AD-A166 188 BOUNDARY LAYER STABILITY MEASUREMENTS OVER A FLAT PLATE AT MACH 3(U) MONTANA STATE UNIV BOZEMAN SUPERSONIC WIND TUNNEL LAB A DEMETRIADES NOV 85 SWT-TR-85-1 1/3

UNCLASSIFIED AFOSR-TR-86-0056 AFOSR-80-0267 F/G 20/4 NL

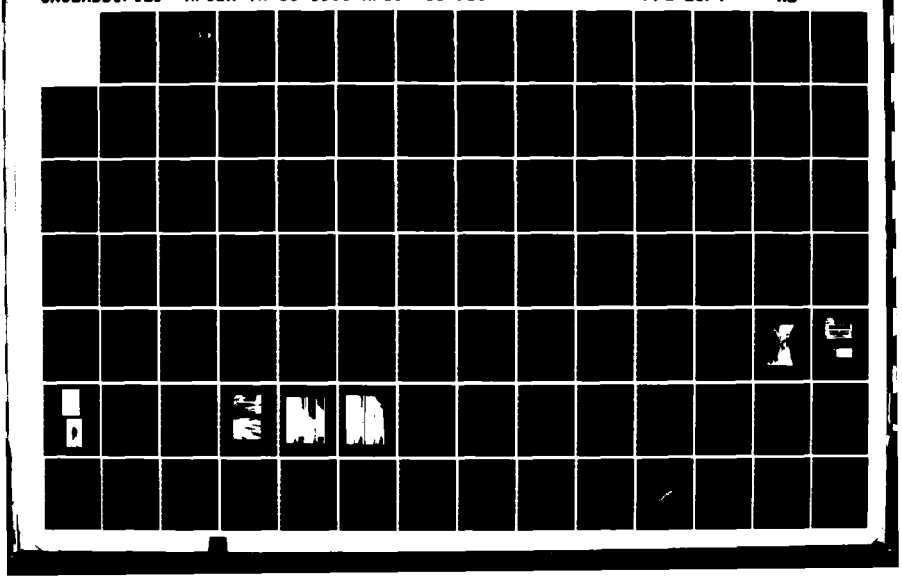

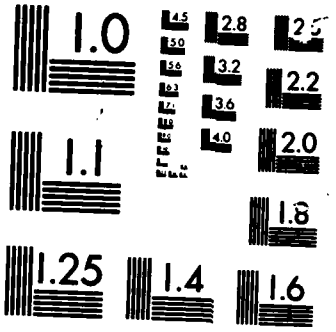

MICROCOPY RESOLUTION TEST CHART

SWT TR 85-1

AFOSR TR_____

BOUNDARY LAYER STABILITY MEASUREMENTS OVER A FLAT PLATE AT MACH 3

Prepared by

Anthony Demetriades
Supersonic Wind Tunnel Laboratory
Mechanical Engineering Department
Montana State University
Bozeman, MT 59717-0007

Prepared for

U.S. Air Force Office for Scientific Research
Building 410, Bolling AFB
Washington, D.C. 20332
Final Report
Under [redacted] AFOSR-80-0267

November, 1985

DISCLAIMER NOTICE

THIS DOCUMENT IS BEST QUALITY PRACTICABLE. THE COPY FURNISHED TO DTIC CONTAINED A SIGNIFICANT NUMBER OF PAGES WHICH DO NOT REPRODUCE LEGIBLY.

UNCLASSIFIED

SECURITY CLASSIFICATION OF THIS PAGE (When Data Entered)

REPORT DOCUMENTATION PAGE	READ INSTRUCTIONS BEFORE COMPLETING FORM
1. REPORT NUMBER: AFOSR-TR- 86-0056 / 2. GOVT ACCESSION NO.: AD-A166188	3. RECIPIENT'S CATALOG NUMBER:
4. TITLE (and Subtitle): Boundary Layer Stability Measurements Over a Flat Plate at Mach 3	5. TYPE OF REPORT & PERIOD COVERED: Final Report
	6. PERFORMING ORG. REPORT NUMBER: SWT TR 85-1
7. AUTHOR(s): Anthony Demetriades	8. CONTRACT OR GRANT NUMBER(s): AFOSR-80-0267
9. PERFORMING ORGANIZATION NAME AND ADDRESS: Montana State University, Bozeman, MT 59717	10. PROGRAM ELEMENT, PROJECT, TASK AREA & WORK UNIT NUMBERS: 61102F, 2307/A2
11. CONTROLLING OFFICE NAME AND ADDRESS: AFOSR/NA, Building 410, Bolling AFB, Washington, DC 20332	12. REPORT DATE: November 1985
	13. NUMBER OF PAGES:
14. MONITORING AGENCY NAME & ADDRESS (if different from Controlling Office)	15. SECURITY CLASS. (of this report): ~~None~~ UNCLASSIFIED
	15a. DECLASSIFICATION DOWNGRADING SCHEDULE

16. DISTRIBUTION STATEMENT (of this Report)

Approved for public release; distribution unlimited.

17. DISTRIBUTION STATEMENT (of the abstract entered in Block 20, if different from Report)

18. SUPPLEMENTARY NOTES

19. KEY WORDS (Continue on reverse side if necessary and identify by block number)

Boundary Layer, Laminar, Stability, Transition, Supersonic

20. ABSTRACT (Continue on reverse side if necessary and identify by block number)

The amplification of natural disturbances in a flat plate laminar boundary layer at edge Mach number 3 have been measured in the MSU Supersonic Wind Tunnel with and without turbulent sidewall boundary layers. Detailed flowfield measurements were made to define the self-similar region and the point where the velocity profile first departs from the Blasius theory. The first instability mode was detected with a minimum critical Re_θ of 190 and a maximum amplified frequency of 0.000225. Amplification rates for this mode agree with the available

DD FORM 1 JAN 73 1473 EDITION OF 1 NOV 65 IS OBSOLETE

UNCLASSIFIED

SECURITY CLASSIFICATION OF THIS PAGE (When Data Entered)

continued

theoretical predictions, and its low-frequency, low-R region is not as distorted by monotonic amplification as previously thought. A second, very prominent and extensive instability was found which extends to much higher frequencies beyond F = 0.00035 and which dominates the pretransitional flow. The neutral branch location of this mode associates it with the second instability mode found in hypersonic flow and serves to clarify and present a stability diagram rational over the M = 0-8 range. The overall amplitude gain before the first departure is still confined to low frequencies with the first mode contributing little net gain, the combined first-second modes contributing a gain of about 3, while an additional factor of 5-10 is provided by a mechanism active near the leading edge and apparently consistent with Mack's forcing-stability approach. Some attempts to gauge the effect of surface roughness on stability are also described.

FOREWORD

This document presents the research performed under support from the U.S. Air Force Office for Scientific Research, under Grant No. 80-0267, in the period 1980-1984 at Montana State University. Principal investigator was the author, Dr. Anthony Demetriades, Professor of Mechanical Engineering at MSU. The AFOSR officer in charge was Captain Michael Francis.

The objective of the research was the study of the hydrodynamic stability of a flat-plate laminar boundary layer in the MSU Supersonic Wind Tunnel by measuring the amplification of natural disturbances in the flow. Initially, some emphasis was placed on the additional effect of surface roughness on stability, and a master's thesis by a graduate student was prepared on the flowfield over a rough wall. Emphasis was gradually shifted to the smooth wall problem, which was found more demanding and potentially more fruitful than originally thought.

The author is indebted to AFOSR for its patience and support throughout this work, and to Glenn McCullough for assistance with the model, the wind tunnel operation and the gathering of the mean-flow data.

TABLE OF CONTENTS

*Interspersed in the text.

LIST OF FIGURES

LIST OF SYMBOLS

A: r.m.s. fluctuation amplitude.

a_1: Coefficient in formula for measured momentum Reynolds no.

a_2: Coefficient in formula for measured momentum Reynolds no.

C: Chapman-Rubesin constant.

c_f: Friction coefficient.

e: r.m.s. hot-wire voltage (=A)

f: Frequency.

F: Non-dimensional frequency.

G: Fluctuation spectrum referred to spectrum at $R = R_o$.

k: Average roughness height.

M: Mach number.

p: Pressure.

R: Square root of Re_x.

Re_x: Reynolds no. based on edge conditions and x.

R_o: Value of R chosen as a reference (R_o = 150 here).

Re_e: Reynolds no. based on k and edge conditions.

Re_k: Reynolds no. based on k and on conditions at y = k.

Re_θ: Momentum Reynolds no.

$Re_{\theta_{NOM}}$: Nominal (calculated) momentum Reynolds no.

$Re_{\theta_{ACT}}$: Actual (measured) momentum Reynolds no.

Re_{θ_T}: Momentum Reynolds number at first departure (transition).

Re_Δ: Reynolds no. based on edge conditions and layer thickness.

Re': Unit Reynolds no. based on edge conditions.

T: Temperature.

T_w: Model surface temperature.

T_o: Total temperature.

T_{o_e}: Stagnation temperature of tunnel flow.

u: Velocity.

x: Distance from the leading edge.

x_i: Entrainment (fluctuation ingestion) point.

x_o: Reference point = x_i.

y: Distance from plate surface.

$\tilde{y}$: Compressible-transformed y.

α_i: Amplification rate.

γ: Ratio of specific heats.

δ: Boundary-layer thickness.

Δx: Increment along x.

θ: Momentum thickness.

λ: Fluctuation wavelength.

ν: Kinematic viscosity.

ρ: Density.

Ψ: Fluctuation wavefront inclination angle.

$( )_e$: Boundary-layer edge conditions.

$( )_o$: Stagnation conditions.

1. Introduction and Motivation

It is common experience that surface roughness promotes transition to turbulence in the laminar boundary layer. Nearly every text on boundary layers includes a summary of the numerous experiments done to date, by which transition to turbulence was found to move upstream when the surface is roughened. The body of available literature is necessarily large because of the large variety of possible roughness geometries and their distribution on the surface, i.e., of the spectrum of the surface contour. There are several prevalent notions of turbulence generation by roughness: one is that the turbulent wakes of a few isolated surface protrusions agitate the boundary layer into a turbulent state; another, that the roughness distorts the mean flow field into a hydrodynamically unstable shape. The latter view has attracted attention especially when the surface is uniformly covered by "distributed" (statistically stationary) roughness of height k much smaller than δ (the layer thickness).

As an ideal example of a formal connection between roughness and transition, one could calculate the mean velocity profile distortion due to small-scale, uniformly distributed roughness, and then subject this profile to hydrodynamic stability analysis; a rational connection between the roughness and transition would thus be found. Such a task would be arduous because of the difficulty of the flowfield calculation and the need to repeat it for every conceivable type of roughness. As an alternative, Reshotko (Reference 1) and Kendall (Reference 2) instead attempted to measure experimentally the velocity profile with roughness, with a view of perhaps using the measured profile as an input to stability analysis. One could then make parallel stability (e.g. disturbance amplification) measurements, and compare the latter with stability characteristics predicted from the measured

mean rough wall flowfield.

The Reshotko and Kendall tests were done at low speeds. The work described here was planned as the analog for supersonic flows. Specifically, the purpose here was to measure both the mean profile and the amplification rates (stability diagram) of a supersonic laminar boundary layer, when the wall surface is rough. Under the best of circumstances, it was hoped that eventual use of the measured mean profile could be made by stability theory for amplification calculations, and that the stability characteristics so calculated would in turn be compared with the measured stability characteristics. No information exists to date on the amplification of small disturbances in a supersonic boundary layer over a rough wall; such information would be in any way invaluable toward the understanding of the role of roughness in promoting transition. Thus, the data could play a dual role as checks of the stability theory and as practical guides to transition prediction.

At the inception of the present program, it was clearly understood that previous knowledge on the supersonic boundary layer stability with a smooth wall should be the necessary base on which the measurements with roughness should rest. It soon became apparent that such knowledge was overestimated. A survey of the experiments done on smooth wall stability showed a number of reports dealing with subsonic edge Mach Number M_e (e.g. References 3 and 4), a series of experiments at $1.5 < M_e < 2.2$ (Reference 5) and a rather heavy concentration at $6 < M_e < 8.5$ (References 6 through 11). Kendall (Reference 12) made another series of measurements at $M_e = 3$ and 4.5, but his presentation deals mainly with the issue of boundary layer response to the free-stream noise with little information on the disturbance behavior within the boundary layer especially at Mach 3.

Those with some experience in amplification measurements at $M_e = 3$ have given discouraging accounts of its suitability as a test-bed of linear stability theory. Laufer and Vrebalovich (Reference 5) limited their published account of stability to $M_e = 1.6$ and 2.2 because "...at M = 3 the detection of self-excited oscillations was much more difficult and less reliable." Kendall notes that in his supersonic experiments "fluctuations of all frequencies were observed to grow monotonically larger in the region of a boundary layer extending from the flat plate leading edge to the predicted location of instability, i.e., in a region where no growth was expected" (Reference 12, p. 291). This statement portends grave difficulties for stability experiments aiming at the observation of neutral boundaries for checking the linear stability theory at or around M = 3. Such experiments, furthermore, also depend on amplified "Tollmien-Schlichting wave" observation as a reliable indicator of ongoing instability, and indeed the accidental discovery of such waves by Schubauer and Skramstadt in the 1940's (Reference 3) supplied the major impetus for modern-day stability research. Even at hypersonic speeds, laminar instability waves are so pronounced that they are routinely visible even with unsophisticated sensors. This selectivity of the boundary layer apparently disappears at $M_e = 3$, however, giving the experimenter no immediate evidence of disturbance amplification.

An interesting theoretical explanation of the exceptional non-selectivity and low amplification in the vicinity of $M_e = 3$ is supplied by Mack (Reference 13, p. 282). It turns out that $M_e = 3$ lies at the minimum of curves one can plot theoretically of maximum spatial amplification rate vs. M_e. This minimum marks the intersection of 3-D, first-mode amplification rates, and the rates due to 2-D second-mode disturbances. Thus $M_e = 3$ occupies a unique spot in boundary layer stability, one which should present difficulties to the

experimentalist and the theoretician alike.

As a result of the ideas expressed above, the objective of measuring the growth of damping of natural disturbances over the smooth wall, rather than being an initial tare measurement, became quite imperative. The smooth wall stability measurement provided, in the end, most of the measurements described and conclusions reached here.

2. Wind-Tunnel Facility

All measurements described here were done in the continuous supersonic wind-tunnel at MSU (MSU/SWT) at Mach number 3.0. A detailed description of the facility appears in Reference 15. The relevant attributes of this facility are its ability to run for long periods (e.g. 8 hours) at constant supply (stagnation) pressures and temperatures, its steadiness and uniformity of flow, its convenience of access to the test section, its broad expanse of optical view of the flow, its automated probe control and data acquisition and the ease of controlling the sidewall boundary layer transition zone. An overall view of the facility is shown in Figure 1.

3. Early Experiments with the Axi-Symmetric Model

This program began as a graduate student thesis experiment to look at the rough wall flowfield, stability and transition on an axi-symmetric (ogive-cylinder) model at Mach 3. This geometry was chosen mainly to alleviate possible problems of model-wall interference common with flat-plate models. This phase of the program is presented in detail in Reference 16.

The model consisted of a 20.3 cm long, 2 cm diameter cylinder attached to an 11.7 cm long ogive with a sharp tip of 5.2° half angle. The rear end of the ogive screwed on and blended smoothly with the front end of the cylinder while the latter was supported in the back by a sting. This model was always

operated at zero angle of attack, in the tunnel stagnation pressure p_o range of 200-600 torr (unit Reynolds number range 20,000 < Re′ < 60,000/cm), and stagnation temperature range 75-125F. The model is pictured on Figure 2.

The boundary layer flowfield over this model was first examined when the cylindrical afterbody had a smooth surface (the ogive was always configured with a smooth surface). The transition dependence on p_o was measured, and it was next attempted to determine the surface roughness suitable for stability measurements by introducing roughness on the cylinder and studying changes in the transition location. Accordingly, duplicates of the cylindrical afterbody were built which were covered by uniformly distributed sand-type roughness; these roughness "overlays", pictured on Figure 3, were made of ordinary shop sandpaper which had earlier been subjected to a measurement of roughness height by profilometry (Reference 17). The random roughness height k, quoted below, was consequently known with some accuracy (as Reference 17 explains, k represents the average peak-to-valley height).

Two important findings emerged. First, it was extremely difficult to trip transition with such sand-type roughness, even though k was gradually increased by changing to coarse overlays. For example, changes in transition were practically imperceptible for 60-grit roughness (k = 0.004" = 0.01 cm). For such k we computed

$$Re_e \equiv \frac{u_e k}{\nu_e} \simeq 500 \tag{1}$$

$$Re_k \equiv \frac{u_k k}{\nu_k} \simeq 23 \tag{2}$$

where "e" refers to boundary layer edge properties and "k" to properties at y = k. Feindt (Reference 18) claims that when the former of these two Reynolds numbers is about 120, the roughness becomes effective as a transition trip in incompressible flows. In view of eq. (1), Feindt's criterion is obviously invalid at high speeds. This is hardly surprising for supersonic

flows where the density is low near the wall and where the roughness has to protrude into higher flux regions to be effective. The proper criterion involves the Re_k of eq. (2) as originally suggested by Schiller (Reference 19) and Smith and Clutter (Reference 20). Kendall (Reference 2) and Reshotko (Reference 1) have re-emphasized that Re_k must reach a value of about 100 for roughness to become effective. In the present instance the resulting required k was computed to be about 0.01" (0.025 cm).

Second, it became clear that such large k values would compound difficulties (already encountered for smaller k) of making meaningful boundary layer measurements. An average k of 0.01" would produce an average ratio of $k/\delta \simeq 1/4$, and on occasion much larger for isolated large grit elements. But unless $k/\delta << 1$ the entire concept of a uniform, statistically homogeneous random surface collapses since k cannot be considered a characteristic length constant from one point on the surface to another. Furthermore, the solid surface itself can no more be defined when k is so large. These conclusions are obviously true for any supersonic/hypersonic flow, and therefore work with the random-distributed sand-type roughness was discontinued.

A roughness type was next sought which would eliminate the difficulties just described. The arrangement settled upon, shown on Figure 4, consisted of a periodic pattern of alternating ridges and grooves ("teeth") machined transverselly over the entire length of a cylindrical afterbody; the top of the ridges defined a cylindrical surface coinciding completely with the largest diameter of the ogive (i.e. the grooves were recessed and the ridges did not protrude from the model surface). The ridge height was 0.036 cm (Figure 4), consistent with the requirement on Re_k as per above. At the same time, however, the spacing between adjacent ridges (= 0.072 cm) was made small to prevent the boundary layer separating at the top of a ridge from

reattaching on the floor of the adjacent groove. It had already been known from the work of Charwat, Dewey and others (References 21 and 22) that for length-to-depth ratios of the type shown on Figure 4, the groove cavity is "open", i.e. the layer separating from one ridge proceeds parallel to the flow to reattach on the top of the next. The present choice of open-cavity flow would seem to create a new virtual surface of the model that is defined by the ridge-tops. In turn, such a flow would be free of point-to-point anomalies in the mean flow profiles, but at the cost of also not taking full advantage of the ridge height. It will be shown later that the profile data taken showed that the flow over a groove was, in fact, very similar to that over a ridge. As to the efficiency of this type of roughness in tripping transition, this was indeed confirmed immediately by Schlieren and pitot measurements, as will be shown in Section 4.2.

At about this time, it also became clear that the boundary layer development over the ogive-cylinder had certain disadvantages. For example, the boundary layer growth was not of the Blasius type, and especially at and downstream of the shoulder the measured momentum Reynolds numbers Re_θ were too large (Figure 5). Such behavior is typical of axi-symmetric ogive-cylinder flows but is not conducive to the study of stability. This phase having exhausted its usefulness, the experiments were continued with a flat plate geometry.

4. Flowfield Measurements

4.1. Flat Plate Model Geometry

Beginning in 1982, the program was continued with the design and fabrication of a 2-dimensional sharp-tipped flat plate model for the stability measurements. Like its axi-symmetric predecessor, this model, pictured on

Figures 6 and 7, had provisions for changing its top surface from a smooth to a roughened one. This was done by the use of interchangeable inserts, one of which was smooth, and the other roughened by parallel "teeth" of the same geometry as used for the axi-symmetric model (Figure 6). All discussion will henceforth pertain to this flat plate model only, which is pictured in Figures 6 and 7.

4.2. Overall Flow Characteristics and the Transition to Turbulence

This report deals with measurements done on the flat-plate model described above placed in the uniform, steady Mach 3 flow of the SWT test section as pictured in Figure 7. Before the amplification data are discussed, however, it is necessary to describe the overall features of the flowfield in the SWT nozzle and the model installed within it.

The overall flow features can be seen in the Schlieren photos of Figures 8 and 9 and in the pitot profiles of the boundary layer included in Figures 10 through 13. The Schlieren picture shows clearly the boundary layer and also the reflection of the leading-edge shock wave. Transition to turbulence is also shown.

The tunnel noise environment is best illustrated via Figure 15. The boundary layer transition onset on the SWT interior sidewalls has been studied at intervals over nearly 15 years, and it has always depended on p_o in the manner illustrated on this figure. In the present measurements, the significant p_o levels chosen were p_o = 350, 475 and 600 torr (mmHg.). The plate model was installed so that its leading edge lay 13.2 inches (33.5 cm) from the nozzle throat. According to the graph of Figure 15, this means that at p_o = 350 turbulence radiation from the sidewalls never reached the plate surface; on the other hand at p_o = 600 the entire length of the plate was irradiated from the sidewalls. The intermediate case of p_o = 475 torr is such

that sidewall radiation along Mach lines first reaches the plate at a distance of order $\sim$ 5 cm downstream of the leading edge.

Transition measurements on the plate were made on several occasions in this research with the Schlieren optics, pitot probes and the hot-wire anemometer. In the present instance transition onset was quantified using the velocity profiles which are summarized on Figures 8 through 14 (the flowfield implications of these profiles will be explained in Section 5.3). If, for the moment, we concentrate on the agreement between the data and the Blasius theory, it is evident from Figures 10, etc. that at a certain x distance for each of the six cases shown, the data depart from the Blasius theory. This "first departure" point (or x) was used here to mark the transition onset. These first-departure points, listed on Table I and plotted on Figure 16, are identified by means of Re_x, R, nominal Re and actual Re ; the latter values represent the momentum Reynolds numbers actually measured, and are discussed in Section 5.3.

TABLE I
TRANSITION DATA SUMMARY

I. REYNOLDS NUMBERS AT FIRST DEPARTURE

SURFACE	P_o (mm)	Re_x (thousands)	$R=(Re_x)^{1/2}$	$Re_{\theta NOM}$	$Re_{\theta ACT}$
SMOOTH	350	353	594	394	446
	475	404	636	422	489
	600	449	670	449	533
ROUGH	350	271	520	345	372
	475	351	593	394	454
	600	415	644	428	523

II. UPPER LIMIT OF MEASUREMENTS (FLOW NOT YET FULLY TURBULENT)

SMOOTH	350	476	690	458	553
	475	706	840	558	768
	600	783	885	588	848
ROUGH	350	462	680	452	576
	475	723	850	564	922
	600	792	890	591	1032

The noteworthy results of Figure 16 are (a) transition as represented by the first departure is a function of Re' for the smooth and rough wall alike, (b) the ridge-groove roughness is effective in moving transition forward, and (c) this effectiveness is pronounced at $Re' = 29{,}000/cm$ but less so at $Re' = 56{,}000/cm$. Note, for example, that at $Re' = 29{,}000/cm$ a decrease of 15% (from $Re_{\theta T} = 400$, say, to 350) in $Re_{\theta T}$ represents a 30% decrease in the x of the transition location. Also to be noted from Figure 16 is that there is no evidence from these data that sidewall irradiation makes any sudden changes in the behavior of $Re_{\theta T}(Re')$.

The lower part of Table I should dispel any illusions that the transition process occurs at Reynolds numbers as small as indicated by the first departure. The best estimates made of C_f, to be presented later, show that fully turbulent flow was not attained even at the farthest positions x examined in this experiment. Especially if the actual Re_θ is considered, the transition process is still incomplete in the range $550 < Re_\theta < 1050$ and depends on p_o and plate surface configuration. The wetted distance x over which transition is in progress is thus quite large.

With the preceding discussion in mind, we have attempted some comparison with transition correlations in wind-tunnels compiled by Pate (Reference 23)

and more recently by Beckwith (Reference 24) and shown in Figures 17 through 20. The comparison is somewhat tenuous since the definition of "transition" varies from one author to the next, but it is made in order to uncover any large and fundamental differences between the MSU/SWT and other facilities. There seems to be no such difference. This finding is important; it inspires confidence that there is no fundamental reason why the present transition, and presumably stability, behavior should be unique to the present wind-tunnel.

TABLE II

MATRIX OF MEAN-FLOW MEASUREMENTS

Mach number (nominal):	3.0
Stagnation pressures:	600 mm Hg abs. (torr)
	475 mm Hg abs.
	350 mm Hg abs.
Stagnation temperature:	100 F (560 R)
	(125 F with p_o = 350 mm only)
Types of surface:	Solid (smooth wall)
	Rough (rough wall)
Distance x from L.E.:	0-16 cm (profiles taken at 1 cm increments)
Data Coding Method:	Data groups consist of a four-digit number with:
-First Digit: Surface code:	"3" for smooth surface
	"2" for rough surface
-Second Digit: Pressure code:	"3" for p_o = 600 mm
	"2" for p_o = 475 mm
	"1" for p_o = 350 mm
-Third & Fourth Digits:	x(cm)

(Note: For the stability measurement done with the anemometer, the third and fourth digits refer to x in tenths of an inch, e.g. 3347 means that the data were obtained at x = 4.7 inch.)

4.3. Instrumentation and Procedures for Flowfield Measurements

Three principal instruments were used for quantitative flow diagnosis of the mean-average flowfield. The model surface temperature was measured by contacting an iron-constantan thermocouple with the underside of each insert. The surface static pressures were measured with a static-pressure probe consisting of a 0.022" dia. tube with 0.013" dia. holes drilled around its circumference and located 0.20" downstream of the closed, sharpened end of the tube. During the measurement the tube was held parallel to the flow and in contact with the surface and traversed slowly backwards (see Figure 21) while the static pressure output was recorded continuously. Tests showed that the spatial resolution of this probe was of order $\hat{\epsilon}/2$; this is satisfactory considering that the stream-wise extent of the mapped region was about 15 cm or 100 δ, and that normal gradients were not expected on theoretical grounds.

Boundary layer profiles were recorded by traversing a 0.004"-dia. pitot probe normal to the surface. Based on an average δ of 0.15 cm, the spatial resolution of this probe was of order 1:15. The SWT probe actuator system served both to suspend the probe and to move it in an advance-pause-measure sequence. A schematic of the system is shown on Figure 22. The pitot signal was translated from pressure to voltage by a Kulite 0-5 psia pressure transducer, so that at each point of measurement two voltages were automatically recorded, one corresponding to distance above the surface. These voltages were converted to digits by a Spectral Dynamics SD133 A/D Converter and stored on cassette by a Texas Instruments Silent 700 computer terminal.

The mean-flow matrix of measurements is shown on Table II. For each of the six combinations of 3 stagnation pressures and 2 types of surface, the plate surface pressure and temperature was determined and boundary layer profiles spaced 1 cm apart were obtained with the pitot probe, each profile

typically containing 60 point measurements. Several profiles were taken in the transitional zone as well. All data were taken at the mid-span position of the plate. Each profile was coded with a four-digit number as explained on Table II.

During the measurements, it was discovered that the boundary layer growth became anomalous at $x > 6$ cm when p_o was 475 and 350 mm. Since the SWT sidewall was laminar at these pressures at the point where it intersected the plate leading edge, it was determined that the latter caused sidewall boundary layer separation and set up a system of waves converging at $x = 6$ cm on the top plate surface. The problem was corrected by limited tripping of the sidewall boundary layer ahead of its intersection with the plate leading edge. Details of this scheme are given in Appendix A.

The mean-flow data were reduced by the standard technique of combining the pitot, static pressure and wall temperature measurements. At each position x chosen, the static pressure was known from the continuous static-probe traverses described above. The total temperature had been measured at only one point, but this was considered adequate because of the expected uniformity of T_w along the plate and the known insensitivity of the data reduction results on T_o. The measured T_w was assumed valid at each point on the surface and each p_o. The distribution of T_o through the layer was assumed linear; T_{oe} at the layer edge was found to be equal to T_o.

The data reduction programs did not account for the distortion of the pitot probe reading due to viscosity (Reference 25). The viscous effect should be most pronounced at the surface, where the minimum diameter-based pitot probe Reynolds number was typically about 10. A viscous error of several percent is possible in this case for the data taken right next to the surface. On the other hand, such data should be in any way rather unreliable

because of probe-surface interference, and their dubious validity did not justify viscous correction (see below for the handling of the first few points next to the wall).

The boundary layer thickness was determined by inspection of preliminary plots of each profile. As always, the choice of δ is somewhat subjective in boundaries of laminar flow which are diffuse, a difficulty compounded by the finite probe size. Generally the method of Kendall (Reference 26) was followed, and once δ was found then final data reduction of the profile was made.

The local "edge" properties (subscript "e") were found from the last profile point, which usually lay at $y \sim 1.3\delta$. The flow within $0 < y < 1.3\delta$ was invariably uniform and constant, so that this method eliminated the propagation of errors in finding δ, to the determination of the edge properties.

During the measurement, the pitot probe tip was always observed with a microscope to ensure that the first recorded datum of each profile was taken with the probe touching the surface, and the second with the probe off the surface. Because of the miniscule motions involved and the finite precision of the hardware, more points than one were always recorded with the probe touching the surface. This could be confirmed with the microscope, however, and a tag notifying the computer of such "bad" points was included in the data analysis. For the rough wall measurements, the "surface" terminology must be replaced with "top of ridge"; note Figure 6 in this connection.

The data thus reduced for the laminar portion of the boundary layer produced velocity profiles which generally agreed well with the Blasius theory, as will be shortly demonstrated, except for a small displacement along the y axis. This displacement ranged from 0 to 10 mils in extreme cases, and

remains unexplained at this writing. To account for this problem, the data were first plotted to measure this displacement ("offset") for each profile, and then reduced for a second time by adding the appropriate offset to the measured vertical distance y. This came to be known as the "offset" method of data reduction. The offset method had the added feature that anomalous points near the surface were eliminated while computing the momentum thickness and also during final plotting of the profiles.

A special problem arising in the rough wall measurement concerned the definition of the "surface". As already mentioned, the succession of two-dimensional cavities formed by the ridge-groove roughness was ignored by the flow, in the main, because each cavity was closed. Pitot profiles taken directly above the ridges gave velocity profiles identical to those taken over the grooves (e.g. midway between two successive ridges). Thus, the plane formed by the tops of the ridges formed the "surface" in the rough wall measurements (see Figure 23).

The management of the data is outlined in Appendix B. The main inputs consisted of tabulations of pitot readings vs. y into files called PITOXXXX or PITXXXX where XXXX is the code given in Table II. The principal reduction program was LAMBL2 which received the PITOXXXX files and produced printouts of the results and, if requested, prepared and stored files GRAFXXXX suitable for graphics plots of these results. Summary graphics plots of integral properties vs. x were also possible by using files called DOTALXX, where here XX refers to the first two digits of the code of Table II.

5. Results of the Flowfield Measurements

5.1. Plate Surface Temperature

The surface temperature measurement gave a recovery factor of 0.937 0.007 for all conditions of p_o and surface configurations.

5.2. Plate Surface Pressure

The surface static pressure distribution along the plate centerline is shown on Figure 21. There are discernible small pressure gradients toward the trailing edge where stability data were not taken in anyway; otherwise the pressure is nearly constant, insensitive to the surface roughness and such as expected from isentropic expansion calculations.

It is of some interest to examine the surface pressure distribution over the rough wall in the greatly magnified detail of Figure 24. The trace shown has been obtained during the static probe traverse (see Section 4.3), has been copied directly from the x-y plotter record, and is a magnified portion of the static pressure distribution in the neighborhood of x = 12 - 13 cm for the rough wall at p_o = 600 torr. For this case the boundary layer included in the graph is turbulent; note the relative dimensions mentioned on the figure (and refer to Figure 8 for a photographic view). The remarkable feature of this trace is its periodicity; there appear two prominent wavelengths, the larger (0.32 cm) being of order δ, the smaller one (0.08 cm) being very close to the spacing between ridges, i.e. to the roughness wavelength. The smaller wavelength is undoubtedly associated with the roughness, i.e. with an equivalent wavy-wall effect. The origin of the larger wave is not known. In either case the periodicity in the pressure is rather small, of order 0.6% for the larger, and an estimated 0.05% for the smaller wave. It should be stressed that the pattern of Figure 24 disappeared when the boundary layer was laminar, in agreement with the notion that pressure features are accented when the flow over the generating surface features increases in speed. No account of this waviness was therefore taken in the analysis of the stability data.

5.3. Boundary Layer Development

The profiles of flow properties through the boundary layer are shown on

Figures 10 through 14; integral properties are shown on Figures 25 through 27 and tabulated in Table III.

These data, together with the preview afforded by Figures 8, 9 etc. collectively support all preconceived ideas about a normal laminar boundary layer ending into a transitional zone. For the smooth wall (e.g. Figure 13) the velocity profile is in agreement with the Blasius theory (Reference 27) up to the "first departure" point already discussed in Section 4.2. Beyond that point an increasing disparity appears between the theory and the data as x increases. The agreement between the theory and the laminar data is most convincing; a few isolated exceptions occur near the leading edge where the laminar boundary layer is so thin that some probe-flow interference is expected. All profiles show no data very near the wall ($y/\delta < 0.2$) for the same reason. Note that the data are shown in terms of the transformed coordinate y normalized with the measured momentum thickness:

$$\frac{\tilde{y}}{\theta} = \frac{\int_0^y \frac{\rho}{\rho_e} dy}{\int_0^\delta \frac{\rho u}{\rho_e u_e}\left(1 - \frac{u}{u_e}\right) dy} \tag{3}$$

where all quantities in the integrands were drawn from the measurements.

The integral properties, etc. from Table III have been compared with their theoretical counterparts:

$$\delta = 5.84 \left(\frac{\nu_e x C}{u_e}\right)^{1/2} \left(1 + .417 \frac{\gamma - 1}{2} M_e^2\right) \tag{4}$$

$$\theta = 0.664 \left(\frac{\nu_e x C}{u_e}\right)^{1/2} \tag{5}$$

$$Re_\delta \delta = Re' \delta^2 = 104 x \tag{6}$$

$$Re_\theta \theta = Re' \theta^2 = 0.441 x \tag{7}$$

$$Re_\theta = 0.664 (Re_x)^{1/2} = 0.664 R \tag{8}$$

where for the three latter formulas we have used $\gamma = 1.4$, $M_e = 3$ and $C = 1$. Eq. (8) has been plotted on Figure 13 and 14, and it is seen that there is a

TABLE III. FLOWFIELD INTEGRAL PROPERTIES

A. Smooth (Solid) Surface

P_o (Torr)	x (cm)	Group	Number of Points	M_e	Re' (cm^{-1})	δ (cm)	θ (cm)	Re_x ($\times 10^{-3}$)	Re_θ
350	3	3103	51	2.98	29800	.095	.0078	89	232
	4	3104	59	2.97	29900	.109	.009	119	270
	5	3105	63	2.94	29600	.122	.0101	132	300
	6	3106	73	2.91	28900	.136	.0115	173	332
	7	3107	75	2.94	29500	.14	.012	206	354
	8	3108	79	2.95	29500	.158	.013	235	385
	9	3109	80	2.97	29900	.155	.013	268	387
	10	3110	86	2.99	29600	.167	.0137	296	405
	11	3111	95	3.00	29800	.188	.0148	327	440
	12	3112	95	3.00	29300	.202	.0158	352	466
	14	3114	97	2.88	27600	.194	.0163	387	452
	16	3116	112	2.86	29100	.225	.0196	465	572
475	3	3203	50	3.04	44100	.08	.0065	132	288
	4	3204	58	3.05	44700	.091	.0073	178	327
	5	3205	67	3.03	44300	.103	.0082	221	364
	6	3206	64	3.02	44000	.107	.0088	263	386
	7	3207	70	3.01	43600	.137	.0112	305	489
	8	3208	87	3.01	43900	.147	.0119	350	522
	9	3209	81	3.01	44400	.156	.0126	399	562
	10	3210	95	3.00	44200	.149	.0121	441	533
	11	3211	93	2.99	43900	.159	.013	482	573
	12	3212	96	3.00	43500	.16	.0133	521	577
	14	3214	107	2.99	42600	.187	.0151	596	645
	16	3216	132	2.95	43300	.229	.0176	692	760

P_o (Torr)	x (cm)	Group	Number of Points	M_e	Re' (cm^{-1})	δ (cm)	θ (cm)	Re_x ($\times 10^3$)	Re_θ
600	3	3303	50	3.06	56400	.075	.006	169	338
	4	3304	60	3.07	56600	.089	.0072	226	406
	5	3305	63	3.06	56400	.099	.077	282	437
	6	3306	64	3.06	56600	.104	.0083	339	468
	7	3307	70	3.05	56300	.116	.0091	393	515
	8	3308	73	3.05	56300	.132	.0101	449	571
	9	3309	75	3.04	57000	.131	.0106	513	606
	10	3310	79	3.02	56500	.133	.011	564	620
	11	3311	84	3.01	55800	.138	.0115	613	642
	12	3312	97	3.02	55100	.153	.0121	661	670
	14	3312	154	3.02	54000	.196	.0153	757	829
				B. ROUGH SURFACE					
350	2	2102	51	2.95	29100	.0737	.00617	58	180
	3	2103	59	2.95	29100	.0878	.00728	87	212
	4	2104	70	2.94	29100	.108	.00883	116	257
	5	2105	77	2.97	30200	.125	.0103	151	310
	6	2106	83	2.9	28200	.12	.0098	169	277
	7	2107	73	2.91	28200	.132	.0115	197	324
	8	2108	82	2.95	29000	.153	.0128	232	370
	9	2109	97	2.94	29200	.16	.0133	262	387
	10	2110	93	2.95	28900	.154	.0129	289	374
	11	2111	95	2.94	28600	.163	.0137	315	391
	12	2112	99	2.94	28200	.177	.0143	338	402
	14	2114	121	2.87	27700	.211	.0176	388	486
	16	2115	133	2.82	28200	.229	.0208	450	586

P_o (Torr)	x (cm)	Group	Number of Points	M_e	Re' (cm^{-1})	δ (cm)	θ (cm)	Re_{x_3} ($\times 10^3$)	Re_θ
475	2	2202	41	2.99	42800	.0628	.00511	86	219
	3	2203	43	3.01	43000	.076	.00623	129	268
	4	2204	49	3.0	42400	.0849	.00716	170	304
	5	2205	71	3.01	43200	.0935	.00772	216	334
	6	2206	65	3.0	43200	.105	.00885	259	382
	7	2207	69	2.99	42700	.121	.0104	298	444
	8	2208	77	3.0	43200	.126	.0108	346	468
	9	2209	87	2.99	43500	.136	.0117	392	510
	10	2210	91	2.97	42900	.154	.0126	429	543
	11	2211	94	2.98	43200	.148	.013	475	560
	12	2212	111	3.0	43000	.172	.0143	516	615
	14	2214	123	3.0	42700	.199	.0159	598	677
	16	2216	141	2.98	44300	.223	.0186	709	826
600	2	2302	46	3.03	56000	.0585	.00465	112	260
	3	2303	54	---	---	---	---	---	---
	4	2304	58	3.01	54400	.0808	.00654	217	356
	5	2305	62	3.02	55100	.0847	.00721	276	398
	6	2306	64	3.01	54900	.0982	.00795	329	436
	7	2307	68	3.01	54700	.108	.00906	383	496
	8	2308	72	3.0	54100	.12	.0101	433	549
	9	2309	81	2.99	54900	.139	.0115	494	634
	10	2310	87	2.97	54700	.158	.0126	548	689
	11	2311	127	2.98	55500	.192	.0136	612	756
	12	2312	127	3.01	56000	.219	.0153	672	860
	14	2314	182	3.01	56200	.319	.0207	787	1161

systematic and growing departure between this formula and the data as x increases, which is apparently independent of p_o (and Re′). Since Re_θ will be needed later for the description of the stability behavior, its departure from eq. (8) was formalized by a least-squares fit of the points shown on Figure 13:

$$Re_{\theta_{ACT}} = Re_{\theta_{NOM}} + a_1 \frac{Re_x}{1000} + a_2 \left(\frac{Re_x}{1000} \right)^2 \qquad (9)$$

where "ACT" and "NOM" refer to actual (measured) and nominal respectively, and where the nominal Re_θ is given by eq. (8). The coefficients a_1, a_2 for the smooth wall were a_1 = -6.609E-3 and a_2 = 4.315E-4.

For the rough wall, the rather surprising fact emerges that the velocity profile shows no characteristic "signature" of the roughness. This can be verified from Figures such as 14, etc. where it is seen that any differences between the rough wall profiles and the Blasius theory or the smooth wall data were very small and irregular so long as the boundary layer remained laminar. Much effort was devoted unsuccessfully in plotting various aspects of the data in order to find any systematic differences between rough and smooth walls. The best that could be done is pictured on Figure 28. Here the abscissa is again in terms of $\frac{y}{\theta}$, and its range covers fully the boundary layer width The ordinate is the

$$\text{INCREMENT} = \left(\frac{u}{u_e} \right)_{\text{SMOOTH}} - \left(\frac{u}{u_e} \right)_{\text{ROUGH}} \qquad (10)$$

As this Figure shows, for low-speed flows with a sandpaper surface Kendall found a positive increment near the wall, meaning that the roughness acted to decelerate the flow. The data points from this experiment indicate a certain acceleration. However, one should note the data scatter; furthermore, the data shown are the end products of a heavy editing process (other data were

much too scattered for inclusion) and are shown as a rather biased attempt at comparison. No conclusions are thus recommended on the basis of this figure, although it is clear that the present data lie sufficiently close to the wall to divulge any chance distortion there due to the roughness.*

The momentum Reynolds number for the rough wall, according to Figure 14, departs from the smooth wall theory, as already observed for the smooth wall in Figure 13 and eq. (9). The actual (measured) Re for the rough wall was therefore fitted with a formula like that of eq. (9), except that in the present case $a_1 = -0.1354$, $a_2 = 8.741E-4$.

6. Stability Measurements

6.1. Instrumentation and Data Acquisition Procedure

The stability data were extracted from the AC signal of a constant-current hot-wire anemometer probe such as pictured on Figure 29. By exercising extreme care in using these probes, such as shielding them during tunnel start or stop, only one probe (No. 9) failed during the many 8-hour days necessary to accumulate the data, so that a total of only two probes sufficed for the measurements. The geometrical and operating characteristics of the probes are shown on Table IV.

---

*The curve due to Kendall shown on Figure 28 was deduced by him from a single boundary layer profile with and without roughness. The scatter of the present data, on the other hand, arises from the superposition of several profiles; there is little scatter within any given profile. The issue therefore is whether Kendall's increment is self-similar and universal at low speeds, for the type of roughness he employed.

TABLE IV

HOT-WIRE ANEMOMETER CHARACTERISTICS

PROBE NO.	5	9
Diameter, microinch	20	20
Material	Pt 10% Rh	Pt 10% Rh
Resistance at 0 C (ohms)	78.57	70.8
Aspect Ratio	175	158
Heating Current, ma	3.4	3.03
Overheat, percent	50	49
Amplifier gain	50	75
Time constant (microsec.)	30	30
High cut-off (KHZ)	500	1000
Low cut-off (HZ)	3	3

The function of the measurement was to make a permanent analog record of the probe output at each of a large number of points x, at constant y/δ , for each combination of p_o and surface condition (rough or smooth). Such a permanent record was made possible with the equipment diagramed on Figure 30. The AC probe output was recorded on a wideband-FM channel of a seven channel analog recorder (Honeywell 7600) at 120 ips (Channel 7), which had a response to 400 KHZ; a direct channel (Channel 2) with a response to 2 MHZ also received this signal, for subsequent study of high-frequency (0.4-2 MHZ) phenomena of possible interest. The signal was monitored in real time by the devices shown on the left on Figure 30, while in the upper right of the Figure is shown equipment by which the probe position was controlled, monitored and recorded. Channel 4 of the recorder was used for a 20 KHZ tone (see lower left hand side of Figure 30) which, on playback, was used as a "valid data on" command for data reduction. Finally, equipment shown on the lower right hand side of the figure was used to ensure that the recording process went smoothly, in real time.

TABLE V
FLUCTUATION MEASUREMENT SUMMARY

				FORWARD POSITIONS					BACK POSITIONS				
		(1)			(2)	(3)	(3)		(2)	(3)	(3)		
SURFACE	P_o (TORR)	BL/FS	CODE	NO. OF X'S	TAPE NO.	START	END	PROBE NO.	TAPE NO.	START	END	PROBE NO.	NO. OF X'S
SMOOTH	350	BL	31--	17	242	6051	8563	5	244	4481	8522	5	28
				19	243	290	3113	5	245	0000	301	5	2
		FS	51--	4	165	8329	END	5	245	587	4938	5	30
				25	186	0000	3981	5					
	475	BL	32--	28	192	4533	8633	5	246	3037	6145	5	21
				8	193	290	1455	5					
		FS	52--	29	188	2948	7509	5	246	6432	END	5	17
									247	0000	602	5	4
	600	BL	33--	36	190	282	5766	5	247	4390	5991	5	11
		FS	53--	29	191	2757	7247	5	247	6278	7873	5	11
ROUGH	350	BL	21--	36	194	0000	5737	5	214	308	6538	9	36
		FS	61--	17	194	6033	8579	5	214	6538	END	9	14
				12	196	0000	1781	5	213	0000	3578	9	22
	475	BL	22--	33	196	2096	7371	5	213	3885	END	9	32
		FS	62--	9	196	7371	8684	5	212	297	6463	9	32
				20	198	000	3171	5					
	600	BL	23--	33	211	3702	END	9	212	6463	END	9	15
				4	161	303	911	9					
		FS	63--	34	161	911	5344	9	211	300	3409	9	21

(1) BL = In boundary layer, FS = In free stream (2) MSU/SWT Analog Tapes (1/2 inch, 7 channel)
(3) Footage marks

The measurement consisted of first positioning the probe tip at the desired x and y/δ (the choice of the latter will be explained in Section 6.2) and recording the probe signal for 10 seconds; then the probe was moved to a new x, keeping y/δ the same, and the process repeated. Each 10-second signal burst was called a "data group" and logged as per the rules of Table II. The collection of groups for each particular p_o and surface condition is called a "data set". Data sets were taken not only inside but also outside the boundary layer, the latter by holding the probe 0.25" (0.625 cm) above the plate surface. The stations x were separated by 0.1" (0.25 cm) and ranged from about 0.2" downstream of the L.E. to a point well into the transitional regime.

The data are summarized in Table V. The "BL" designation refers to the data taken within the boundary layer, while "FS" refers to those taken in the free stream, as just explained above; there are thus 2 x 3 x 2 = 12 sets of data altogether. The number of x positions, i.e. data groups, is seen to vary from one set to another. For example, for p_o = 350 torr with the rough wall, there were 12 + 17 = 29 groups recorded in the free stream outside the layer in the "forward" probe position with probe No. 5, and another 14 + 22 = 26 groups recorded in the "back" position with probe No. 9. Thus there was a plate lenth equal to (29 + 26) / 10 = 5.5 inches of flow covered at 0.1" intervals. In all, 690 data groups were recorded on 20 reels totaling about 210,000 feet of tape.

It is important to note that the hot-wire anemometer responds jointly to fluctuations in the fluid speed, its temperature, density and pressure. The process by which the latter fluctuations are extracted from the wire AC voltage is called "modal analysis". In practice (References 5, 8 and 12 for example) modal analysis is put aside in stability experiments because of its

great complexity, because of the theoretically-confirmed insensitivity of the stability to the precise mode of fluctuation (Reference 13) and because of recent experimental confirmation of such insensitivity by Stetson et al (Reference 10). Therefore, in this work the quantity A(f;x), while in reality the spectral density of the AC anemometer voltage output, is equated to the rms spectral density of a typical fluctuation. Spectral densities or amplitudes were in anyway unimportant in this work, and only the amplitude change was studied. The complex and lengthy process of computing this change (i.e. the amplification rates) from the anemometer signal is explained in Appendices C and D.

6.2. Initial Observations

Initial observations with the hot-wire anemometer confirmed that the zone of transition to turbulence varied in the manner shown on Figure 16. In the free stream the rms output of the wire was generally so low as to be almost indistinguishable from the electronic noise. The wire signal always increased in the laminar boundary layer, however. Traces of the wideband signal vs. y/δ are shown on Figure 31. In the range $0.2 < y/\delta < 0.9$ this increase consists of a "double-peaked" curve which appeared to maintain a self-similar form along x, independent of p_o and surface condition. Of these two peaks, the one occurring at about $y/\delta = 0.45$ was slightly larger than the other, occuring at about $y/\delta = 0.68$. Similarity of this profile stopped at the first departure point.

At low speeds, Schlichting's theory (Reference 28) and wind-tunnel data (Reference 3) suggest such a double-peaked distribution because of shifting phase of neutral oscillations across the boundary layer. The experimental record at hypersonic speeds, on the other extreme, speaks of a similarly

"noisy" laminar boundary layer profile but with a single peak (References 6, etc.). A double peak is noticed in the early data shown at M = 2.2 by JPL (Reference 5), but more recent JPL measurements by Kendall in the $2 < M_e < 5$ range indicate a double-peak only at $M_e = 3$. It seems, therefore, that in the supersonic/hypersonic regime this double-peaked wideband fluctuation profile is specific to or around Mach 3, although for reasons presently unknown.

Another peculiarity obvious from Figure 31 is that the wideband peak signals do not always intensify along x, and that these signals are already large at very small x, of order 1 cm. One possible answer is that considerable amplification occurs very near the leading edge (say at x < 1 cm) where linear stability theory, however, predicts nothing but damping (Re_θ at distances so close to the leading edge are of order 100). Coupled with the greatly suppressed fluctuation levels in the free stream, as mentioned above, this implies a sudden large increase of the disturbance level as the fluctuations first enter the layer very near the leading edge. We shall return to this subject later from another direction, when we discuss the total amplifications measured in the boundary layer.

All measurements reported hereafter were taken at $y/\delta = 0.68$, that is on the energy peak of Figure 31 which was farther from the wall. Using this peak as a landmark simplified the task of keeping y/δ constant from one x to another. Use of the peak at $y/\delta = 0.45$ was rejected for fear of increased risks of wire breakage and wall-probe interference.

The data taken outside the boundary layer (sets 51, 52..., 61, ...) were used to scrutinize the effect of p_o on the stream turbulence, via Figure 32. Even though the signal was not modally analyzed, it is clear from this figure that there exist two general levels of stream turbulence intensity, both of which incease with Re_x. At the top level, marked "with B.L. radiation" in the

figure one finds the data recorded when the wire was immersed in the sound radiation field from turbulent sidewall boundary layers. The lower level, marked "w/o B.L. radiation" corresponds to laminar sidewall boundary layers. The figure confirms an earlier projection, based on Figure 15, about the location of sidewall transition (see Section 4.2). These "free stream" wideband signals range from 0.015 to 0.04 vrms compared to the boundary layer signals (Figures 33 and 34) which range from about 0.06 to 1.6 vrms. The latter signals also scale, approximately, with Re_x as shown on Figures 35 and 36. This is a most important result, since it says that the sidewall radiation has little, if any, systematic effect on the growth of disturbance level in the boundary layer.

In all circumstances the wideband rms signal along the boundary layer was found to increase considerally some distance before the point of first departure. Figures 37 to 42 have been prepared to set this increase in context with observed profile shapes and friction coefficients discussed in Section 5. It is seen that this increase amounts to a factor of 3 in typical cases, and it starts much closer to the leading edge than sometimes thought especially if one keeps in mind the relation $x \sim Re_x^2$. For example, for the rough wall at p_o = 350 torr (Figure 40) the x at which the wideband rms starts increasing is half the x at the first departure. Wideband rms observations alone would thus be most unsuitable for locating the transition zone.

6.3. Results of the Stability Measurements

6.3.1 Spectra of the Fluctuations

The spectra of the fluctuations are shown typically in Figures 43 and 44, to an upper limit of 120 KHZ. In accord with expectations from linear stability, the spectral density seems to decrease, generally, at the high frequencies. The rough wall data appear, too, to be much more "selective"

than the smooth wall data, with peaks in the 10-40 KHZ range. In contrast to results presented at subsonic, low supersonic and hypersonic speeds in References 3, 5, 6, etc. the present smooth wall results are quite unselective. This is so despite the practice in most earlier works to present the mean-square spectral density $A^2(f)$, as opposed to the rms density $A(f)$ shown on Figures 43 and 44 which, incidentally, is therein labeled "amplifier output." Figure 45 shows a comparison between the spectra in the boundary layer and those in the free stream under the same conditions.

A three-dimensional view of spectrum development for the six cases under study is shown on Figure 46. The selectivity of the rough wall boundary layer becomes very obvious in these plots. Note that the plots extend into the boundary layer transition zone.

As mentioned above, the smooth wall data had very low selectivity. Even so, peaks in their spectra could be faintly identified toward the end of the laminar range. Figure 47 shows the position, on the stability diagram (F, Re_θ), of all the spectrum peaks thus observed. The locus is often called "maximum amplification" line in the literature, which should not be confused with the "maximum amplification rate" line in the (F, Re_θ) space. The data shown on this figure were taken directly from the spectrum peaks found from figures such as 45, etc.

The point made by Figure 47 is that, first, the maximum amplitude line is quite independent of Re'; second, there seems to be no effect of the roughness; third, the data agree with those of Laufer (Reference 5) in that they form with the latter a logical progression in the range $M_e = 1.5 - 3$. In this respect, note that the agreement improves when the actual Re_θ is considered.

6.3.2. Characteristic Wavelengths

At this point it is appropriate to remark about an interesting generalization implied by Figure 47. Motivated by similarities between the incompressible and compressible boundary layers when coordinates in the latter are compressed by the compressibility transformation, Laufer and Vrebalovich found (Reference 5, Fig. 32) that their neutral amplification data coincided with those at M = 0, by Schubauer, if F is plotted vs.

$$Re_\delta = \frac{u_e \delta}{\nu_e} \tag{11}$$

A coincidence similar to that indicated in Reference 5 for the neutral branches is bound to occur also for the maximum amplitude line which follows closely the upper neutral branch, inviting an inclusion of the Schubauer-Skramstad data in Figure 47. We can, however, do better. The upper neutral branch for the amplified region observed in References 3 and 5 is very nearly a hyperbola, so that in the correlation scheme of Reference 5 the maximum amplitude should occur along a line of the type

$$F \simeq \frac{\text{CONST.}}{Re_\delta} \tag{12}$$

which in turn gives

$$FRe_\delta = \frac{2\pi f}{u_e Re}, Re'\delta = 2\pi \left(\frac{f}{u_e}\right)\delta = 2\pi \frac{\delta}{\lambda} = \text{CONST.} \tag{13}$$

where λ is the disturbance wavelength based on the edge fluid (not the phase) velocity. Thus the Laufer-Vrebalovich correlation implies that the wavelength is independent of M_e, a point which can now be formally checked by also including the present data. In fact one can also make a comparison with the hypersonic data, where $\frac{\lambda}{\delta}$ has been found to be fairly independent of Re_δ as well.

This comparison, where λ was computed from the edge velocity and the measured peak frequencies, is shown on Figure 48 for all stability data. A

few points obtained by Kendall (Reference 12) at $M_e = 7.7$ are not shown, but these data fall almost exactly on top of the other hypersonic results included. Below the bottom margin of the figure lie "higher harmonic" results about which there is good agreement among References 6, 9, and 12. In passing it must also be noted that (a) the present data are plotted using the actual, measured momentum thickness (see previous discussion), (b)both smooth wall and rough wall data from the present test are included and (c) the M = 7 data of this author represent three different experiments and include hot- and cold-wall results (to $T_w/T_o = 0.4$).

It is evident from this figure that the prominent wavelengths for $0 < M_e < 3$ are of order 30 , while at hypersonic speeds they are much smaller in terms of δ ($\lambda \simeq 2\delta$, as previously found in References 6 , 9 etc.). The $0 < M_e < 3$ results seem unaffected by roughness, while the M = 7 results seem unaffected by moderate cooling. Thus this large difference foretells of fundamentally different instability behavior between these two Mach number regimes.

The data shown plotted on Figure 48 have been reduced by assuming that the phase velocity equals the edge flow velocity, as is evident from eq. (13). This is probably quite true for the hypersonic data, where the prominent instability is supposed to be of the second, two-dimensional mode, and where the critical layer occurs very near the boundary layer edge. For the $0 < M_e < 3$ data, however, the instability mode generating the data shown in the figure is thought to be the first 3-D mode, with phase velocities fundamentally different from the edge velocities.

6.3.3. The Amplification Rates and the Stability Diagram

The amplification rates

$$-\alpha_i(R;f) = \frac{1}{2A}\,\frac{\partial A(R;f)}{\partial R} \qquad (14)$$

were determined by first curve-fitting the A(f;R) data vs. R by the least-squares polynomial method. This curve-fitting became a major issue because of our desire to minimize bias by using the same polynomial degree for all data, because of the wide and ondulatory variation of the observed amplitudes and also because of the sensitivity of the curve-fits to the number of data points included in the fitted range. One can produce serious differences in the magnitude of the derivatives of the polynomials A(R;f) which enter (14), by choosing different ranges of data to fit or by choosing inappropriate polynomial degrees. Details of these difficulties, as they arose, are described in Appendix D, and can be appreciated best by scrutinizing the figures of that Appendix (Figures D.1, D.2, etc.). The end result was to reduce data always in the range $0 < x < 10$ cm and to use a 7th degree polynomial in that interval.

Figures 49 through 51 present typical results comparing data points on the variation of A(R;f) vs. R (in this case, A(x;f) vs. x) with the polynomial chosen to represent each case. With few exceptions the fidelity of representation is very good. Here care must be exercised not to compare amplitudes at different p_o or wall surface conditions since two different hot-wire probes were used. Although the solid curves cannot be taken seriously at the very extremes of the range (e.g. at $x < 1$ cm, $x > 9$ cm) it is already clear from these figures that the disturbance magnitudes tend to increase greatly in the downstream direction beginning at an x which appears dependent on p_o, even though the range $0 < x < 10$ cm is almost always in the laminar regime. Figure 52 is a copy of the CRT screen display made during the curve-fitting process and is included to illustrate the ease with which the operator could examine the validity of the curve-fits.

The amplification-rate findings are exposed here in a number of ways:

the "relief" plots of Figures 53 through 55, frequency-dependence plots of Figures 56 and 57, Reynolds-dependence plots of Figures 58 and 59, and finally Figure 60 which attempts to extract the smooth vs. rough effect.

To those familiar with stability theory, the relief plots of Figures 53 through 55 afford a convenient means of judging the amplification rate results. There are, in essence, three main features worthy of note: first, an up-down-running ridge which is sometimes nearly vertical (e.g. p_o = 475 torr, smooth wall) or inclined (p_o = 600 torr, rough wall) in a way reminiscent of the classic first-mode unstable region at low speeds. Second, there is a weak evidence of a small amplification region at low F and low R, which occasionally blends with the "principal" unstable region just mentioned. Third, there is a consistent and prominent onset of amplification at "large" R which actually dominates the picture. Note that this latter feature, marked by a minimum (trough) in the amplification rates, always lies considerably upstream of the first departure point, marked on Figures 53 - 55 by a vertical dashed line (the abscissa on the figures is $R \sim x^{1/2}$, obscuring the actual wetted-length of plate dominated by this feature, which length is typically one-half of the distance from the L.E. to the first departure).

Considerable scrutiny of Figures 53-60 is required before the principal lessons taught by them are stated; first, however, we present on Figures 60 and 61 the stability diagrams for the smooth and rough walls in the familiar R-F coordinates. As the symbol key explains, these figures show the points on the F-R plane where $\alpha_i = 0$ (the neutral branches) with a distinction of the "lower" and "upper" branch ($-\alpha_i$ increasing or decreasing through zero, respectively). Dots and crosses identify points of minima and maxima in $-\alpha_i$, respectively; note that a maximum in $-\alpha_i$ may not necessarily lie in an amplified region, and a minimum may not necessarily lie in a damped region.

That is, one can have "hilltops submerged under the sea" and "canyon bottoms on dry land." The value of this presentation is that the imminence of a stable region in the F-R plane can be signalled by a minimum in $-\alpha_i$ (the dots) long before a neutral branch appears. For example at $p_o = 350$ for the smooth-wall (Figure 61) the lower neutral branch at $R \simeq 250$ is signaled first by the trough in $-\alpha_i$ occurring near $R = 150$, and the second amplified region starting at $R \simeq 450$ is signaled first by the trough around $R = 400$.

It is crucial to understand that the R range shown on Figures 61 and 62 covers the region before the first departure, i.e. it represents entirely laminar, self-similar flow. The apparent clutter of points includes scatter, as usual, and probably some instrumentation problems at large F, at the very tops of the figures.

At $p_o = 600$ torr it is clear that the data clutter becomes so pronounced that it is impossible to detect amplified on damped regions with any certainty. This phenomenon occurs for both the smooth and the rough wall. It will be recalled that at this pressure the boundary layer on the sidewalls was completely turbulent. The problem with the 600 torr data has therefore been tentatively ascribed to the increased disturbance level in the stream and, in the main, these data will be excluded from further discussion.

6.3.4. The First Unstable Mode for the Smooth Wall

We will now attempt to identify and discuss specific features of the amplification rate and stability diagram results shown on Figures 53-62, limiting our comments to the smooth wall unless otherwise specified.

Figure 61 shows an unstable region in the lower center of the stability diagram. The neutral branches, replotted on Figure 63, are seen to be independent of unit Reynolds number. Also plotted on the latter figure are the $M_e = 2.2$ data of Laufer and Vrebalovich. In their paper (Reference 5) the

latter had compared their results with early numerical results by Mack (Reference 13) and found good qualitative agreement regarding the general location of this unstable region and excellent quantitative agreement with theory as regards to the location of the upper branch. Theoretically, this so-called first instability mode predicted by theory and found experimentally by Laufer and Vrebalovich does not shift greatly in the F-R plane as M_e changes from 2.2 to 3; since numerical predictions for this mode at $M_e = 3$ are not sufficiently in existence from comparison, the similarity with the $M_e = 2.2$ data on Figure 63 prompt the statement that the present data plotted in that figure represent the first instability mode.

An improvement over earlier measurements is noted in that the minimum critical Re_θ ($\sim$190) and maximum "amplified frequency" F ($\sim$ 0.000225) are quite clearly defined. Two fundamental features of the present data deserve attention, however. One is the shortness of the upper branch which appears to stop at $Re_\theta = 300$, $F = 0.00013$, thereafter "merging" with the lower neutral branch of a second unstable region (consult Figure 61) to be discussed shortly. Another is the presence of amplification at low frequencies; below $F = 0.0001$ the present data show amplification at all F beyond about $Re_\theta = 180$ whereas theory and Laufer's tests indicate stability, i.e. damping, at very low F. As already mentioned, this low-frequency amplification had already been encountered at $M_e = 3$ by Kendall, reportedly in an extreme form of disturbance growth at all Re_θ. It is not yet clear whether this phenomenon is an aberration common to wind-tunnel flows or a true feature of stability.

6.3.5. The First-Mode Amplification Rates

Figures 56 and 58 show typical amplification rates and Figures 64-65 show typical amplification spectra; use of R in the abscissa removes the need to

choose between nominal and actual Re_θ. The striking feature of Figures 56-58 is the large rates observed near the leading edge when p_o = 600 torr, which bears on the discussion just concluded regarding low-frequency amplification. The examples in the figures show that at p_o = 600 torr, $-\alpha_i$ is very large near the plate leading edge. This would indicate an increased efficiency of the leading edge region as a conduit and cultivator of spurious noise into the boundary layer, when the latter is irradiated by external disturbances.

An attempt has been made in Figure 66 to compare the measured amplification rates with theory. The only numerical amplification rate results available for the first, three-dimensional mode at Mach 3 are due to L. Mack,* and they are shown on Figure 66 also. The computation pertains to oblique waves in the range $55^\circ < \psi^\circ < 65^\circ$, for which the rates are presumably the highest. At the lower R (e.g. R = 300) the present data are obviously influenced by the low-frequency gain phenomenon, while at higher R (e.g. R = 500) there is an apparent influence of other amplification mechanisms, to be discussed later. Otherwise, however, the data of Figure 66 are not far from the theory, thus justifying their identification with the first mode.

The practice of plotting neutral branches alone does not yield the maximum information on stable and unstable regions. Additional knowledge can be gained from other topographical features of the stability diagram by including the extrema in the amplification rates (the "ridge tops" and "canyon bottoms"). A case in point is Figure 67 where the maxima in $-\alpha_i$ (the maxima found in Figure 61 for example) are shown. The fact that such maxima usually run down the middle of unstable regions is confirmed by the cluster of points "down the middle" of the unstable region. The Figure also shows the topographical relation among this maximum amplification line, the maximum

---

* The author is indebted to Mr. Mack for these unpublished computations.

amplitude line (see Figure 47) and the neutral branches; it also finds little differences between use of the actual and nominal Re_θ.

The important feature of Figure 67 is that the p_o = 600 torr data (Re′ = 56100/cm), despite scatter, are also well represented along the line of maximum $-\alpha_i$. Thus, whereas neutral branches at this Re′ are hard to discern (see Figure 61), a strong hint toward the presence of the first mode is afforded by this type of plot even in this case of the boundary layer irradiated by stream noise.

6.3.6. Effect of Roughness, Turbulence and Unit Reynolds No. on the First Mode

Reviewing the effect of unit Reynolds number Re′ on the first mode, we realize that we can at best study this effect by comparing the Re′ = 29400/cm and 43900/cm data; use of the 56100/cm data is questionable because the latter also includes the stream-irradiation effect (the "turbulence"). Within this context, we have seen that Re′ changes do not affect the location of the unstable region on the stability diagram. There appears to be, however, an effect on the amplification rates. From Figures 64 and 65 we see that the higher Re′ data are more damped especially at low R or Re_θ. This must be connected with the observed effect of Re′ on transition (Figure 16).

For this particular experiment it appears that noise irradiation increases the "noise" of the measurement, causes amplification near the leading edge at practically all frequencies and obscures the neutral branch location. The end effect, however, is not to aid and abet the first mode in accelerating the transition process; the transition data of Figure 16 do not show any abrupt changes of behavior when sidewall radiation sets in. Furthermore, the stream disturbance levels of Figure 32 show only a moderate increase in level when sidewall radiation arrives at the point of measurement.

By contrast, the data of Beckwith and Kendall (Reference 24) show a much larger stream noise increase upon irradiation, accompanied by markedly earlier transition. At this point, therefore, the stream noise effect in the present test appears much more benign than expected.

The rough wall results are much less conclusive than Figure 62 indicates. Since the roughened surface did not start until 3 cm from the leading edge (R $\simeq$300 at p_o = 350 torr), one is at a loss to explain the unstable region shown on Figure 62. The same puzzlement can be expressed regarding the elevated amplification rates over the rough wall at low R, as per the amplification spectra of Figures 64 and 65. Discussion of the effect of roughness on instability will therefore be postponed until further data are discussed later.

6.3.7. The Second Instability Region

It is evident from the overall stability diagrams of Figures 61 and 62 that a second amplification region exists to the right of the first mode described in the previous section. We will refer to this additional region of amplification as the "second instability mode" partly for distinguishing it from the first mode results, and partly because of evidence of its connection to the second mode of instability in hydrodynamic theory.

Evidence of the second mode, as R increases, first appears as the locus of minima in $-\alpha_i$ located nearly vertically in Figures 61 and 62 at R$\simeq$400, followed by a lower neutral branch in the region 450 < R < 550. The latter branch has been for clarity replotted on Figure 68 (and also on Figure 69 for the rough wall). It is seen that this amplification phenomenon considerably precedes the first departure, that it "intercepts" the upper neutral branch of the first mode, that it extends to high frequencies (of order F = 0.0004) and that it is strongly Reynolds-number dependent.

Typical amplitude and amplification data, which generated the stability-diagram plots of Figure 61, are shown on Figures 70 through 73. The amplitudes A(f) shown on Figure 70 for typical cases at p_o = 350 and 475 torr are especially illuminating because they show the relative insignificance of the first compared to the second mode. The former creates a rather minor disturbance in the evolution of fluctuations along the plate, while the latter involves a pronounced increase in the signal. Note that the wetted length of plate over which the second mode is active in the self-similar laminar region is quite long. For example, Figure 70 shows that for F = 0.000207 the first mode activity lies between R = 260 and 330, roughly, corresponding to Δx = 1.4 cm at p_o = 350 torr; while the second mode is active from R = 460 and is still so at the first departure (R $\simeq$ 600), for an "active length" Δx = 5 cm. When p_o = 475 torr, from Figure 70 we get Δx = 2.6 cm for the region of first mode activity in 300 < R < 450, and Δx = 3 cm for the second mode activity region in 525 < R < 640. Similar plots, stressing the relative extent of the two modes in the physical coordinate x along the plate are shown on Figures 71-73. The top plot of each figure is one of amplitude and the bottom two of amplification. The two "bulges" in the latter are the two instability modes under discussion. The predominance of the second mode over the first is evident even for F as low as 0.000056. Note, too, that the second mode becomes more prominent as F increases. For example at F = 0.00021 which is near the highest amplified frequency for the first mode, considerable amplification of the natural disturbances due to the second mode alone occurs in the range 7 < x < 12 cm when $Re' = 29400/cm$. It is also evident that at very low frequencies, say F < 0.00005, the two modes merge and amplification (starting at an unexpectedly early point, as already discussed) continues uninterruptedly throughout the self-similar region since the second mode "sets

in" before the first mode is done with amplification. This merging process makes it difficult to discuss any further the topography of the second mode at the low frequencies, a topic which will be left aside until total amplification is discussed later.

According to the figures shown so far, the amplification rates for the second mode appear to be much higher than those of the first mode, especially at large F and R. To show numerical results, the amplification spectra of Figures 64, 65, etc. have been extended by plotting on Figures 74 to 77 such spectra to R = 600. For these plots, the computations were made using Option 11 in the program STABLE02 (see Appendix C) but, in contrast to the first mode presentations of Figures 64, 65, etc., the curve-fitted data extended to x = 15 cm (for Figures 64, 65, etc. the range extended only to 10 cm, which is where the second mode becomes most active and might have, therefore, missed or misrepresented the second-mode results).

Figures 74 through 77 show the second-mode amplification spectra $-\alpha_i$ vs. F in plots similar to those of Figures 64, 65, etc. The frequency range extends to F = Q0004 and the R values displayed are R = 300, 400, 500 and 600. These ranges again display some of the amplification-spectrum results shown earlier but in a way which now allows a good comparison between the two modes, and also of the individual mode behavior along the plate. If, for the moment, we concentrate on the smooth wall results (Figures 74 and 75) we note the ease with which the first mode shift toward the lower frequencies can be followed as R increases. Maximum rates for this mode reach about 0.005. The second mode appears to set in almost abruptly at $R \simeq 450$ and to involve maximum rates of order 0.012. Therefore, the second mode predominates at locations on the model just preceding the first departure (transition), and involves much higher amplifications than ever attained by the first mode. On occasion (e.g.

Figure 75 at R = 600 for $Re' = 43900/cm$, which occurs just before the first departure) the first mode even appears as a minor superposition on the second mode spectrum. This is very significant because it implies that the second mode activity extends to low frequencies (lower than F = 0.0001) where, as we shall later see, one must look for the causes of transition. In other words, the second mode may here be at the least a participant in, if not the cause of, transition.

A final point concerns the chosen "first mode" and "second mode" terminology. In the context of stability theory modes are specific "groups" of eigenvalue solutions of the small disturbance equations which can coexist at a certain R with different amplification behavior; furthermore, at the same R the amplification spectrum ($-\alpha_i$, F) of a mode can depend on the disturbance wavefront orientation relative to the flow vector. It is experimentally difficult to attribute an observed disturbance amplification to the action of any particular mode, although sometimes the observed amplification spectra can be decomposed into individual mode contributions. A familiar case in point is the plot on Figure 77, taken from Reference 9, showing amplification spectra for $M_e = 6.8$ to 7.7 and $R \simeq 1740$. For reasons clear from this plot, the community has interpreted the data shown on it as a superposition of two theoretical instability modes, a three-dimensional one with orientation $\psi = 55^\circ$ and a two-dimensional one with $\psi = 0^\circ$. Based on obvious similarities between this plot and the present amplification spectra from Figures 74 through 77, it is evident that the latter also shows the merging of two different modes, shown by single or double arrows and called "first" and "second" respectively. From what has been shown, it is also evident that the use of the word "first" (for "first 3-D") is justified, but

we know little at this point on whether the second mode is two- or three-dimensional.*

6.3.8. The Character and Mach-Number Dependence of the Instability

It is seen from the previous discussion that the unstable region found is rather complex, consisting of two merged instability modes which provide two separate peaks in the amplification spectra. At lower R (say $R < 400$) these two modes are separated by a damped region which disappears when R increases.

As was already indicated by the example of Figure 77, this type of mixed-mode or merged-mode instability is common at hypersonic Mach numbers. The experiments of this author (References 6, 7 and 8) and of Stetson et al. (Reference 9) show the existence of a large region of instability in the range $1000 < R < 2000$ in which the first and second modes co-exist.** The present day experimental knowledge of the Mach number dependence of the stability diagram, typified by the present data and those of References 3, 5, 8 and 9 is pictured on Figures 78 and 79. The interesting feature here is that the "second mode" lower neutral branch claimed by the present data appears to form the natural extension of the hypersonic results (at present limited to $R > 1000$) at the lower Reynolds numbers.

---

*There are, strictly speaking, several possibilities for second mode mechanisms including some not related to Tollmien-Schlichting phenomena such as three-dimensional or Taylor-Goertler instabilities. There may also be tunnel-peculiar phenomena, such as finite-span problems wherein instabilities generated by three-dimensionalities at the plate-sidewall intersection propagate to the plate centerline.

**The authors of these references found additional unstable regions, consisting of "higher harmonics" of the main instability under discussion here.

This opinion is reinforced by Figure 79 where the abscissa is the Reynolds number based on the kinematic thickness of the boundary layer. This plot was motivated by Laufer's original observation that such scaling brings the neutral-branch data of References 3 and 5 into coincidence. To extend this test to the present data, the latter were converted from R-values to Re_δ values using the measured thickness δ . The hypersonic results were converted to the coordinate Re by using this author's measured relation (see Reference 8, Figure 3) between Re_δ and R:

$$Re_\delta \simeq 12R$$

Figure 79 thus shows the neutral branch location, on the F-Re_δ plane, of the instabilities most likely to be experimentally detected over a wide range of M_e. Of course, observability is mainly a question of amplification rate; low-speed measurements cannot discern the "hypersonic" instability because the latter has no amplification (is not present) at low M_e.

6.3.9. Roughness and Reynolds Number Effects on the Second Mode

It has already been mentioned that the lower neutral branch of the second mode is Reynolds-number sensitive. The results of Figure 68 supporting this claim pertain to the smooth wall, and in this case the effect is a systematic shift of the neutral curve toward larger R as Re′ increases. It is worth repeating here that this constitutes a possible explanation of the unit Reynolds number effect on transition.

The corresponding effect of Re′ for the rough wall gives the surprising results of Figure 69. Increasing Re′ in this case changes completely the character of the lower neutral branch, from one with positive slope in the F, R plane when Re′ = 29400/cm, to one with negative slope when Re′ = 43900/cm. No explanation is available at this stage, and no definite conclusions were

therefore pursued about the effect of Re′ when the wall was rough.

6.4. Boundary-Layer Response and the Transition Question

While the presentation and discussion of the data have so far dealt with details of the small disturbance development along the laminar boundary layer, we are ultimately interested in the cumulative effect of amplification or damping and in the total amplification experienced by each wave number between entry into the boundary layer and arrival at the first departure zone. This net cumulative effect, presently termed the "boundary layer response", associates the total "gain" experienced by each wave number with its likelihood of triggering transition, the presumption being that those disturbances displaying the maximum total gain before the first departure are responsible for causing the transition phenomenon. Typical targets for such gain computations would be to find a net factor by which a disturbance must increase before causing transition or even an absolute disturbance magnitude needed to cause transition.

The disturbance amplitude gain within the boundary layer can be discussed with the aid of Figure 80. The line of constant y/δ along which data were obtained can be roughly approximated with a "disturbance track" originating at a point $x = x_o$ (entrainment point) on the layer edge, close to the plate leading edge, where small convected or radiated stream disturbances enter the boundary layer. Comparison of the disturbance amplitude at any point on this track with its "entry" amplitude at x_o will give the cumulative effect of boundary layer instability on the disturbance up to that point; thus the gain up to a certain point $R \sim x^{1/2}$ for a Fourier component F is simply the "spectrum ratio" $A(R;F)$ to $A(R_o;F)$:

$$G(R;F) \equiv \frac{A(R;F)}{A(R_o;F)} \quad ; \; R_o \equiv R(x=x_o) \tag{16}$$

Since the entrainment point is difficult to fix or define, gain calculations for the present data were made by picking, for x_o, a point x_i near the most forward probe position; for convenience, the x_i was chosen so that $R_o = 150$ always (this gave $x_i = 0.8$ cm for $Re' = 29400/cm$ and 0.8 cm for $Re' = 43900/cm$). Results are shown on Figures 81 and 82. As has been increasingly evident in this report, the disturbances have gained little in amplitude between the leading edge and R = 450. For the smooth wall at $Re' = 43900/cm$ all disturbances have in fact experienced net damping, up until R = 450 (Figure 81). The disturbance amplitude gain seems to be large only when the second mode becomes active, in the interval between $R \simeq 450$ and the first departure. Figures 81 and 82 show that the maximum gain at the first departure is of order 2.5 to 3 and is confined to the low frequencies ($F \sim 0.00005$). This result is of course obvious even at the early stages of this narrative during discussion of the amplitude histories (Section 6.3.3 and Figures 49, 50, etc.).

The factor of 3 is too small to be a credible mechanism for initiating transition in the boundary layer. It must be observed from the data shown so far that the disturbance magnitude at the beginning of the process (i.e. near x_o or x_i, that is near the leading edge) is already substantial compared to the stream disturbance level. Previous observations (Reference 12) have already shown that much larger gain factors obtain when the disturbance magnitudes just before transition are compared with the stream disturbance level A_e, which must be correctly considered to be the "initial" disturbance magnitude. Mack (Reference 14) has formulated a "forcing" variant of stability theory which accounts for the boundary layer stability together with the stream noise environment. At a Mach number of 4.5, Kendall has qualitatively verified the forcing theory and found gains A/A_e just before

transition which amount to factors 10-100 depending on frequency.

To investigate the total gain in the boundary layer of a disturbance which starts out with a magnitude $A_e(F)$ in the stream, we present the spectra $A(F)/A_e(F)$ of Figures 83 and 84. The gain intrinsic to the boundary layer, just discussed above, can be seen in these Figures as the difference between A/A_e at, say, R = 200 and the first departure R ($R \gtrsim 600$ for smooth wall). For example, for the smooth wall at $Re' = 29400/cm$ the gain at R = 229, F = 0.00005 is about 5 and at R = 592 it is 15, giving the factor 3 previously discussed. The principal message of Figure 83 is that at low R, of order 200 (or of order 150 in the vicinity of x_i, Figure 84) the disturbance magnitude is a factor of as high as 5 larger than that in the stream. Note that the growth is nil or "sluggish" for a certain range of R thereafter. Translating R into x for the typical case of $Re' = 29400/cm$, we can put together the following physical picture of disturbance gain for low F: upon "entering" the layer between the L.E. and x = 1.8 cm (R = 229) the disturbance increases by a factor of 5 in size, and gains an additional factor of 3 or so between x = 1.8 cm and x = 12 cm (R = 592).

This point is further demonstrated in the cross-plot A/A_e vs. R of Figure 84 for F = 0.00005. Qualitatively similar results, plotted on the same Figure, have been reported by Kendall (Reference 12). The latter's data show a slower gain process, with "non-similarity" at $M_e = 3$ and $Re' = 43,000/cm$ indicated at R = 900 vs. our own first departure point around R = 600. For this reason Kendall's final gain before transition seems to be $A/A_e = 25$ at this F, while ours is about 15. In other words, Kendall's finding says that transition begins around 19 cm, after the disturbance magnitude has increased 25-fold, while we find it occurring at 12 cm following a 15-fold increase. This difference might be attributed to differences between the two wind-

tunnels, although in both cases there was no irradiation from turbulent sidewall boundary layers. On the other hand, there may be other, simpler explanations dealing with interpretation of the measurements. For instance, it is not clear from Kendall's article that his "non-similarity" corresponds to our "first departure." More important, in both cases the changes in hot-wire sensitivity and frequency response are not really accounted for in measuring A and A_e; strictly speaking, therefore, all data on Figure 84 are qualitative. Finally, whereas our A_e was measured just over the plate boundary layer, Kendall himself cautions that his A_e was measured ahead of the plate and thus is probably overestimated; in comparing his data with theory he increases his A/A_e by a factor of 2 for comparison purposes (Reference 12, p. 245). If the solid curve is also increased by 2 on Figure 84, then Kendall's and the present data come into much better agreement.

No theoretical results from Mack's combined forcing-and-stability theory are available for $M_e = 3$, but a comparison of the present data with his theory (quoted by Kendall, Reference 12, p. 295) at $M_e = 4.5$ is also shown on Figure 84, as a matter of some interest.

Conclusions

Based on the results obtained from the present measurements, the following conclusions can be drawn for the flat-plate boundary layer at Mach 3:

1. An unstable region has been found which has been identified with the first unstable mode. Supporting evidence consists of the shape and location of this region on the stability diagram and the agreement of its amplification rates with the available theoretical expectations. Minimum critical Re_θ for this region is 190 and maximum amplified frequency is F =

0.000225, independently of unit Reynolds number.

2. An extensive second unstable region was also found with amplification rates much larger than those of the first mode, extending to frequencies higher than F = 0.00035 and strongly dependent on unit Reynolds number. This region separates from the first-mode at low R, merges with the latter at high R and appears to connect with, and forms the low-R terminus of, the merged first- and second-mode instability found earlier at high Mach numbers. For this reason, this second unstable region has been associated with the second instability mode.
3. The net gain in disturbance amplitude from the free stream to the first departure is about 15 and is confined to a frequency band centered near F = 0.00005. Of this gain, a factor of about 3 is due to the detected boundary layer instabilities and is almost entirely due to the second mode; the remaining factor of 5 is experienced very near the leading edge of the plate.
4. Transition delay, expressed as an increased Re_θ of transition as the unit Reynolds number increases, seems to be caused mostly by a shift to higher Reynolds number of the second unstable mode and much less so by decreases in the first-mode amplification rates as the unit Reynolds number increases.
5. When computed with the stream rather than the phase velocity, the maximum-amplitude waves ("laminar waves" or "Tollmien-Schlichting waves") of the first mode had a length of about 30δ in agreement with the previous stability data for $M_e < 3$; by contrast the second-mode wavelengths, reported so far only at hypersonic speeds, have a primary wavelength of about 2δ.
6. The effect of sound irradiation from turbulent sidewall boundary layers

was a doubling of the stream fluctuations without any discernible effect on transition on the model. In the boundary layer such irradiation caused large increases in the amplification rates near the leading edge, and scatter of data which tended to obscure the first mode, but left the second mode largely unaffected.

7. A clearly recognizeable effect of the surface roughness was to make the layer more selective, i.e. to produce peaks in the fluctuation spectra. Otherwise, peculiar behavior observed of the boundary layer stability with roughness, and its connection to the observed earlier transition has been left uninterpreted because of the unique (non-generalizable) nature of the roughness.

REFERENCES

1. Reshotko E. and Leventhal L.: "Disturbances in a Laminar Boundary-Layer Due to Distributed Surface Roughness," AIAA Paper No. 81-1224, Palo Alto, CA, June 1981.

2. Kendall J.M. Jr.: "Laminar Boundary Layer Velocity Distortion by Surface Roughness: Effect Upon Stability," AIAA Paper No. 81-0195, St. Louis, MO, January 1981.

3. Schubauer G.B. and Skramstad H.K.: "Laminar Boundary Layer Oscillations and Transition on a Flat Plate," NACA TR 909, Washington, DC, 1948.

4. Strazisar A.J., Prahl J.M. and Reshotko E.: "Experimental Study of the Stability of Heated Laminar Boundary Layers in Water," Case Western Reserve University, Dept. of Fluid, Thermal and Aerospace Science, FTAS/TR-75-113, 1975.

5. Laufer J. and Vrebalovitch T.: "Stability and Transition of a Supersonic Laminar Boundary Layer on an Insulated Flat Plate," J. Fluid Mechanics, Vol. 9, No. 2, pp. 257-299, 1960.

6. Demetriades A.: "Hypersonic Viscous Flow Over a Slender Cone, Part III: Laminar Instability and Transition," AIAA Paper No. 74-535, Palo Alto, CA, June 1974.

7. Demetriades A.: "Boundary Layer Instability Observations at Mach No. 7," J. of Applied Mechanics, ASME, Vol. 99, No. 1, pp. 7-10, 1977.

8. Demetriades A.: "New Experiment on Hypersonic Boundary Layer Stability Including Wall Temperature Effects," Heat Transfer and Fluid Mechanics Inst., Stanford University Press, pp. 39-55, 1978.

9. Stetson K.F., Thompson E.R., Donaldson J.C. and Siler L.G.: "Laminar Boundary Layer Stability Experiments on a Cone at Mach 8, Part 1: Sharp Cone," AIAA Paper No. 83-1761, July 1983.

10. Stetson K.F., Thompson E.R., Donaldson J.C. and Siler L.G.: "Laminar Boundary Layer STability Experiments on a Cone at Mach 8, Part 2: Blunt Cone," AIAA Paper No. 84-0006, January 1984.

11. Stetson K.F., Thompson E.R., Donaldson J.C. and Siler L.G.: "Laminar Boundary Layer Stability Experiments on a Cone at Mach 8, Part 3: Sharp Cone at Angle of Attack," AIAA Paper No. 85-0492, January 1985.

12. Kendall J.M. Jr.: "Wind-Tunnel Experiment Relating to Supersonic and Hypersonic Boundary Layer Transition," AIAA J., Vol. 13, No. 3, pp. 290-299, March 1975.

13. Mack L.M.: "Linear Stability Theory and the Problem of Supersonic Boundary Layer Transition," AIAA J., Vol. 13, No. 3, pp. 278-289, March 1975.

14. Mack L.M.: "Review of Linear Compressible Stability Theory," ICASE/NASA Workshop on Stability of Time-Dependent and Spatial Varying Flows, Hampton, VA, 1985.

15. Drummond D., Rogers B. and Demetriades A.: "Design and Operating Characteristics of the Supersonic Wind-Tunnel," MSU TR 81-1, Montana State University, January 1981.

16. D'Sa J.M.: "Characteristics of a Supersonic Laminar Boundary Layer Over a Rough Wall," Thesis, Mech. Engr. Dept., Montana State University, 1982.

17. Demetriades A.: "Roughness Effects on Boundary Layer Transition in a Nozzle Throat," AIAA J., Vol. 19, No. 3, pp. 282-289, March 1981.

18. Feindt E.G.: "Untersuchangen uber die Abhangigkeit des Umschlages Laminar-Turbulent Von Der Oberflachenrauhigkeit and der Druckverteilung," Jahrbuch 1956 der Schiffbautechnischen Gesellschaff, Vol. 50, pp. 180-203, 1957.

19. Schiller L.: Handbook of Experimental Physics, Vol. IV, Part 4, pp. 1-207, Leipzig 1932.

20. Smith A.M.O. and Clutter D.W.: "The Smallest Height of Roughness Capable of Affecting Boundary Layer Transition," J. of Aero Sciences, Vol. 26, No. 4, p. 229, April 1959.

21. Charwat A.F., Roos J.N., Dewey C.F. Jr. and Hitz J.A.: "An Investigation of Separated Flows, Part I: The Pressure Field," J. of Aerospace Sci., Vol. 28, No. 6, p. 457, July 1961.

22. Charwat A.F., Dewey C.F. Jr., Roos J.N. and Hitz J.A.: "An Investigation of Separated Flows, Part II: Flow in the Cavity and Heat Transfer," J. of Aerospace Sci., Vol. 28, No. 7, p. 513, July 1961.

23. Pate S.R.: "Dominance of Radiated Aerodynamic Noise on Boundary Layer Transition in Supersonic-Hypersonic Wind-Tunnels: Theory and Application," Ph.D. Thesis, University of Tennessee, Knoxville, 1977.

24. Beckwith I.E., Creel T.R. Jr., Chen F.J. and Kendall J.M.: "Free Stream Noise and Transition Measurements on a Cone in a Mach 3.5 Pilot Low-Disturbance Tunnel," NASA TP 2180, 1983.

25. Chambre P.L. and Schaaf S.A.: "The Impact Tube," Physical Measurements in Gas Dynamics and Combustion, R.W. Ladenburg, Ed., Princeton University, Princeton, NJ, pp. 111-122, 1954.

26. Kendall, J.M. Jr.: "An Experimental Investigation of Leading-Edge Shock Wave/Boundary Layer Interaction at Mach 5.8," J. of Aerospace Science, Vol. 24, No. 1, p. 47, January 1957.

27. Cohen C.B. and Reshotko E.: "Similar Solutions for the Compressible Laminar Boundary Layer with Heat Transfer and Pressure Gradient," NACA TR 1293, 1956.

28. Schlichting H.: "Boundary Layer Theory," McGraw-Hill Book Co., New York, Seventh Edition, pp. 449-544.

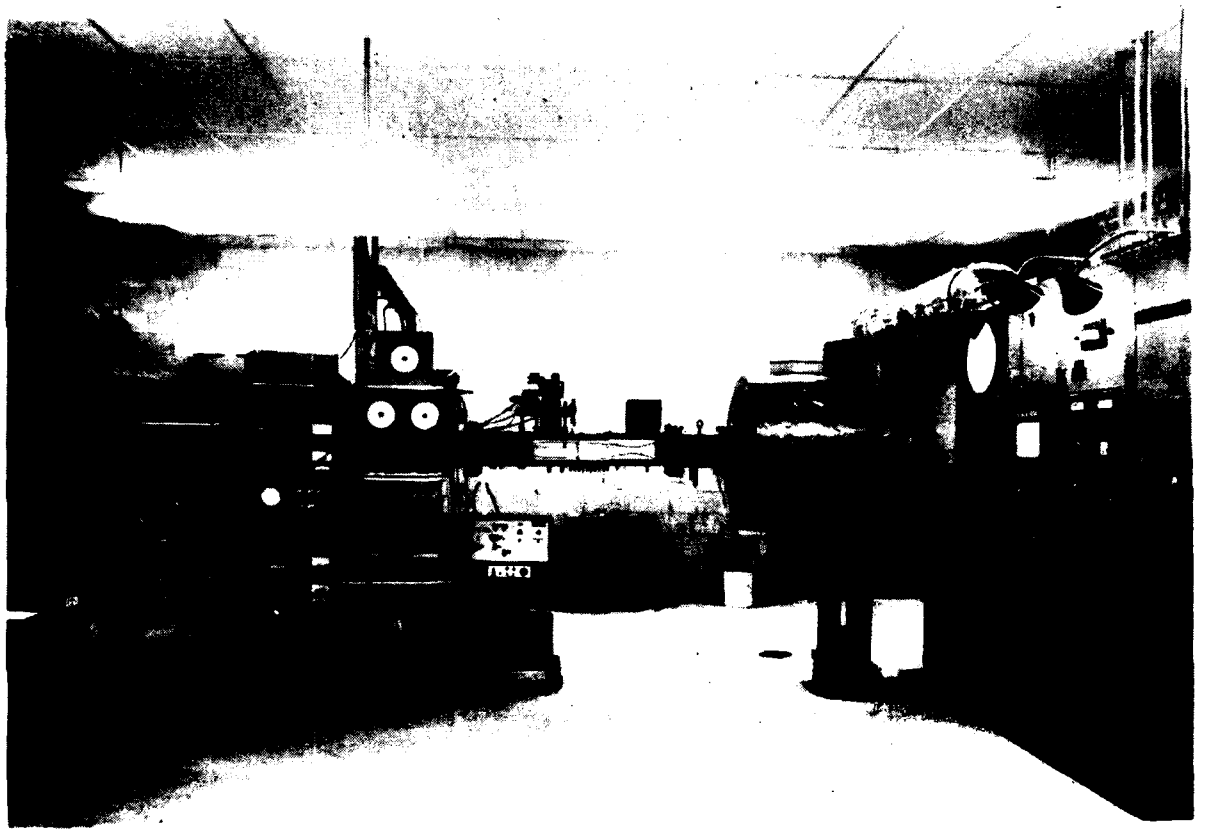

Figure 1. Overview of the Supersonic Wind-Tunnel.

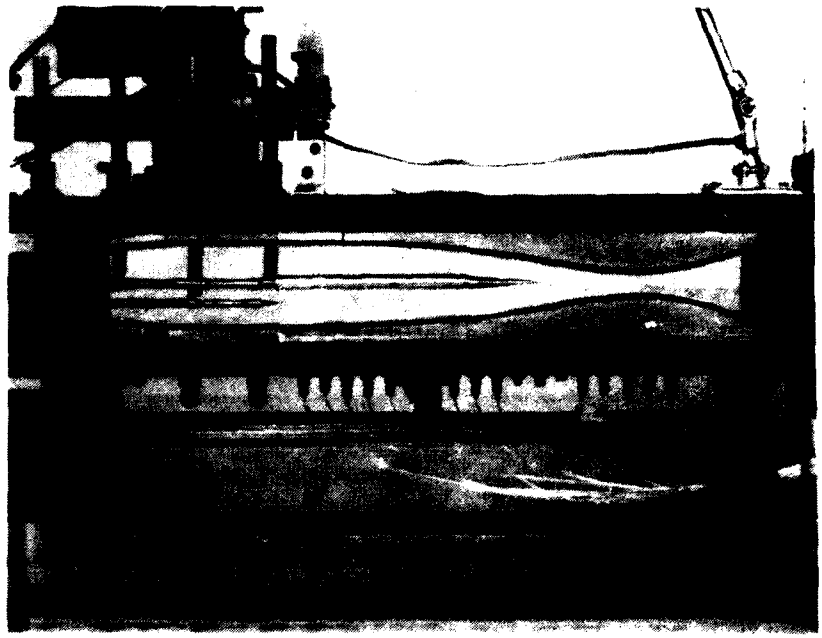

Figure 2. Axisymmetric model installed in the SWT test section.

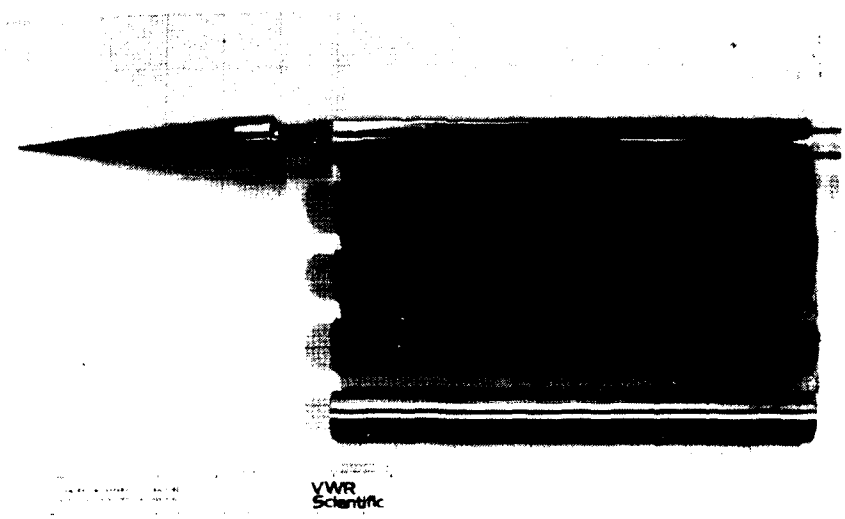

Figure 3. Axisymmetric model, shown disassembled, with a variety of rough surface afterbodies.

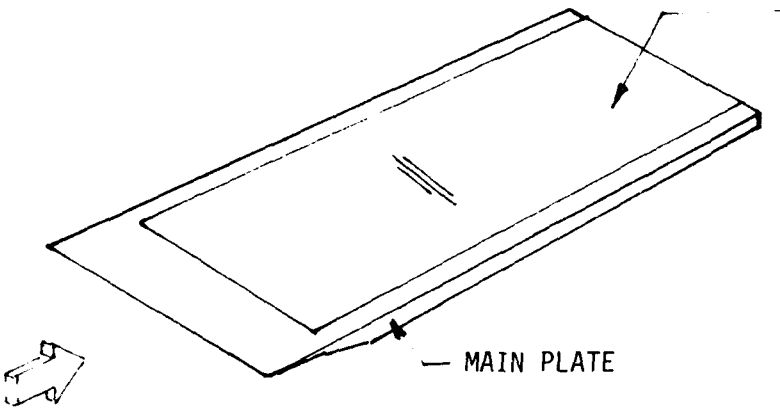

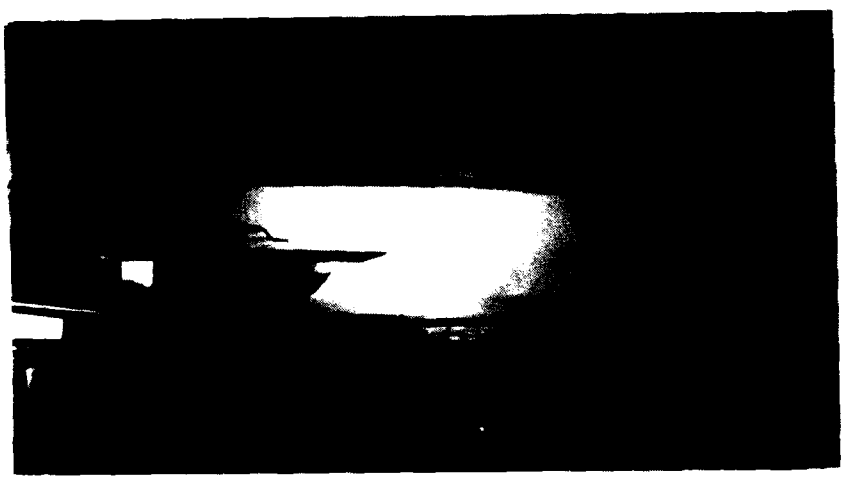

FLAT PLATE MODEL INSTALLED IN MSU SUPERSONIC WIND-TUNNEL (WITH PROBE SHOWN NEAR SURFACE)

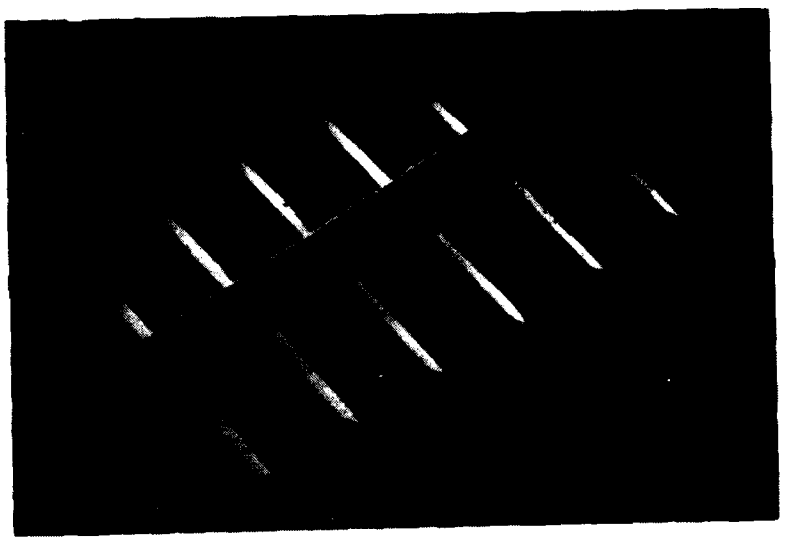

ELECTRON MICROSCOPE PHOTO OF GROOVES (20-MIL TUBE SHOWN FOR REFERENCE).

Figure 4. Flat plate model. The rough surface geometry shown at right was also used in the axisymmetric model. Note static-pressure probe (photo at right) and its orifice location. Dimensions in cm.

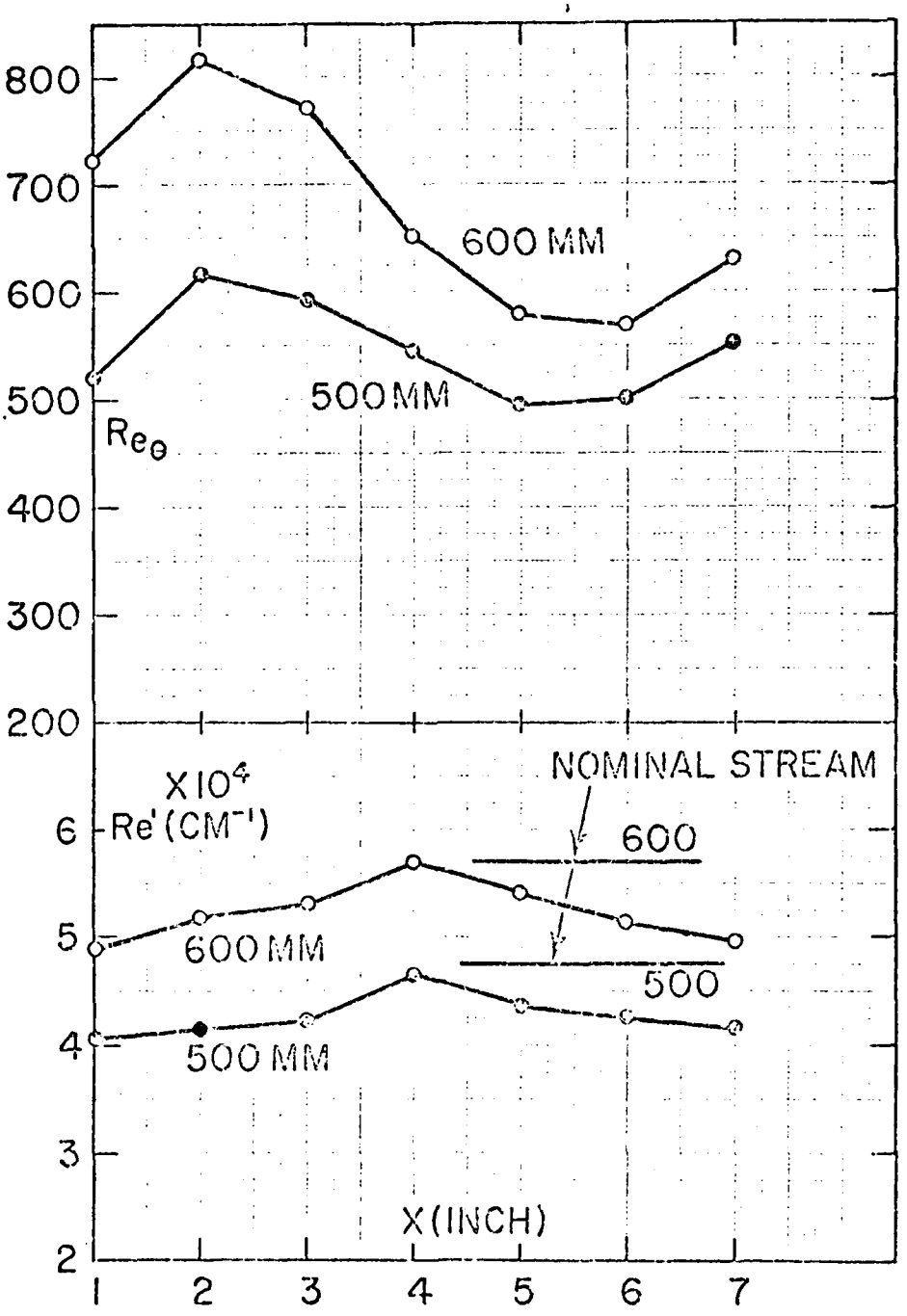

Figure 5. Measured momentum Reynolds number (top) and edge Re' for the axi-symmetric model vs. distance x from model base. (Flow from right to left.)

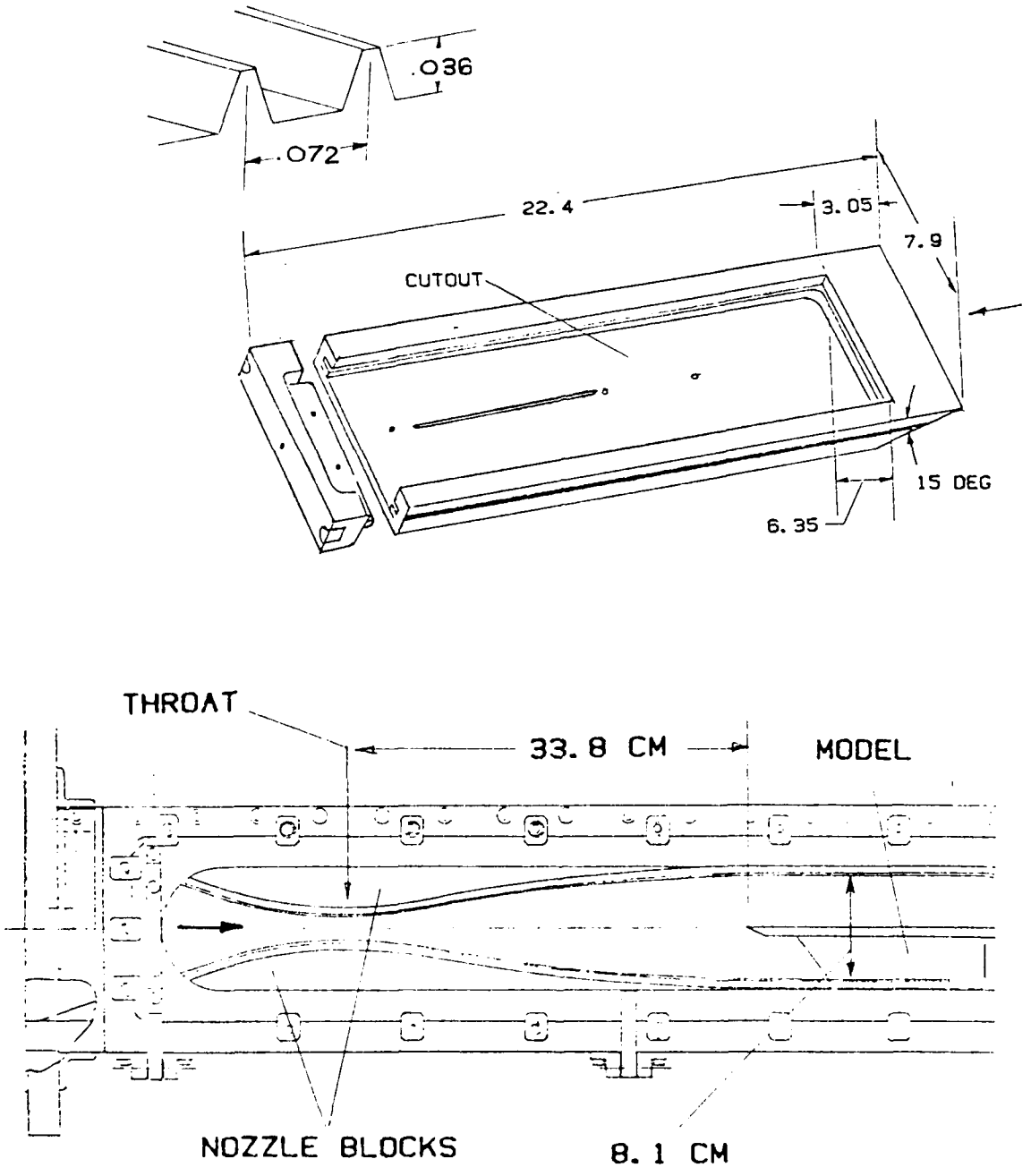

Figure 6. Flat plate geometry (minus surface insert). Dimensions in cm.

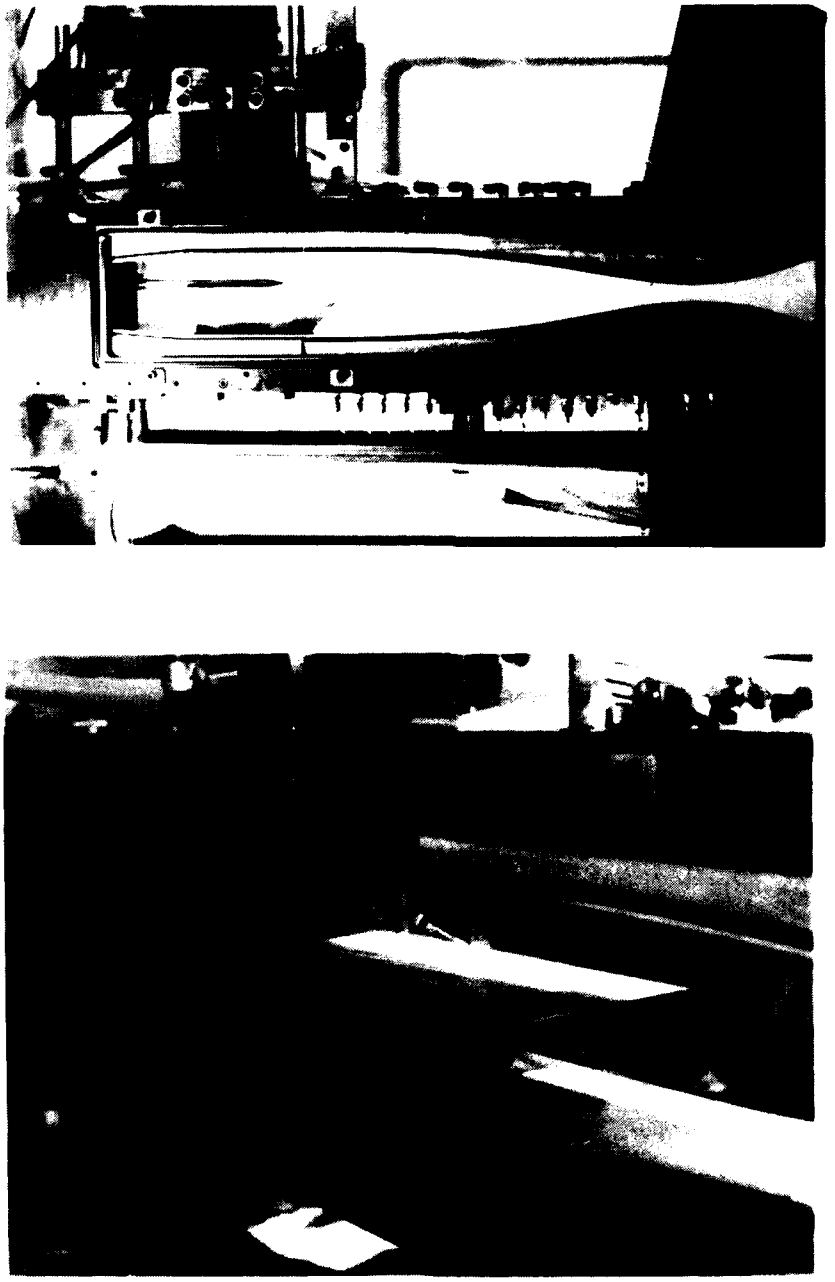

Figure 7. Flat plate model installation in the SWT test section.

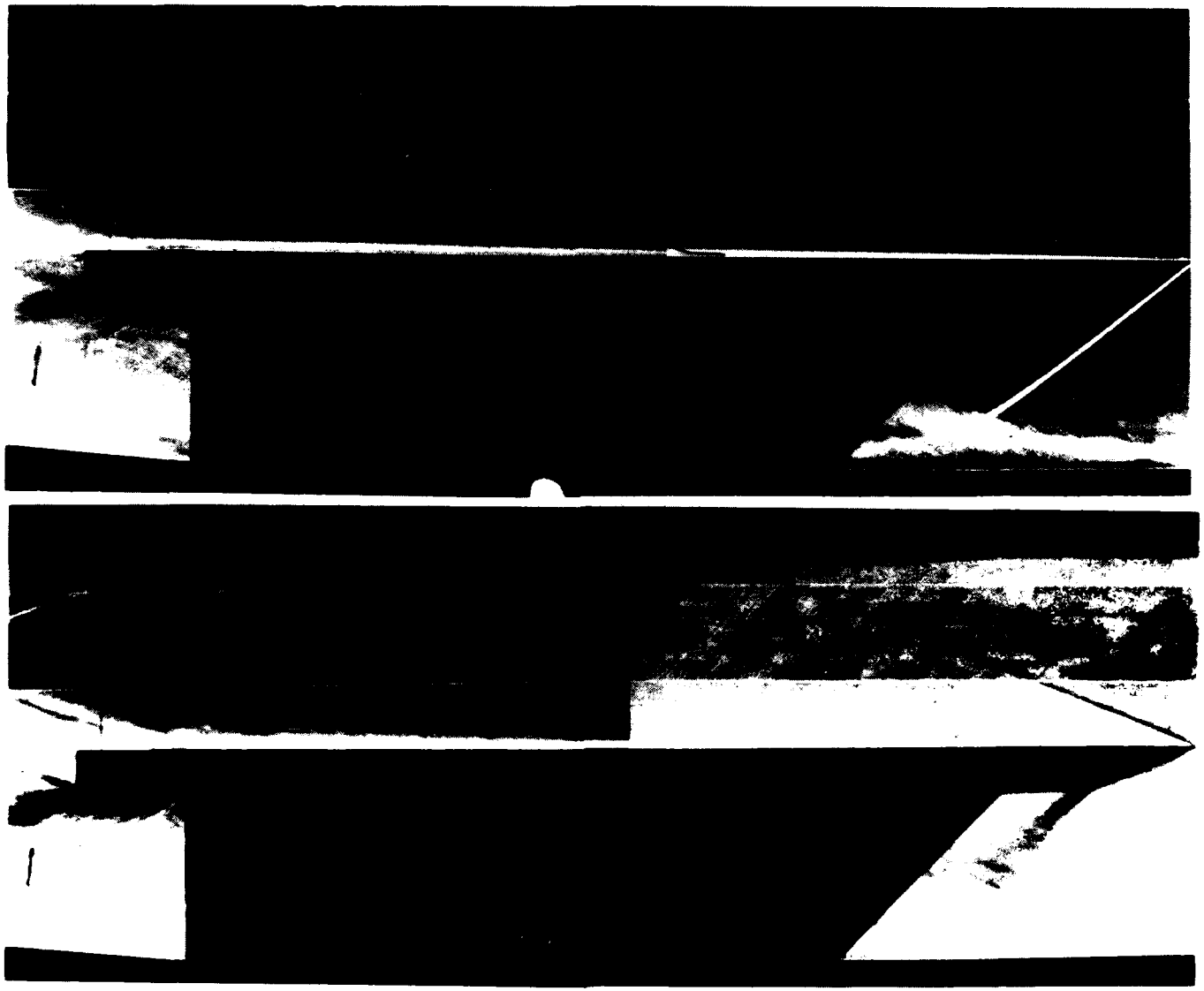

Figure 8. Spark Schlieren photo of boundary layer over smooth wall for 350 torr (top) and 600 torr (bottom).

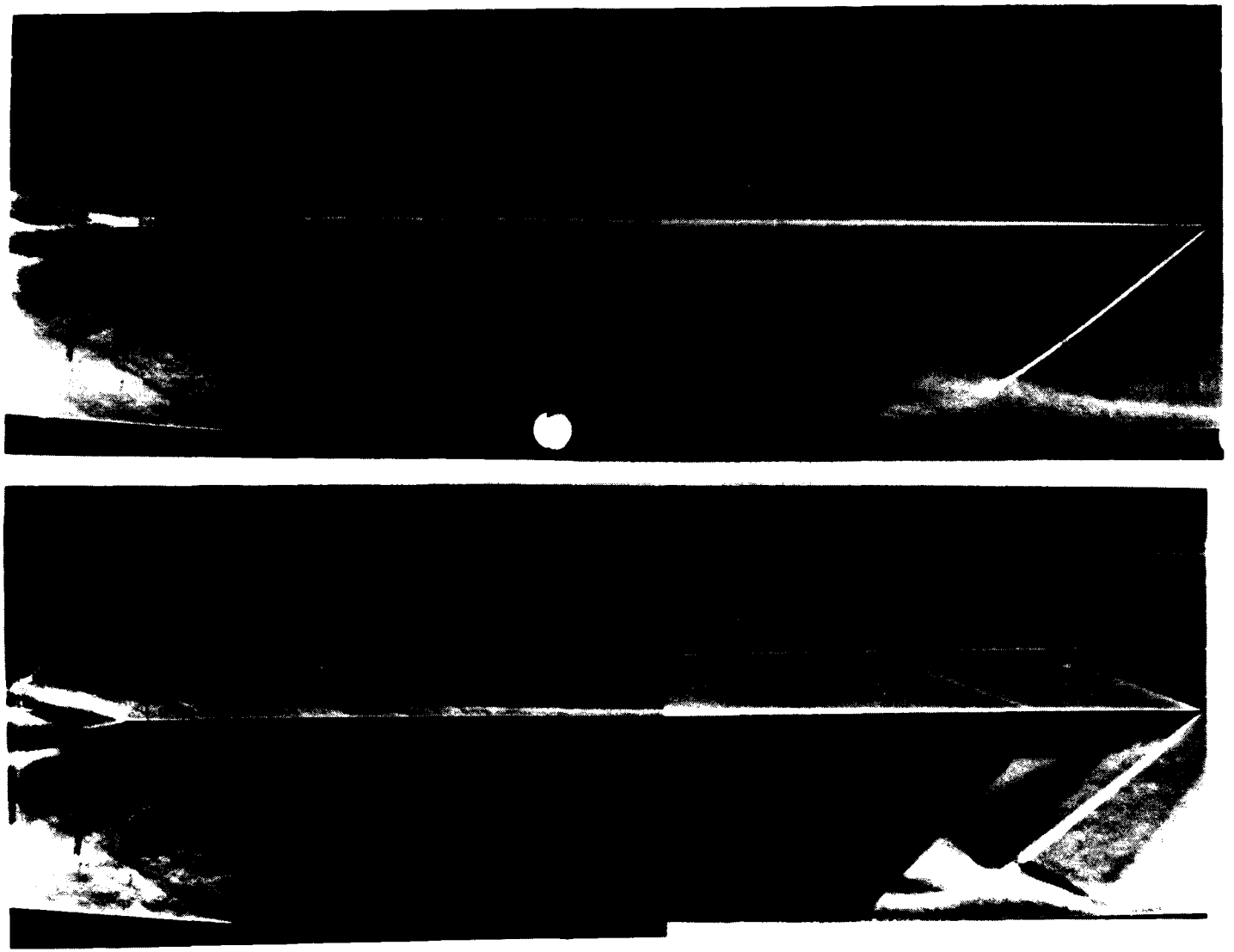

Figure 9. Spark Schlieren photo of boundary layer over rough wall for 350 torr (top) and 600 torr (bottom).

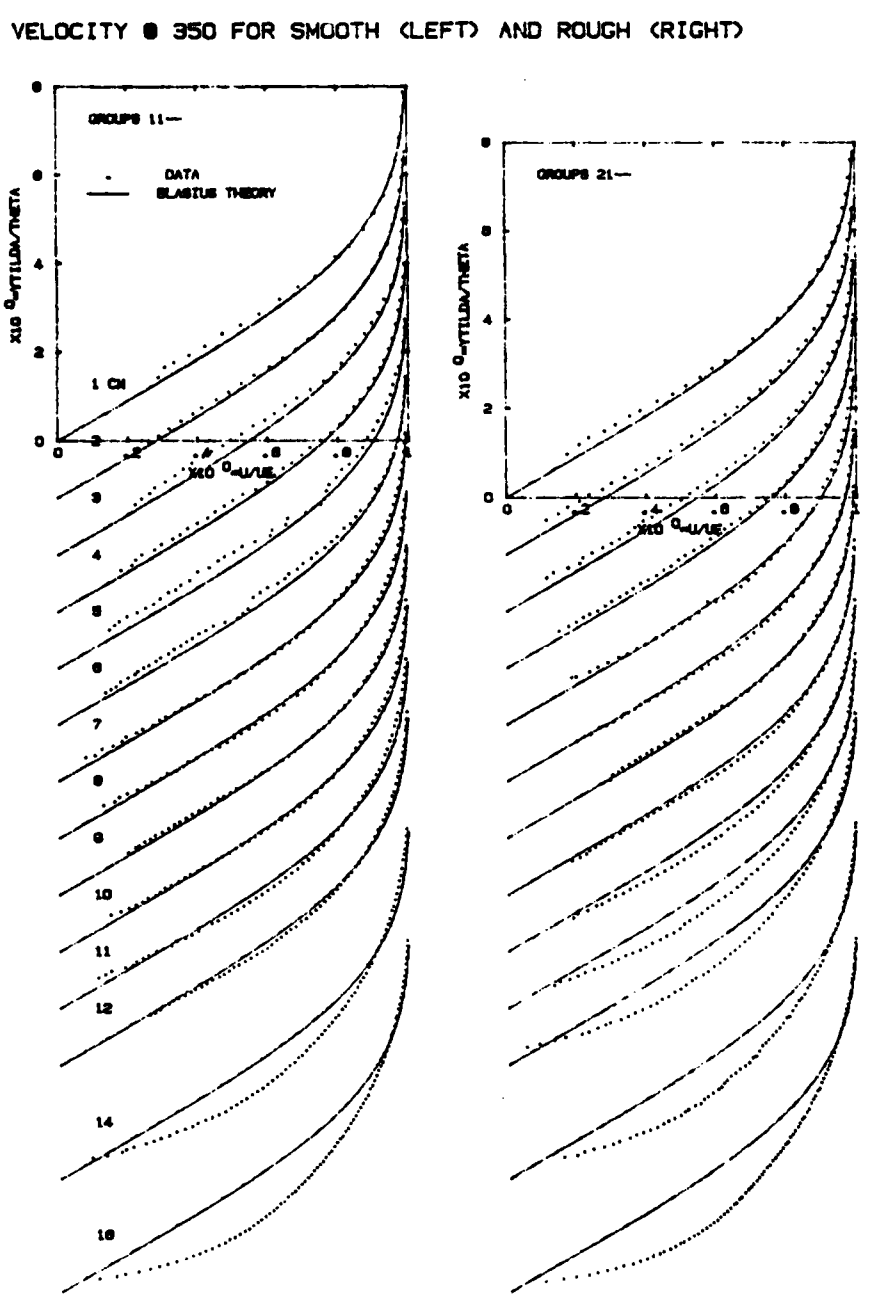

Figure 10. Velocity profiles at 350 torr.

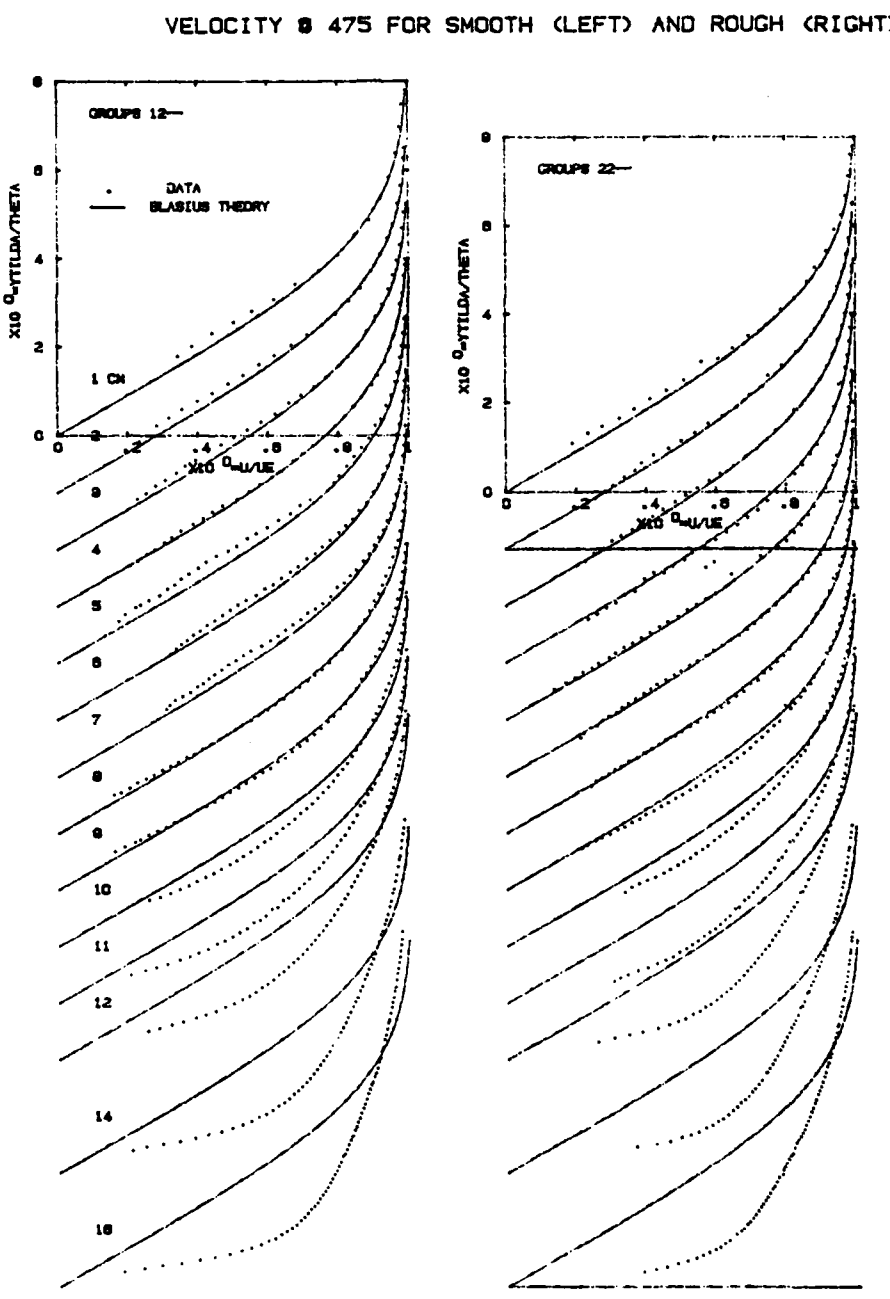

Figure 11. Velocity profiles at 475 torr.

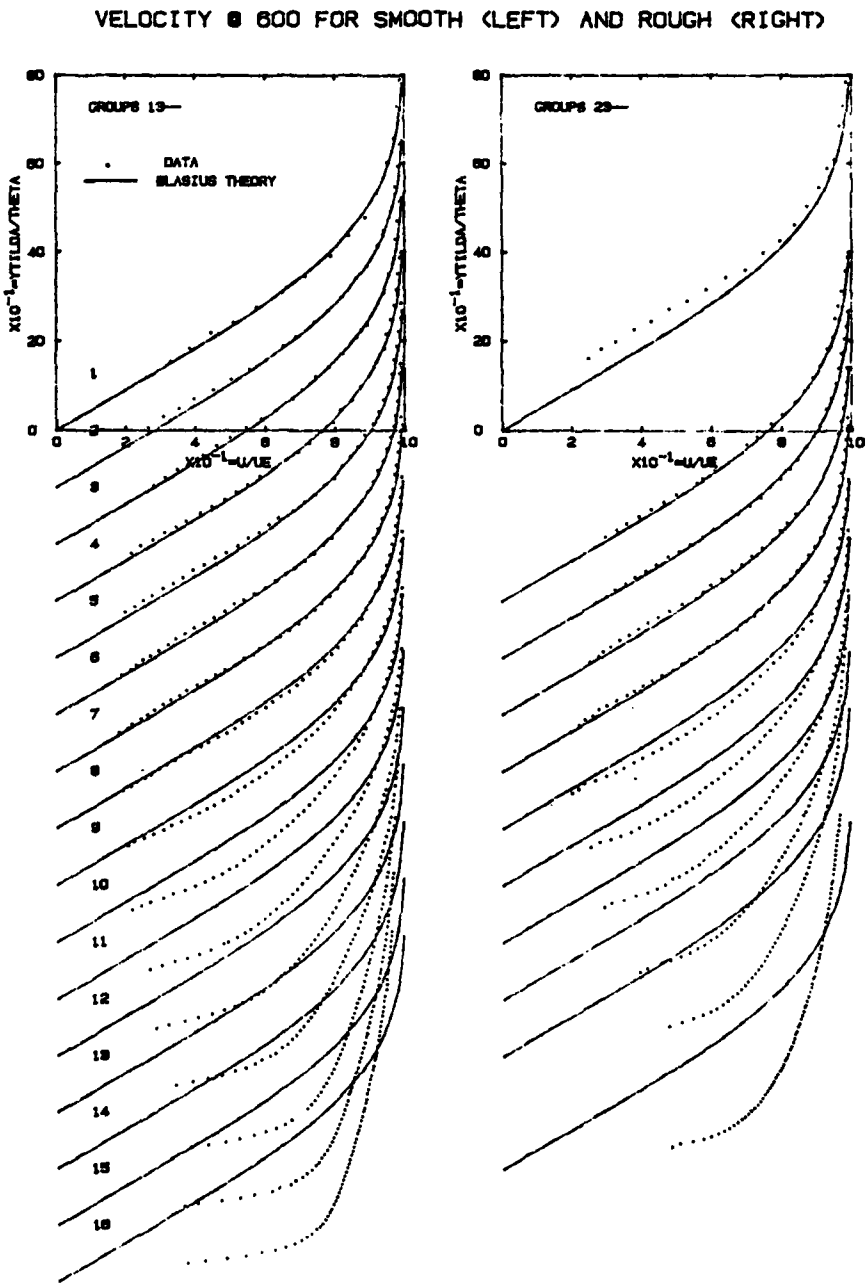

Figure 12. Velocity profiles at 600 torr.

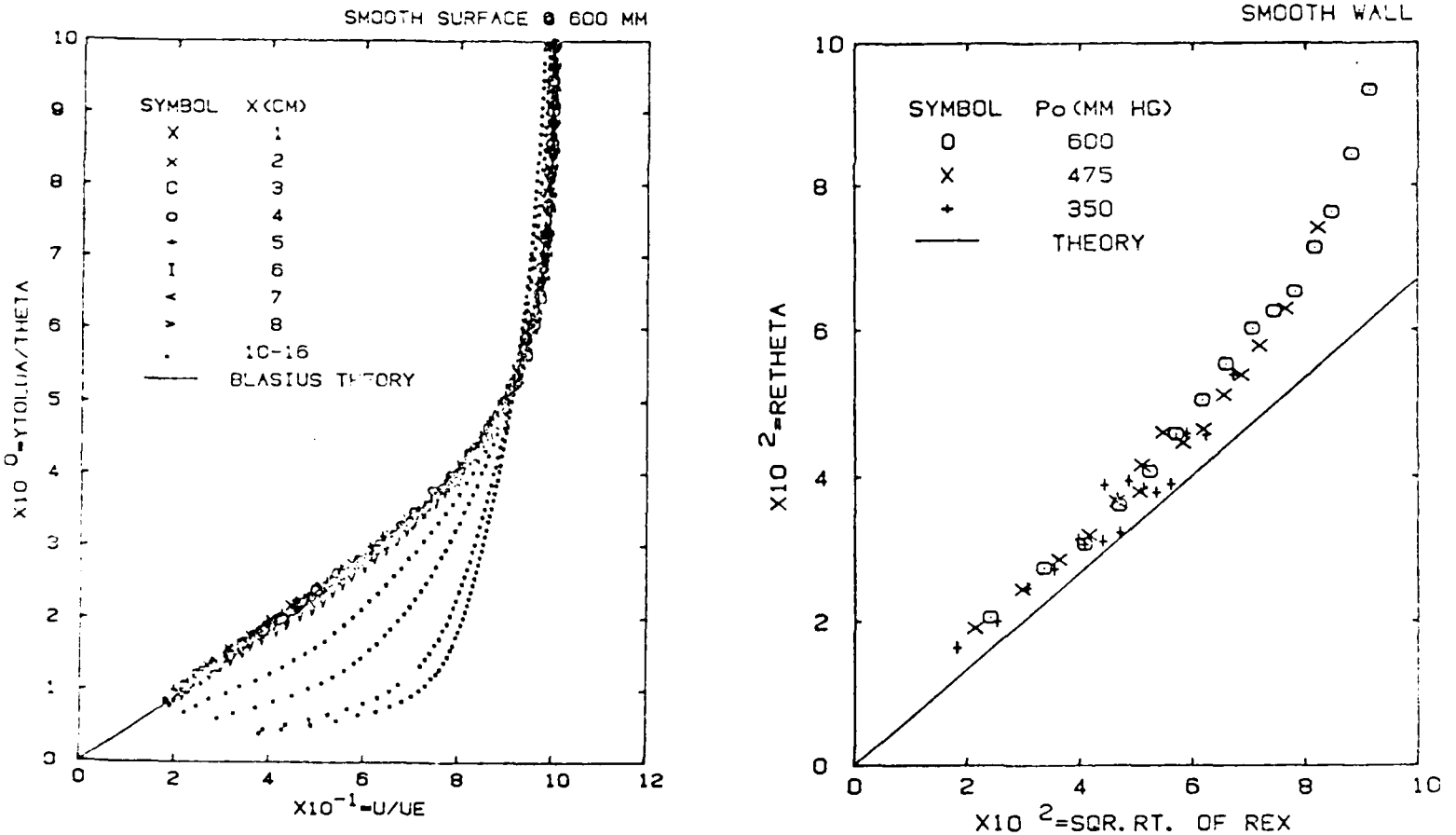

Figure 13. Typical velocity profiles (left) and Re_θ variation (right) for the smooth wall.

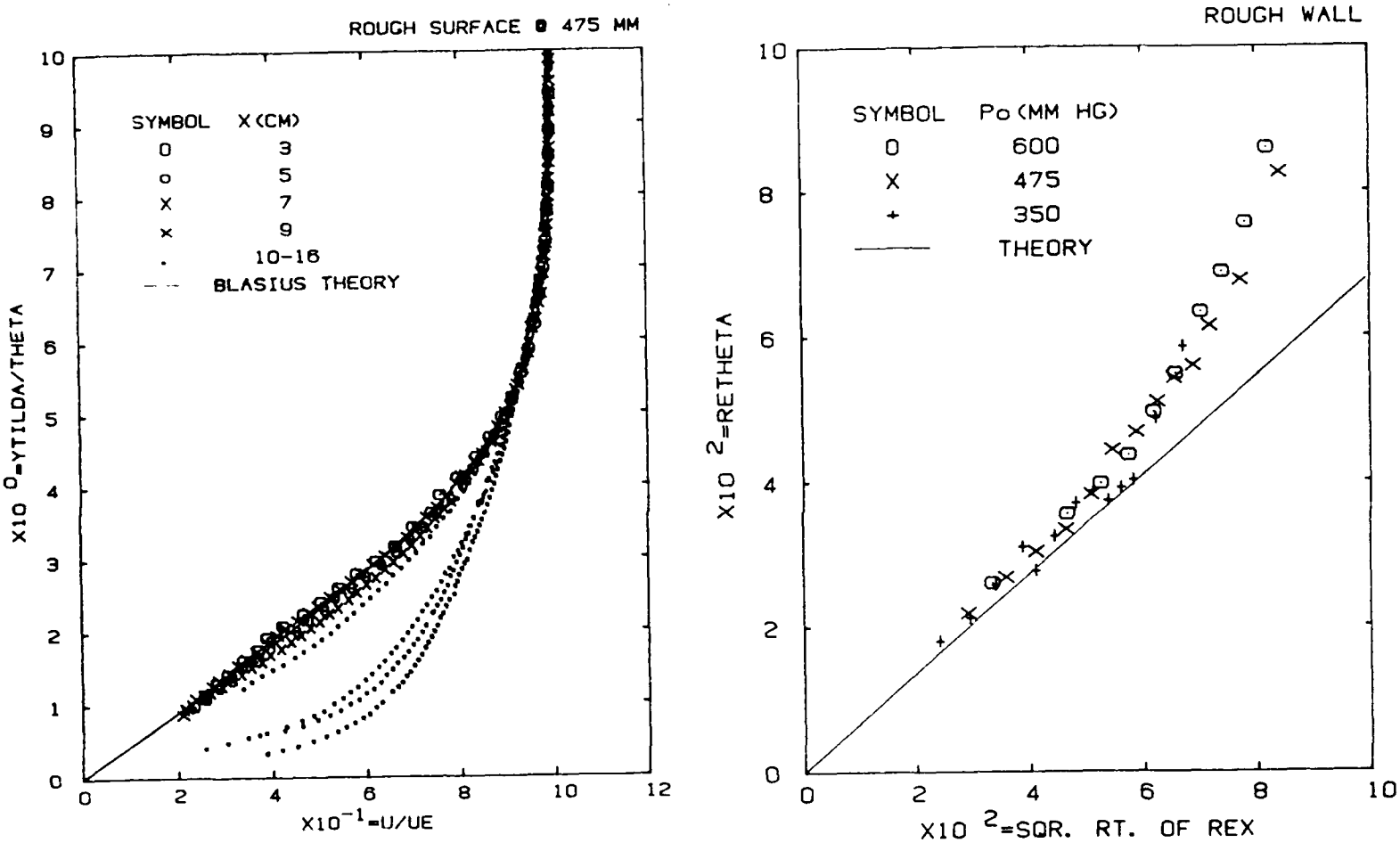

Figure 14. Typical velocity profiles (left) and Re_θ variation (right) for the rough wall.

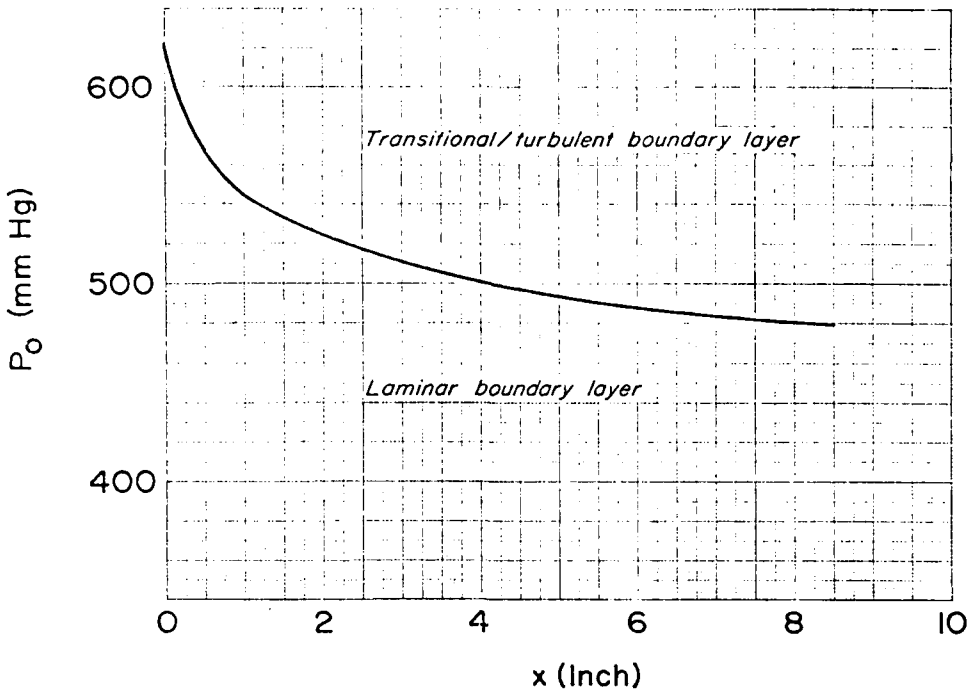

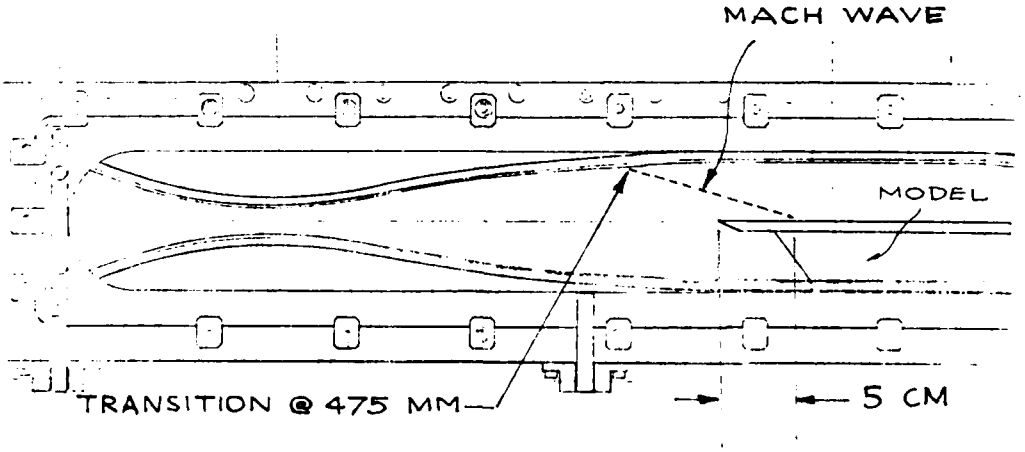

Figure 15. State of the boundary layer on the interior surfaces of the tunnel and the resulting irradiation from sidewall turbulence.

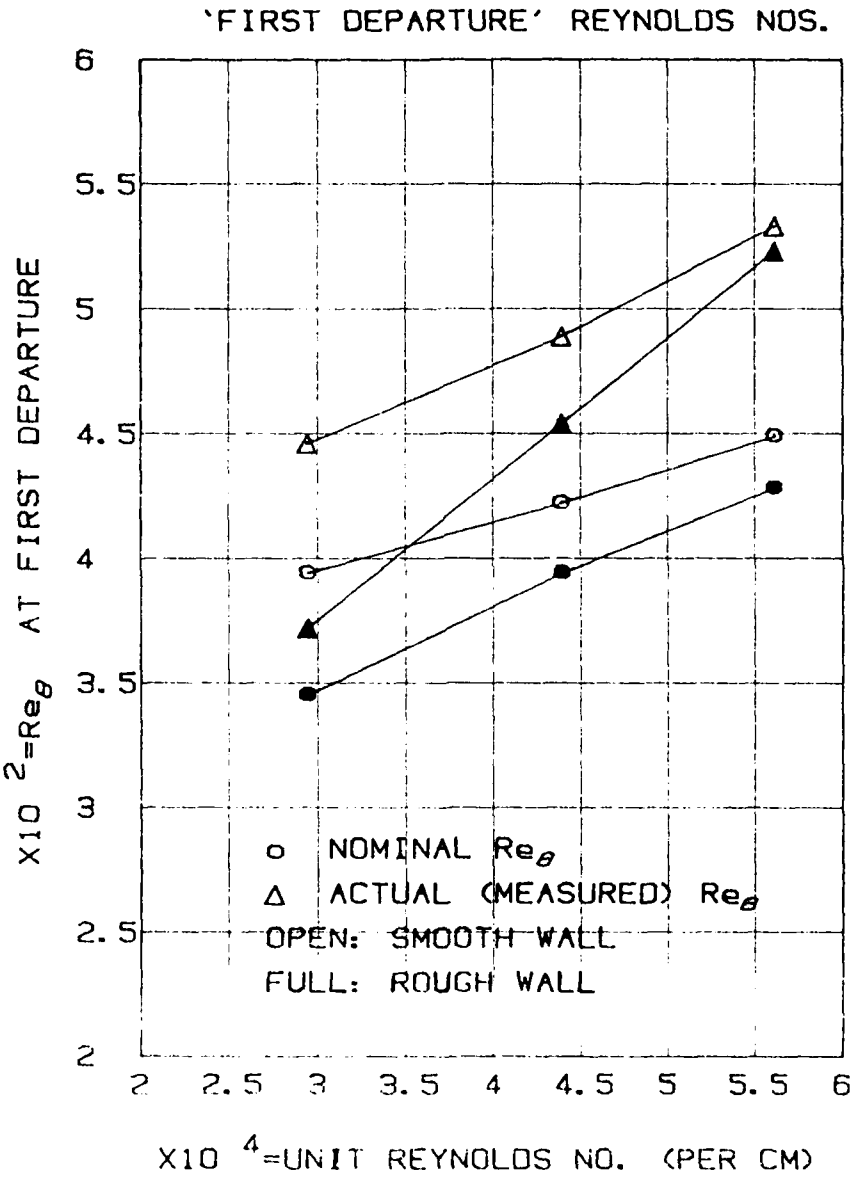

Figure 16. Momentum Reynolds number at first departure.

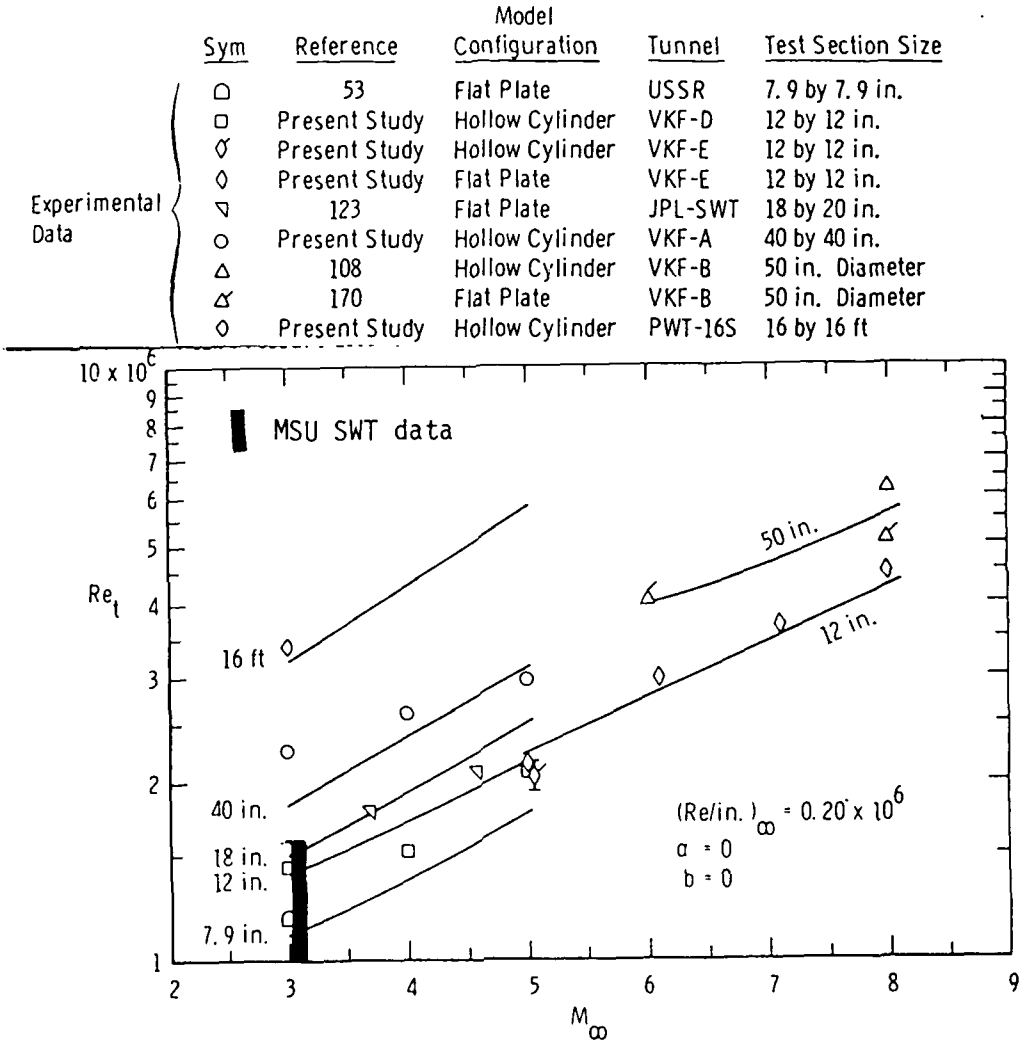

Figure 17. Transition data on the flat plate superposed on a correlation by Pate (Reference 23, p. 258) for various wind-tunnels.

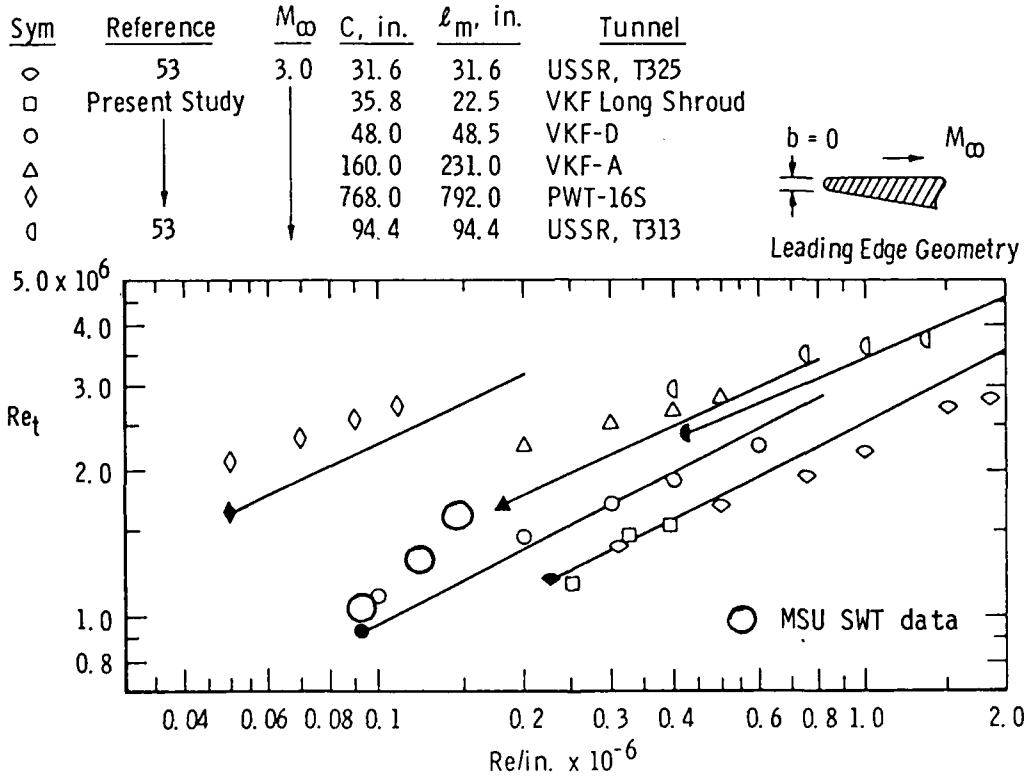

Figure 18. Unit Reynolds number effect on transition observed on the flat plate superposed on a correlation by Pate (Reference 23, p. 245).

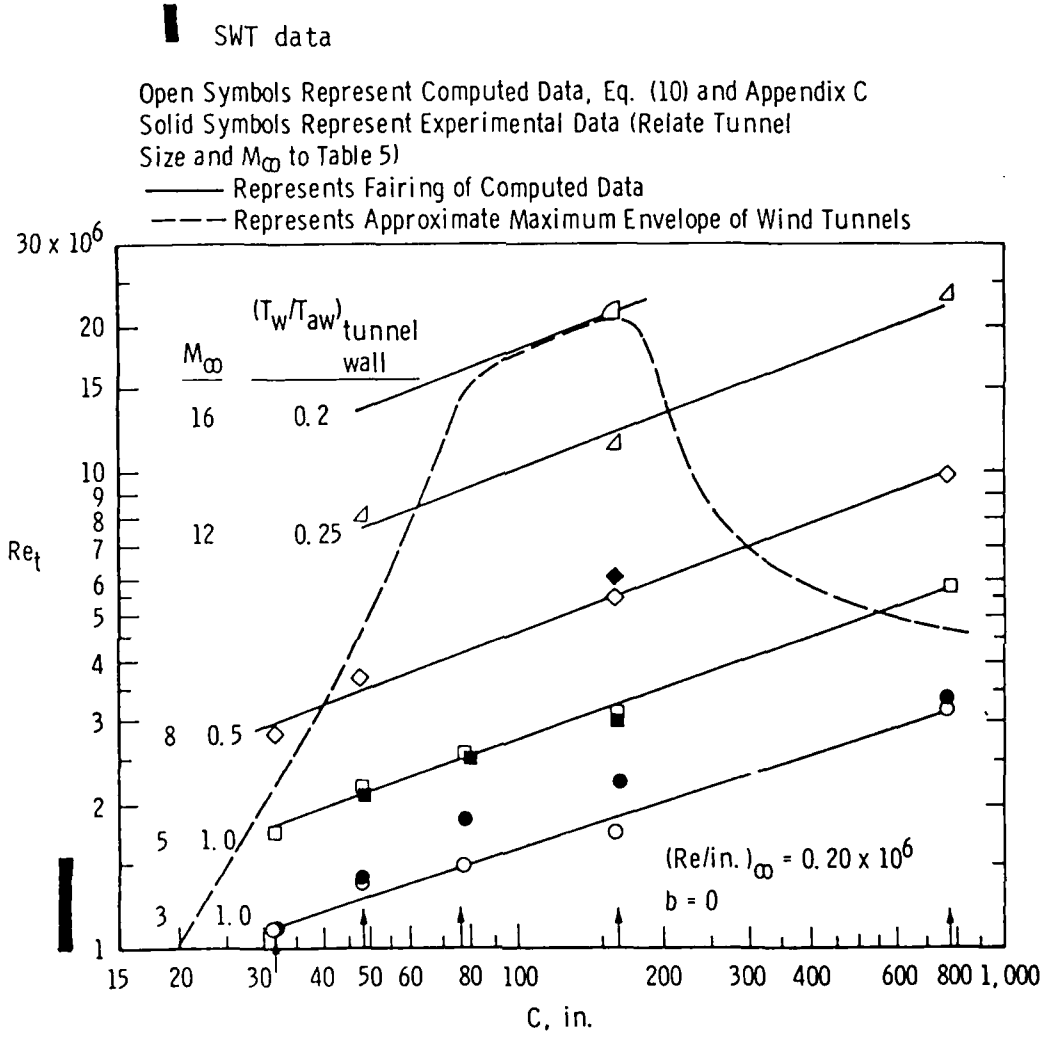

Figure 19. Test-section cross-section perimeter effect on transition for the flat plate superposed on a correlation by Pate (Reference 23, p. 241).

FACILITY		θ_c, deg	M_e	T_w/T_o	REF
AEDC "C" 12-in.	○	5	2.9-4.3	T_{aw}/T_o	22
AEDC "A" 40-in.	□	↓	2.9-4.3	↓	22
JPL 12-in.	◇	↓	2.7-3.7	↓	23
JPL 12-in.	◇	↓	1.9	↓	23
JPL 20-in.	△	2.5	2.5-4.4	↓	24
JPL 12-in. & 20-in.	◺	↓	2.5-4.4	↓	25
JPL 12-in. & 20-in.	◣	↓	1.7	↓	25
FLIGHT	⬠	7.5	1.4-4.6	.3-.8	26
FLIGHT	⬡	10	1.4-2.1	.5-.7	27
FLIGHT	◇	5	2.0-3.5	.4-.7	28
FLIGHT	◇	↓	1.6-3.7	.4-.7	29
FLIGHT	⬠	↓	1.6-1.8	T_{aw}/T_o	30

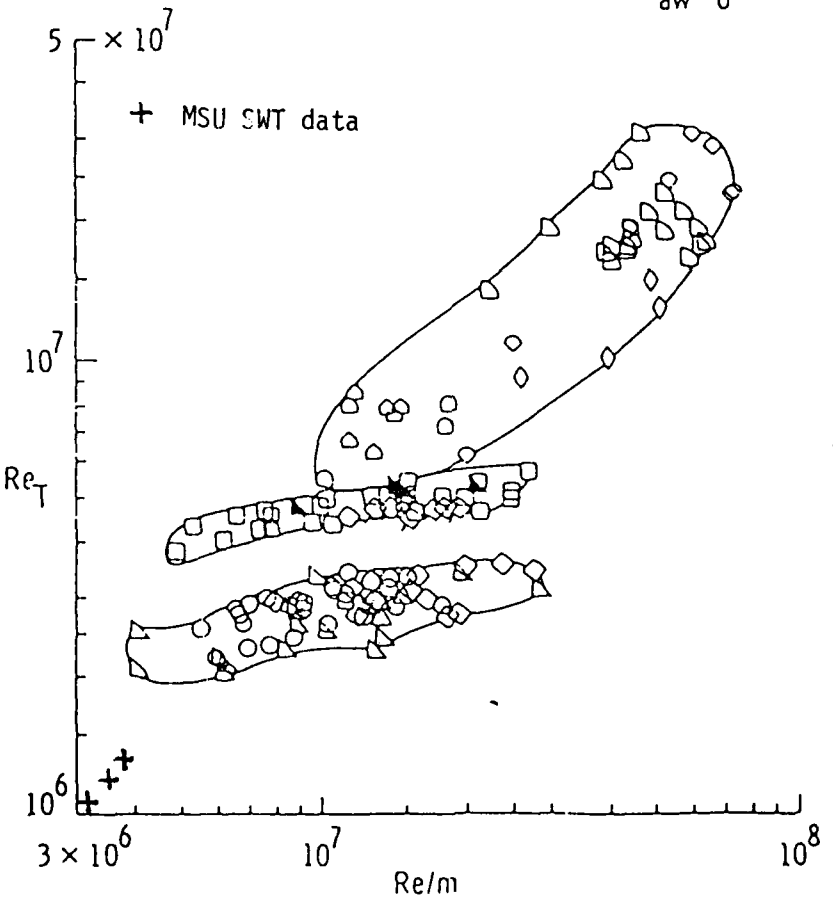

Figure 20. Unit Reynolds number effect on the flat plate transition superposed on a correlation by Beckwith et al. (Reference 24, Figure 17).

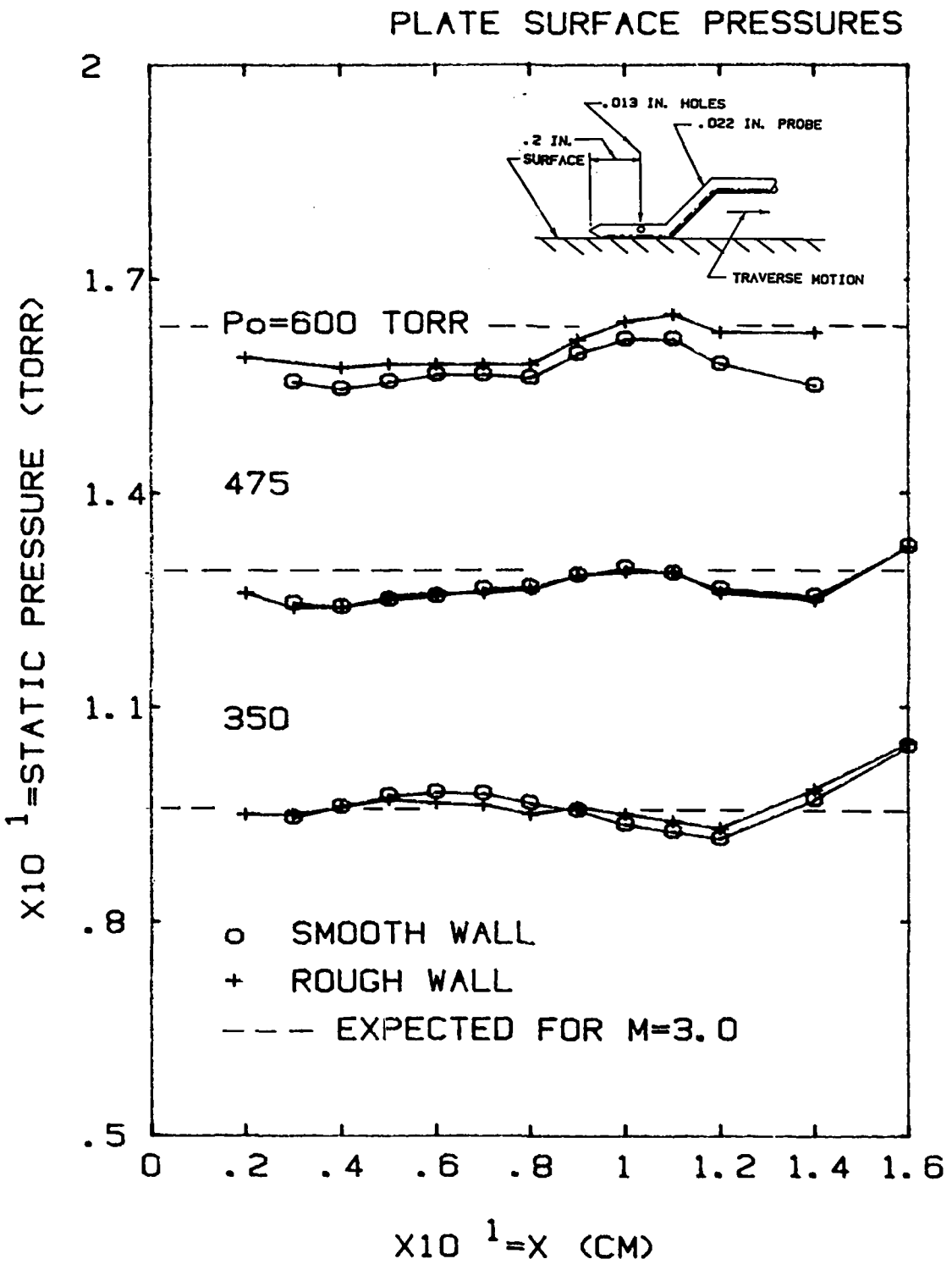

Figure 21. Static pressures measured on the plate surface.

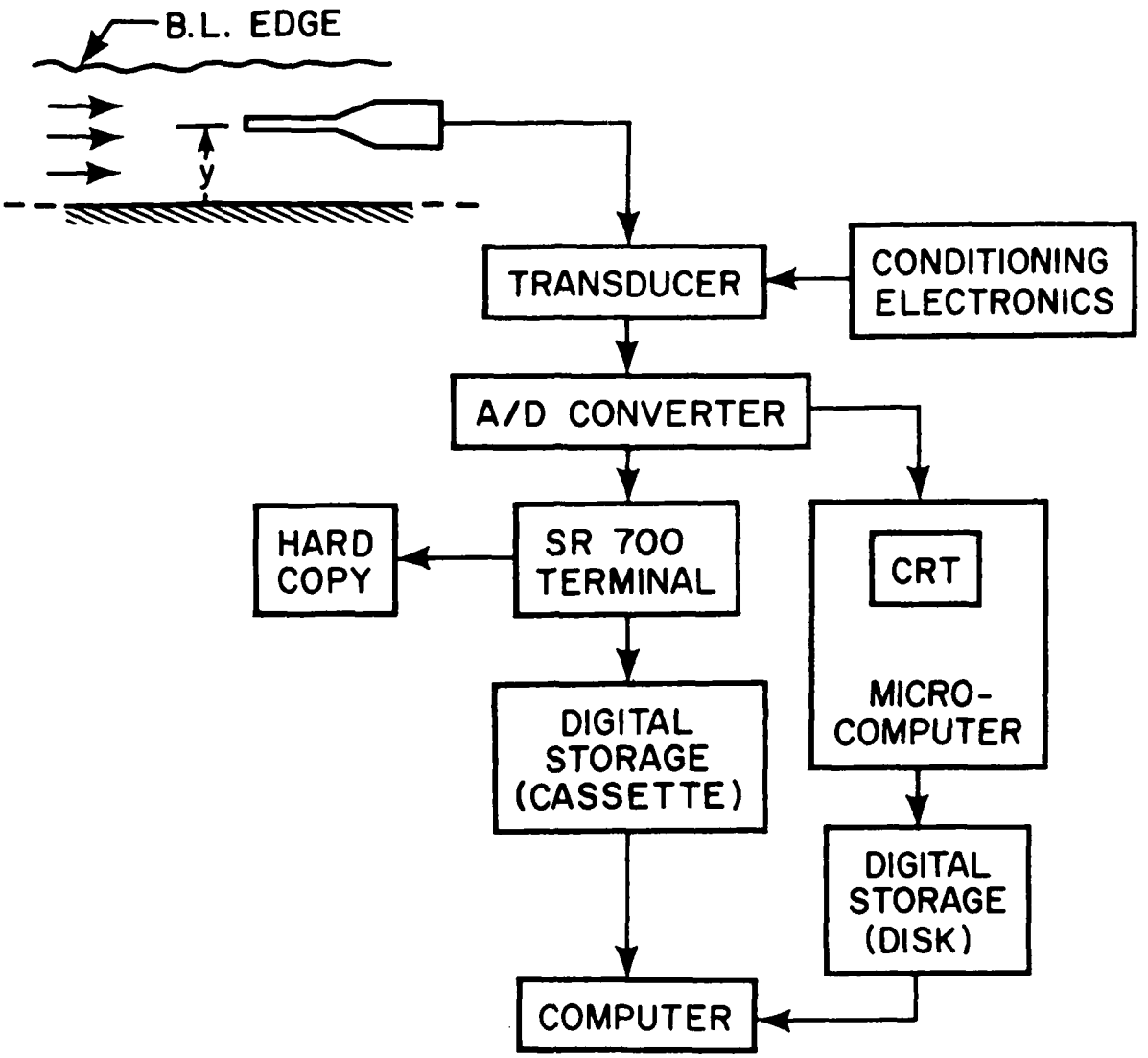

Figure 22. Basic elements in the pitot-probe location on the velocity profile.

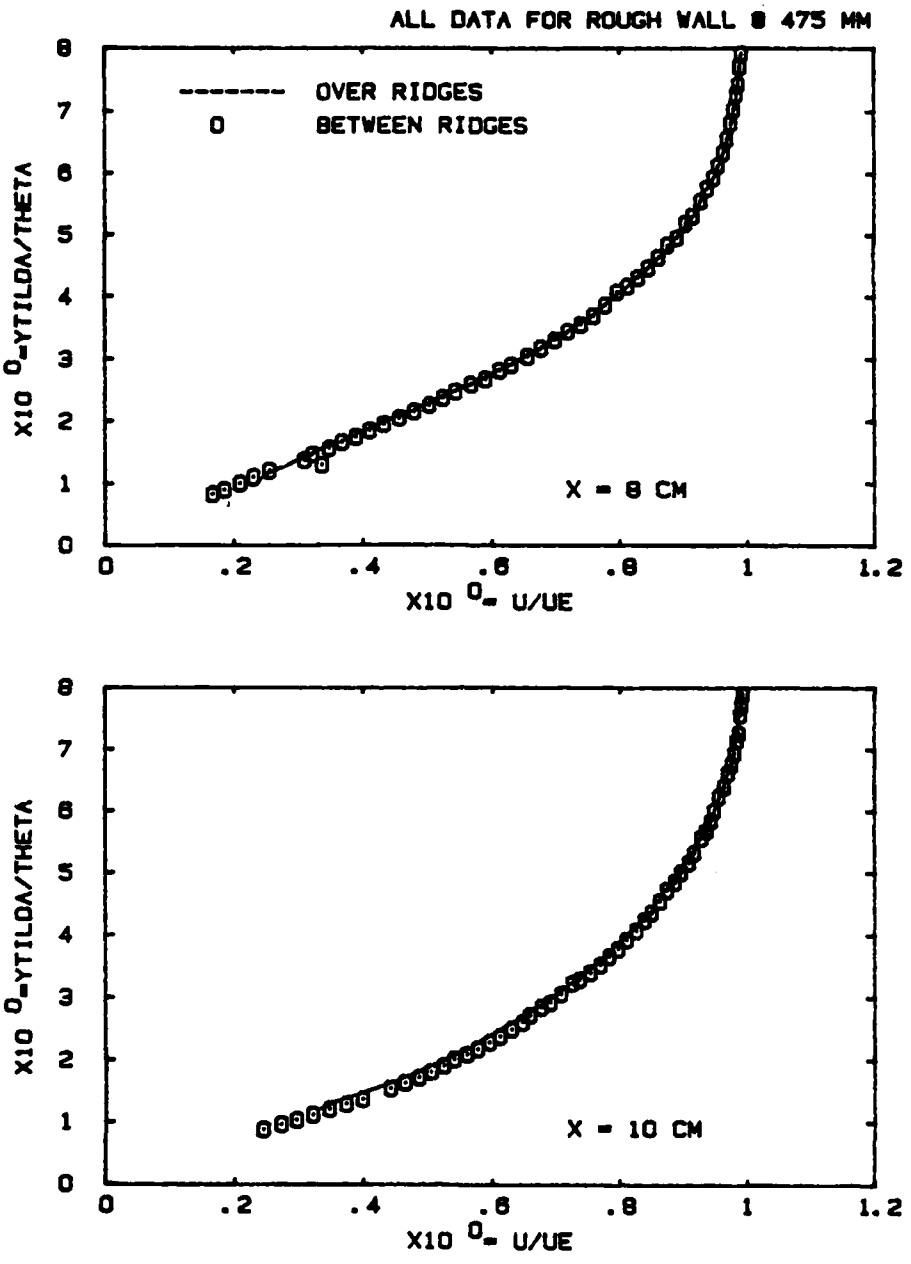

Figure 23. Test of the effect of pitot-probe location on the velocity profile.

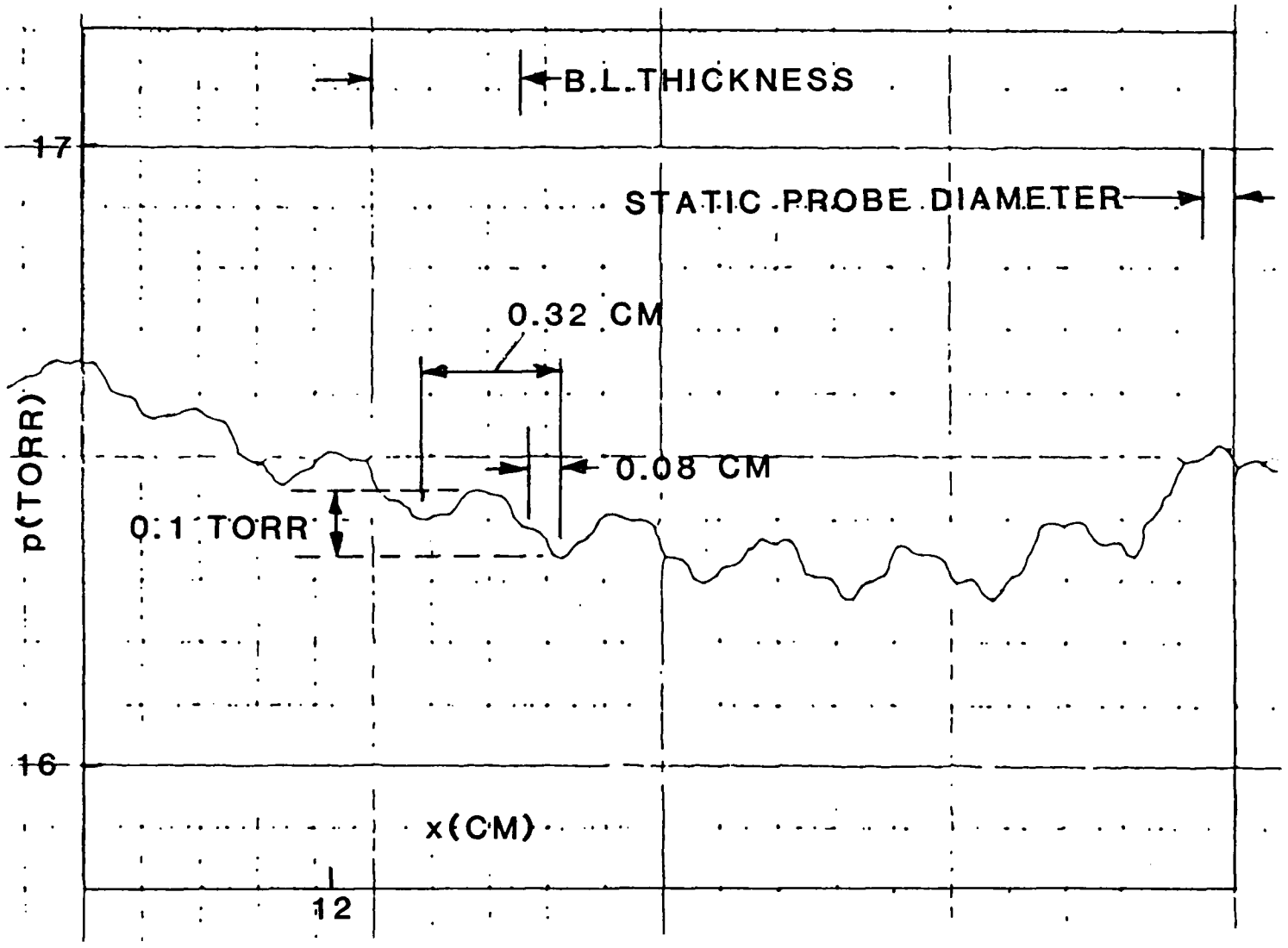

Figure 24. Detailed view of static-probe output over the rough wall for turbulent boundary layer.

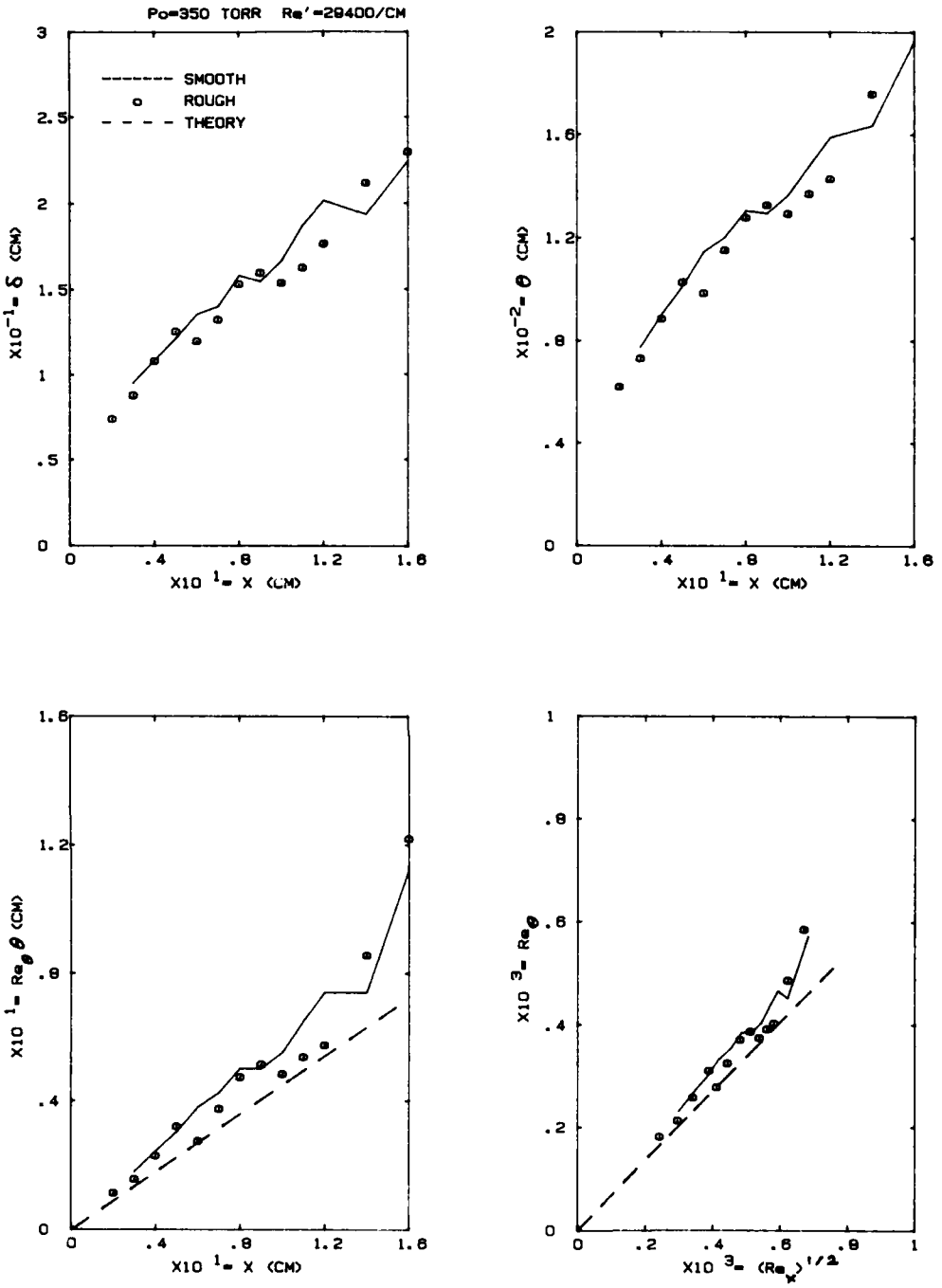

Figure 25. Effect of roughness on the measured integral properties at 350 torr.

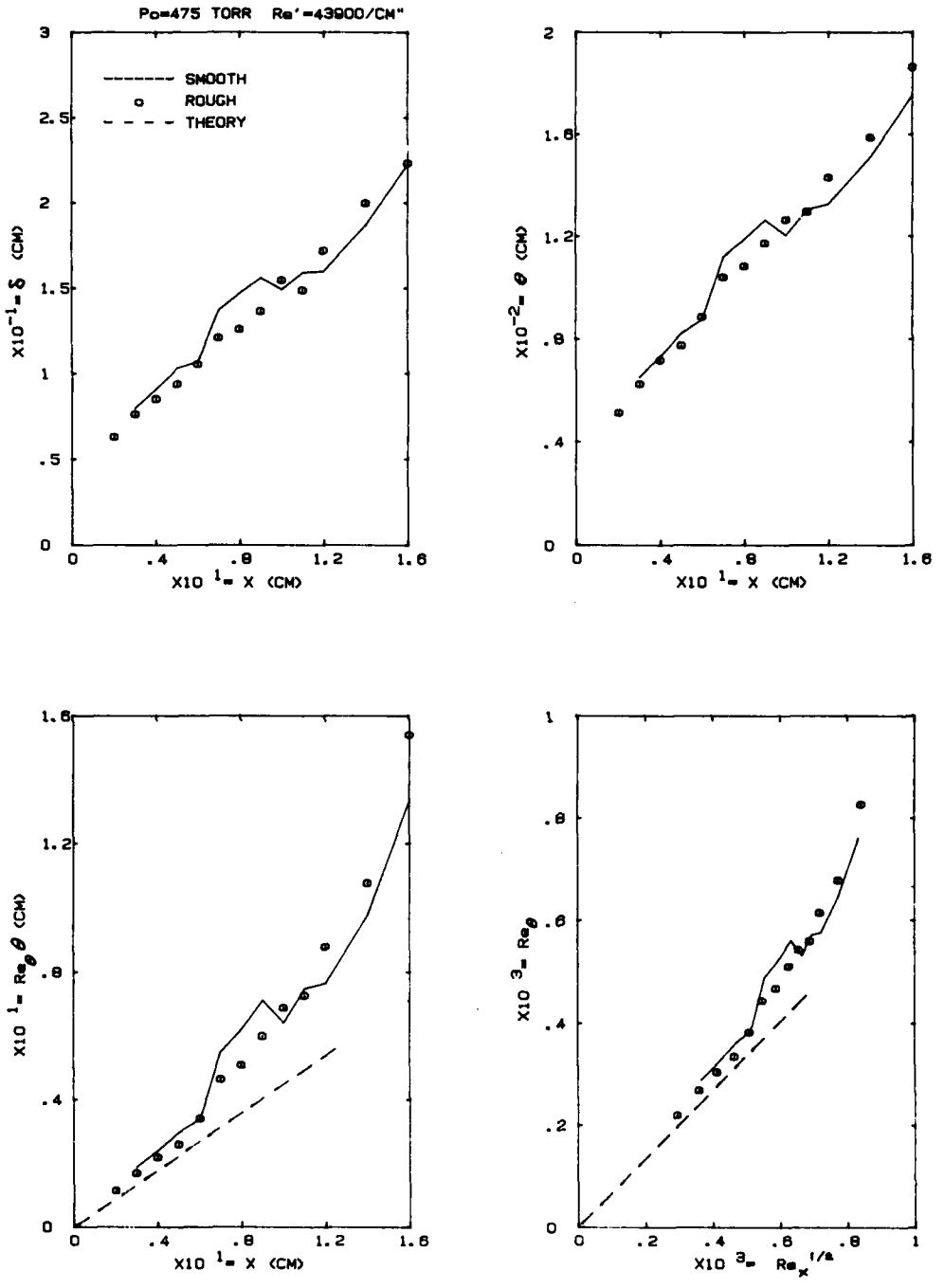

Figure 26. Effect of roughness on the measured integral properties at 475 torr.

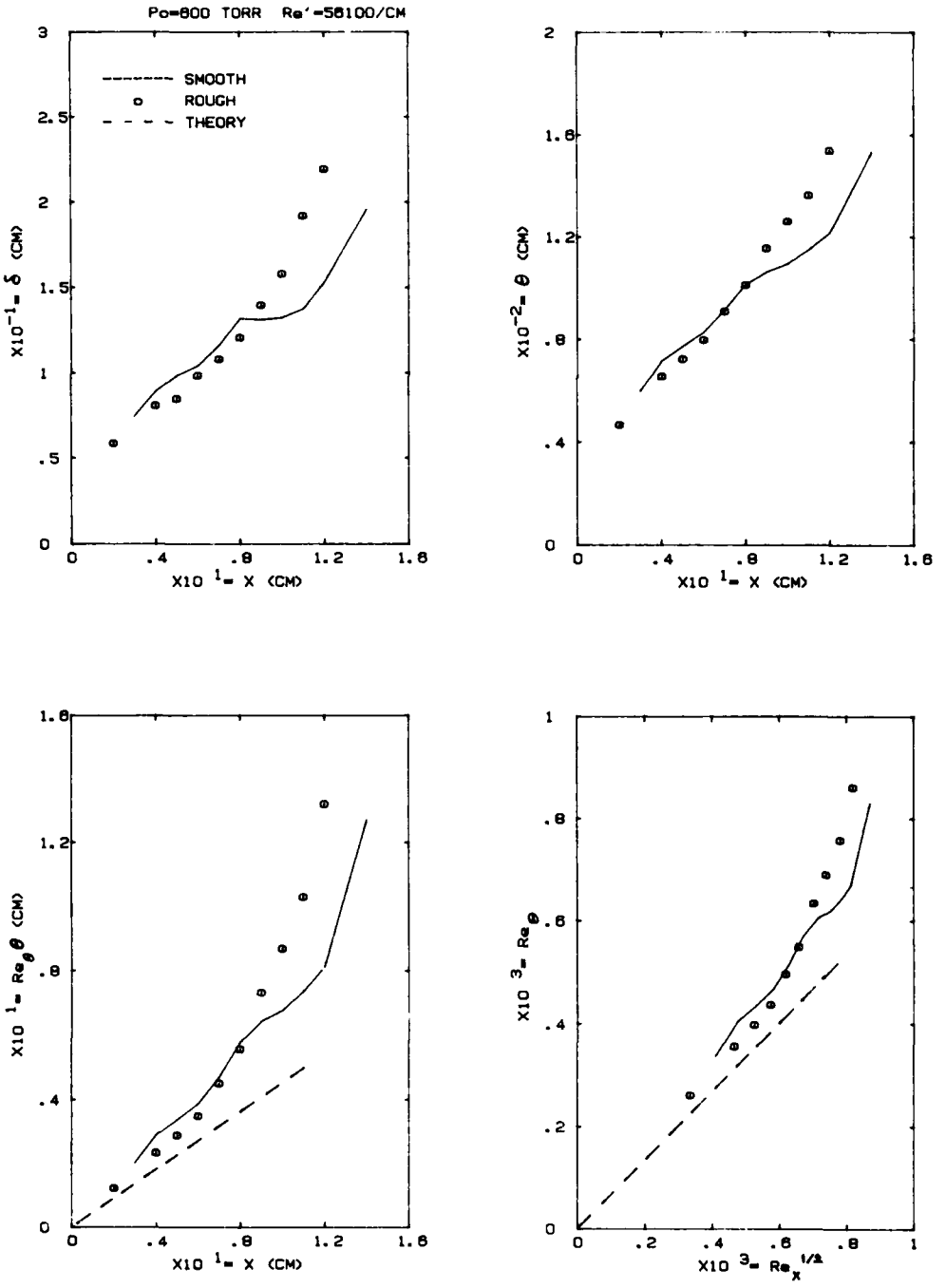

Figure 27. Effect of roughness on the measured integral properties at 600 torr.

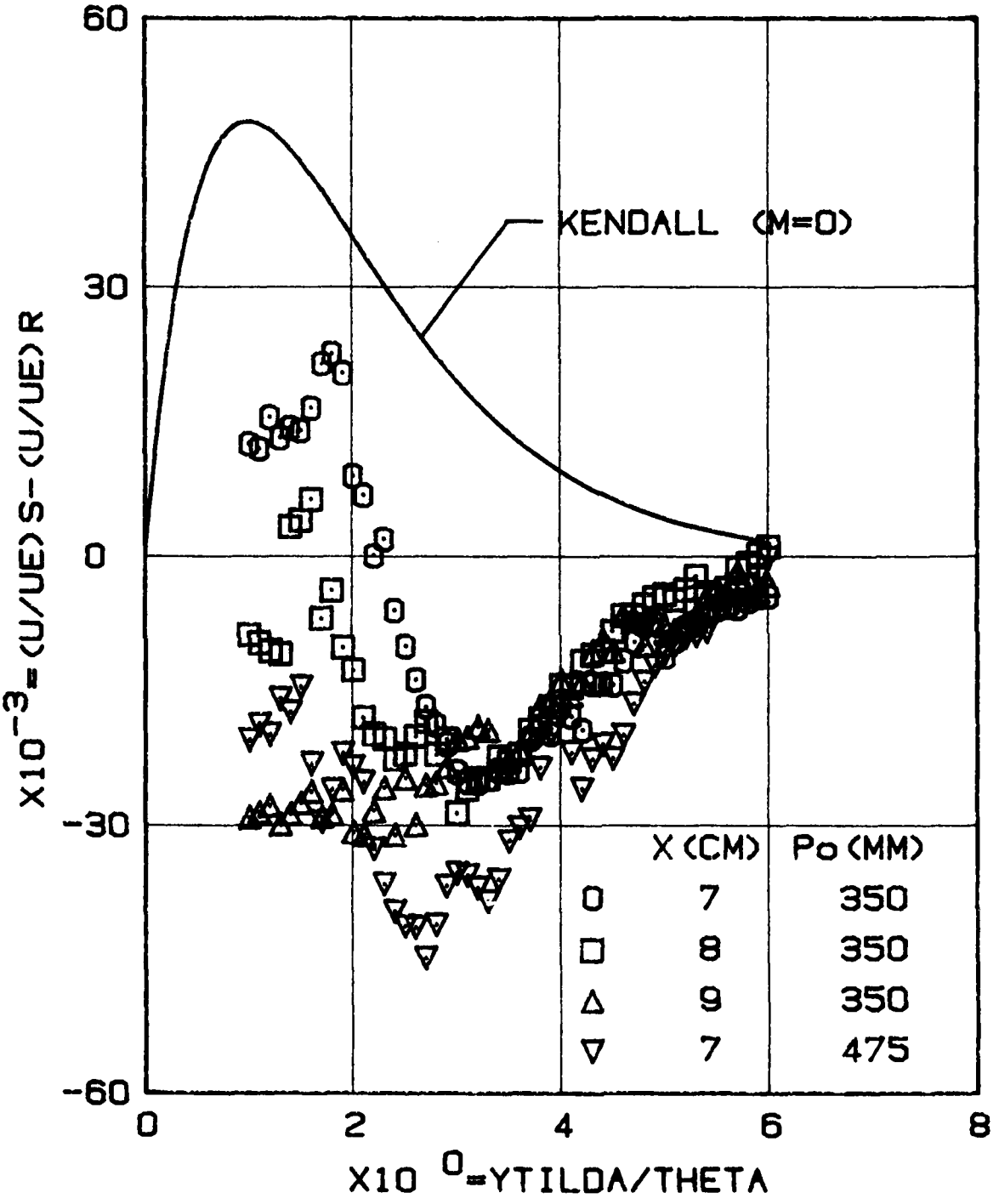

Figure 28. An attempt to find a systematic effect of the roughness on the velocity profile.

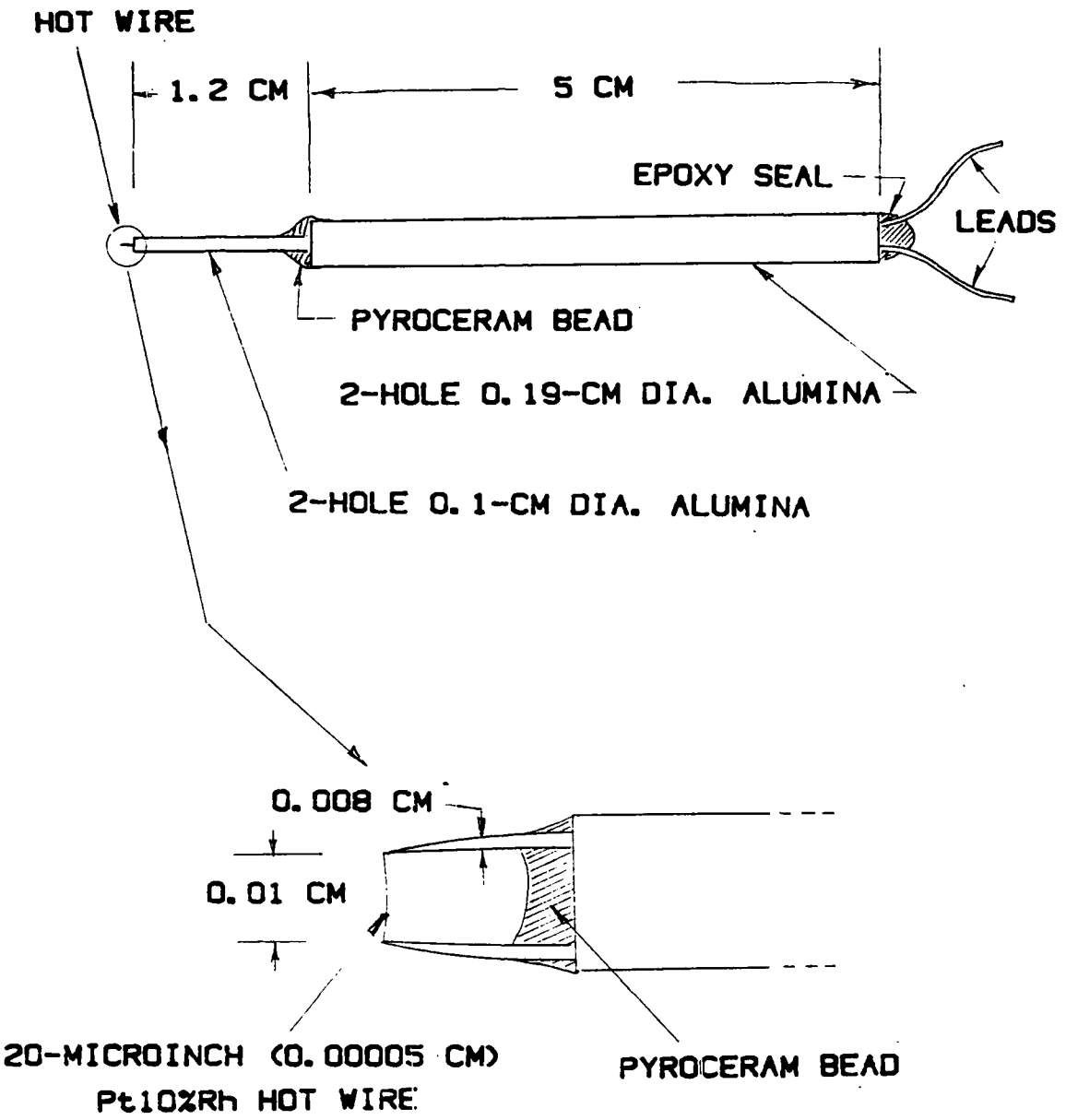

Figure 29. Schematic of the hot-wire anemometer probe.

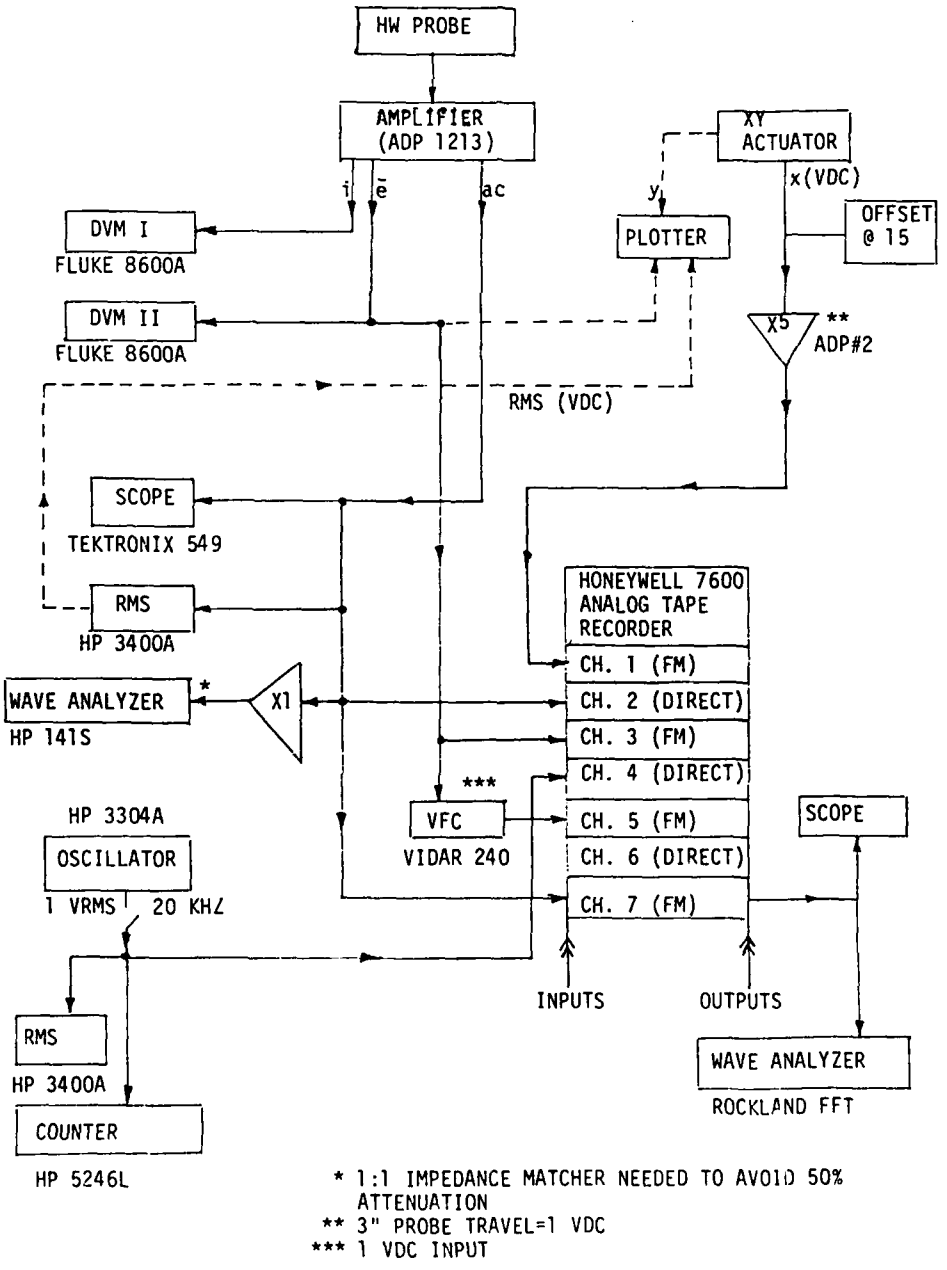

Figure 30. The test set-up for the hot-wire measurements.

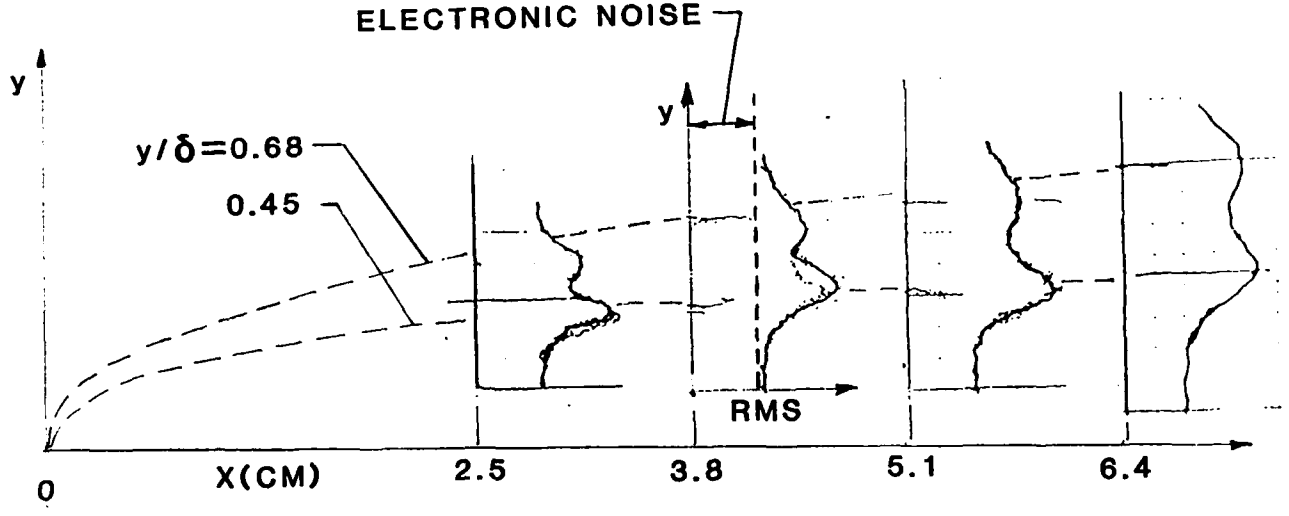

Figure 31. Unresolved wideband hot-wire profiles across the laminar boundary layer (typical).

AD-A166 188 BOUNDARY LAYER STABILITY MEASUREMENTS OVER A FLAT PLATE AT MACH 3(U) MONTANA STATE UNIV BOZEMAN SUPERSONIC WIND TUNNEL LAB A DEMETRIADES NOV 85 SWT-TR-85-1 2/3

UNCLASSIFIED AFOSR-TR-86-0056 AFOSR-80-0267 F/G 20/4 NL

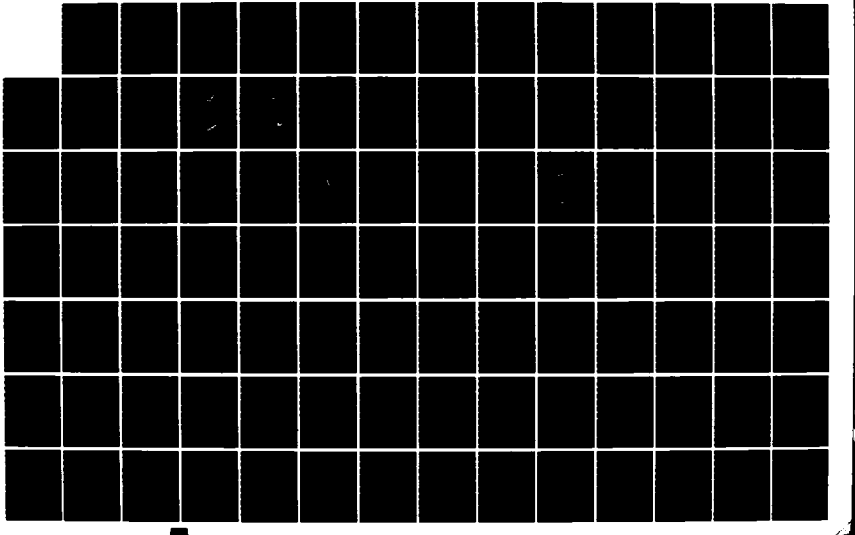

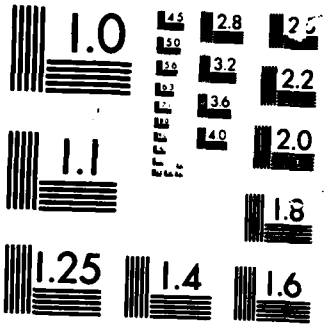

MICROCOPY RESOLUTION TEST CHART

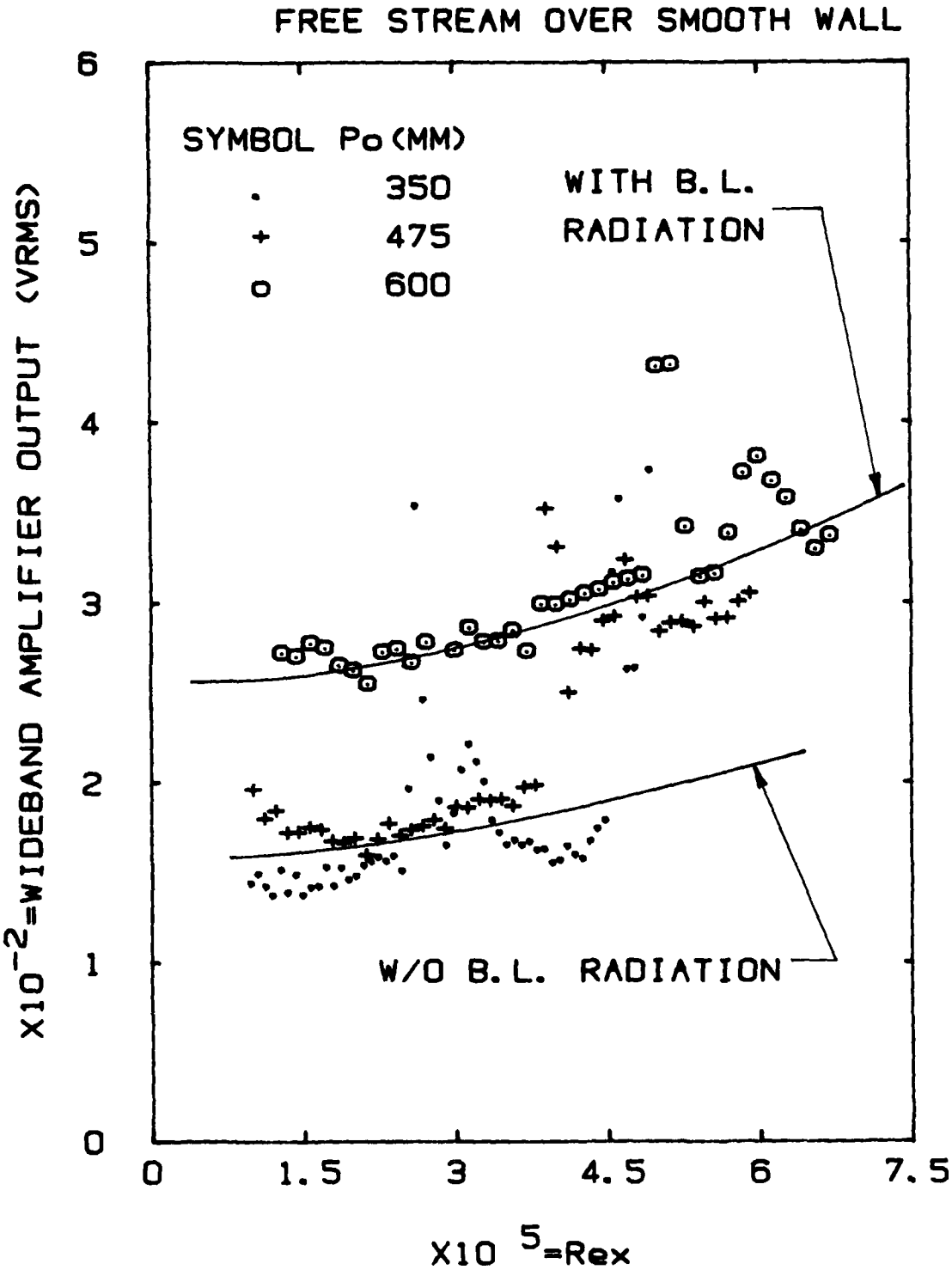

Figure 32. Reynolds number effect on stream noise detected just outside the boundary layer.

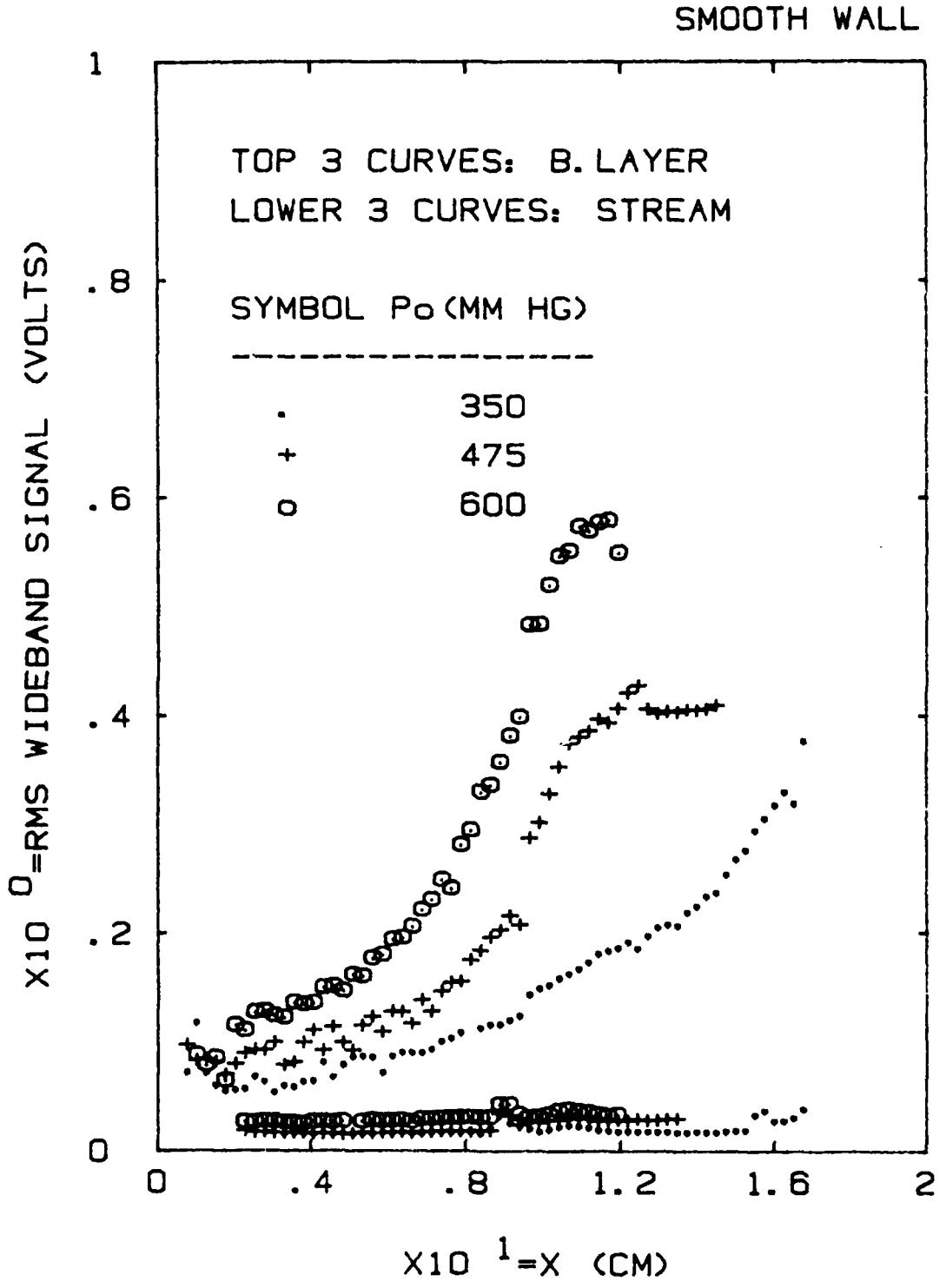

Figure 33. Wideband hot-wire output variation along plate (smooth wall).

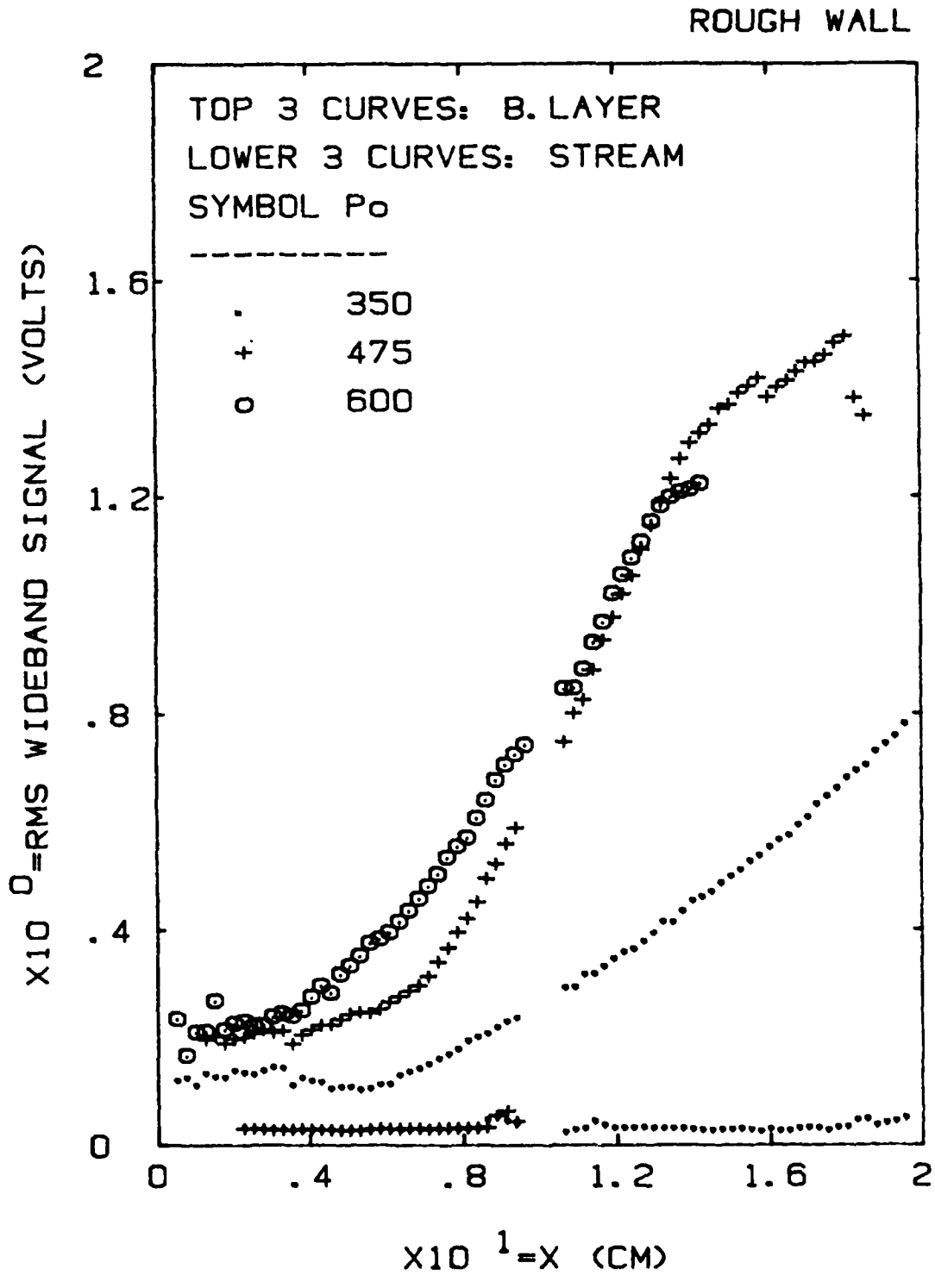

Figure 34. Wideband hot-wire output variation along plate (rough wall).

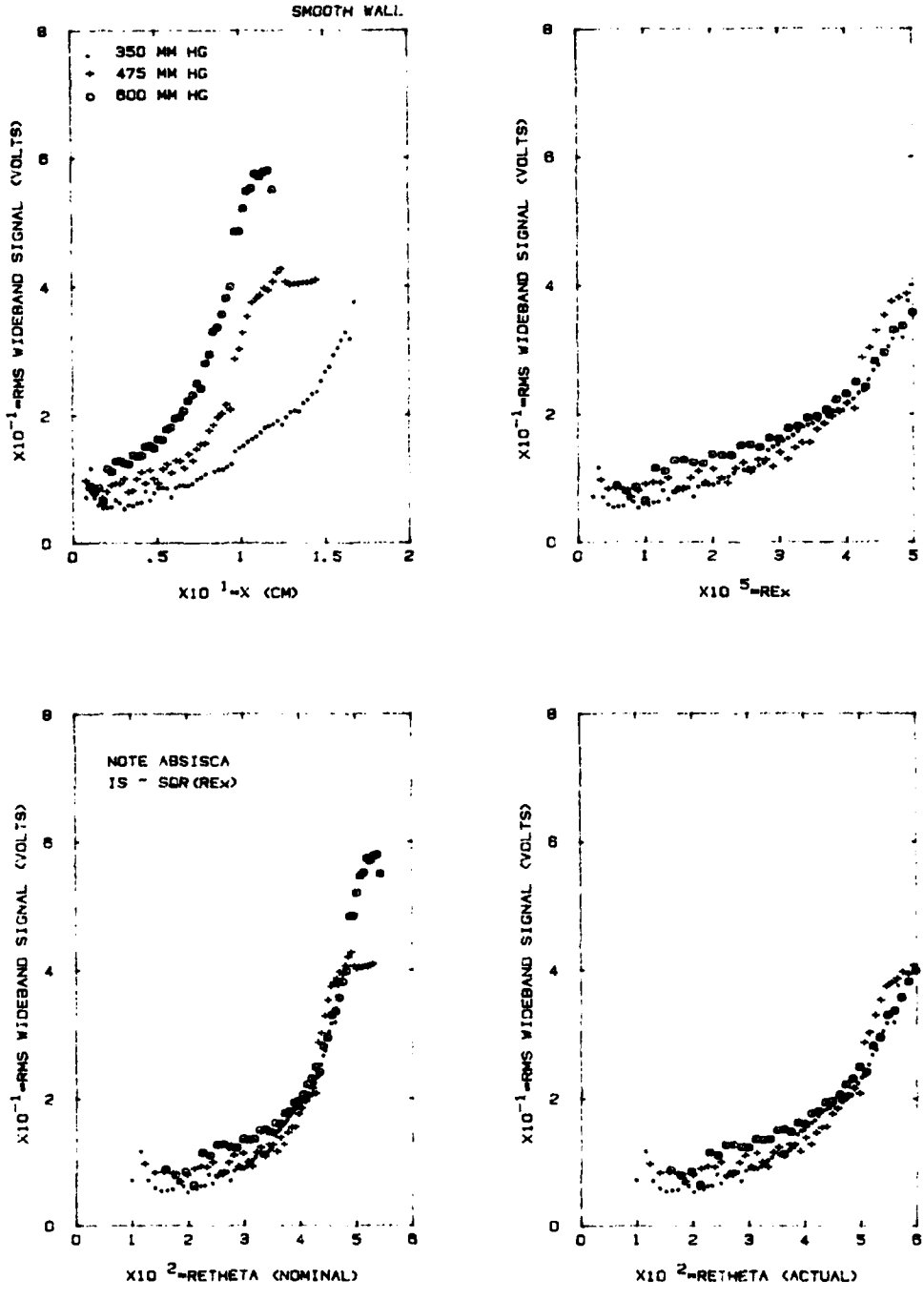

Figure 35. Reynolds number effects on wideband signal along plate (smooth wall).

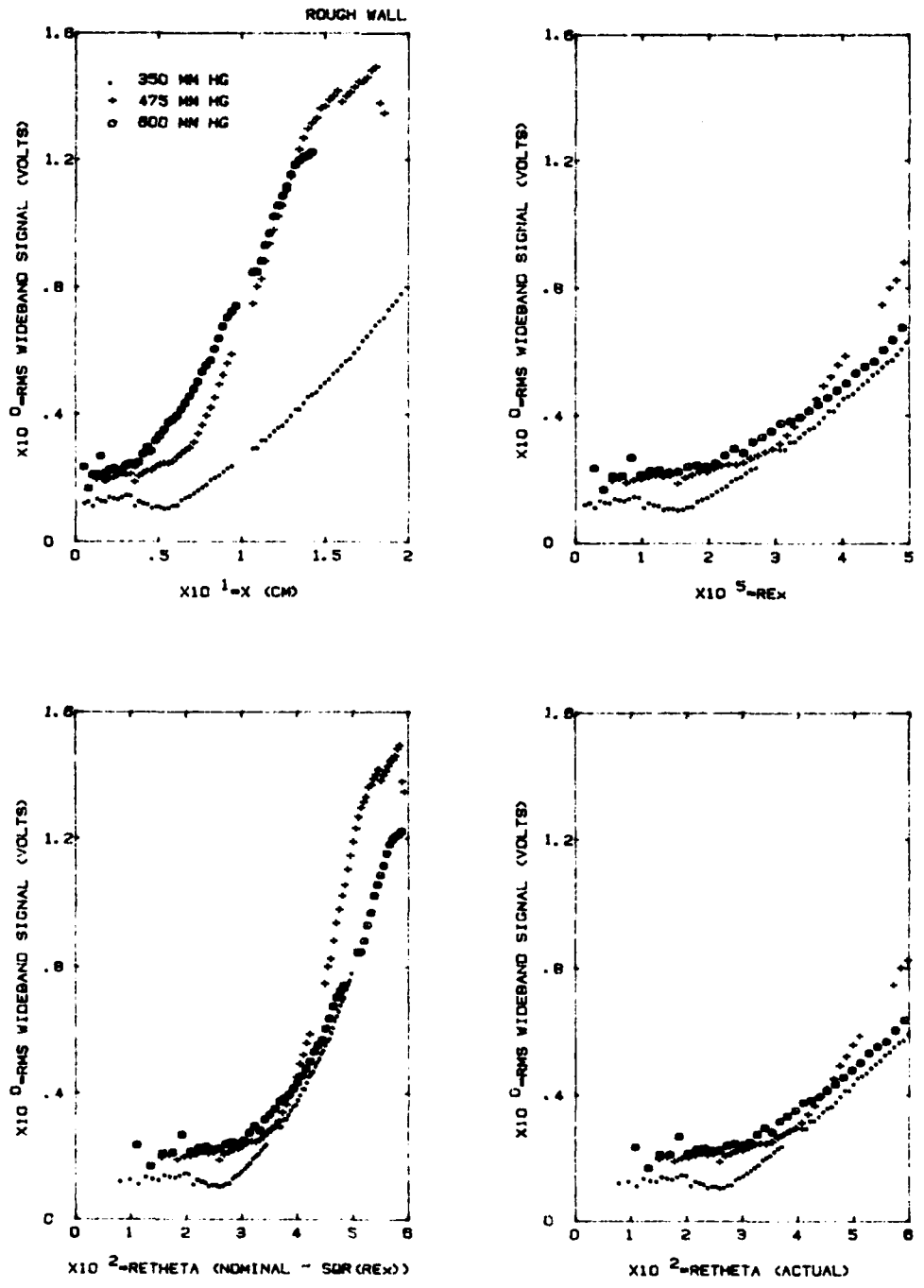

Figure 36. Reynolds number effects on wideband signal along plate (rough wall).

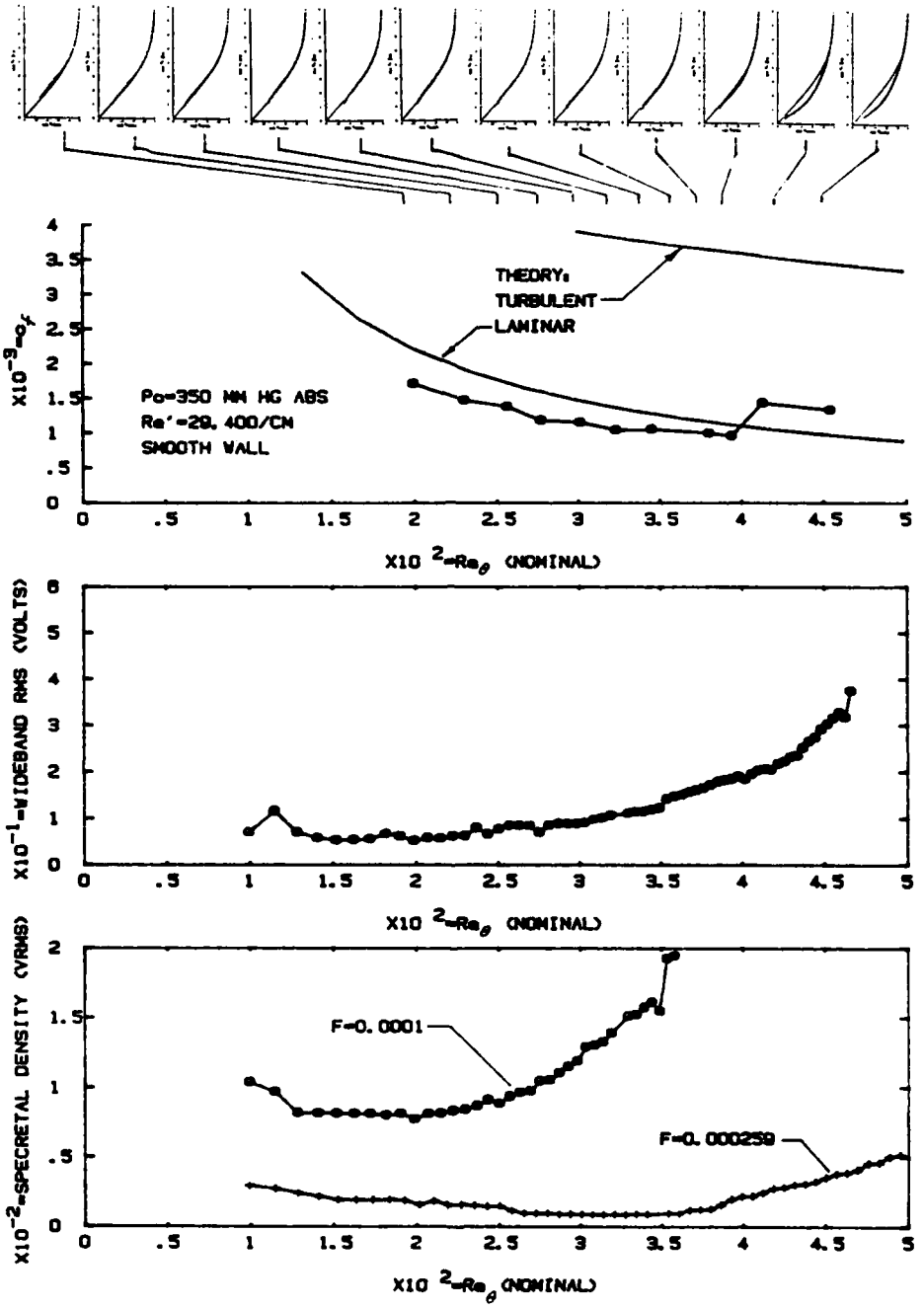

Figure 37. Relative behavior of (from top) the velocity profiles with solid curves showing the Blasius theory, friction coefficient, wideband output and selected Fourier components represented nondimensionally. Smooth wall at 350 torr.

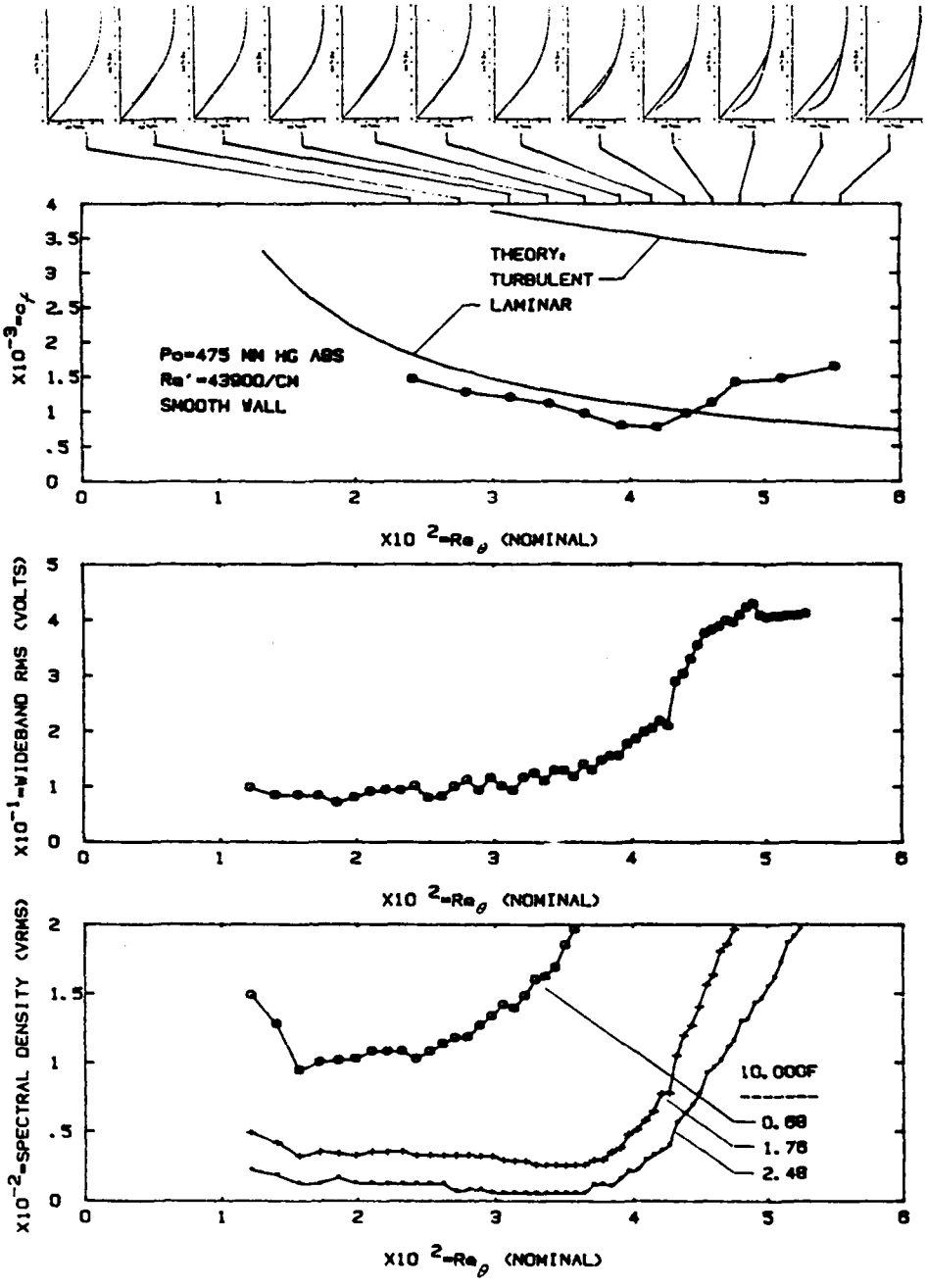

Figure 38. As in Figure 37; smooth wall at 475 torr.

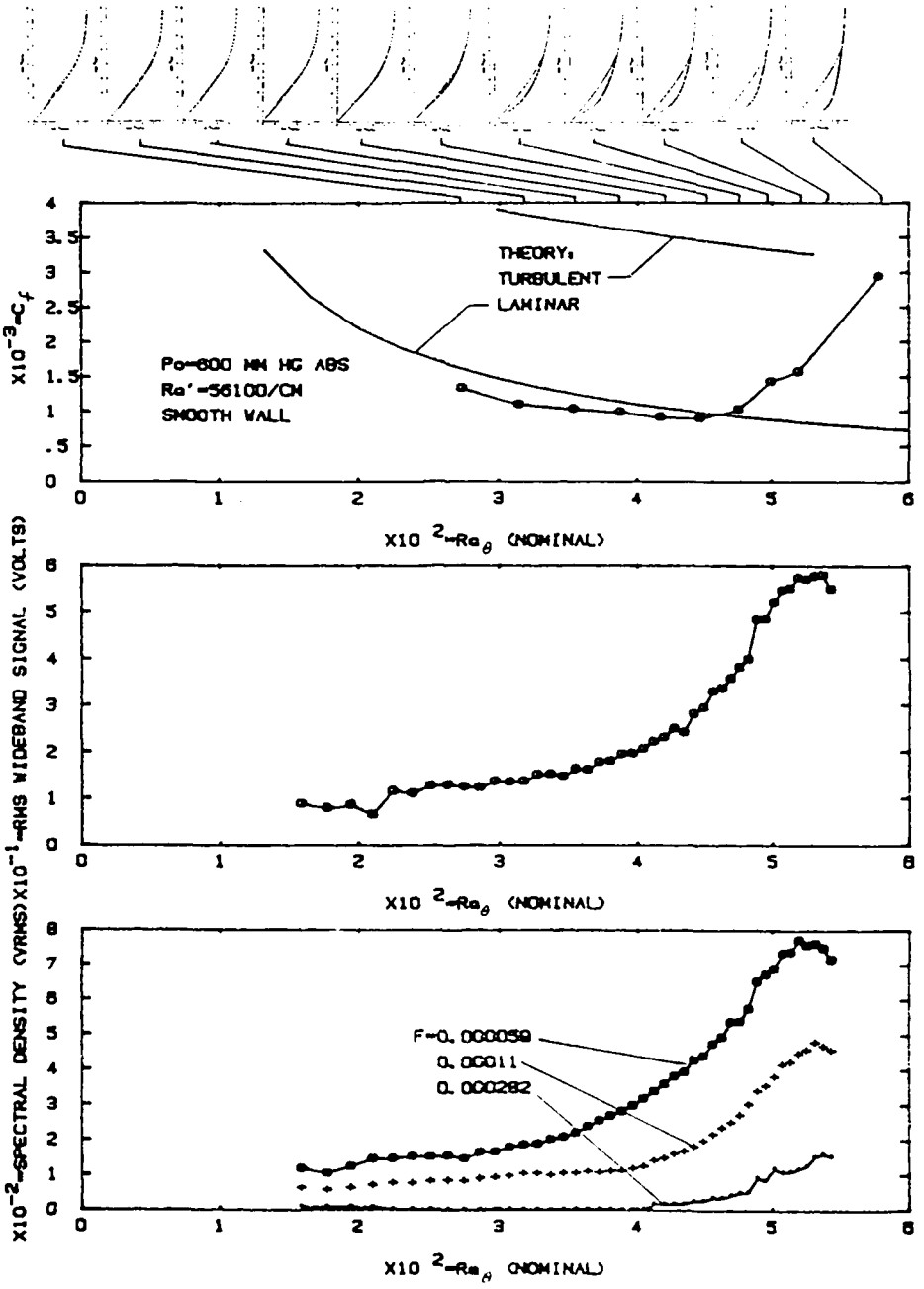

Figure 39. As in Figure 37; smooth wall at 600 torr.

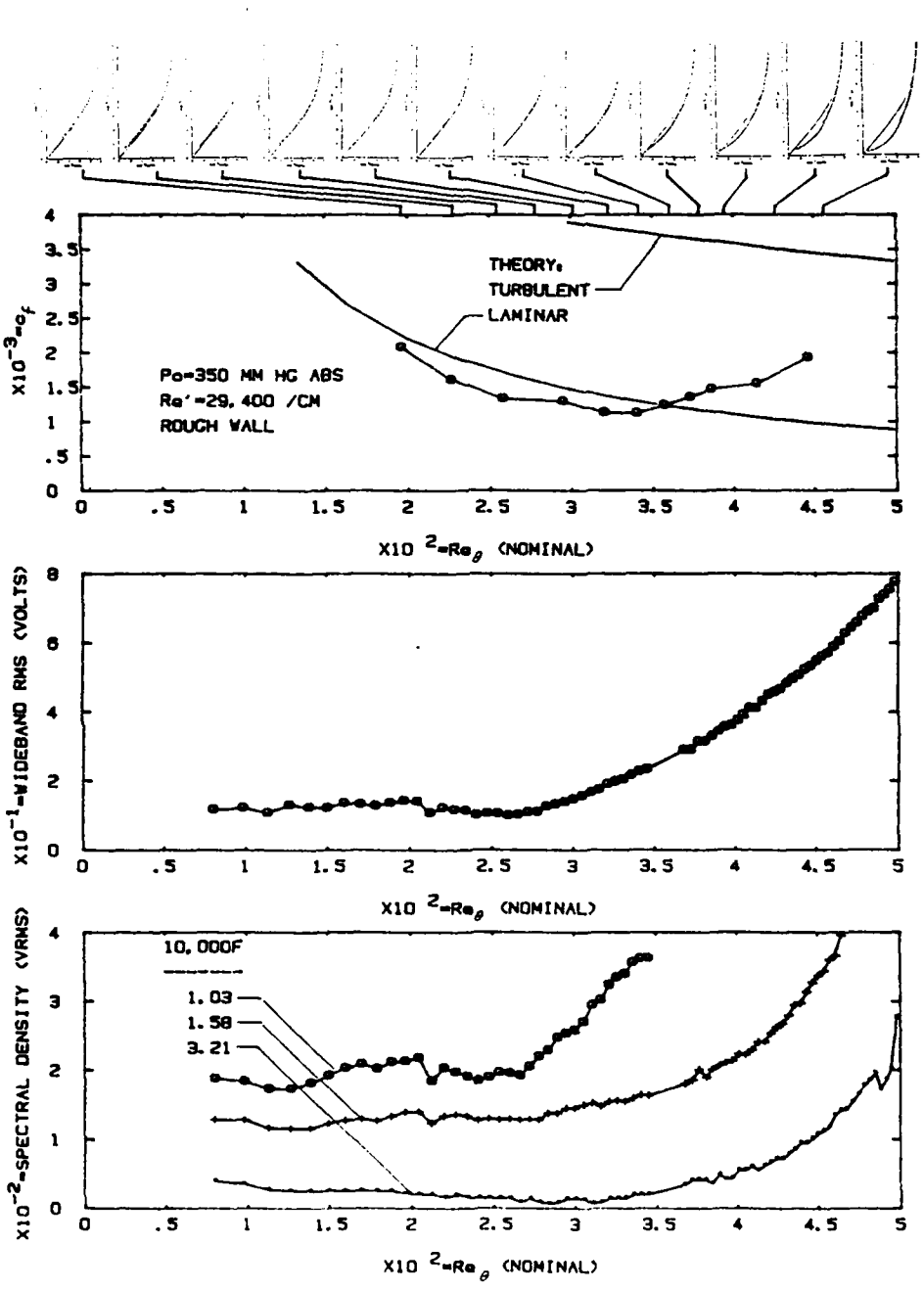

Figure 40. As in Figure 37; rough wall at 350 torr.

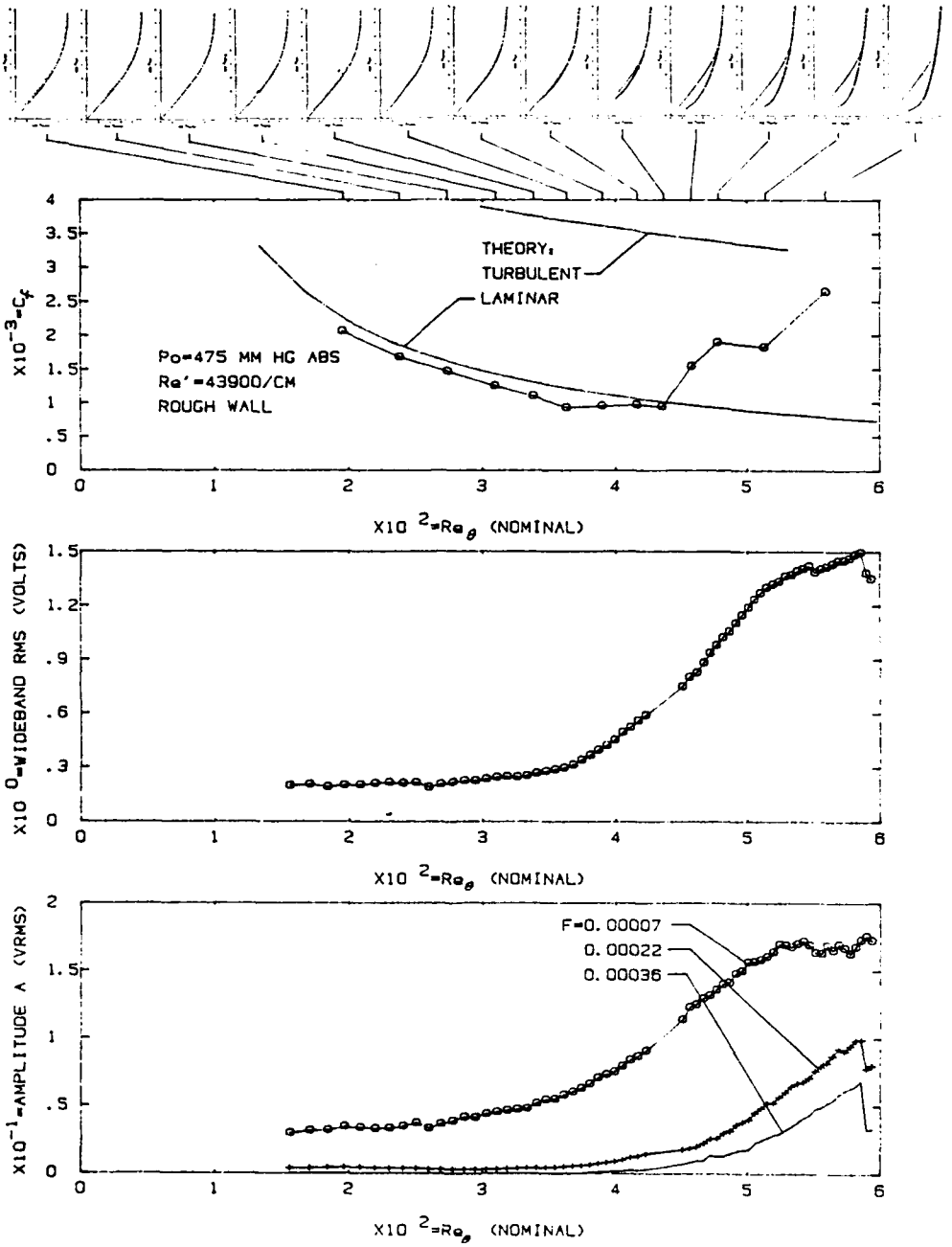

Figure 41. As in Figure 37; rough wall at 475 torr.

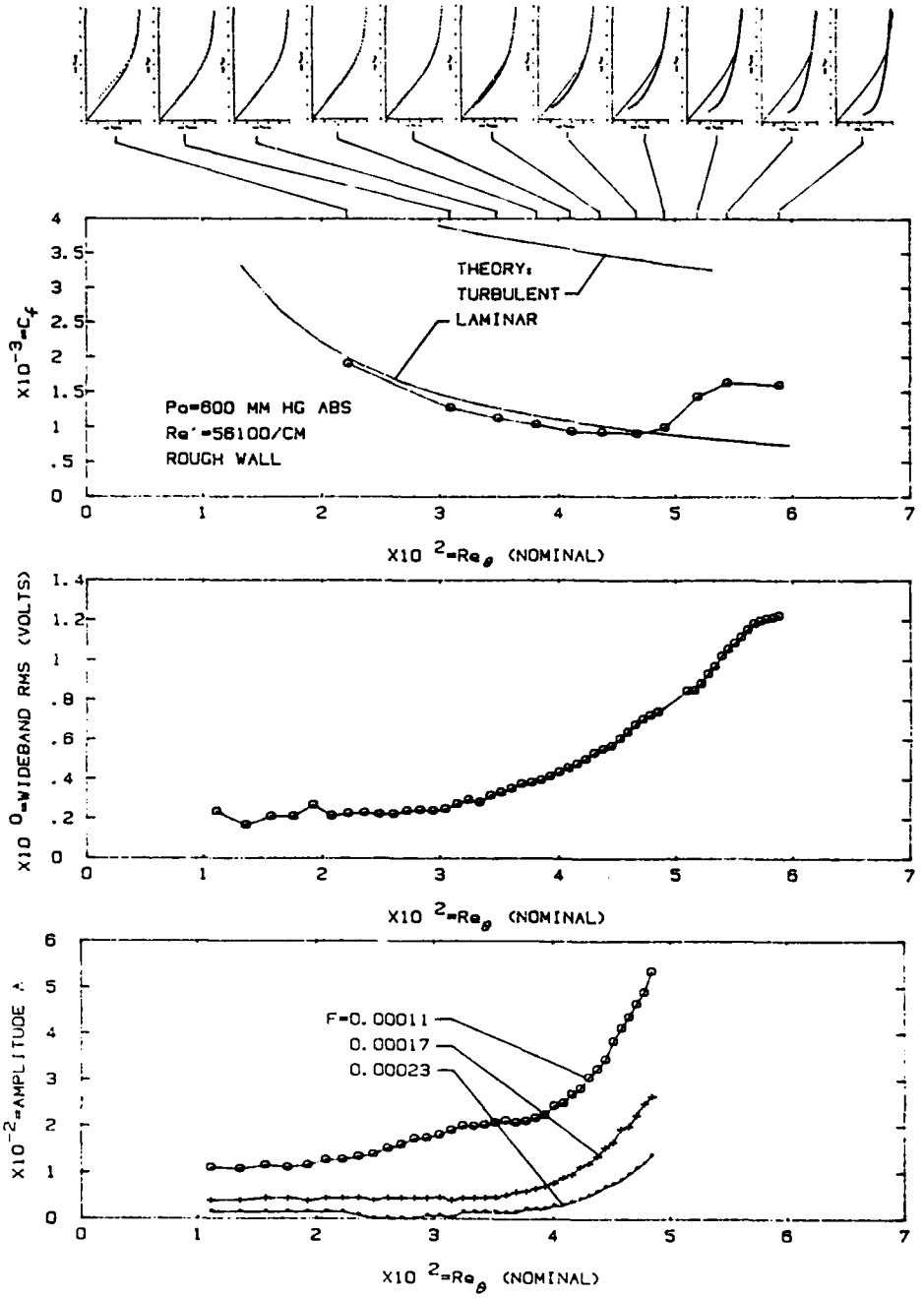

Figure 42. As in Figure 37; rough wall at 600 torr.

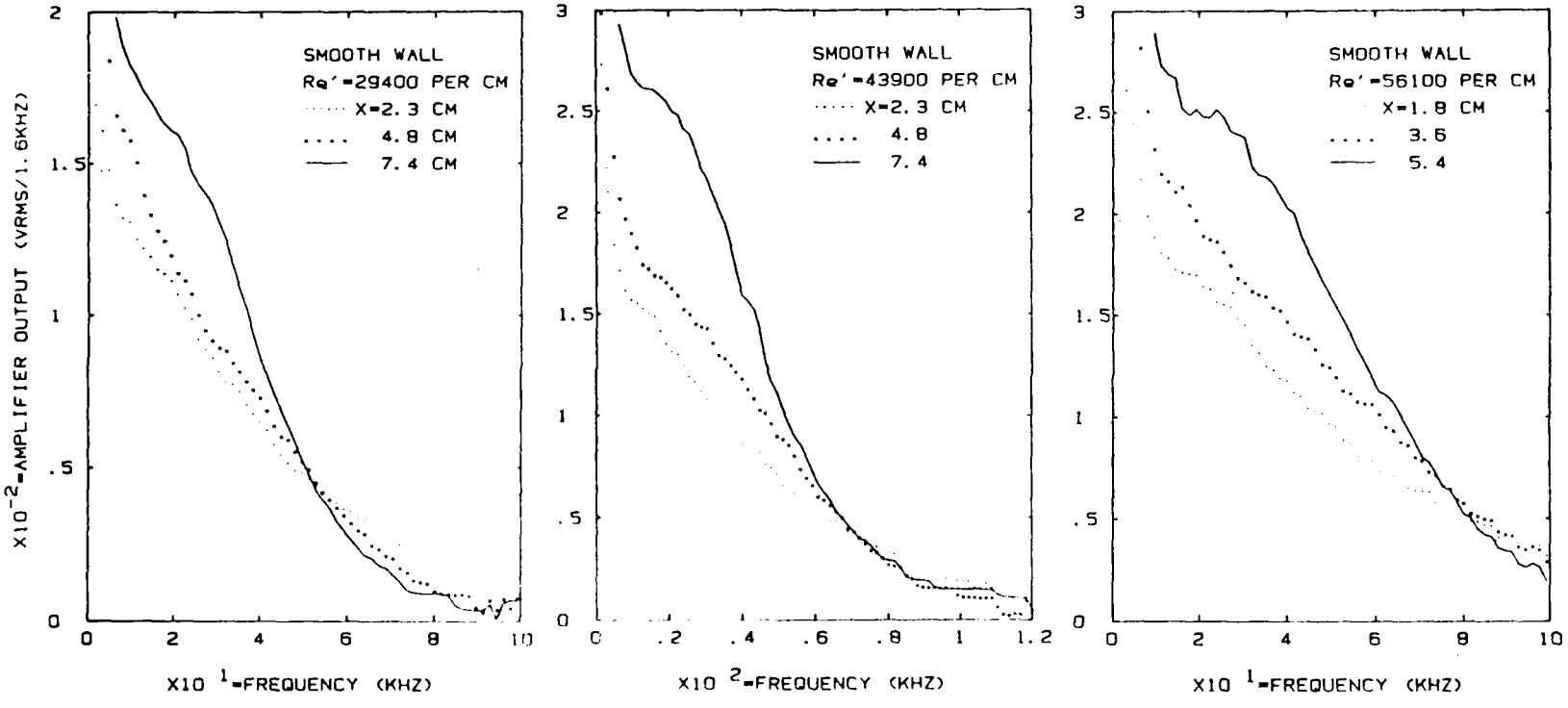

Figure 43. Typical spectra in the laminar boundary layer; smooth wall.

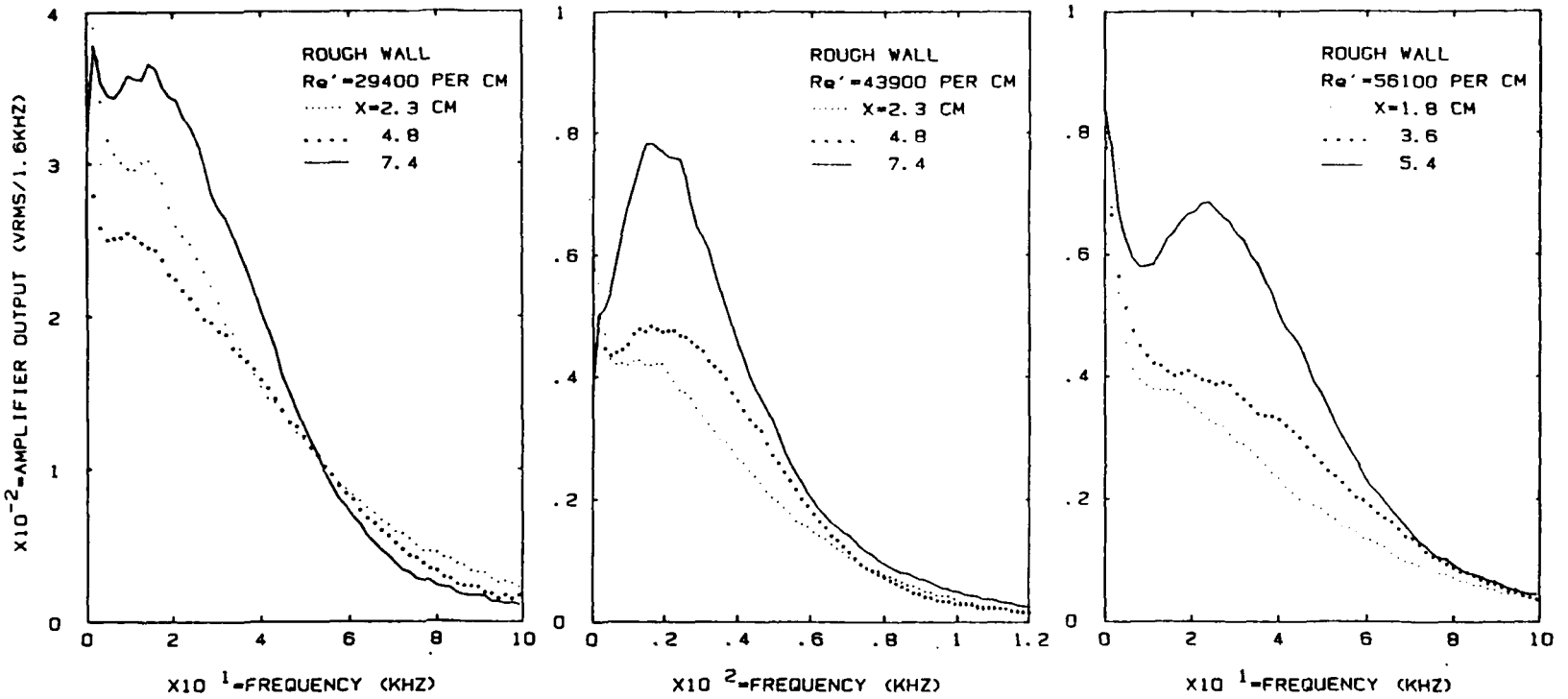

Figure 44. Typical spectra in the laminar boundary layer; rough wall.

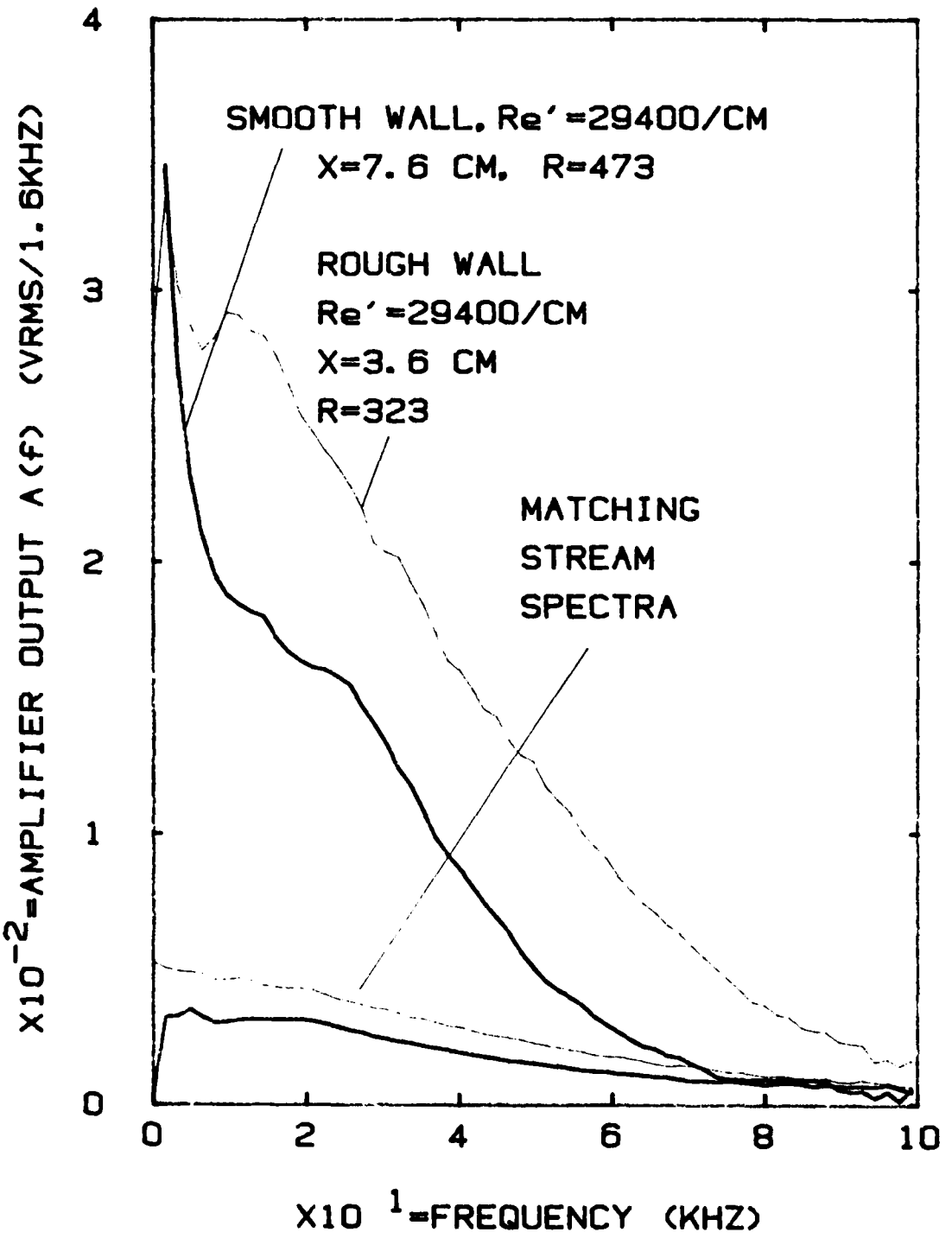

Figure 45. Typical differences between spectra in the boundary layer and in the stream.

Figure 46. Three-dimensional views of the spectrum development along the plate. Curves closest to the coordinate origin are nearest the leading edge.

ROUGH WALL, Po=350 MM
0.5 < X < 15.2 CM

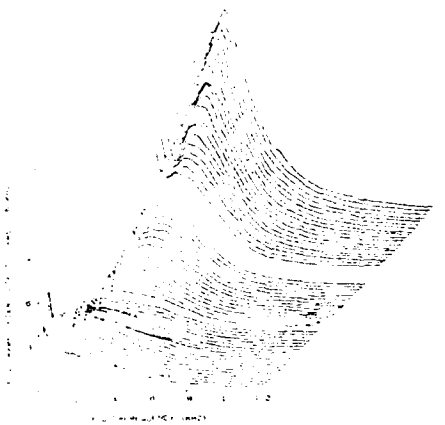

ROUGH WALL, Po=475 MM
1.3 < X < 16.5 CM

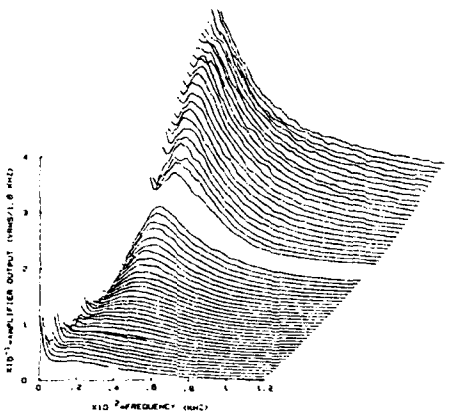

ROUGH WALL, Po=600 MM
0.5 < X < 14.2 CM

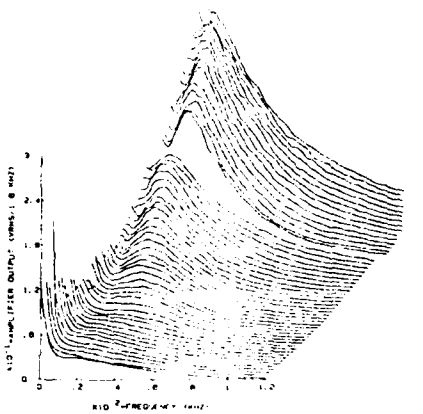

SMOOTH WALL, Po=350 MM
0.8 < X < 15 CM

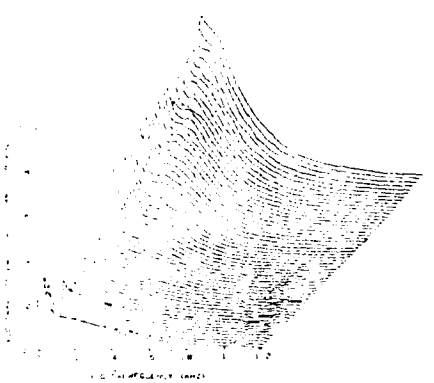

SMOOTH WALL, Po=475 MM
0.8 < X < 14.5 CM

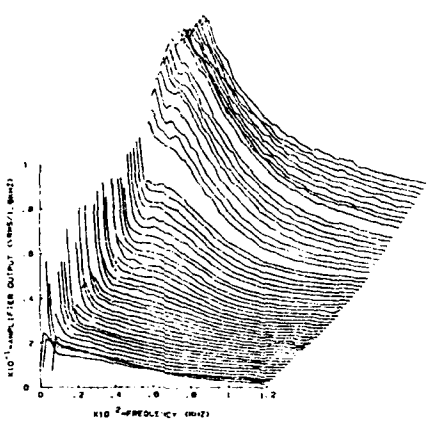

SMOOTH WALL, Po=600 MM
1 < X < 11.9 CM

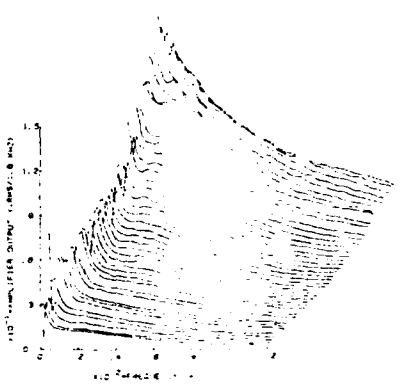

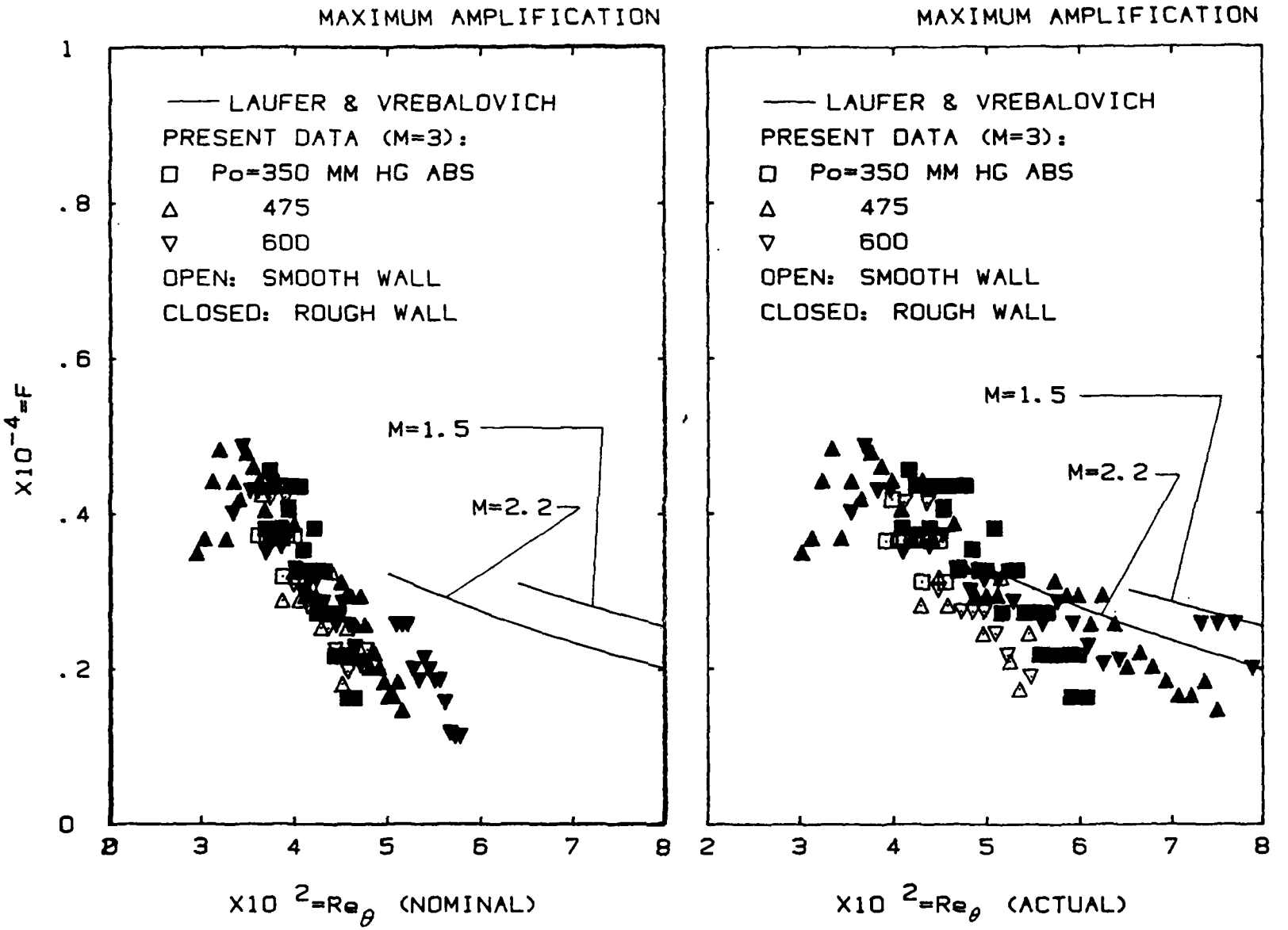

Figure 47. The "maximum amplification" (spectrum peak) data.

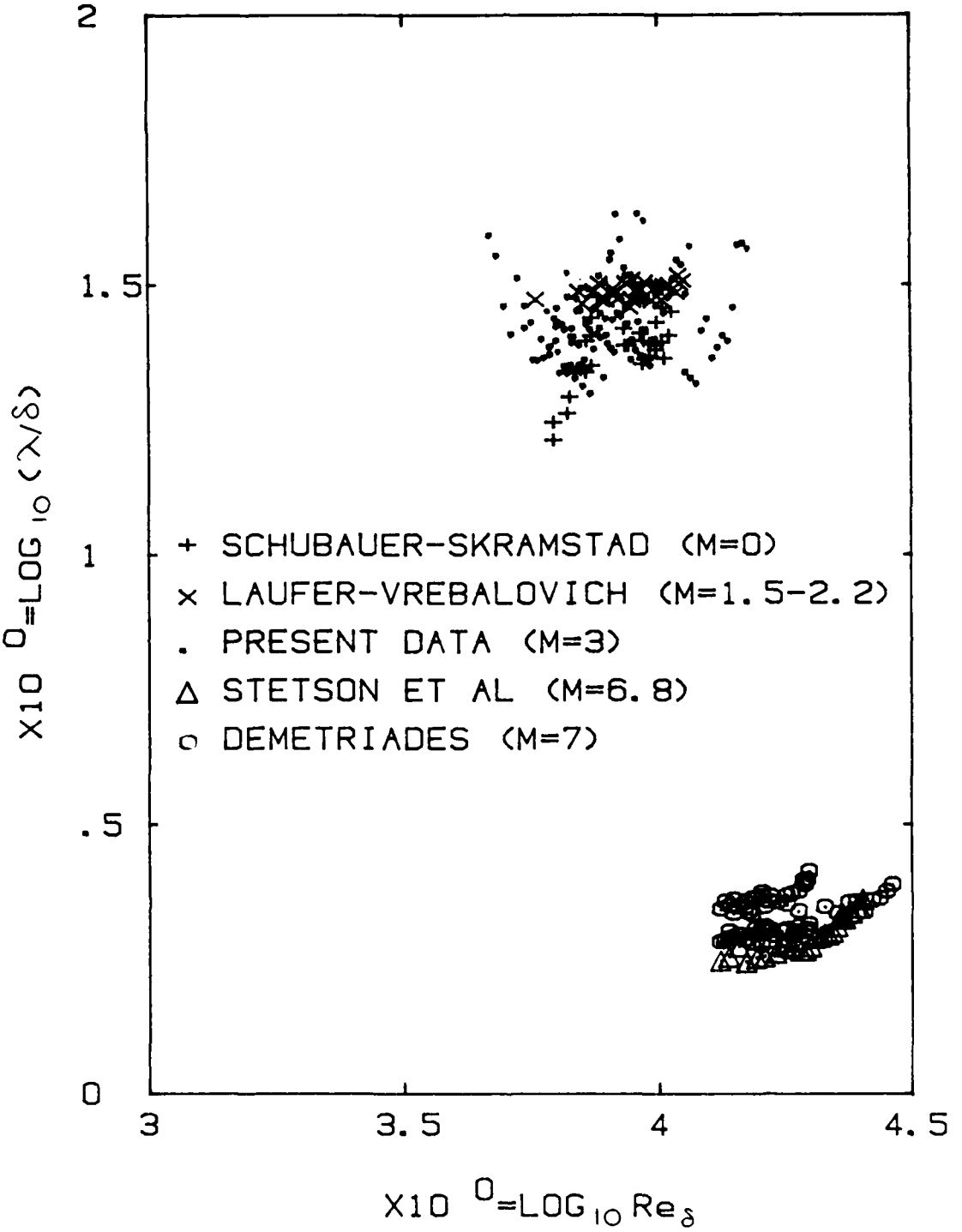

Figure 48. Prominent "T-S" wavelengths λ visible in boundary layers (here computed using the stream as opposed to the phase velocity) group themselves in clusters depending on the active instability mode. "Higher harmonic" cluster found at hypersonic speeds by Demetriades and later by Stetson et al with $\lambda < \delta$, lie below the bottom margin.

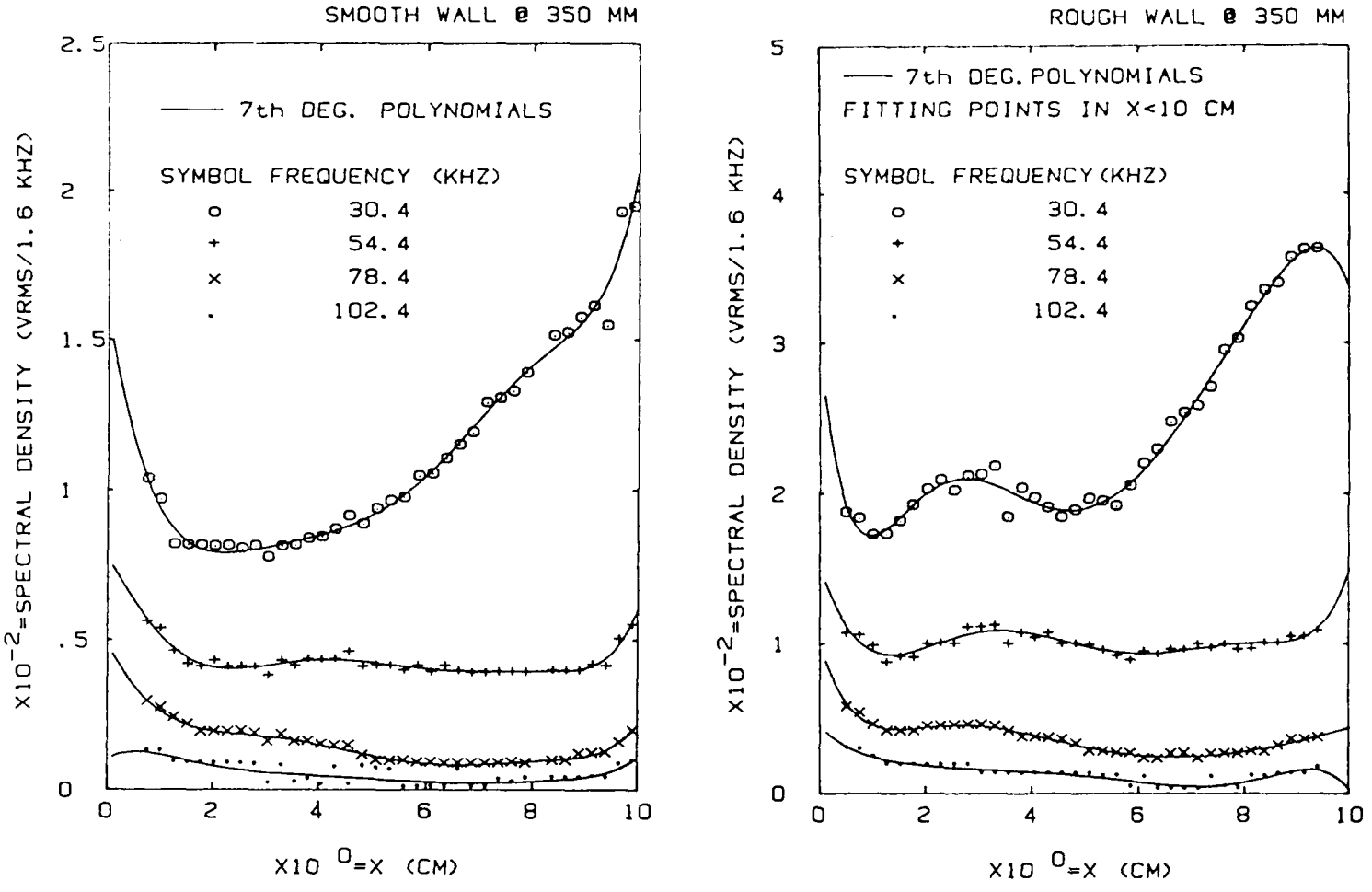

Figure 49. Typical curve-fits of A(x;f) at 350 torr.

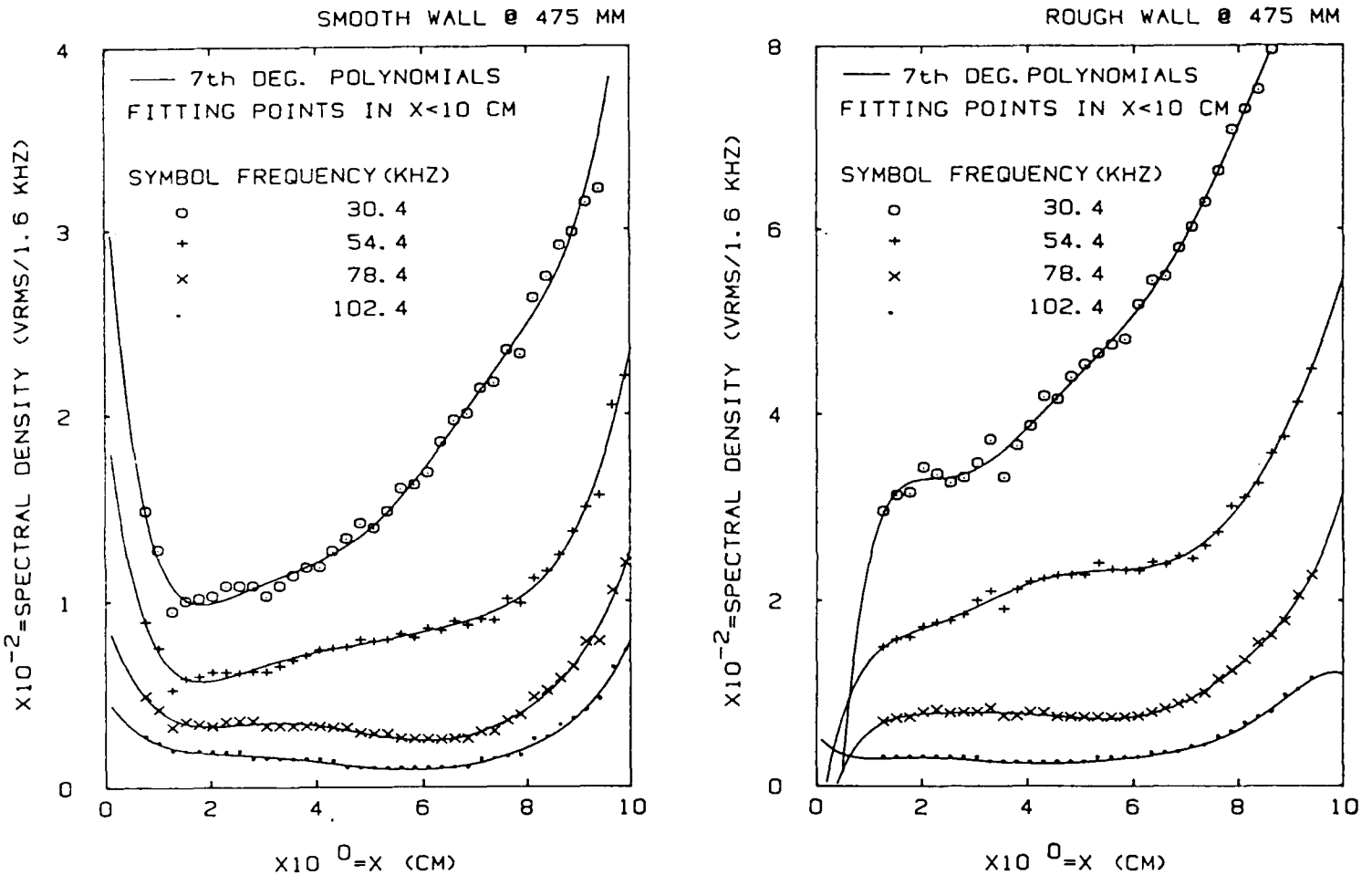

Figure 50. Typical curve-fits of A(x;f) at 475 torr.

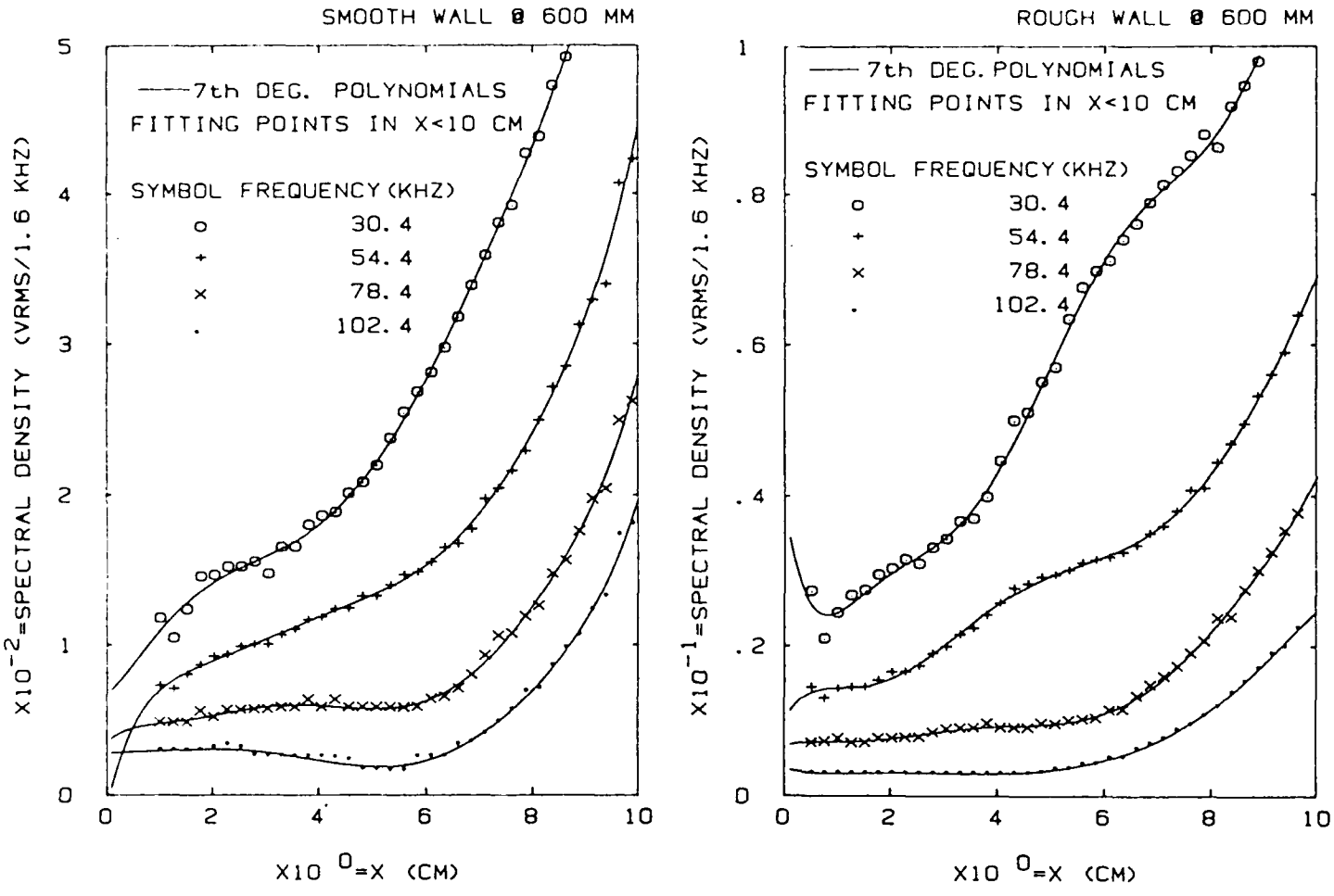

Figure 51. Typical curve-fits of A(x;f) at 600 torr.

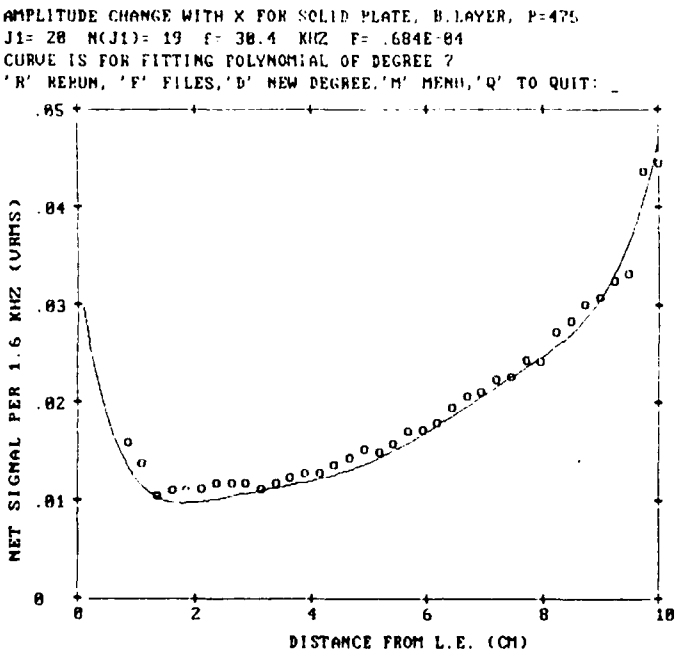

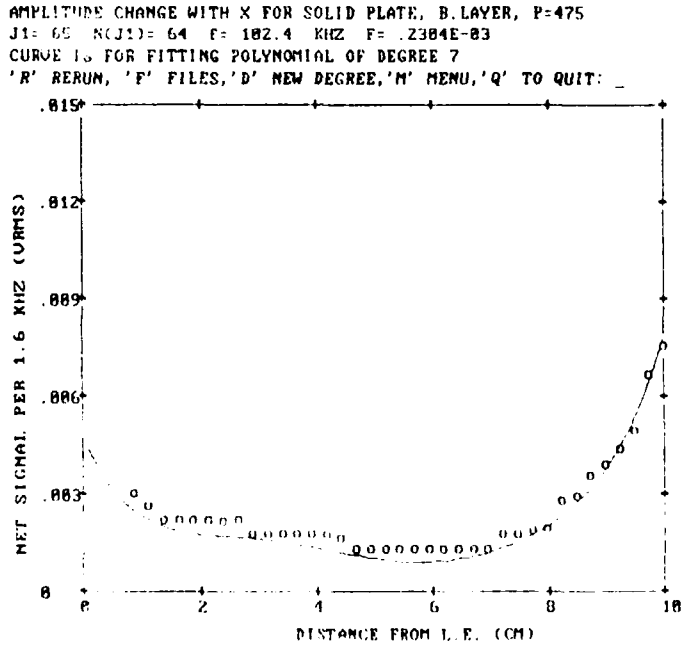

Figure 52. Demonstration of the data-reduction system performance: typical curve-fits of A(x;f) vs. x (STABLE02 Program, Option 9).

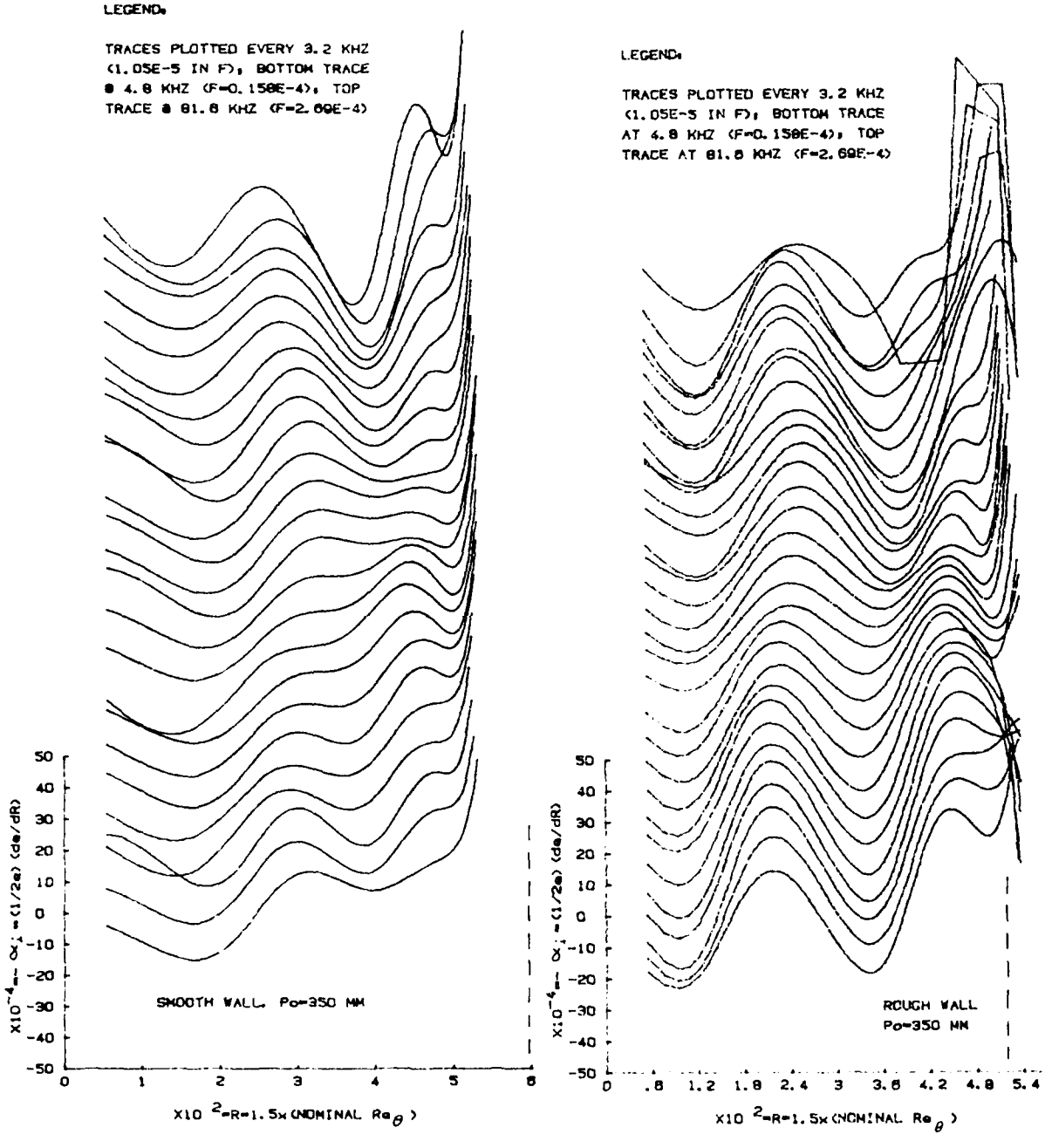

Figure 53. Development of amplification rate for various frequencies. First departure point is shown by dashed line on the right. Pressure is 350 torr.

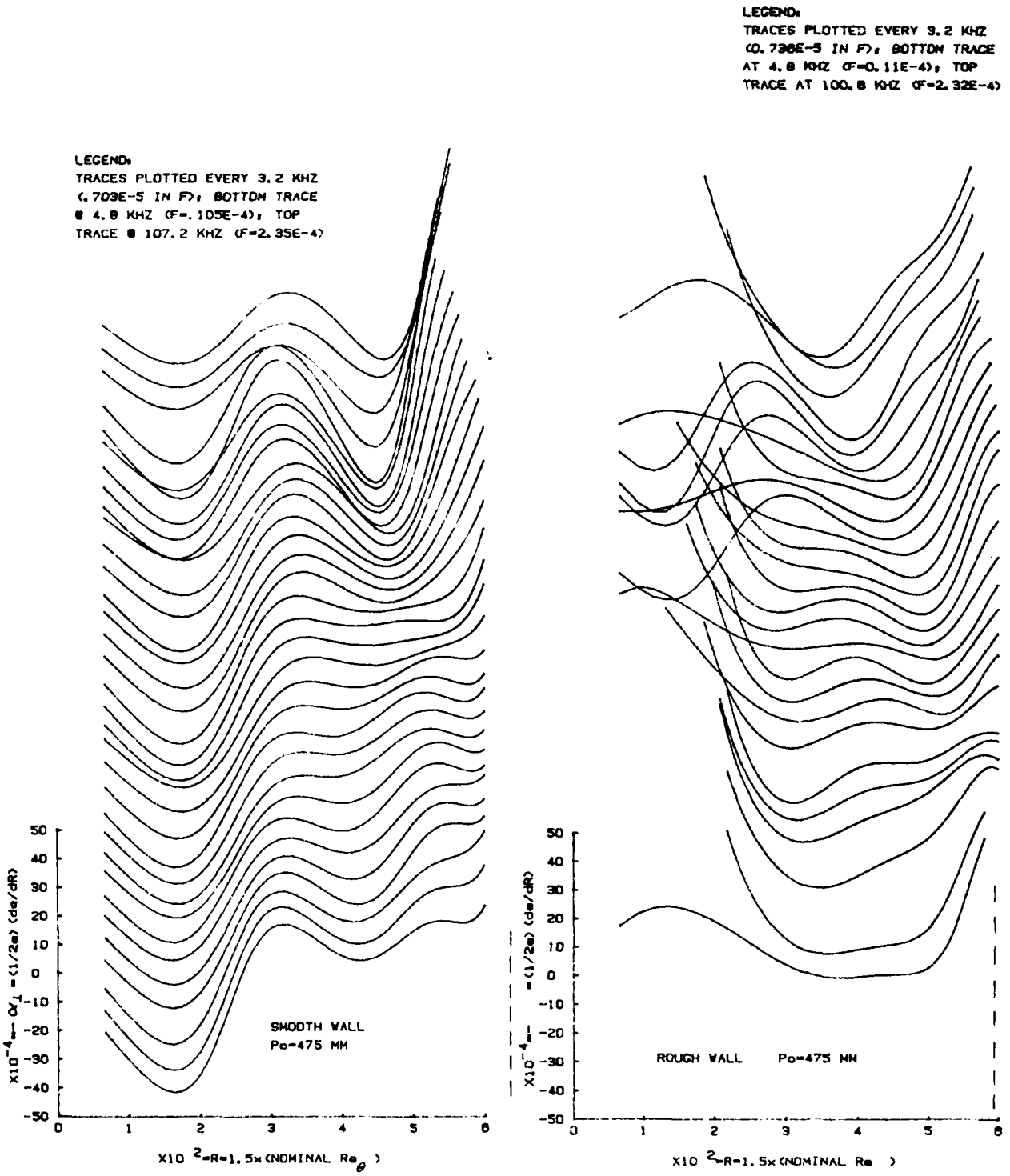

Figure 54. As in Figure 53 for 475 torr.

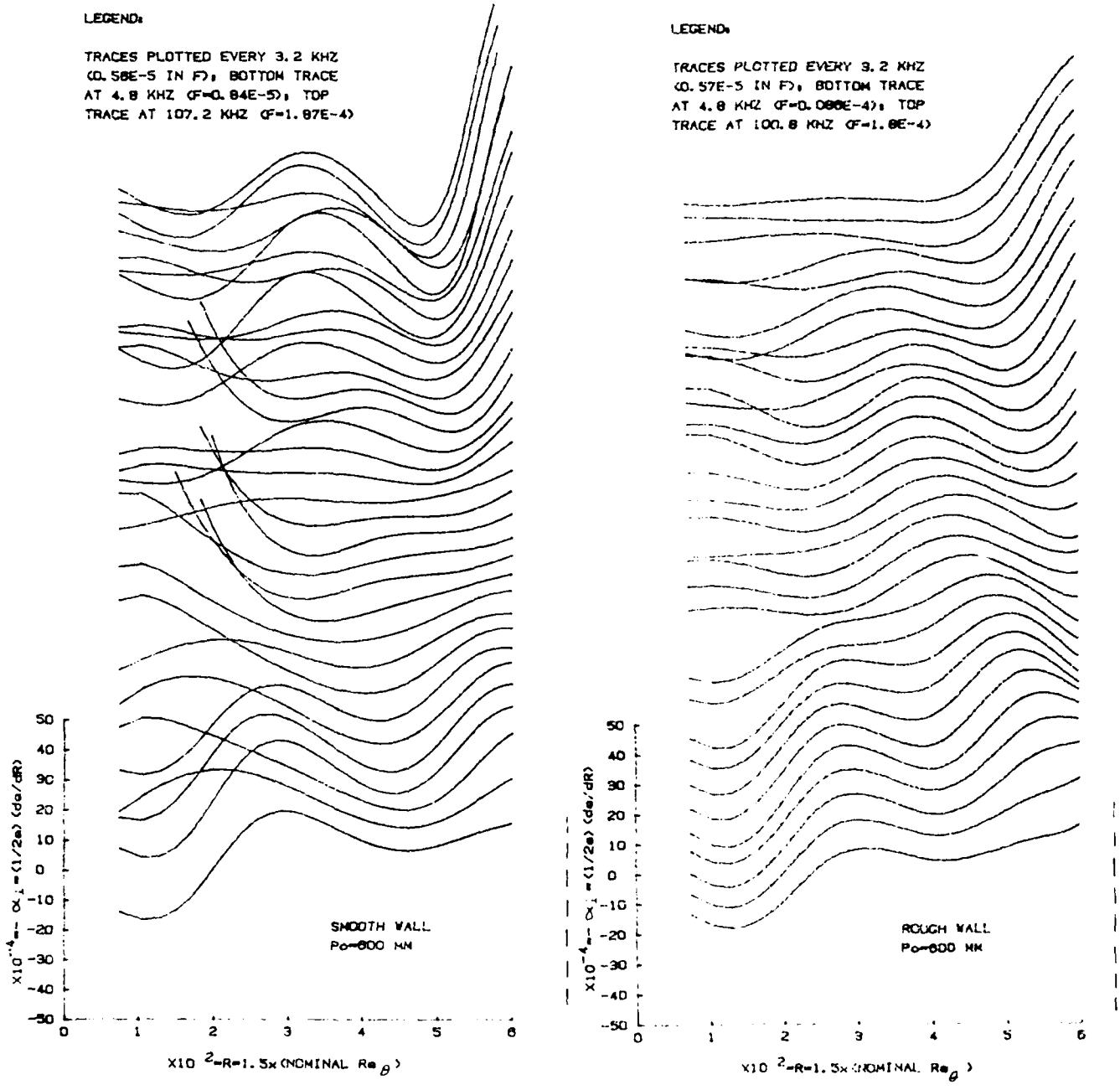

Figure 55. As in Figure 53 for 600 torr.

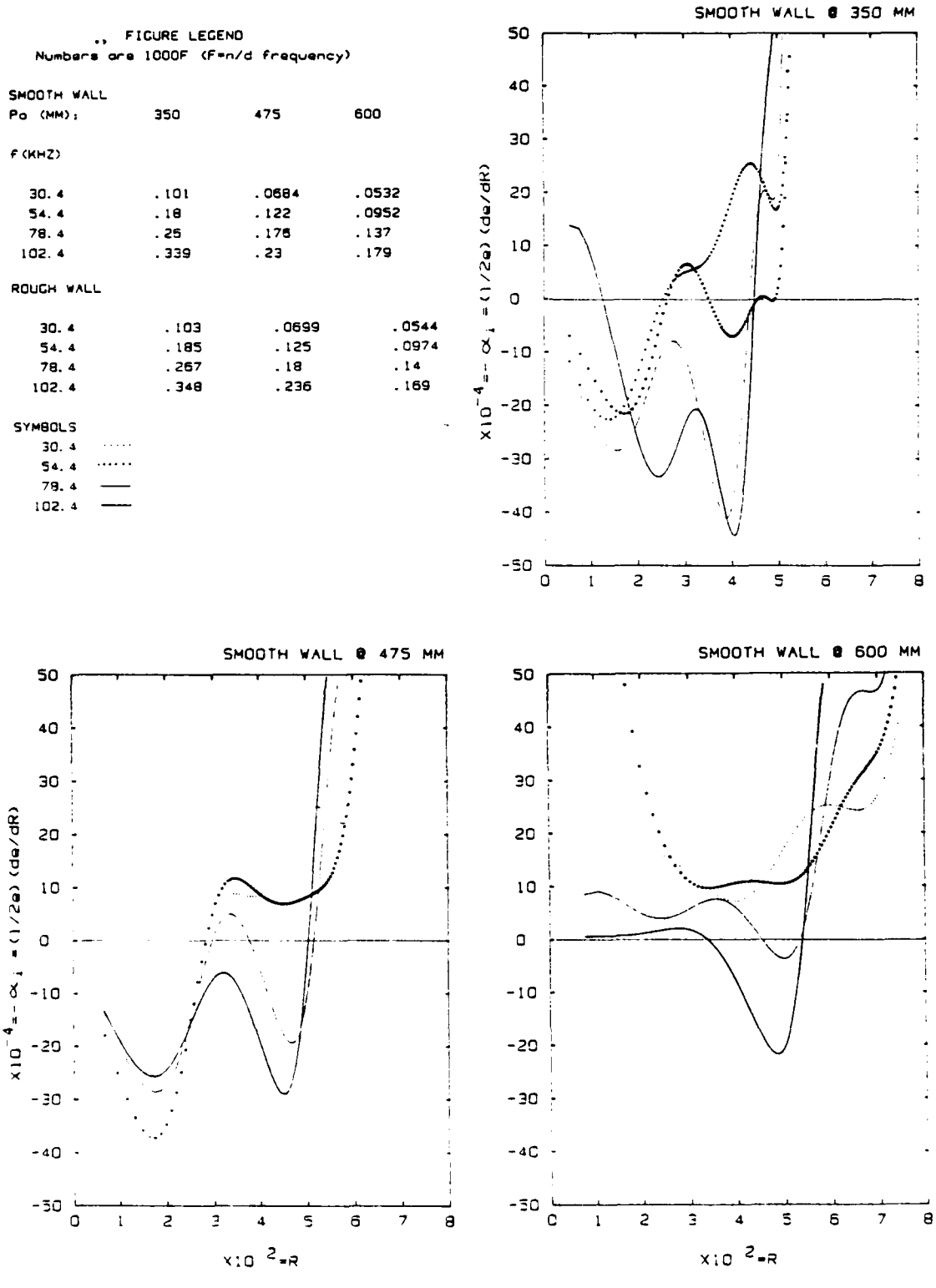

Figure 56. Smooth-wall amplification-rate dependence on R for various frequencies.

FIGURE LEGEND

Numbers are 1000F (F=n/d frequency)

SMOOTH WALL

Po (MM):	350	475	600
F(KHZ)			
30.4	.101	.0684	.0532
54.4	.18	.122	.0952
78.4	.26	.176	.137
102.4	.339	.23	.179

ROUGH WALL

30.4	.103	.0699	.0544
54.4	.185	.125	.0974
78.4	.267	.18	.14
102.4	.348	.236	.169

SYMBOLS

30.4 ·····

54.4 ·····

78.4 ——

102.4 ——

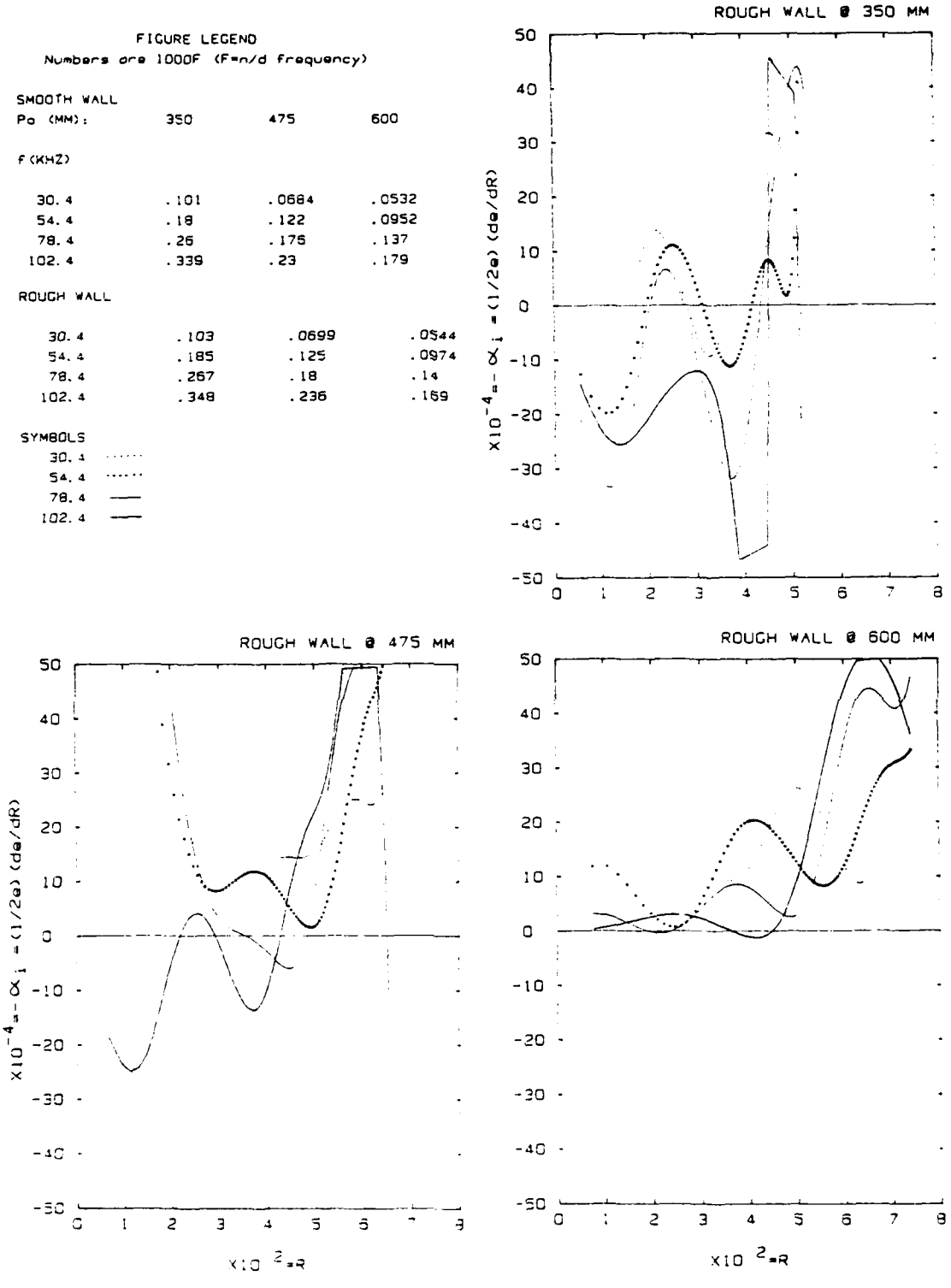

Figure 57. Rough-wall amplification-rate dependence on R for various frequencies.

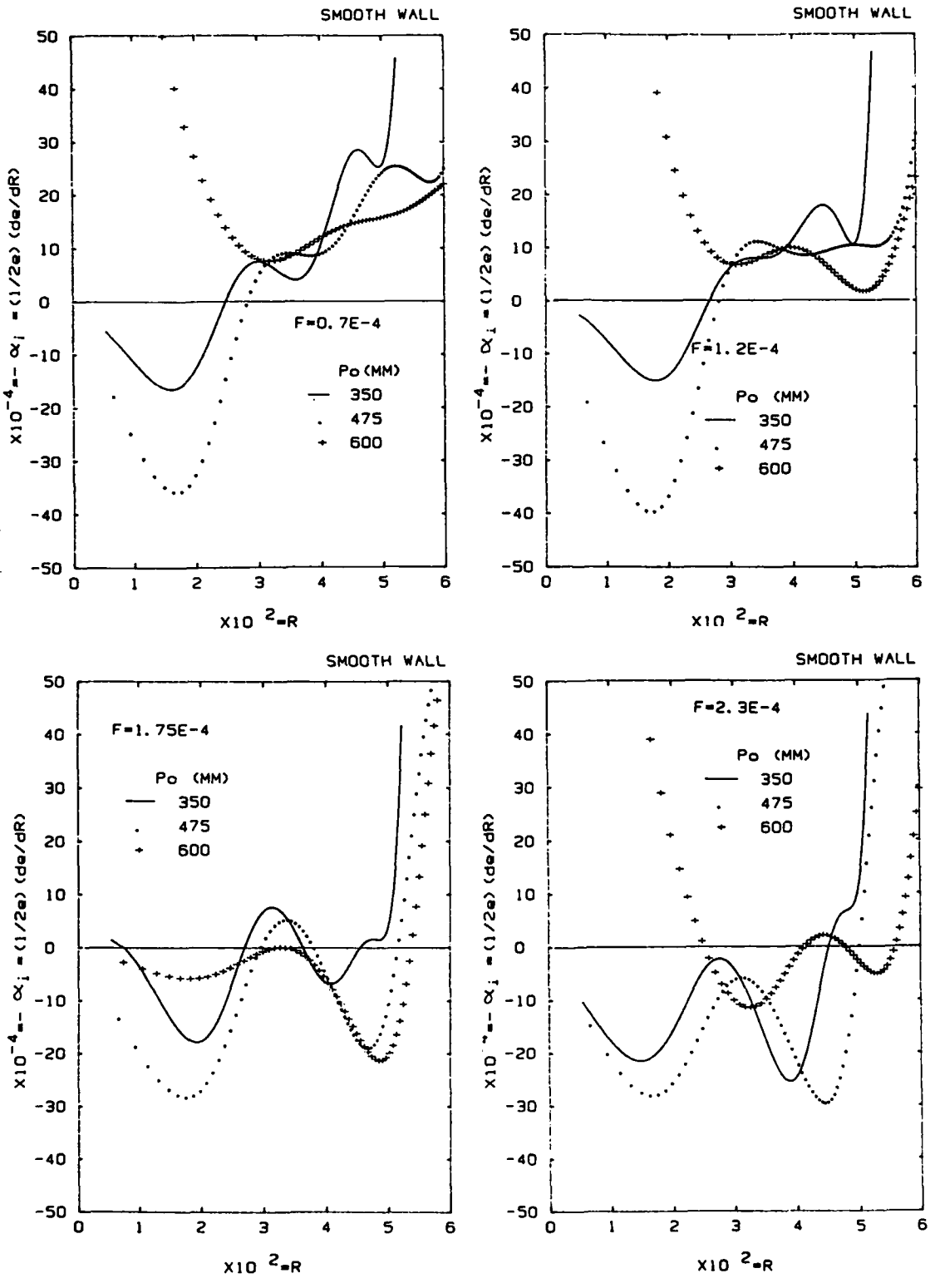

Figure 58. Effect of Unit Re^{θ} on amplification rates, smooth wall.

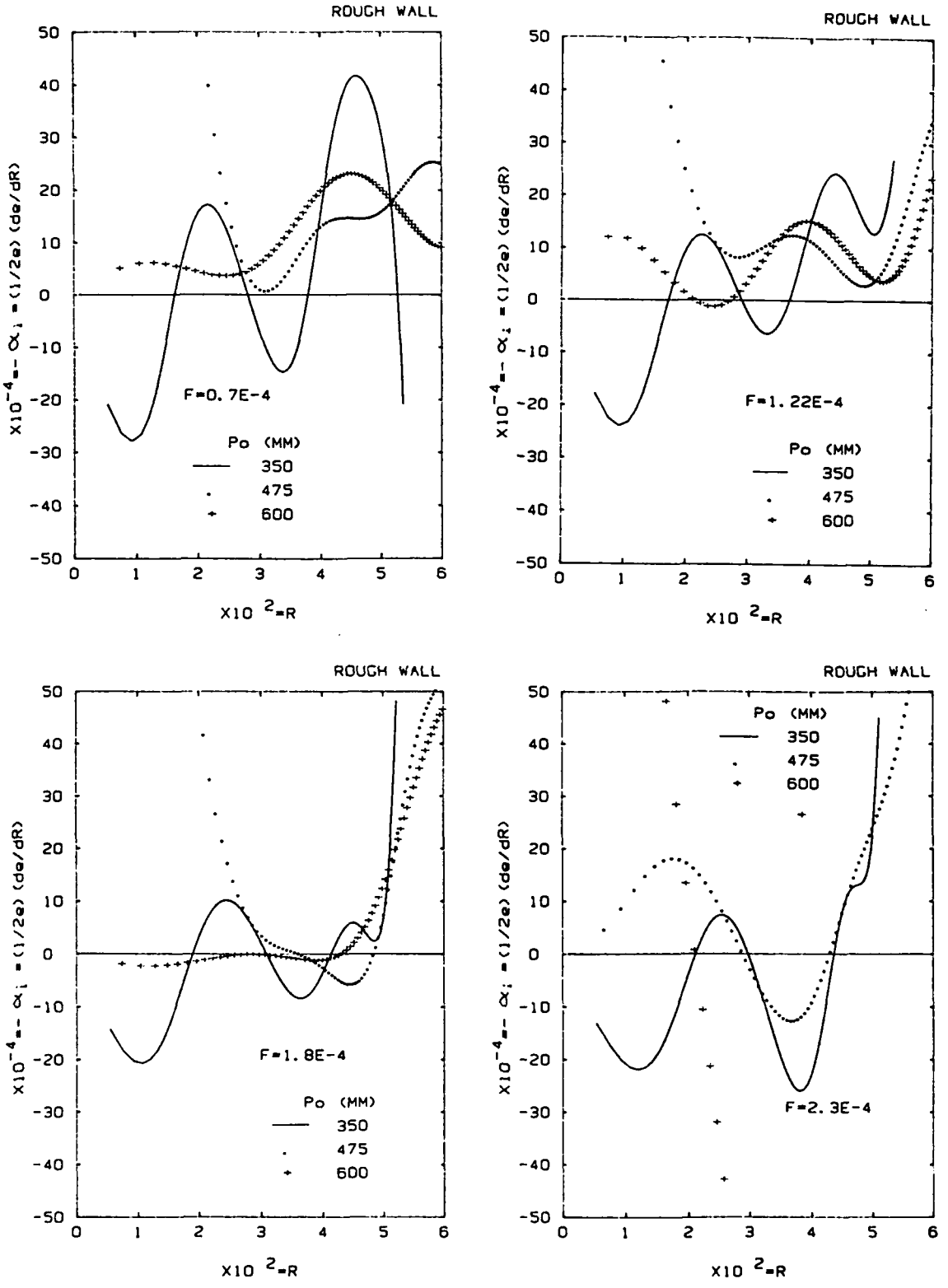

Figure 59. Effect of Unit Re' on amplification rates, rough wall.

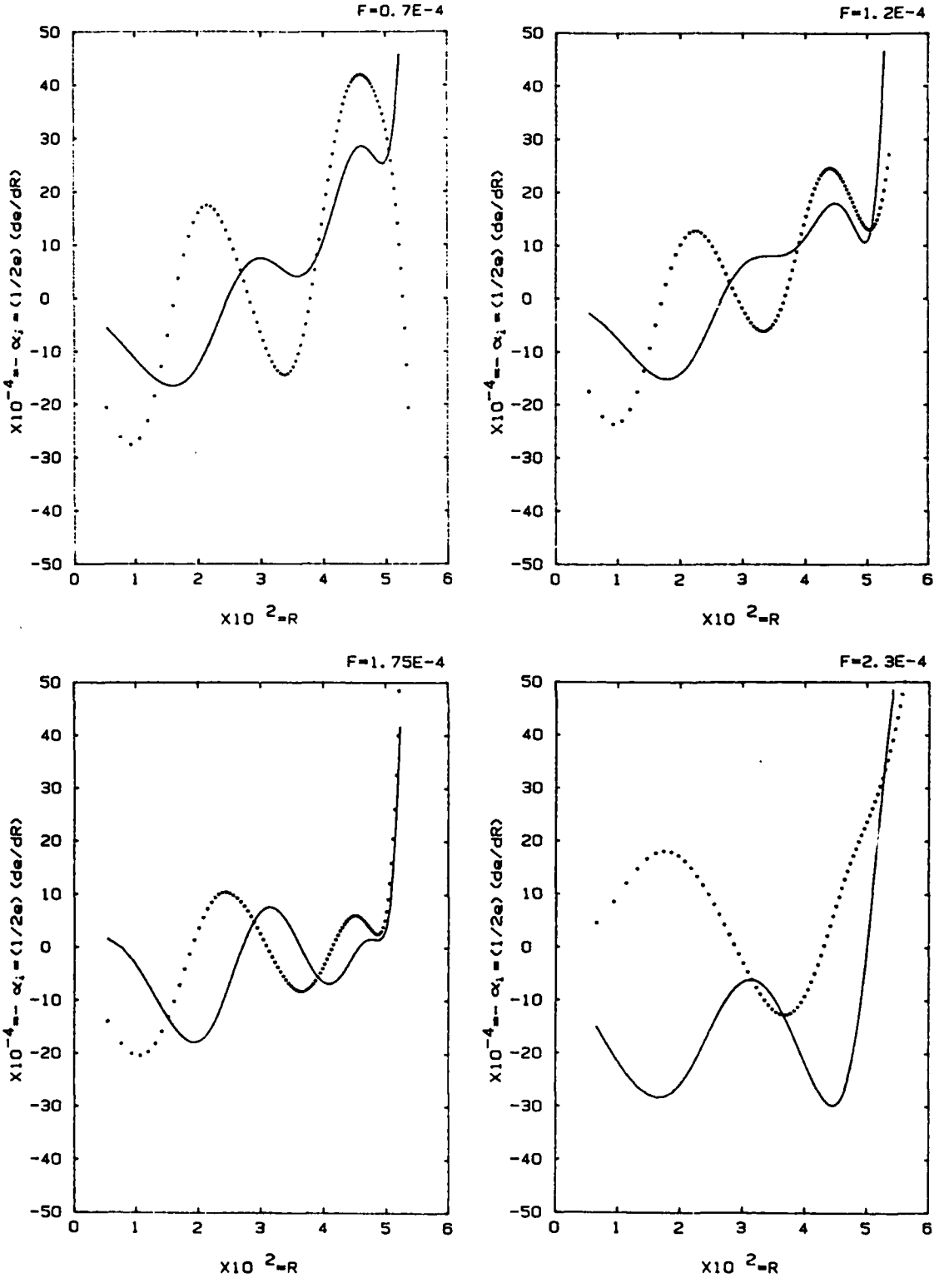

Figure 60. Typical amplification rates for the smooth (solid) and rough (dotted) walls.

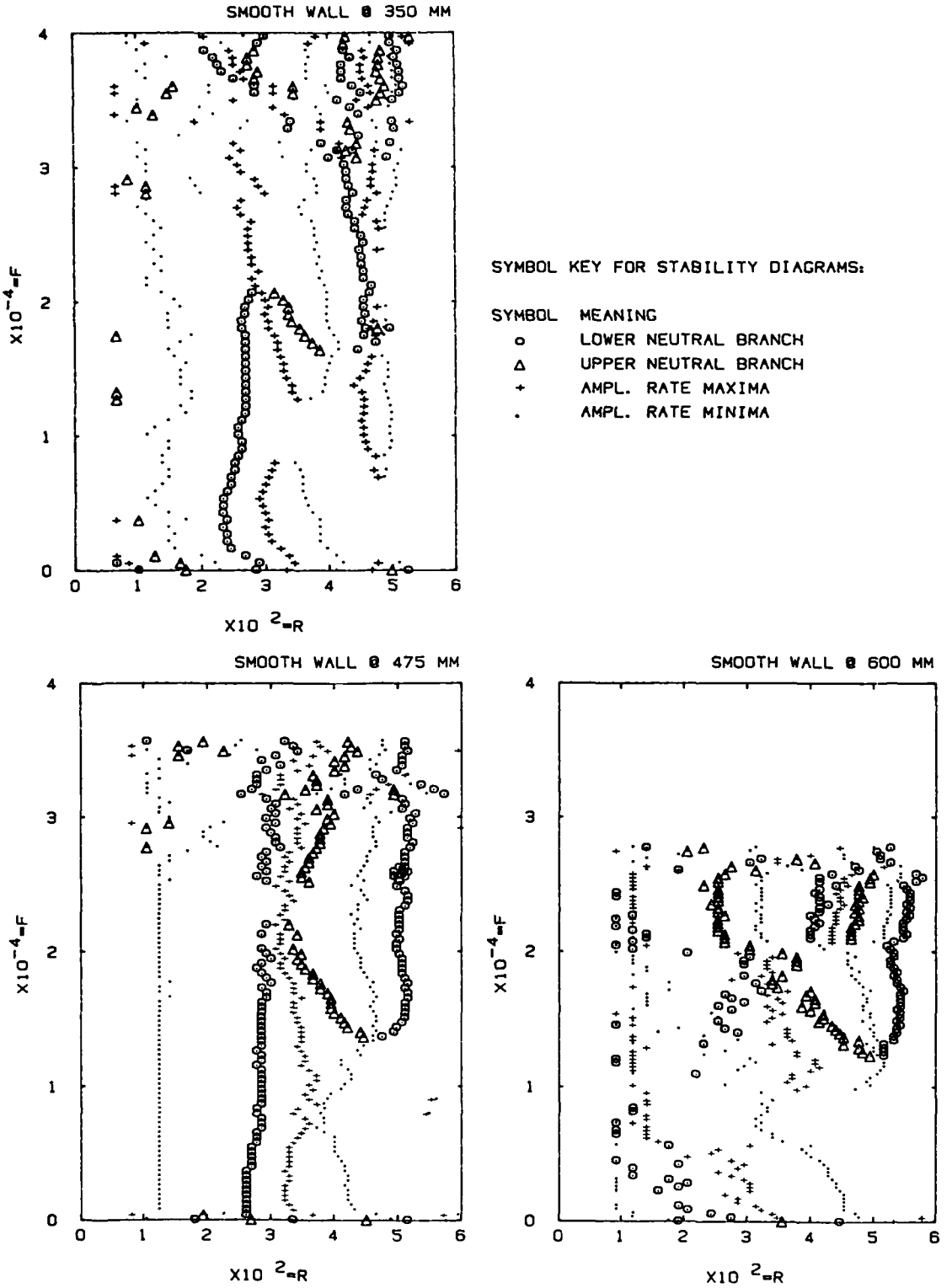

Figure 61. Unedited stability diagrams for the smooth wall.

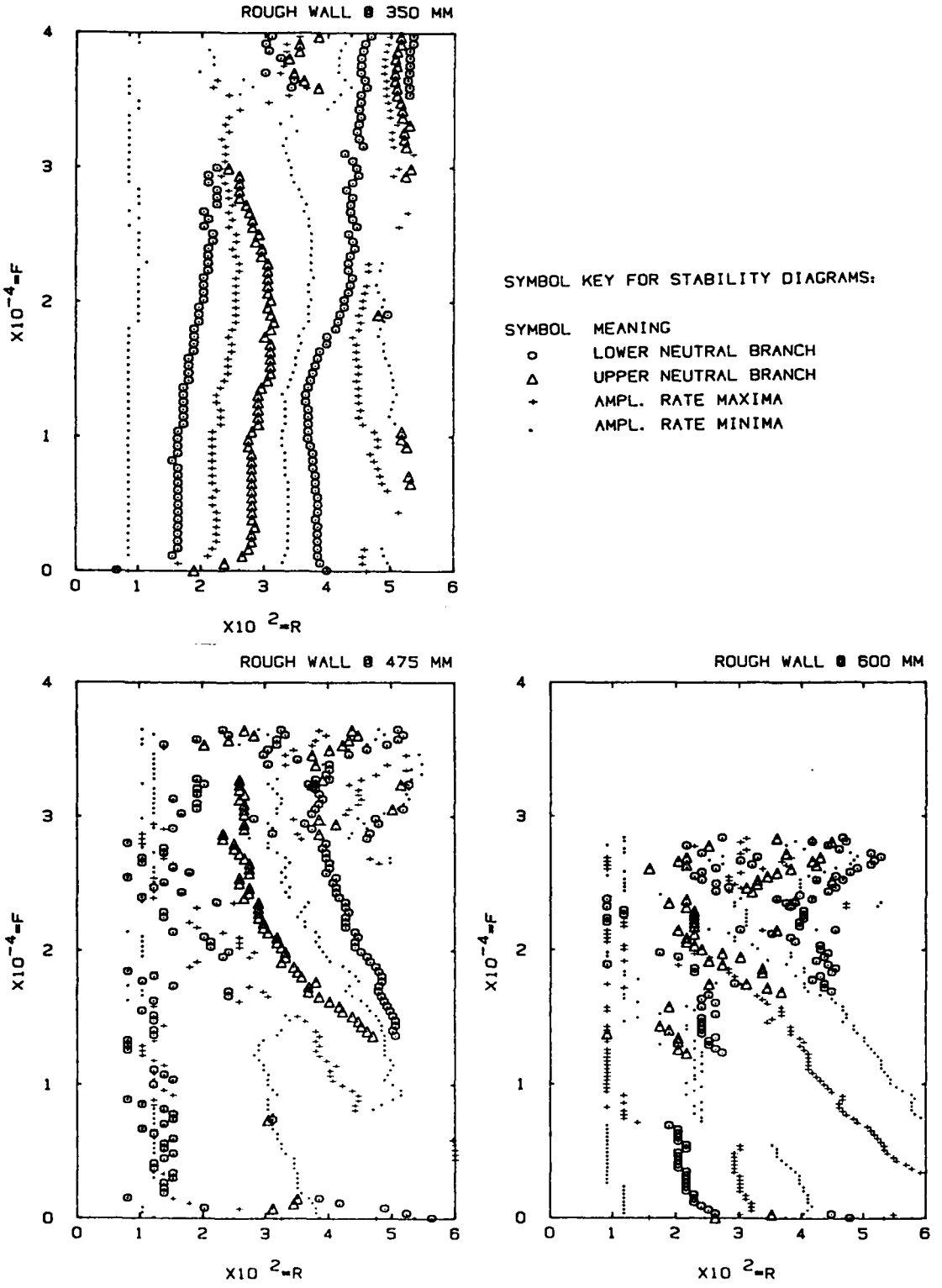

Figure 62. Unedited stability diagram for the rough wall.

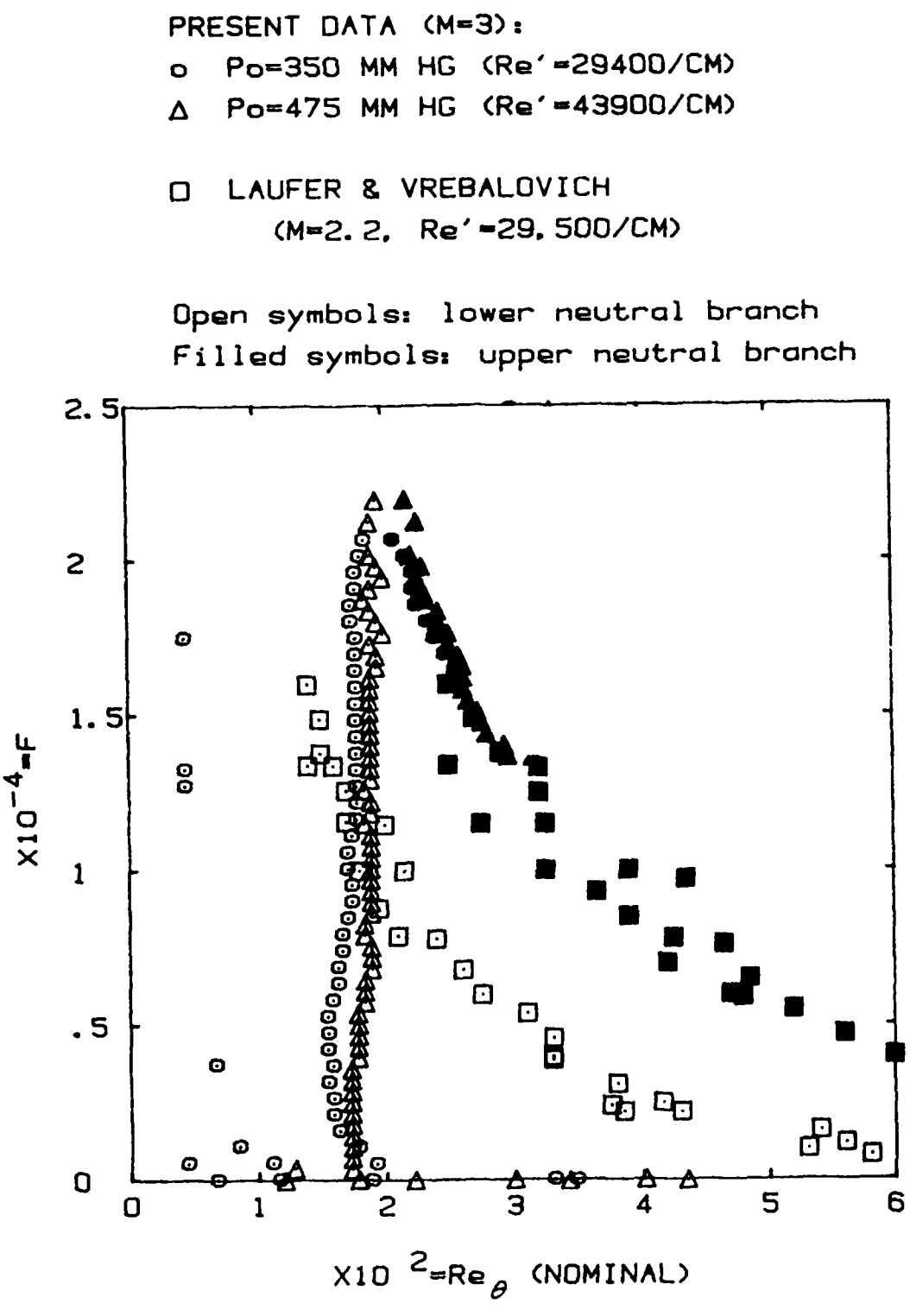

Figure 63. First mode stability.

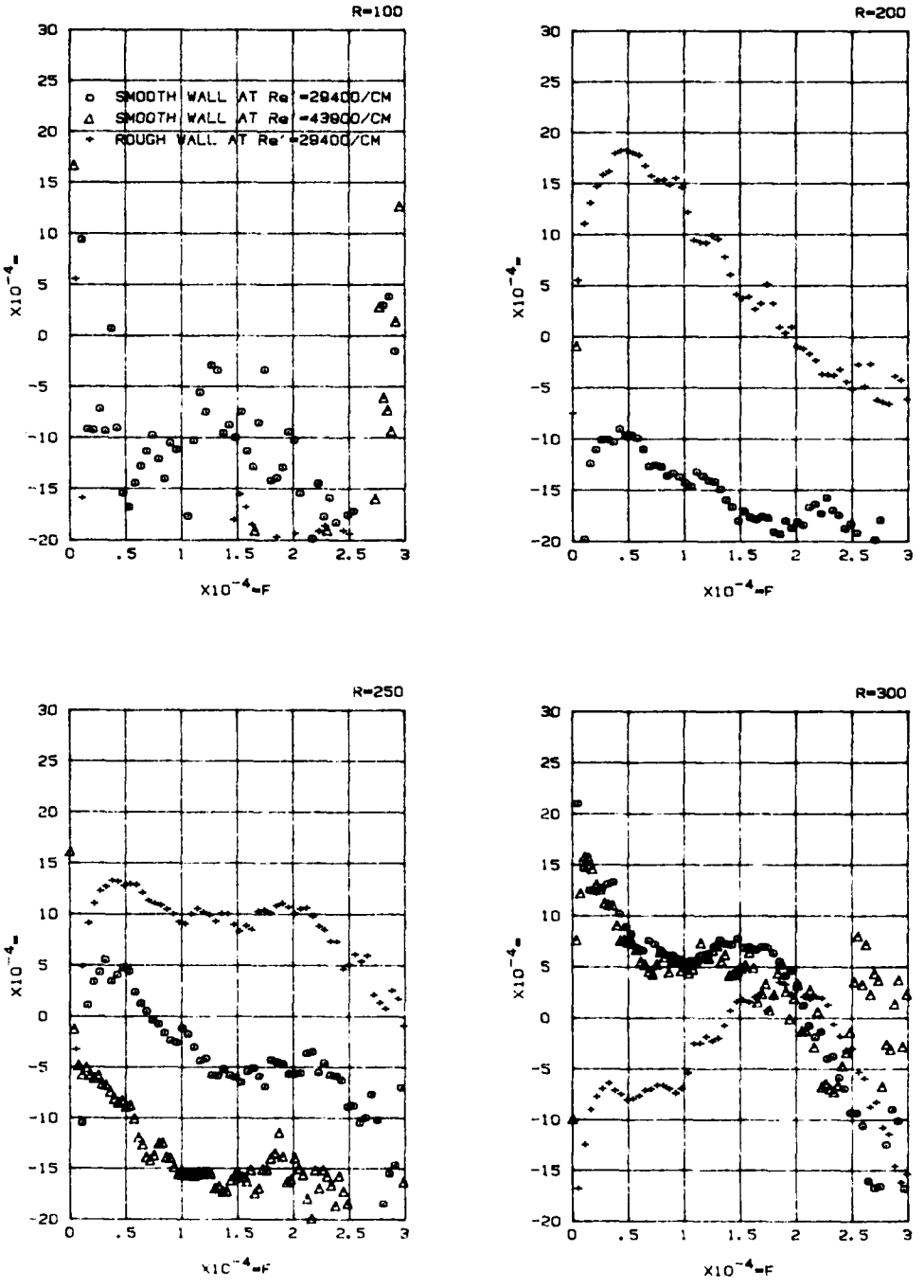

Figure 64. Unedited amplification-rate spectra (typical).

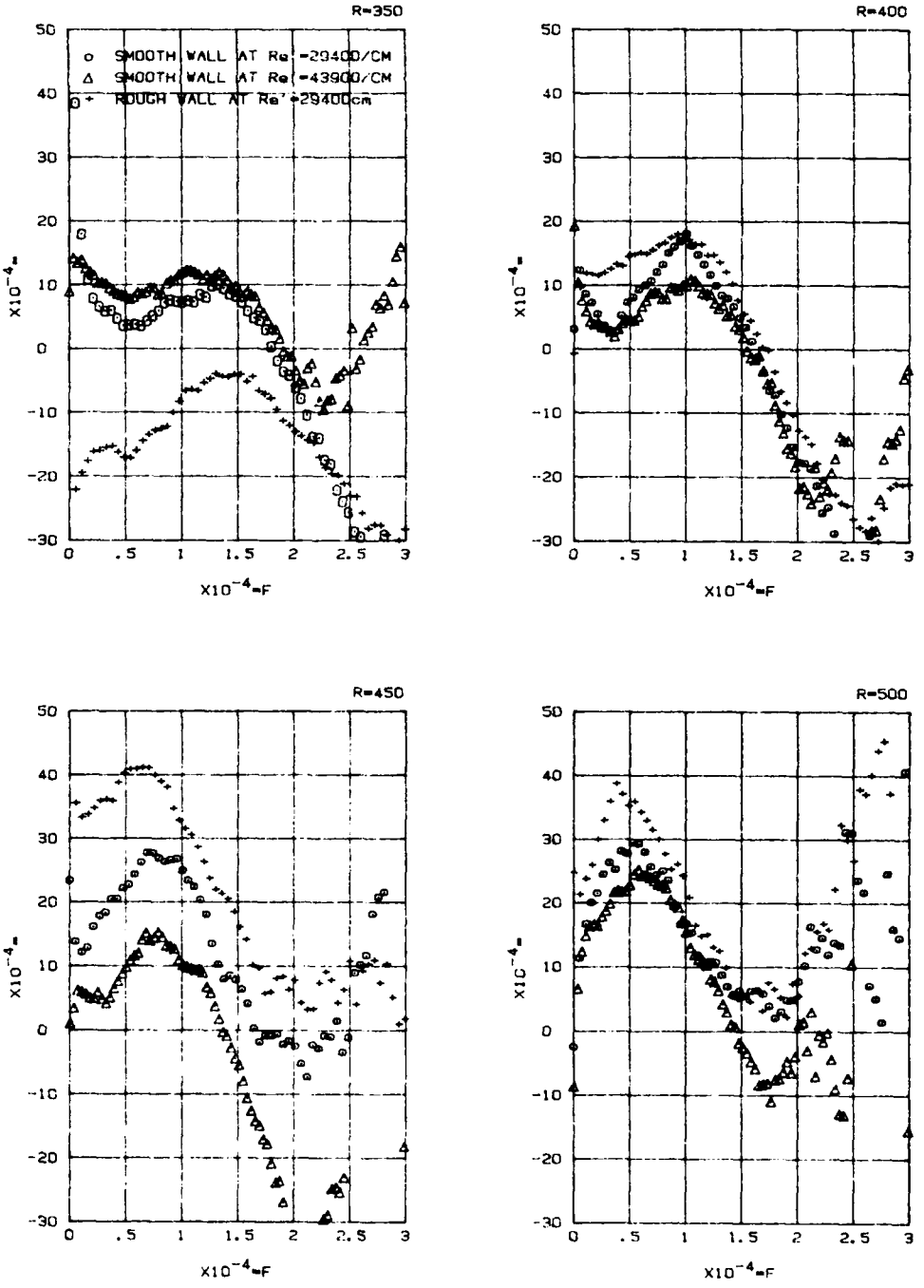

Figure 65. Unedited amplification-rate spectra (typical).

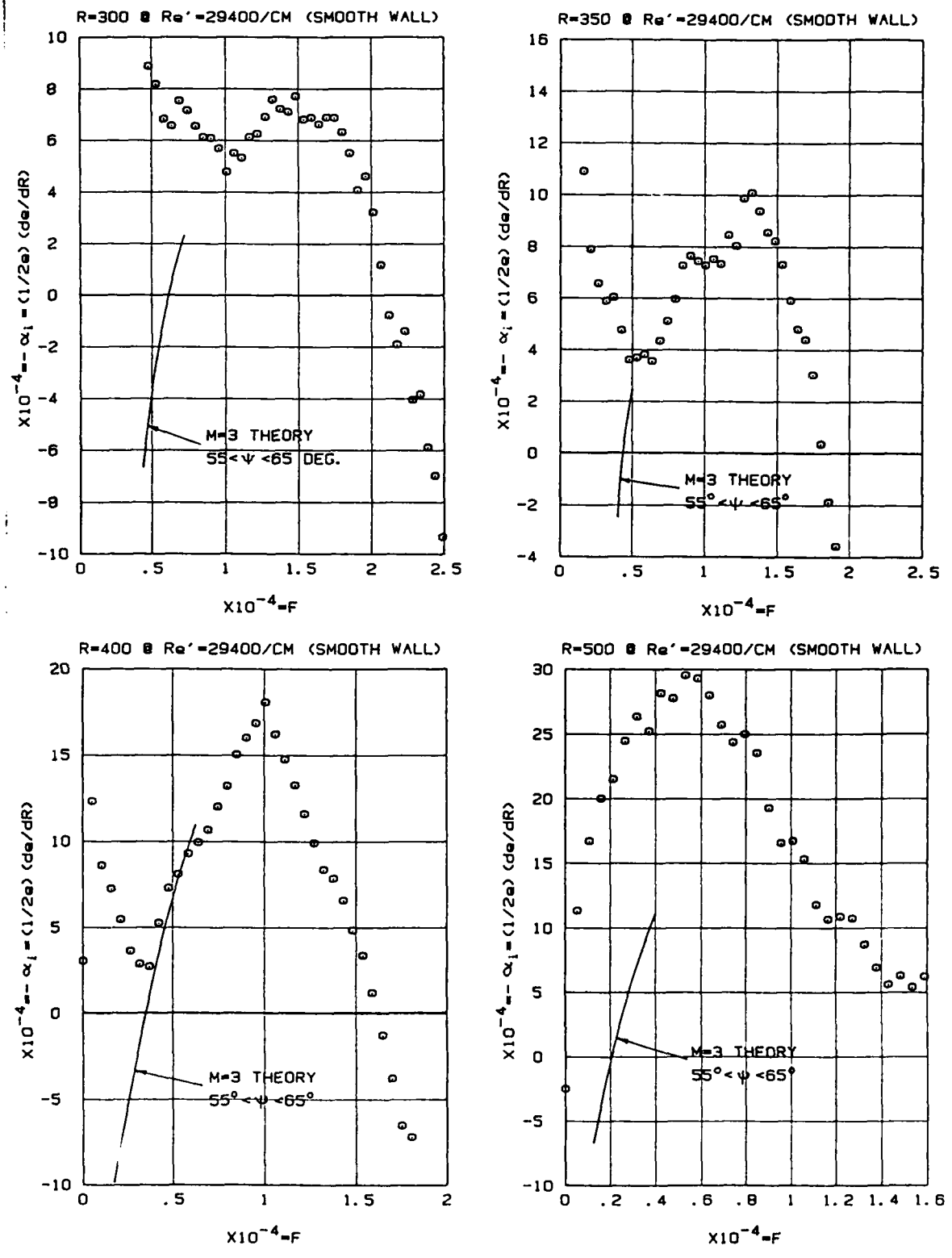

Figure 66. First-mode amplification-spectrum data compared with numerical results ("theory") supplied by Mack. Low-frequency anomaly has been also previously reported. High-R spectrum reflects contamination by the second mode.

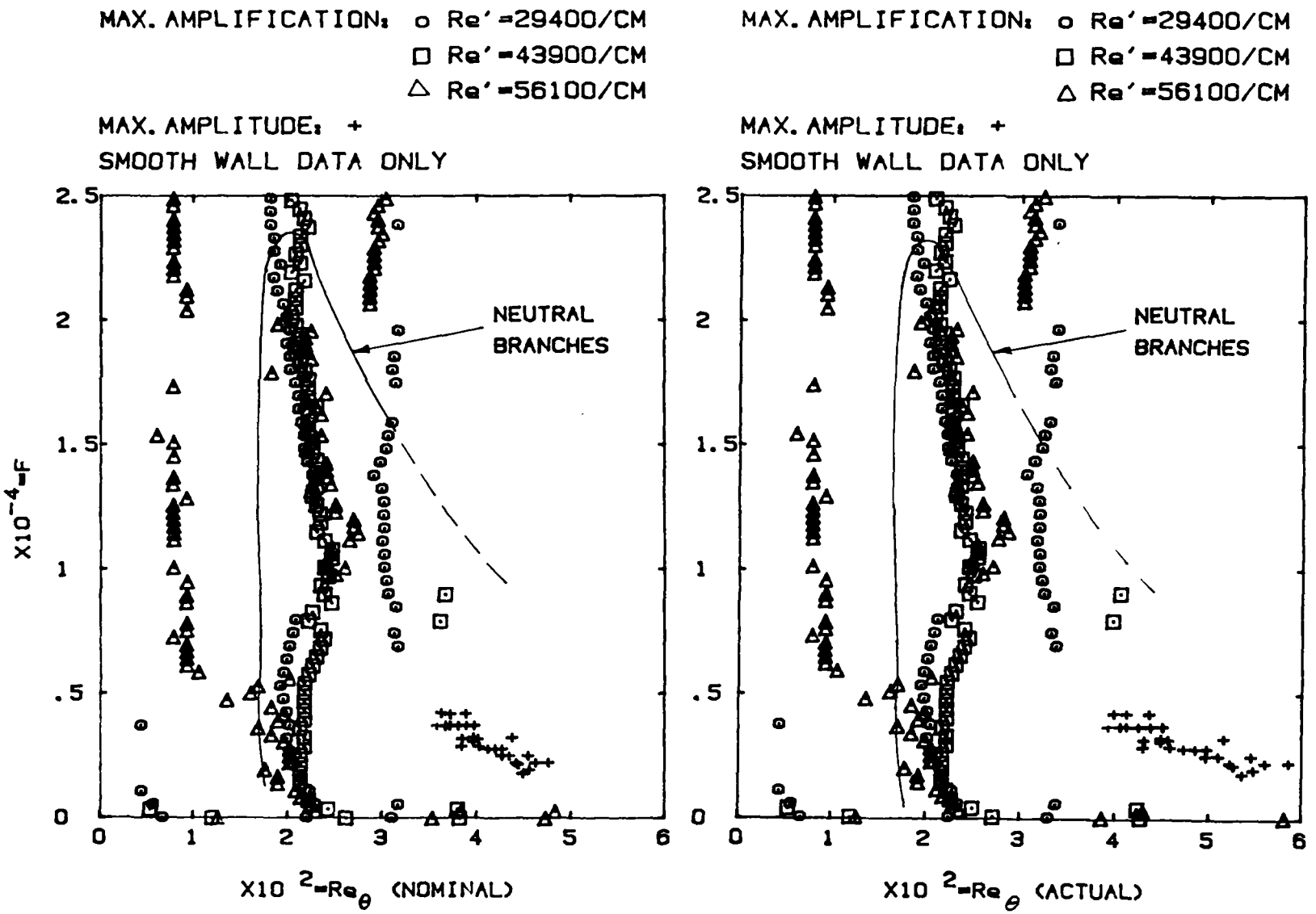

Figure 67. Maximum amplification-rate points, smooth wall.

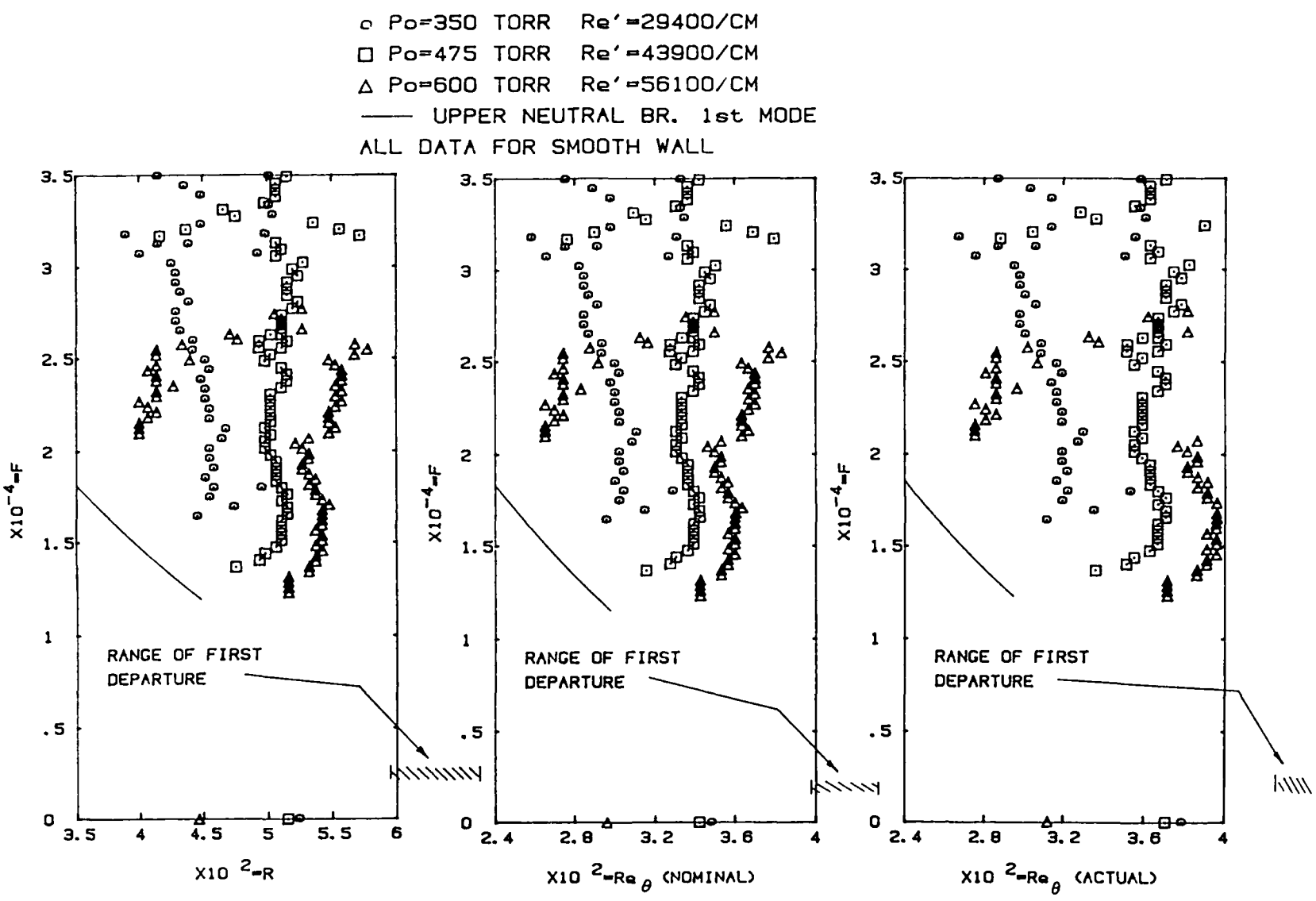

Figure 68. Lower neutral branch of the second mode, smooth wall.

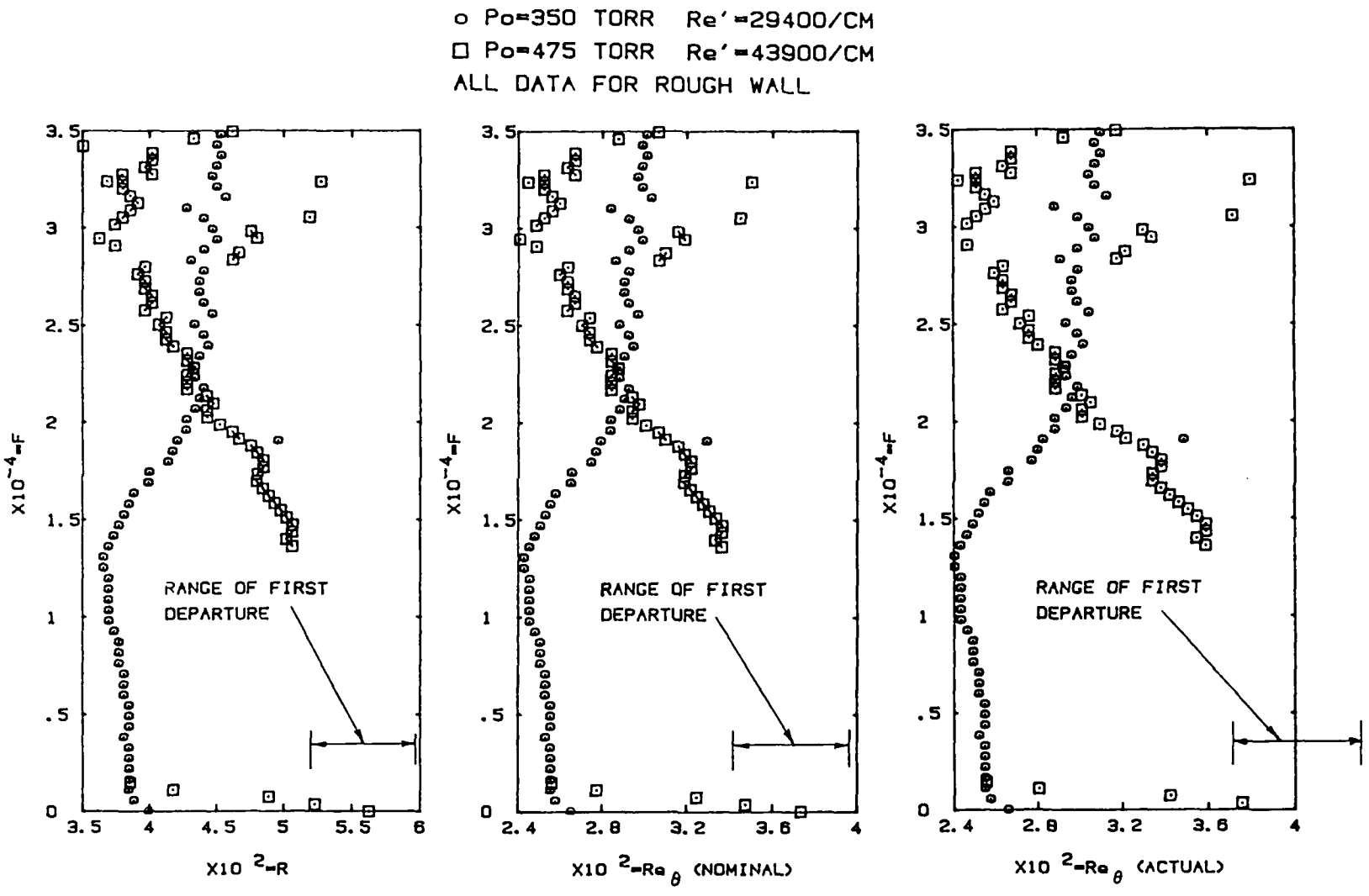

Figure 69. Lower neutral branch of the second mode, rough wall.

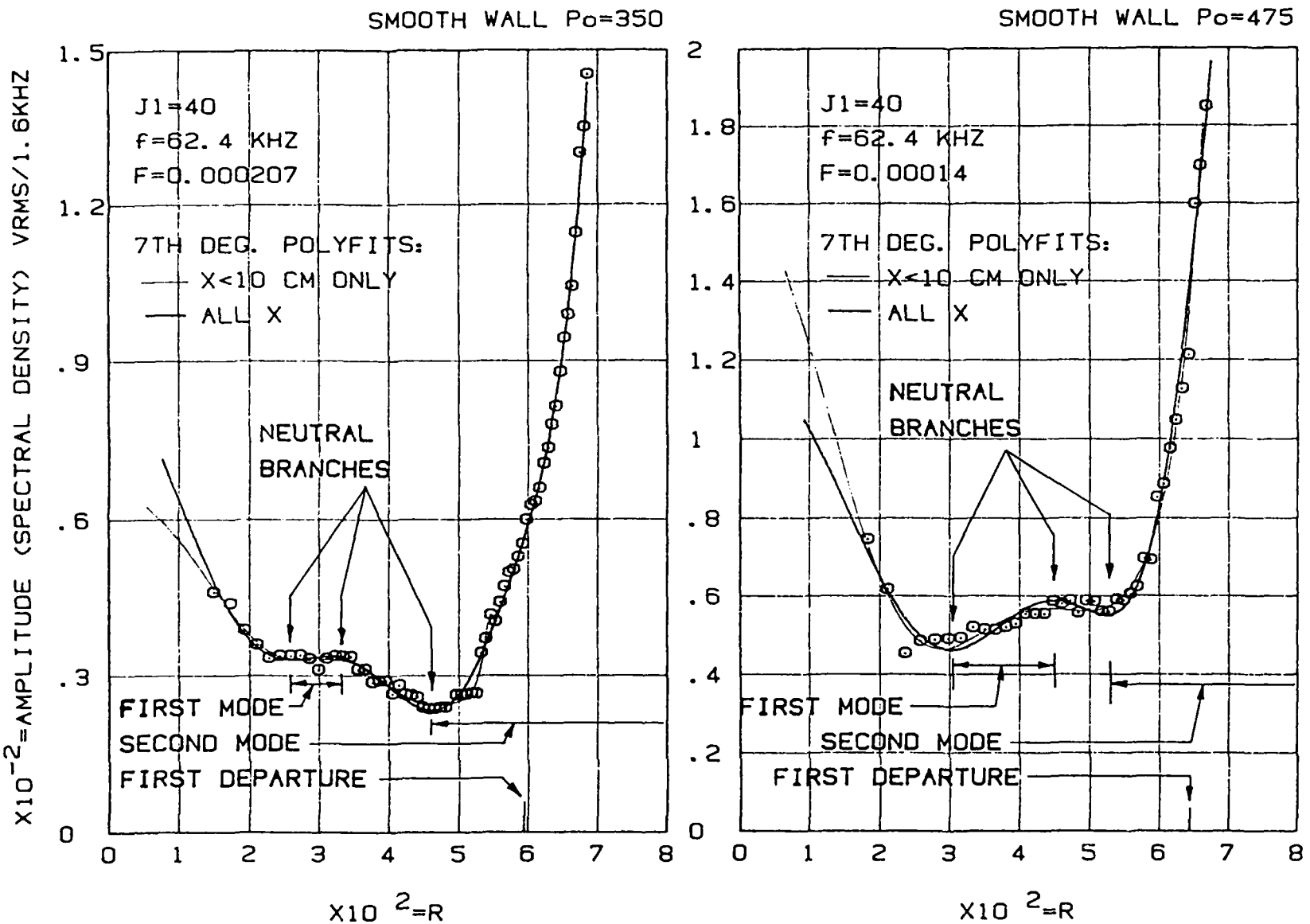

Figure 70. Amplitude histories illustrate the minor role played by the first mode. Note position where boundary layer velocity profile "first departs" from the Blasius theory.

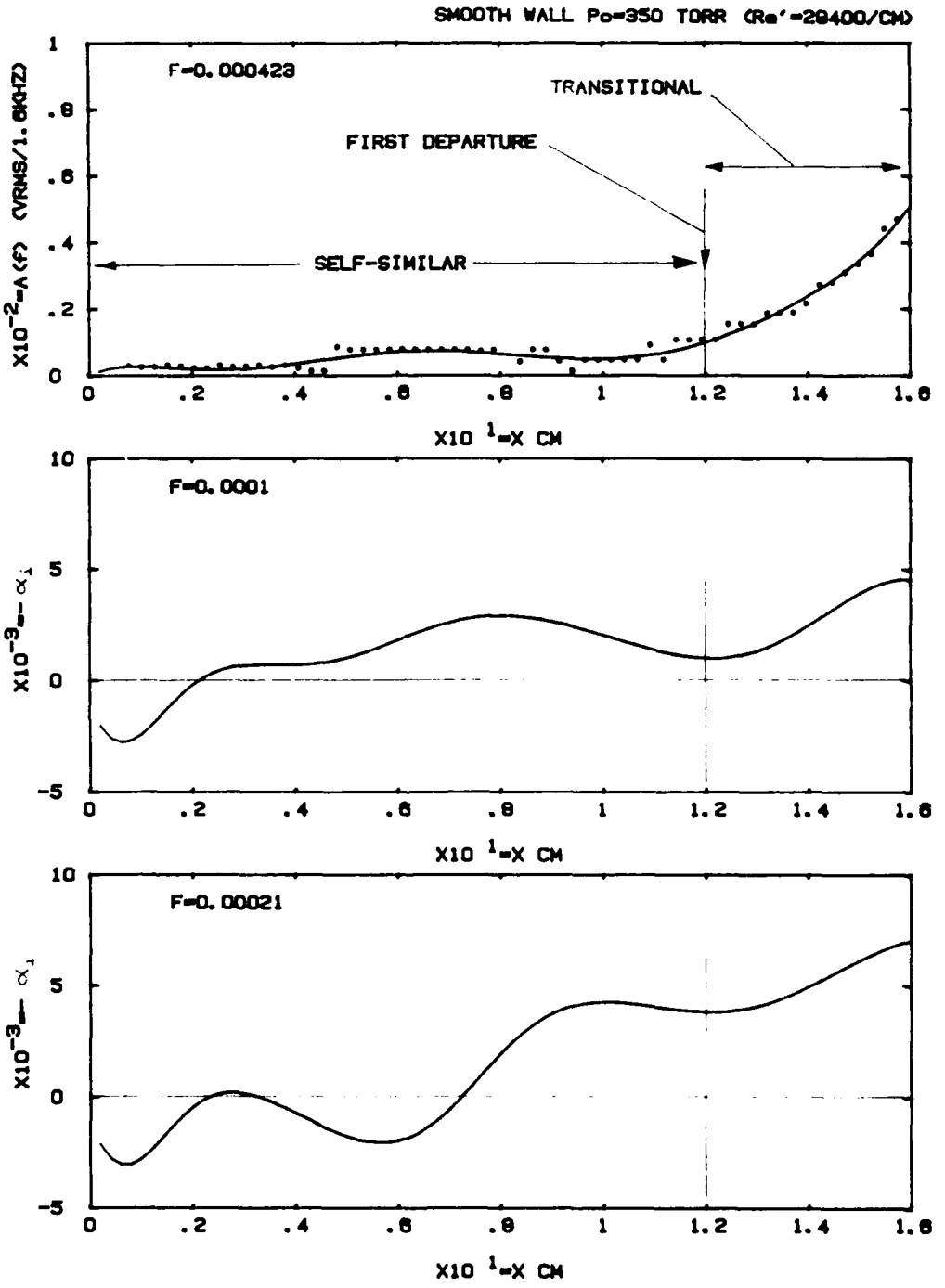

Figure 71. Typical smooth-wall amplitude (top) and amplification-rate histories (middle and bottom), 350 torr.

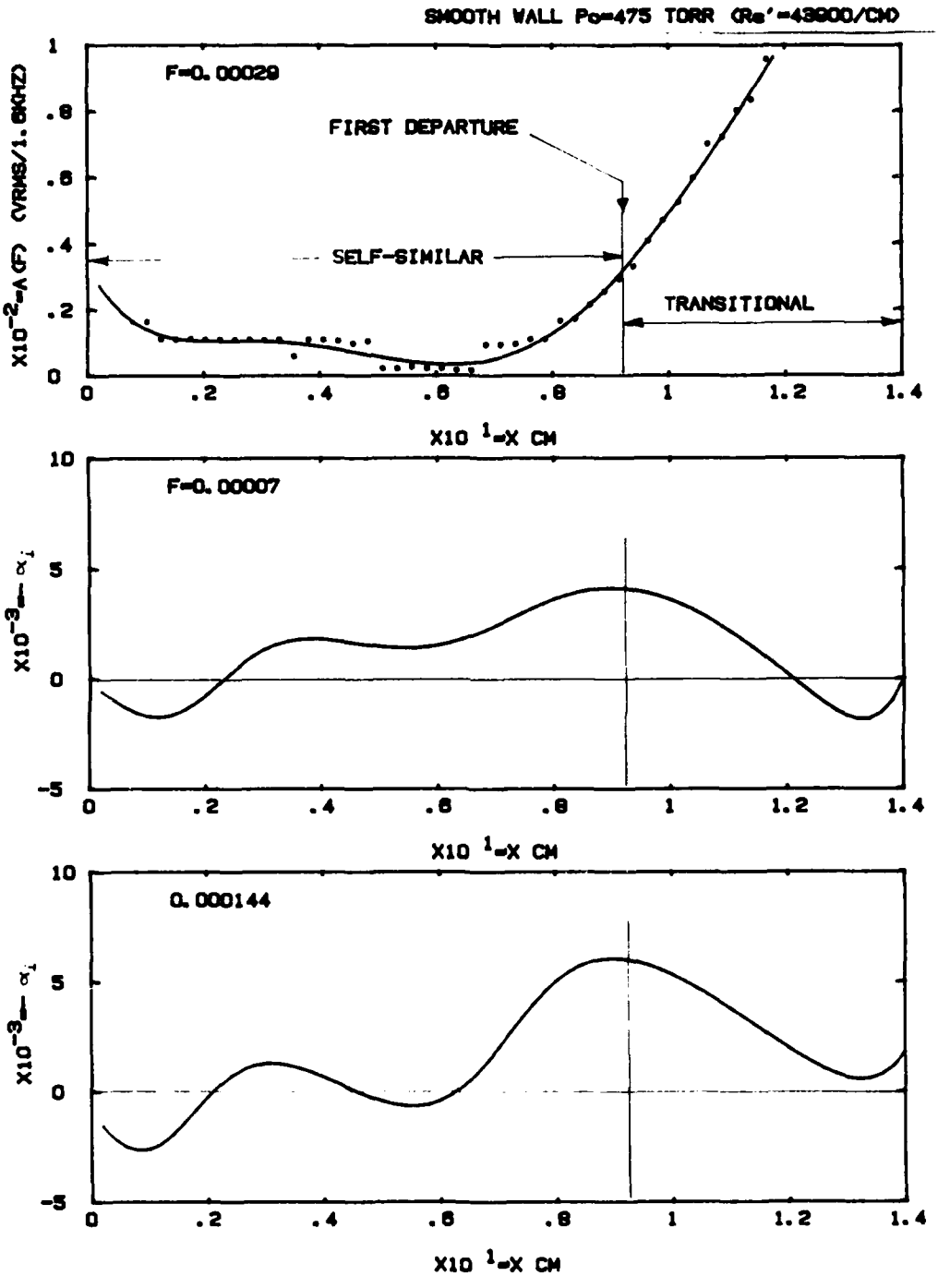

Figure 72. As in Figure 71, 475 torr.

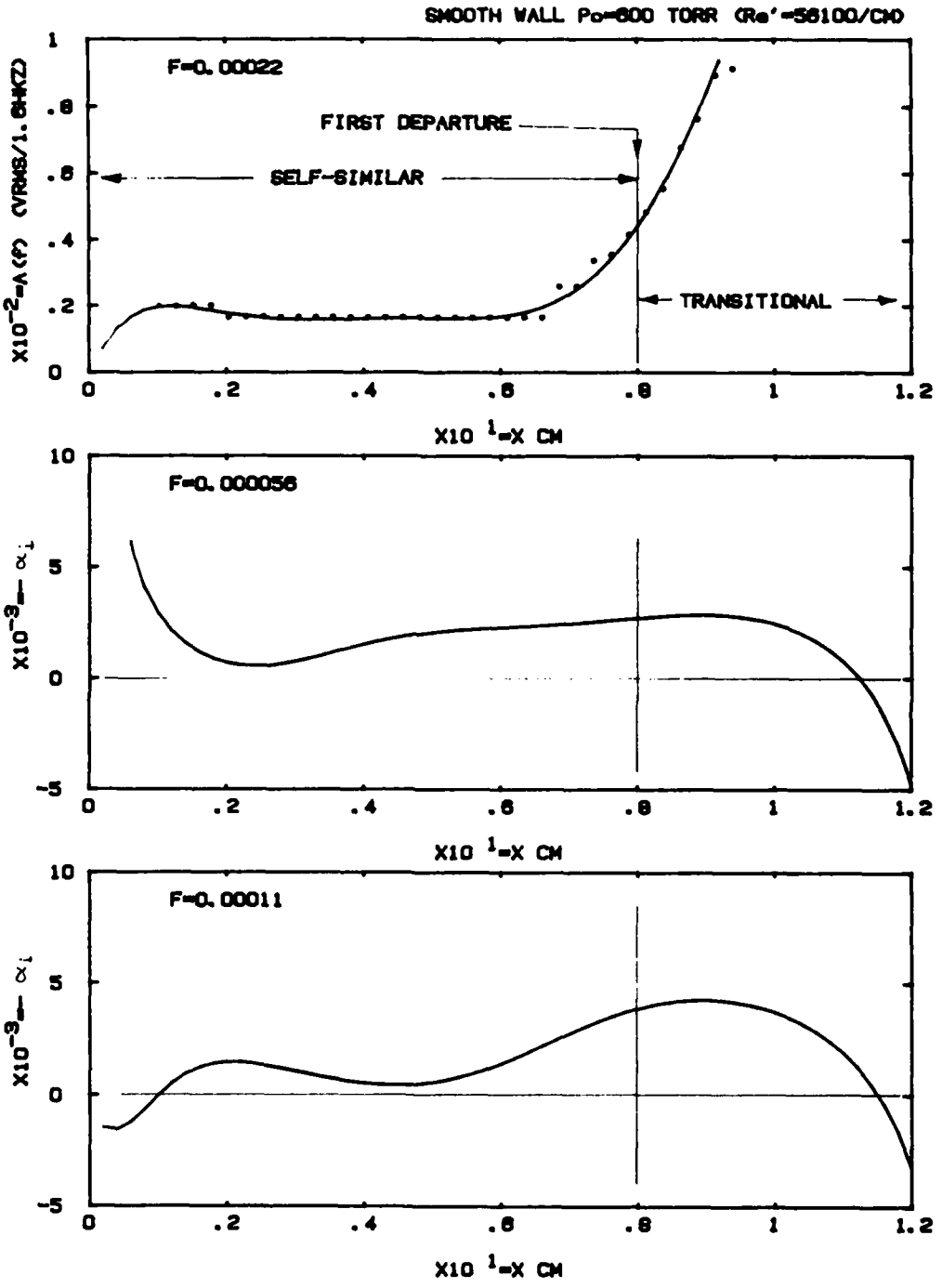

Figure 73. As in Figure 71, 600 torr.

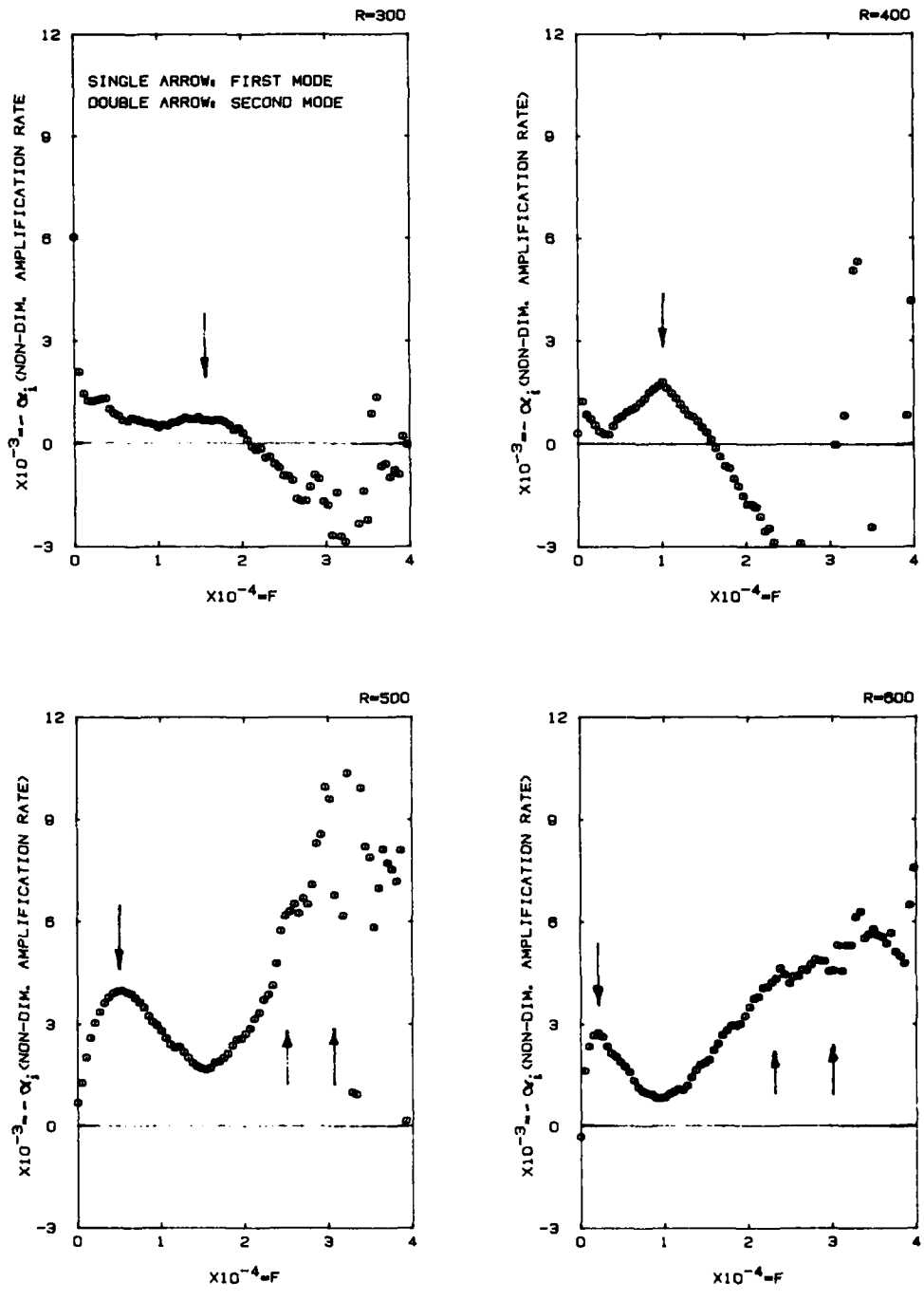

Figure 74. Amplification spectra at Re'=29400/cm, showing clearly the movement of the first-mode peak to low F as R increases and the eventual preponderance of the second mode.

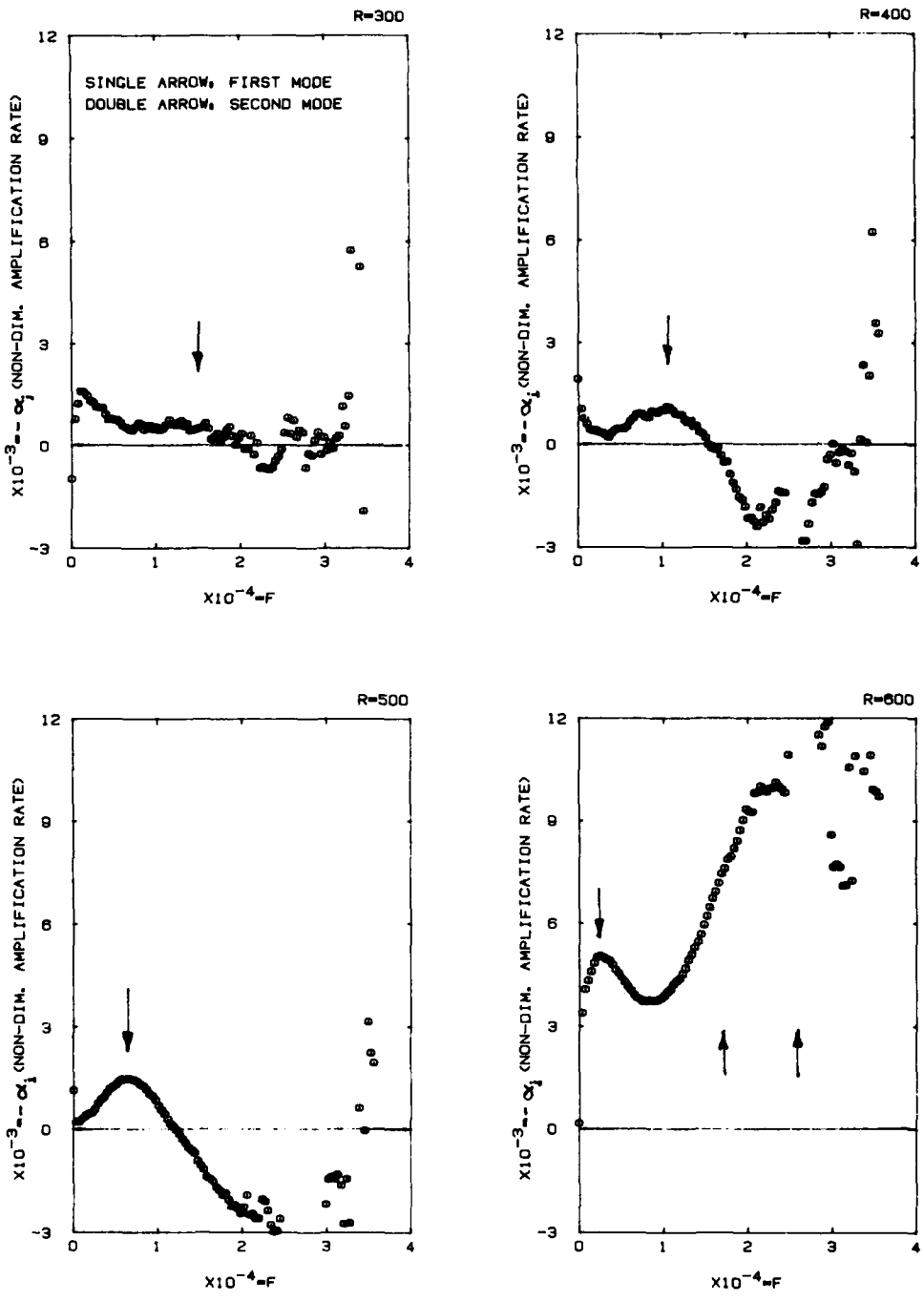

Figure 75. As in Figure 74, at 475 torr.

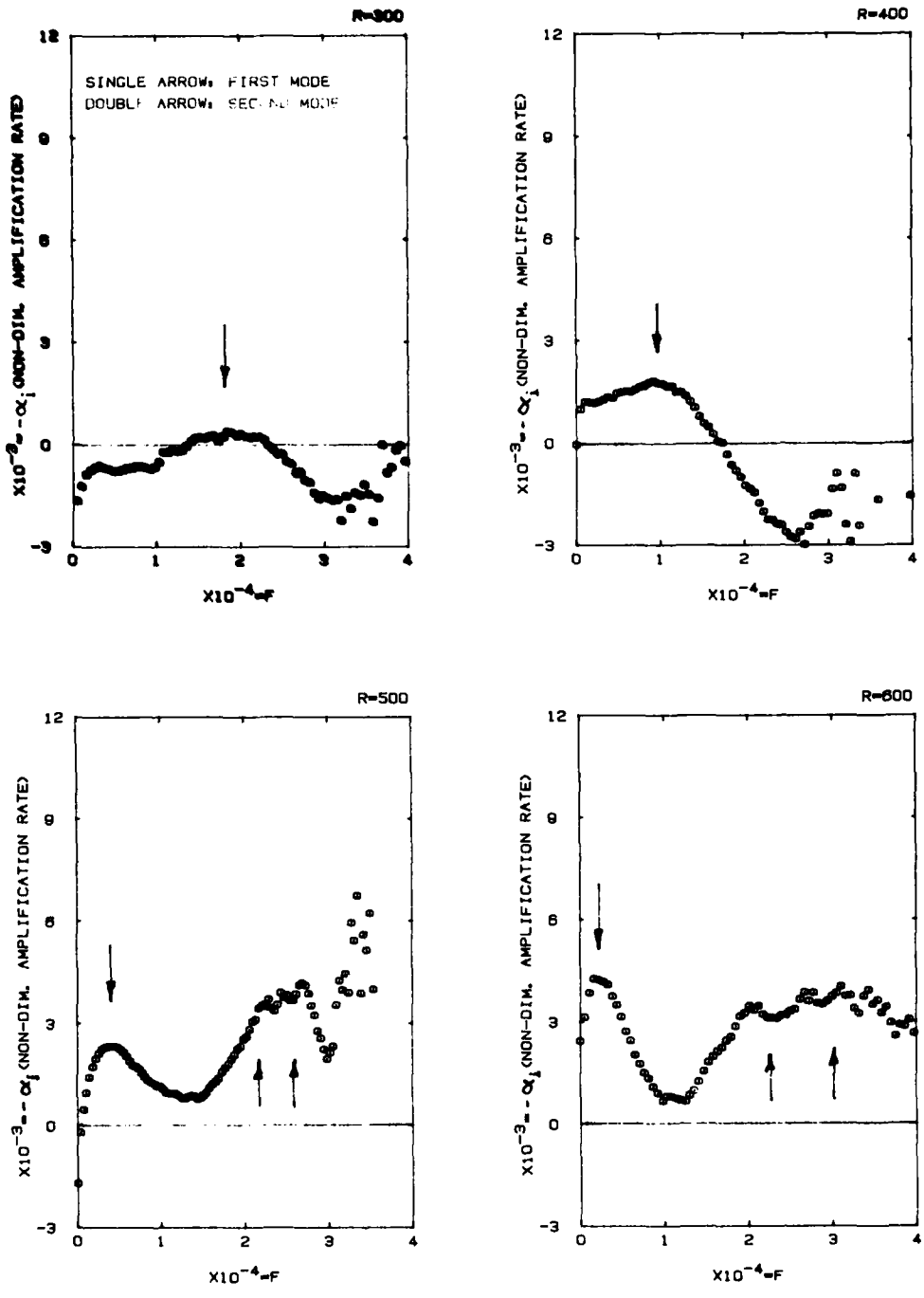

Figure 76. As in Figure 74, rough wall at 350 torr.

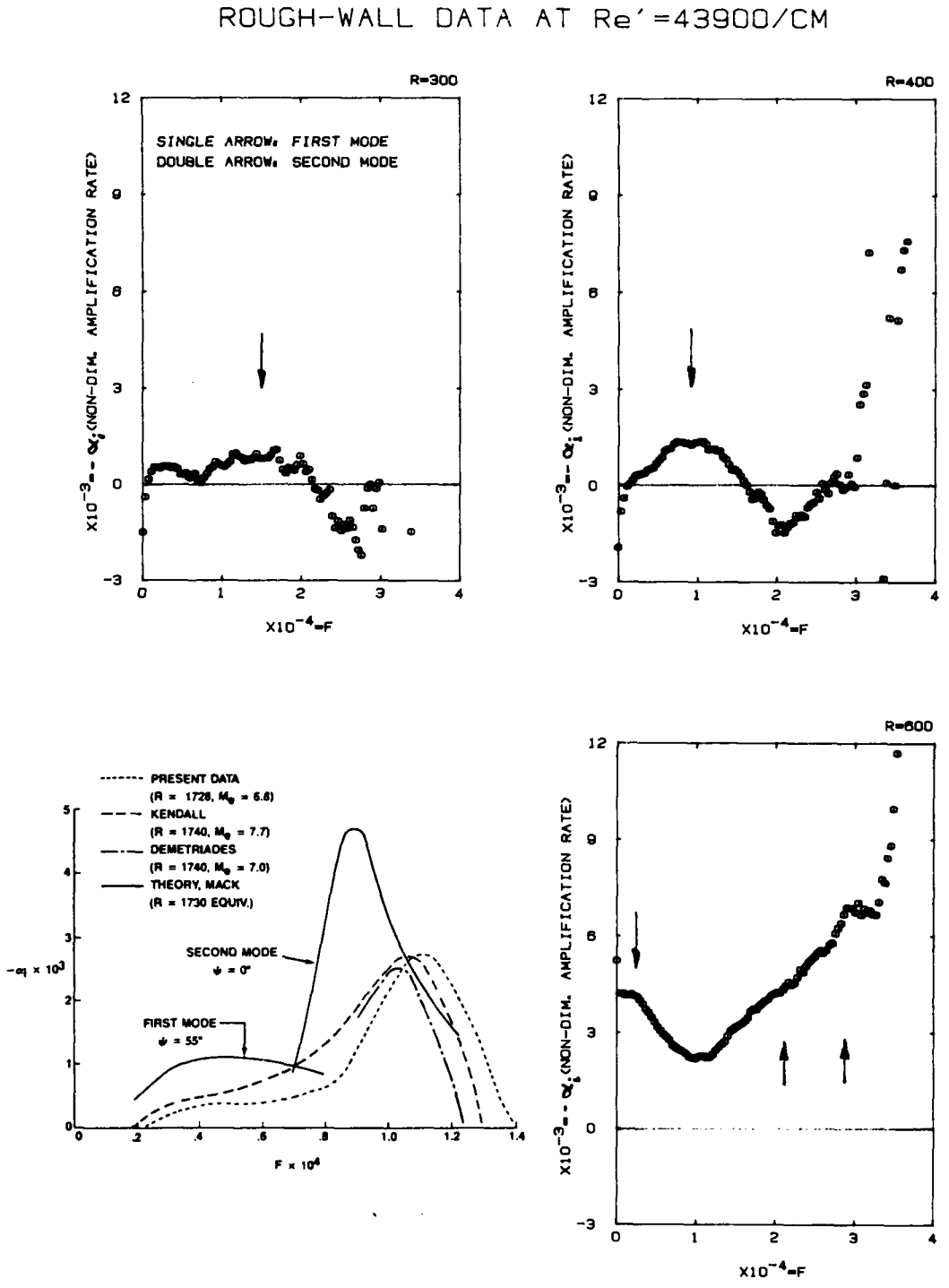

Figure 77. As in Figure 74, rough wall at 475 torr, except for lower left where a similar amplification-rate spectrum pattern at hypersonic speeds is taken from Reference 9.

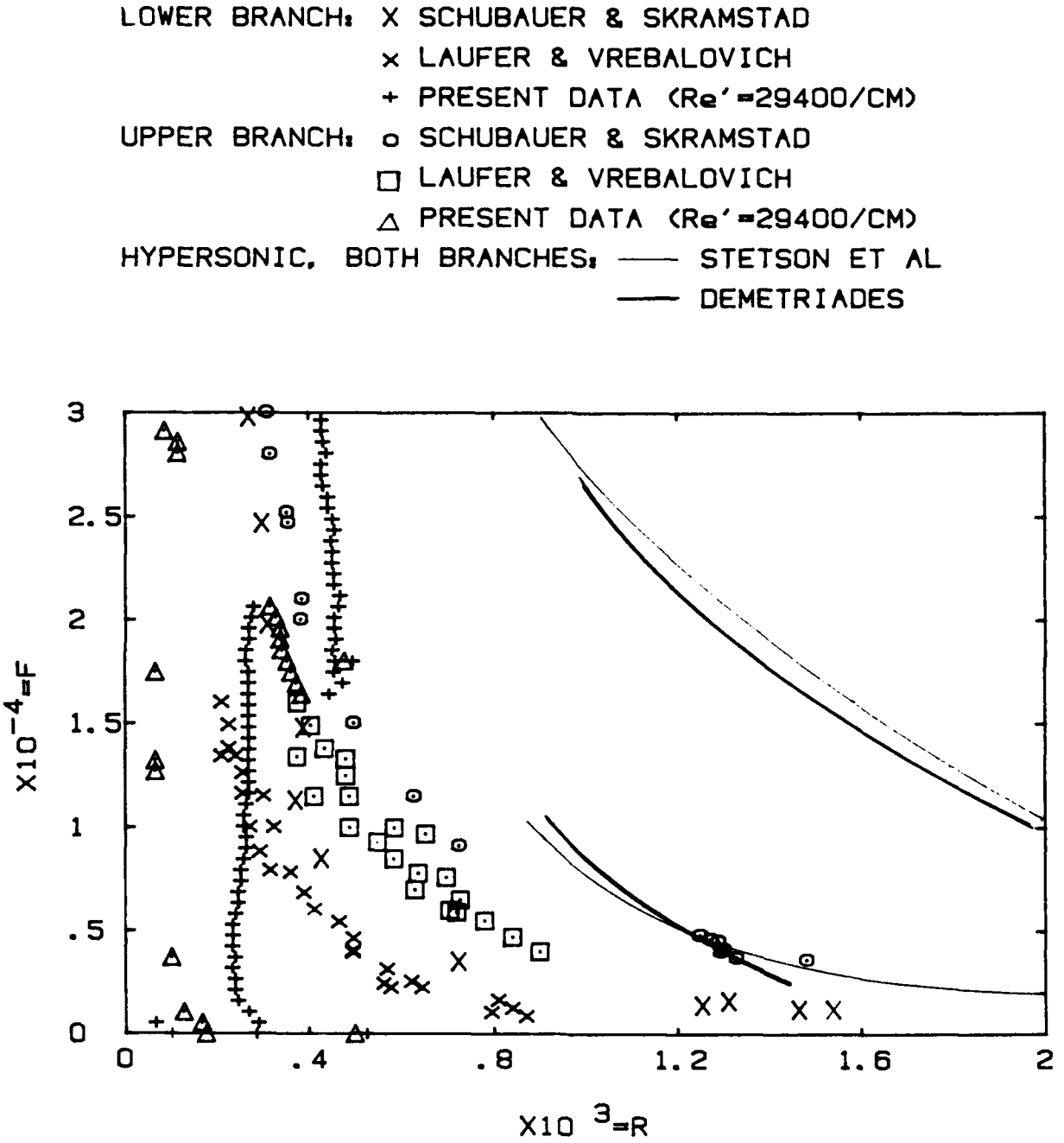

Figure 78. Updated overview of the experimentally determined unstable regions in boundary layers. Low-frequency, low-R instability shown here has been previously reported in more severe form. The indicated second-mode lower neutral branch (upper left) seems to be part of the hypersonic instability loop discovered in the 1970's, possibly indicating the missing low-R end of that loop and implying the need to look for instabilities at very large F (hypersonic higher harmonics not shown).

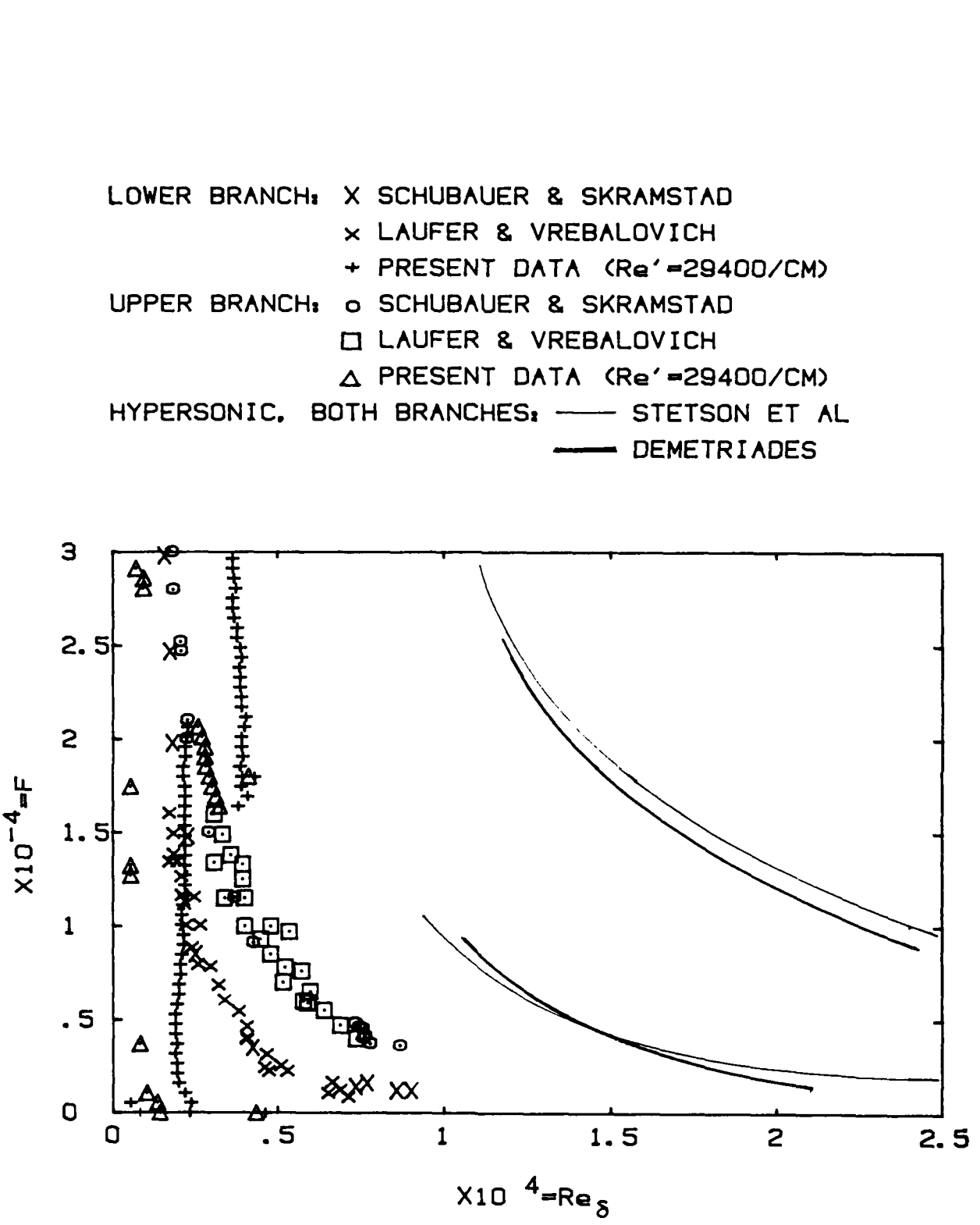

Figure 79. Same as Figure 78 but plotted vs Re_δ as suggested by Laufer to bring all low-M data into coincidence.

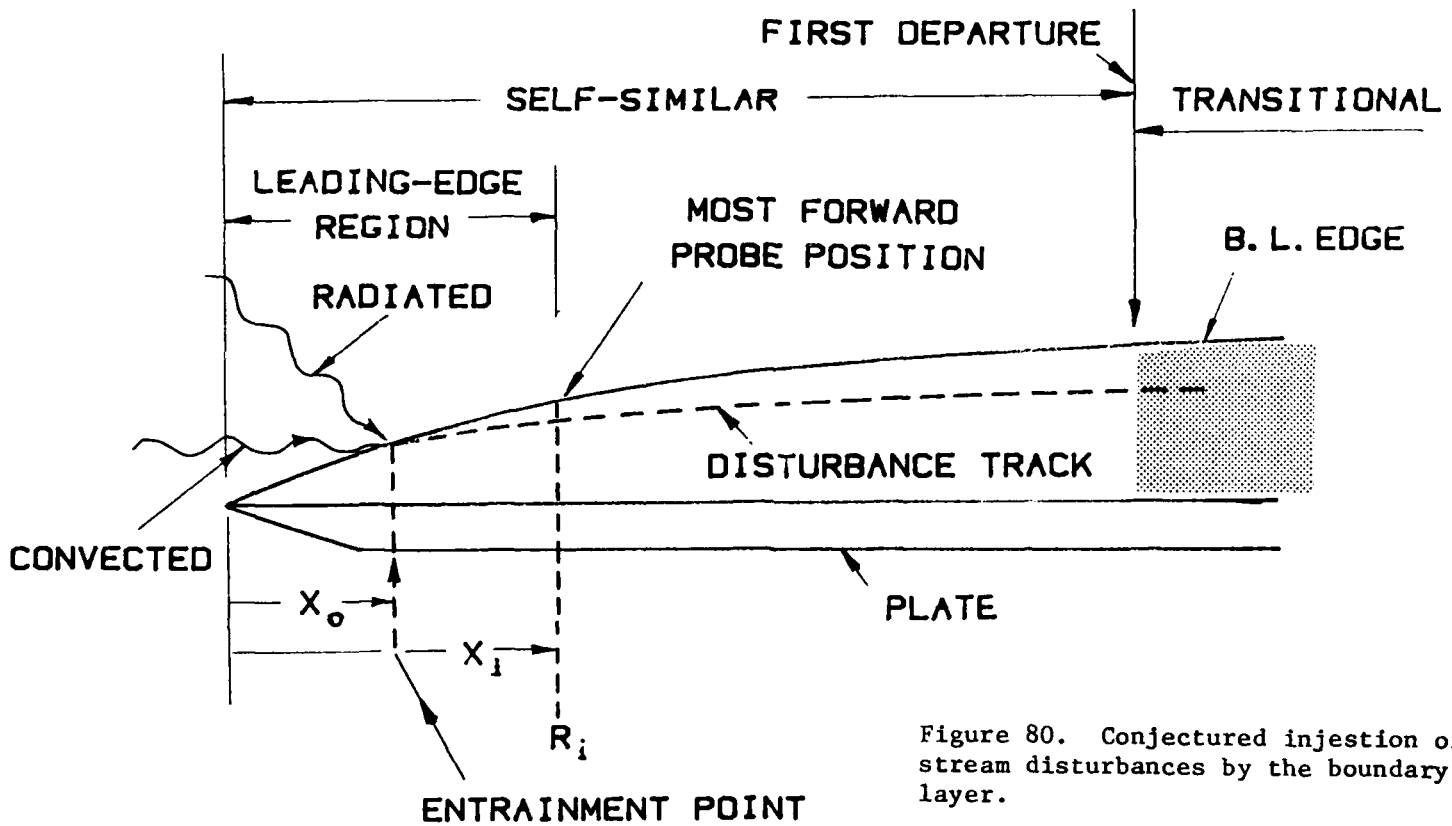

Figure 80. Conjectured injestion of stream disturbances by the boundary layer.

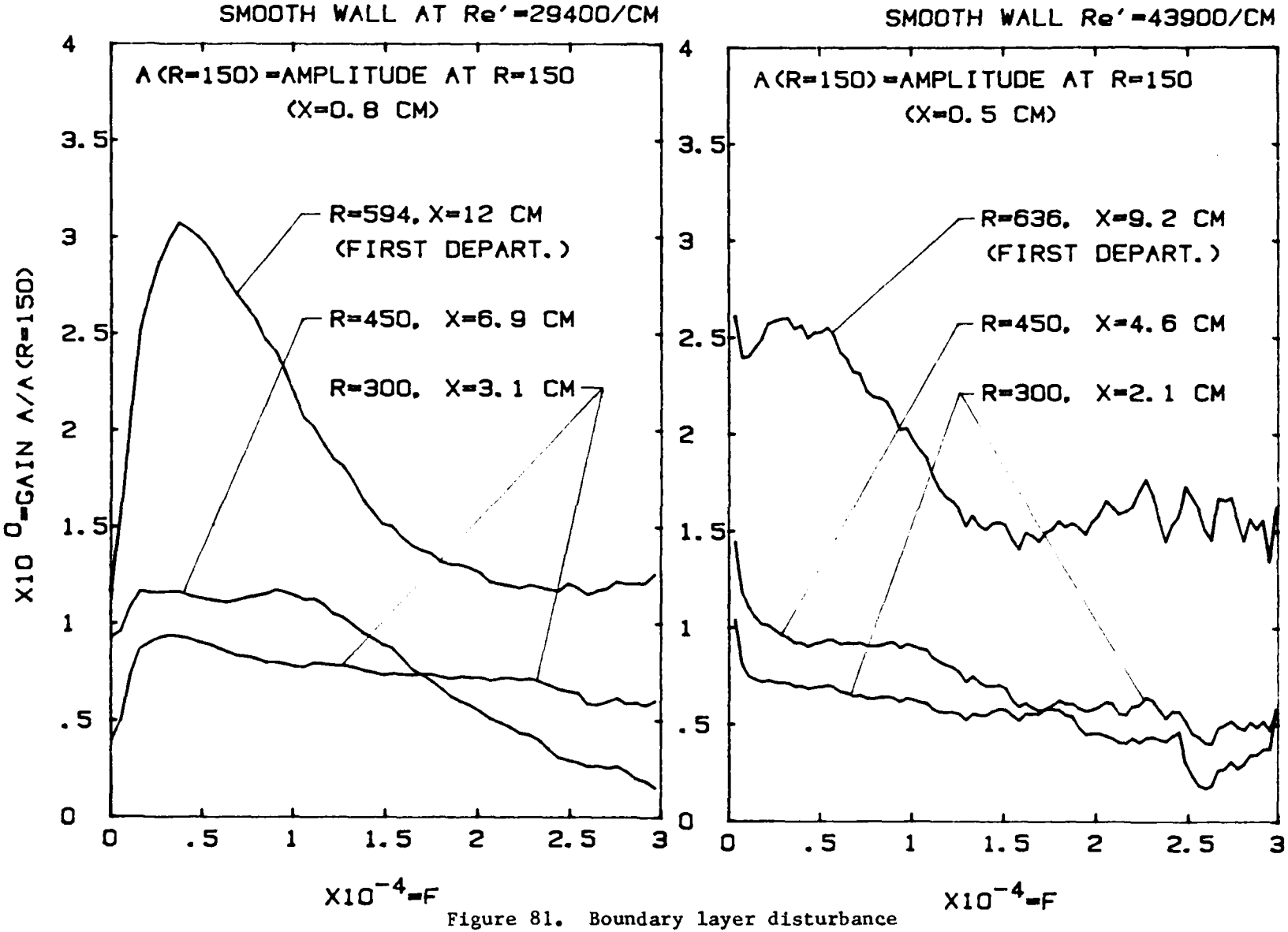

Figure 81. Boundary layer disturbance amplitude gain referred to the amplitudes at R = 150, smooth wall.

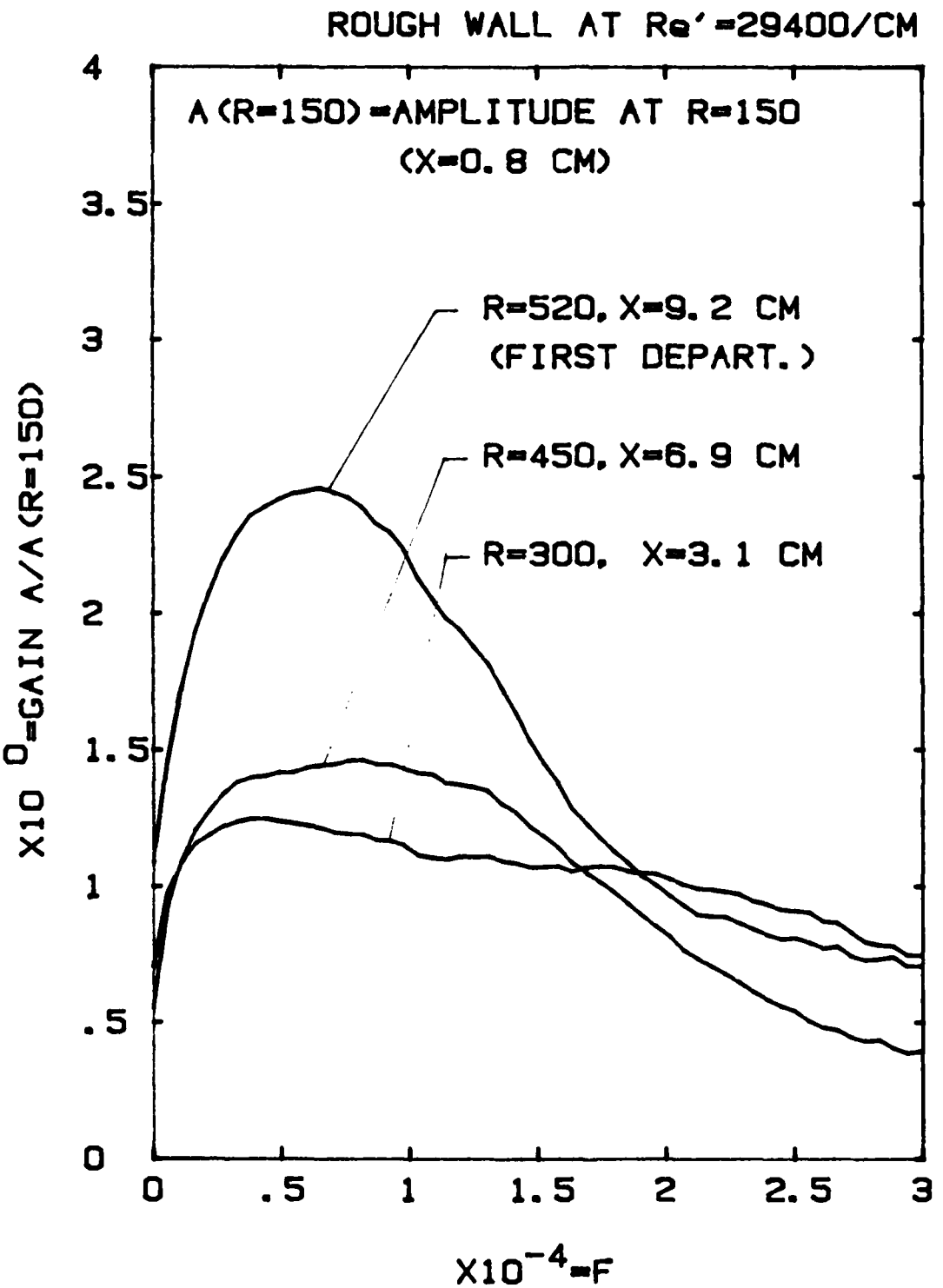

Figure 82. Boundary layer disturbance amplitude gain referred to the amplitude at R = 150, rough wall

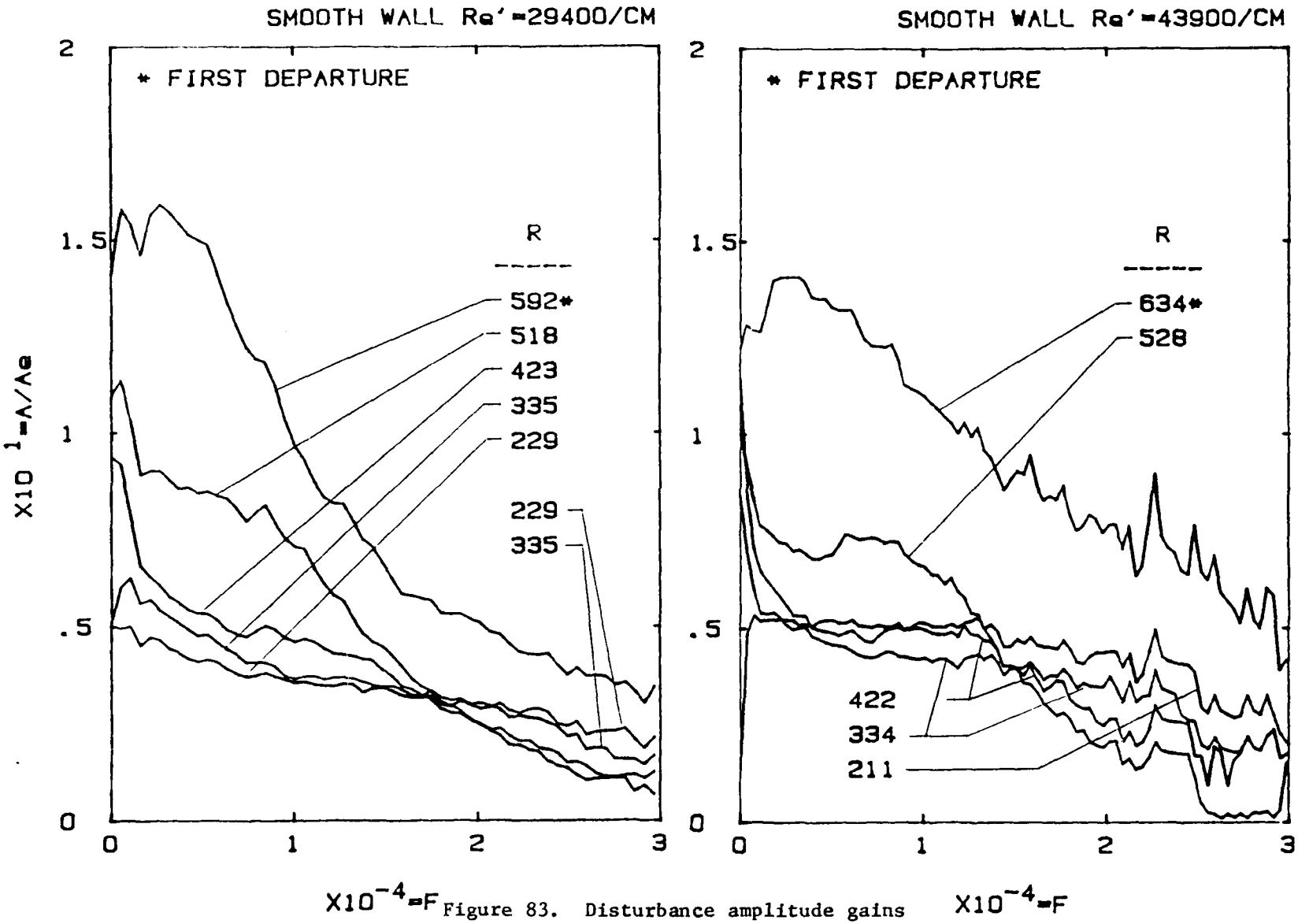

Figure 83. Disturbance amplitude gains referred to the stream disturbance levels.

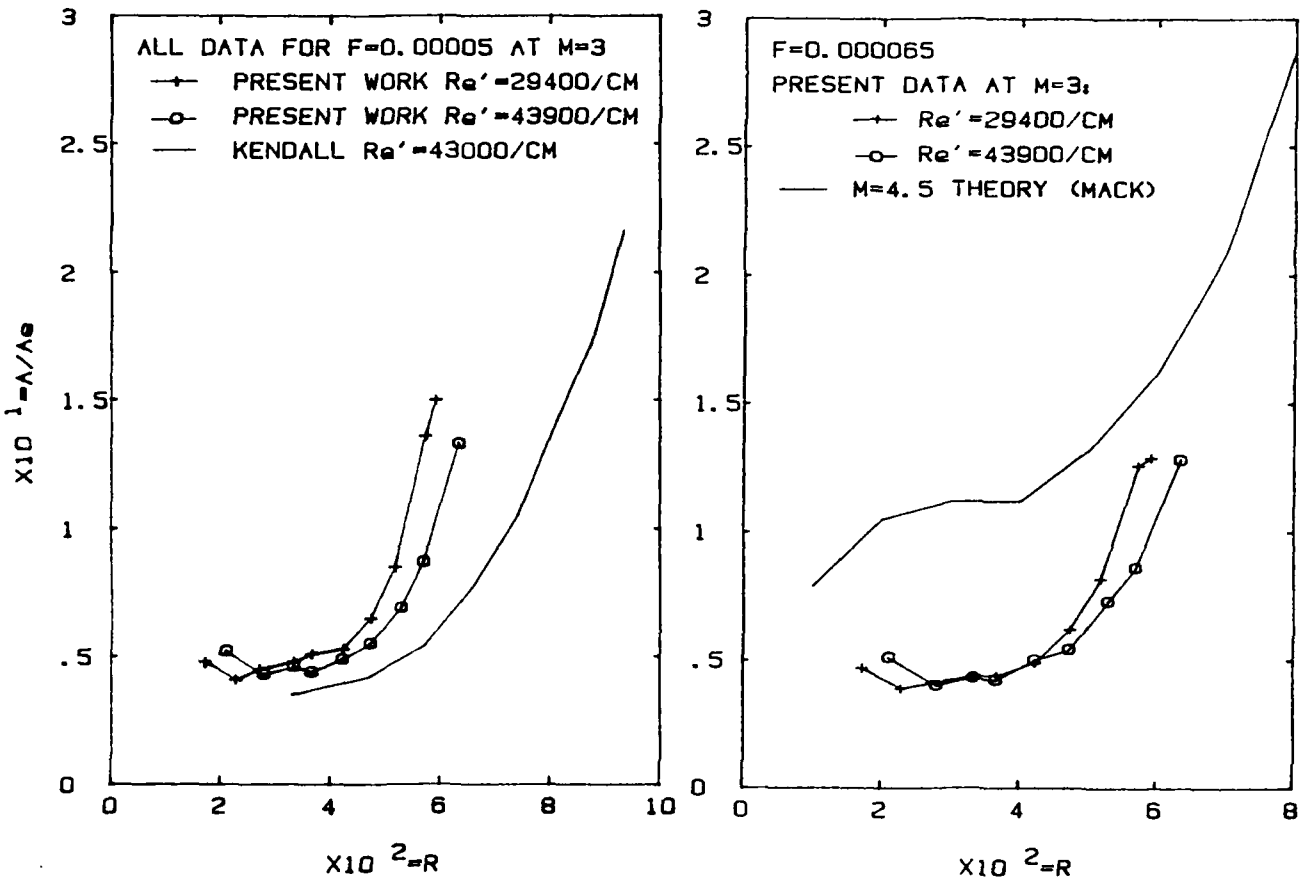

Figure 84. Typical response data, where A_e is the stream signal level, compared with earlier findings by Kendall (left) and, for illustration only, with Mack's forcing-stability theory at M=4.5 (right). As previously surmised the leading-edge region substantially amplifies incoming stream disturbances.

APPENDIX A

Method of Decreasing the Model-Wall Interference

Boundary layers tend to separate in an adverse pressure gradient. A classical example of separation can be found around the base of an object protruding from an otherwise flat surface over which the boundary layer forms. In the present experiment, the plate model spanned the test section from one sidewall to the other. The mechanism mentioned above, which is potentially capable of separating the layer, is present at the two points where the plate leading edge meets the two sidewalls.

Observation made during this experiment showed anomalous flow along the model centerline beginning at about x = 6 cm and present at the two lower pressure conditions (P_o = 475, 350 mm Hg abs.). Mach wave tracing indicated that disturbances at that location would originate at the points of model-wall intersection. Furthermore, it has been established (Reference 15) that at the pressures quoted above, the sidewall boundary layer is largely laminar whereas at P_o = 600 mm Hg it is turbulent. This gave added strength to the view that the anomaly was caused by sidewall boundary layer separation at the model-wall intersection points since turbulent (rather than laminar) boundary layers are much more resistant to separation. A schematic of this situation appears on Figure A.1.

According to the above remarks, the diagnosis of the problem also suggests its cure which would be to cause the sidewall boundary layer to become turbulent upstream of the model-wall intersection. This can be accomplished by "tripping" the boundary layer by means, for example, of artificial roughness. Fortunately, a great deal of information about transition-tripping of the test-section boundary layers in the SWT was available, and specifically about using surface roughness for the purpose

(Reference 17). A 0.5" x 4" strip of 120-grit sandpaper was therefore affixed on the glass sidewall by adhesive with the leading edge of the strip upstream of and the trailing edge downstream of the sonic throat; a similar strip was placed at the corresponding position on the opposite sidewall. According to Reference 17, the streamwise extent of these strips should be sufficient to generate turbulence downstream of them all the way to the diffuser entrance along a narrow band which covers the model wall intersection point. The placement at the sonic throat, where the nozzle boundary layers are thin, allows for the use of fine-grit sandpaper (grit finer than 120 could, in fact, be used according to Reference 17) and thus minimizes wavelets radiated into the flow by the grit particles. Futhermore, the leading edge of the strip, being in the subsonic portion of the nozzle, generates no shock waves, and the strips themselves were in anyway so far upstream of the nozzle that they caused no inviscid disturbances to the model flow.

Subsequent testing showed that the installation of these trips restored the measured boundary layer growth on the model to that expected from theory. All data shown in this report were taken with the trips in place.

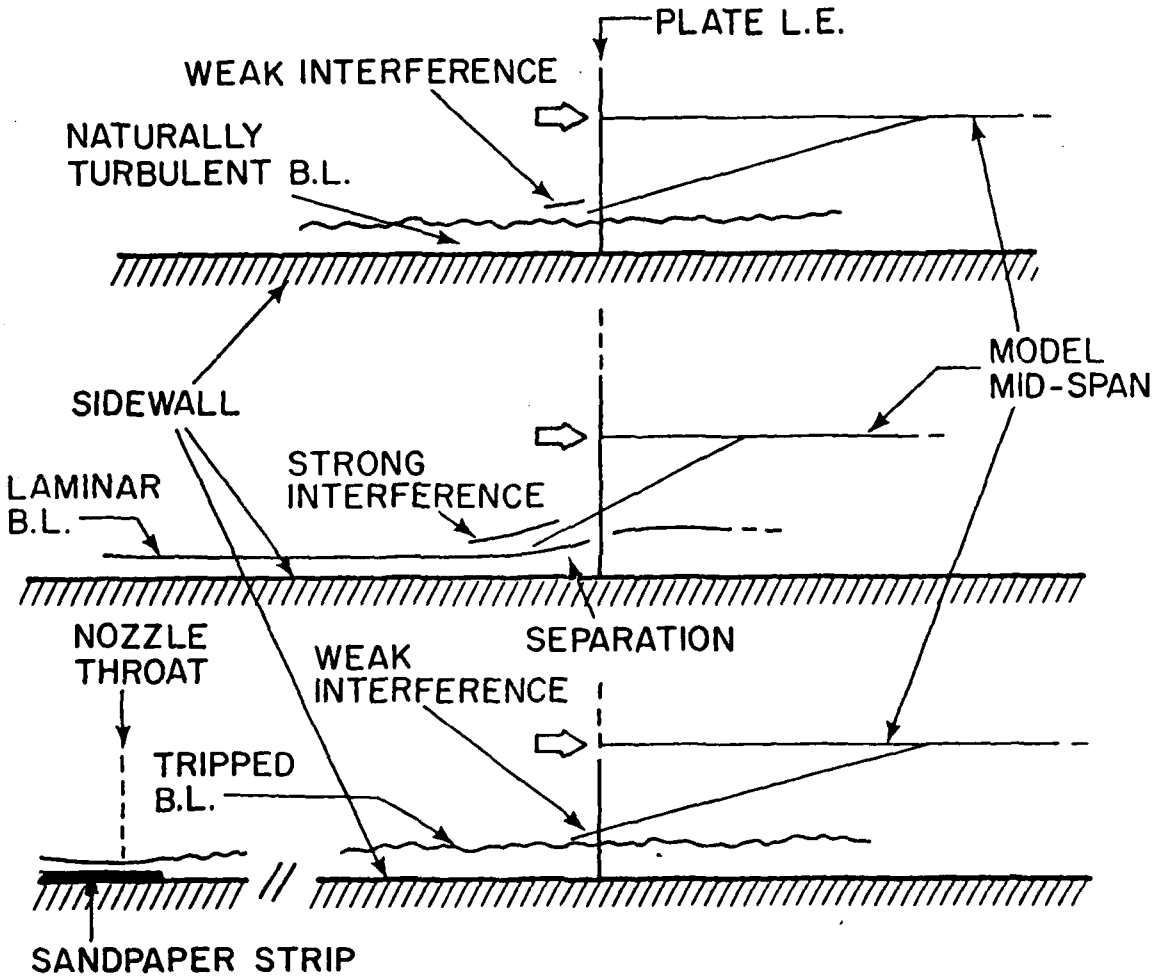

Figure A.1 Explanation of model-wall interference effect and its alleviation

APPENDIX B

Mean Flowfield Computer Programs

In order of presentation, the following are included here:

B.1 The PITOXXXX data file (example), which is used as an input to the LAMBL-series programs. Note: This file is translated into an indentical one put without line numbers, by the DATAFORM program, before insertion in such programs.

B.2 The LAMBL2 program. When asked to RUN, this program requests a PITOXXXX input. The program produces full printouts of the boundary layer profile, using offset-type data reduction; a typical output is shown under B.4. (This program, as well as all other LAMBL-type programs, also creates graphics files called GRAFXXXX.)

B.3 The LAMBL3 program, which is identical to LAMBL2, except that it prints only a summary of the profile properties (item 3 of the example under B.4).

B.4 Sample run of the LAMBL2 program.

B.5 Format of the GRAFXXXX output files (these are used for producing data plots of profile properties).

B.6 Format of the TOTALXX output files (these are used for producing data plots along x).

B.1 The PITOXXXX Data File (Example)

```
10 +1                  Surface Code (see Table I)
15 +600                P_o (mm Hg abs)
20 +4                  x (cm)
25 +100                T_o (deg F)
30 +2.1278             Intercept of transducer calibration (mm Hg)
35 +.1046              Slope of transducer calibration (mm Hg/count)
40 +0                  Intercept of y-position calibration (cm)
45 +.0001875           Slope of y-position calibration (cm/count)
50 +15.45              Local surface pressure (mm Hg)
55 +.01016             Probe diameter (cm)
60 +67                 Number of points in profile
65 +29                 Number of points at the boundary layer edge
70 +.008               Offset (cm)
120 +1304              Profile Code (Table I)
121 +4                 Number of anomalous points near wall
130 +307,+142,         Beginning of data (y(counts), p_T(counts))
140 +307,+143,
150 +310,+143,
160 +323,+143,
170 +336,+145,
180 +351,+150,
190 +364,+158,
200 +378, 167,
210 +390,+178,
220 +402,+189,
230 +417,+207,
240 +429,+224,
250 +444,+248,
260 +456,+272,
270 +469,+303,
280 +484,+340,
290 +495,+389,
300 +509,$443,
310 +522,+505,
320 +536,+568,
```

B.2 THE LAMBL2 PROGRAM

```
10 REM LAMBL2
20 DIM N(200),C1(200),C2(200),P2(200),Y(200),Y1(200)
25 DIM Y3(200)
30 DIM M(200),T1(200),T2(200),U(200),R(200),I(200)
40 PRINT "WHAT ARE FILES PITOXXXX";
50 INPUT F1$
60 OPEN "I",#1,F1$
70 INPUT #1,A1,P,X,T,D1,D2,D3,D4,P1,D5,J,D,F,H,J1
80 PRINT
90 PRINT "BOUNDARY-LAYER PROFILE OF GROUP NO.:";H
100 IF A1=1 GOTO 150
110 IF A1=2 GOTO 180
120 IF A1=3 GOTO 200
130 IF A1=4 GOTO 220
140 IF A1=5 GOTO 240
150 IF A1=6 GOTO 260
160 PRINT "SMOOTH SURFACE"
170 GOTO 270
180 PRINT "ROUGH SURFACE"
190 GOTO 270
200 PRINT "POROUS SURFACE, ZERO INJECTION"
210 GOTO 270
220 PRINT "POROUS SURFACE, LOW INJECTION"
230 GOTO 270
240 PRINT "POROUS SURFACE, MEDIUM INJECTION"
250 GOTO 270
260 PRINT "POROUS SURFACE, HIGH INJECTION"
270 PRINT "STAGNATION PRESSURE (MM HG ABS)=";P
280 PRINT "STAGNATION TEMPERATURE (DEG F)=";T
290 PRINT "DISTANCE FROM THE L.E. (CM)=";X
300 PRINT "LOCAL STATIC PRESSURE (MM HG)=";P1
310 PRINT "------------------------------------------------------------"
315 PRINT "NO. OF POINTS JUDGED INVALID DUE TO WALL-PROBE INTERFERENCE:";J1
320 PRINT
330 PRINT
340 PRINT "1.RAW DATA FOR GROUP";H
350 PRINT "---- ---------------------"
360 PRINT
370 PRINT "POINT NO.","Y(COUNTS)","PT(COUNTS)","PT(MM)","PT/PW"
380 PRINT
390 FOR N=1 TO J
400 INPUT #1,C1(N),C2(N)
410 LET P2(N)=D1+D2*C2(N)
420 PRINT N,C1(N),C2(N),P2(N),P2(N)/P1
430 NEXT N
440 PRINT
450 PRINT
460 PRINT "2.DIMENSIONLESS PROFILES OF GROUP";H
470 PRINT "-------------------------------------"
480 PRINT
490 PRINT "N","Y/DELTA","M","U/UE","T/TE"
500 PRINT
510 FOR N=1 TO J
520 LET Y(N)=D4*(C1(N)-C1(1))+F+(D5/2)
530 LET Y(D)=D4*(C1(D)-C1(1))+F+(D5/2)
540 LET Y1(N)=Y(N)/Y(D)
550 IF P2(N)/P1>=1.8929 GOTO 580
560 LET M(N)=SQR(5*(((P2(N)/P1)^(1/3.5))-1))
570 GOTO 660
580 LET M(N)=(.5*P2(N)/P1)^(1/1.6)
590 LET F1=(1.2*(M(N))^2)^3.5
600 LET F2=(6/((7*(M(N)^2))-1))^2.5
610 LET F3=F1*F2
620 LET Z=((P2(N)/P1)-F3)/(P2(N)/P1)
630 IF ABS(Z)<=.001 GOTO 660
640 LET M(N)=M(N)+Z
650 GOTO 590
660 IF Y1(N)>1 GOTO 690
670 LET T1(N)=(.94+.06*Y1(N))*(T+460)
680 GOTO 700
690 LET T1(N)=T+460
700 LET T2(N)=T1(N)/(1+.2*(M(N)^2))
710 LET U(N)=2009*M(N)*SQR(.5556*T2(N))
720 LET R(N)=.0008338*P1/T2(N)
730 NEXT N
740 FOR N=1 TO J
750 PRINT N,Y1(N),M(N),U(N)/U(J),T2(N)/T2(J)
760 NEXT N
770 PRINT
780 PRINT
790 PRINT "3.SUMMARY FOR GROUP NO.";H
800 PRINT "---------------------------"
810 PRINT
820 PRINT "SURFACE CODE:";A1
830 PRINT "DISTANCE FROM L.E.(CM)=";X
840 PRINT "STAGNATION PRESSURE (MM HG ABS)=";P
850 PRINT "STATIC PRESSURE (MM HG)=";P1
860 PRINT "NO. OF BAD POINTS:";J1
870 PRINT
880 PRINT "EDGE MACH NO.=";M(J)
890 PRINT "EDGE VELOCITY (CM/SEC)=";U(J)
900 PRINT "EDGE TEMPERATURE (DEG K)=";5*T2(J)/9
910 PRINT "EDGE DENSITY (CGS)=";R(J)
915 LET M1=.0000109*(T2(J)^1.5)/(T2(J)+198.6)
920 PRINT "EDGE VISCOSITY (CGS)=";M1
930 PRINT "EDGE UNIT REYNOLDS NO.)CM-1)=";U(J)*R(J)/M1
940 PRINT
950 PRINT "B.L.THICKNESS DELTA (CM)=";Y(D)
960 FOR N=J1+1 TO J
970 LET I(J1)=0
980 LET Y(J1)=0
990 LET I(N)=((R(N)*U(N))/(R(J)*U(J)))*(1-(U(N)/U(J)))
1000 LET D6=D6+(I(N)+I(N-1))*(Y(N)-Y(N-1))/2
1010 NEXT N
1020 PRINT "MOMENTUM THICKNESS THETA (CM)=";D6
1030 PRINT "DELTA SQUARED (CM2)=";Y(D)^2
1040 PRINT "THETA SQUARED (CM2)=";D6^2
1050 PRINT "DELTA/THETA=";Y(D)/D6
1060 PRINT "MOMENTUM REYNOLDS NO.=";U(J)*R(J)*D6/M1
1070 PRINT "REDELTA*DELTA=";(U(J)*R(J)/M1)*(Y(D)^2)
1080 PRINT "RETHETA*THETA=";(U(J)*R(J)/M1)*(D6^2)
1090 LET G=(1+.0934*(M(J)^2))^2
1100 PRINT "REDELTA*DELTA/F(ME)=";(U(J)*R(J)/M1)*(Y(D)^2)/G
1105 PRINT "SQYARE ROOT OF REX=";SQR(X*U(J)*R(J)/M1)
1110 PRINT
1120 PRINT
1130 PRINT "4.COMPRESSIBLE-TRANSFORMED PROFILE OF";H
1140 PRINT "-----------------------------------------"
```

B.2 (contd)

```
1150 PRINT
1160 PRINT "N","Y(CM)","YBAR(CM)","YBAR/THETA","U/UE"
1170 PRINT
1180 FOR N=J1+1 TO J
1190 LET Y(J1)=0
1195 LET Y3(J1)=0
1200 LET R(J1)=.000833*P1/(.94*(T+460))
1210 LET Y3(N)=Y3(N-1)+((R(N)+R(N-1))/(2*R(J)))*(Y(N)-Y(N-1))
1220 PRINT N,Y(N),Y3(N),Y3(N)/D6,U(N)/U(J)
1230 NEXT N
1235 PRINT
1276 PRINT
1240 PRINT "DO YOU WISH A FILE MADE FOR GRAPHICS (CR FOR YES,1 FOR NO)";
1250 INPUT A2
1260 IF A2=1 GOTO 2000
1270 INPUT "GRAPHICS FILE NAME (GRAFABCD)";F2$
1280 OPEN "O",#2,F2$
1290 FOR N=J1+1 TO J
1300 WRITE#2,N,Y(N),Y1(N),Y3(N)/D6,M(N),U(N)/U(J),T2(N)/T2(J),R(N)/R(J)
1310 NEXT N
2000 END
Ok
```

B.3 THE LAMBL3 PROGRAM

```
10 REM LAMBL3
20 DIM N(200),C1(200),C2(200),P2(200),Y(200),Y1(200)
25 DIM Y3(200)
30 DIM M(200),T1(200),T2(200),U(200),R(200),I(200)
40 PRINT "WHAT ARE FILES PITOXXXX";
50 INPUT F1$
60 OPEN "I",#1,F1$
70 INPUT #1,A1,F,X,T,D1,D2,D3,D4,P1,D5,J,D,F,H,J1
80 PRINT
90 PRINT "BOUNDARY-LAYER PROFILE OF GROUP NO.:";H
100 IF A1=1 GOTO 160
110 IF A1=2 GOTO 180
120 IF A1=3 GOTO 200
130 IF A1=4 GOTO 220
140 IF A1=5 GOTO 240
150 IF A1=6 GOTO 260
160 PRINT "SMOOTH SURFACE"
170 GOTO 270
180 PRINT "ROUGH SURFACE"
190 GOTO 270
200 PRINT "POROUS SURFACE, ZERO INJECTION"
210 GOTO 270
220 PRINT "POROUS SURFACE, LOW INJECTION"
230 GOTO 270
240 PRINT "POROUS SURFACE, MEDIUM INJECTION"
250 GOTO 270
260 PRINT "POROUS SURFACE, HIGH INJECTION"
270 PRINT "STAGNATION PRESSURE (MM HG ABS)=";P
280 PRINT "STAGNATION TEMPERATURE (DEG F)=";T
290 PRINT "DISTANCE FROM THE L.E. (CM)=";X
300 PRINT "LOCAL STATIC PRESSURE (MM HG)=";P1
310 PRINT "-------------------------------------------------------"
315 PRINT "NO. OF POINTS JUDGED INVALID DUE TO WALL-PROBE INTERFERENCE:";J1
320 PRINT
330 PRINT
360 PRINT
380 PRINT
390 FOR N=1 TO J
400 INPUT #1,C1(N),C2(N)
410 LET P2(N)=D1+D2*C2(N)
430 NEXT N
440 PRINT
450 PRINT
480 PRINT
500 PRINT
510 FOR N=1 TO J
520 LET Y(N)=D4*(C1(N)-C1(1))+F+(D5/2)
530 LET Y(D)=D4*(C1(D)-C1(1))+F+(D5/2)
540 LET Y1(N)=Y(N)/Y(D)
550 IF P2(N)/P1>=1.8929 GOTO 580
560 LET M(N)=SQR(5*(((P2(N)/P1)^(1/3.5))-1))
570 GOTO 660
580 LET M(N)=(.5*P2(N)/P1)^(1/1.6)
590 LET F1=(1.2*(M(N))^2)^3.5
600 LET F2=(6/((7*(M(N)^2))-1))^2.5
610 LET F3=F1*F2
```

```
620 LET Z=((P2(N)/P1)-F3)/(P2(N)/P1)
630 IF ABS(Z)<=.001 GOTO 660
640 LET M(N)=M(N)+Z
650 GOTO 590
660 IF Y1(N)>1 GOTO 690
670 LET T1(N)=(.94+.06*Y1(N))*(T+460)
680 GOTO 700
690 LET T1(N)=T+460
700 LET T2(N)=T1(N)/(1+.2*(M(N)^2))
710 LET U(N)=2009*M(N)*SQR(.5556*T2(N))
720 LET R(N)=.0008338*P1/T2(N)
730 NEXT N
740 FOR N=1 TO J
750 NEXT N
770 PRINT
780 PRINT
790 PRINT "3.SUMMARY FOR GROUP NO.";H
800 PRINT "----------------------------"
810 PRINT
820 PRINT "SURFACE CODE:";A1
830 PRINT "DISTANCE FROM L.E.(CM)=";X
840 PRINT "STAGNATION PRESSURE (MM HG ABS)=";P
850 PRINT "STATIC PRESSURE (MM HG)=";P1
860 PRINT "NO. OF PAD POINTS:";J1
870 PRINT
880 PRINT "EDGE MACH NO.=";M(J)
890 PRINT "EDGE VELOCITY (CM/SEC)=";U(J)
900 PRINT "EDGE TEMPERATURE (DEG K)=";5*T2(J)/9
910 PRINT "EDGE DENSITY (CGS)=";R(J)
915 LET M1=.0000109*(T2(J)^1.5)/(T2(J)+198.6)
920 PRINT "EDGE VISCOSITY (CGS)=";M1
930 PRINT "EDGE UNIT REYNOLDS NO.(CM-1)=";U(J)*R(J)/M1
940 PRINT
950 PRINT "B.L.THICKNESS DELTA (CM)=";Y(D)
960 FOR N=J1+1 TO J
970 LET I(J1)=0
980 LET Y(J1)=0
990 LET I(N)=((R(N)*U(N))/(R(J)*U(J)))*(1-(U(N)/U(J)))
1000 LET D6=D6+(I(N)+I(N-1))*(Y(N)-Y(N-1))/2
1010 NEXT N
1020 PRINT "MOMENTUM THICKNESS THETA (CM)=";D6
1030 PRINT "DELTA SQUARED (CM2)=";Y(D)^2
1040 PRINT "THETA SQUARED (CM2)=";D6^2
1050 PRINT "DELTA/THETA=";Y(D)/D6
1060 PRINT "MOMENTUM REYNOLDS NO.=";U(J)*R(J)*D6/M1
1070 PRINT "REDELTA*DELTA=";(U(J)*R(J)/M1)*(Y(D)^2)
1080 PRINT "RETHETA*THETA=";(U(J)*R(J)/M1)*(D6^2)
1090 LET G=(1+.0834*(M(J)^2))^2
1100 PRINT "REDELTA*DELTA/F(ME)=";(U(J)*R(J)/M1)*(Y(D)^2)/G
1105 PRINT "SQUARE ROOT OF REX=";SQR(X*U(J)*R(J)/M1)
1110 PRINT
1120 PRINT
1150 PRINT
1170 PRINT
1180 FOR N=J1+1 TO J
1190 LET Y(J1)=0
1195 LET Y3(J1)=0
1200 LET R(J1)=.0008338*P1/(.94*(T+460))
1210 LET Y3(N)=Y3(N-1)+((R(N)+R(N-1))/(2*R(J)))*(Y(N)-Y(N-1))
1230 NEXT N
1233 PRINT
1236 PRINT
1238 PRINT CHR$(7)
1240 PRINT "DO YOU WISH A FILE MADE FOR GRAPHICS (CR FOR YES,1 FOR NO)";
1250 INPUT A2
1260 IF A2=1 GOTO 2000
1270 INPUT "GRAPHICS FILE NAME (GRAFABCD)";F2$
1280 OPEN "O",#2,F2$
1290 FOR N=J1+1 TO J
1300 WRITE#2,N,Y(N),Y1(N),Y3(N)/D6,M(N),U(N)/U(J),T2(N)/T2(J),R(N)/R(J)
1310 NEXT N
2000 END
Ok
```

B.4 SAMPLE LAMBL2 OUTPUT

```
WHAT ARE FILES PITOXXXX? POTO1304.BAS

BOUNDARY-LAYER PROFILE OF GROUP NO.: 1304
SMOOTH SURFACE
STAGNATION PRESSURE (MM HG ABS)= 600
STAGNATION TEMPERATURE (DEG F)= 100
DISTANCE FROM THE L.E. (CM)= 4
LOCAL STATIC PRESSURE (MM HG)= 15.45
-------------------------------------------------------------
NO. OF POINTS JUDGED INVALID DUE TO WALL-PROBE INTERFERENCE: 4
```

1.RAW DATA FOR GROUP 1304

POINT NO.	Y(COUNTS)	PT(COUNTS)	PT(MM)	PT/PW
1	307	142	16.981	1.09909
2	307	143	17.0856	1.10586
3	310	143	17.0856	1.10586
4	323	143	17.0856	1.10586
5	336	145	17.2948	1.1194
6	351	150	17.8178	1.15326
7	364	158	18.6546	1.20742
8	378	167	19.596	1.26835
9	390	178	20.7466	1.34282
10	402	187	21.0972	1.41729
11	417	207	23.78	1.53916
12	429	224	25.5582	1.65425
13	444	248	28.0686	1.81674
14	456	272	30.579	1.97922
15	469	303	33.8216	2.1891
16	484	340	37.6918	2.4396
17	495	389	42.8172	2.77134
18	509	443	48.4656	3.13693
19	522	505	54.9509	3.55669
20	536	568	61.5406	3.98321
21	551	640	69.0718	4.47067
22	564	730	78.4858	5.07999
23	579	792	84.971	5.49974
24	591	910	97.3138	6.29863
25	607	1012	107.983	6.98919
26	618	1112	118.443	7.66621
27	632	1227	130.472	8.44479
28	645	1360	144.384	9.34523
29	659	1382	146.685	9.49418
30	672	1468	155.681	10.0764
31	685	1543	163.526	10.5842
32	698	1604	169.906	10.9972
33	712	1646	174.299	11.2815
34	725	1682	178.065	11.5252
35	739	1717	181.726	11.7622
36	751	1738	183.923	11.9044
37	766	1756	185.805	12.0262
38	778	1767	186.956	12.1007
39	794	1776	187.897	12.1616
40	806	1780	188.316	12.1887
41	823	1784	188.734	12.2158
42	833	1786	188.943	12.2293
43	847	1789	189.257	12.2497
44	863	1791	189.466	12.2632
45	876	1793	189.676	12.2767
46	892	1794	189.78	12.2835
47	903	1795	189.885	12.2903
48	917	1796	189.989	12.2971
49	930	1796	189.989	12.2971
50	944	1798	190.199	12.3106
51	954	1799	190.303	12.3174
52	966	1798	190.199	12.3106
53	980	1800	190.408	12.3241
54	992	1801	190.512	12.3309
55	1007	1802	190.617	12.3377
56	1021	1802	190.617	12.3377
57	1031	1803	190.722	12.3444
58	1047	1803	190.722	12.3444
59	1057	1804	190.826	12.3512
60	1073	1804	190.826	12.3512
61	1087	1804	190.826	12.3512
62	1098	1805	190.931	12.358
63	1113	1805	190.931	12.358
64	1126	1805	190.931	12.358
65	1139	1806	191.035	12.3648
66	1149	1807	191.14	12.3715
67	1167	1806	191.035	12.3648

2.DIMENSIONLESS PROFILES OF GROUP 1304

N	Y/DELTA	M	U/UE	T/TE
1	.165402	.36989	.192445	2.63457
2	.165402	.381889	.202632	2.62966
3	.172515	.381889	.202717	2.63094
4	.203338	.381889	.203916	2.61936
5	.234162	.404677	.215917	2.62191
6	.269727	.455966	.24252	2.61544
7	.30055	.52597	.278195	2.58636
8	.333744	.592784	.31166	2.55553
9	.362197	.662832	.345966	2.51868
10	.390649	.723797	.376718	2.48454
11	.426214	.809698	.415291	2.43205
12	.454666	.879402	.446813	2.38666
13	.490231	.964357	.483997	2.32875
14	.518684	1.03804	.515067	2.27621
15	.549507	1.12197	.549114	2.21449
16	.585072	1.21151	.583917	2.14765
17	.611153	1.31822	.622992	2.06491
18	.644347	1.42499	.659946	1.98293
19	.675171	1.53693	.696233	1.8972
20	.708365	1.64329	.728619	1.81755
21	.74393	1.75612	.760776	1.73507
22	.774753	1.88684	.79509	1.64163

23	.810319	1.97151	.816237	1.5847
24	.838771	2.1244	.850829	1.48294
25	.876707	2.24745	.876697	1.40679
26	.902788	2.36182	.898768	1.3388
27	.923983	2.4869	.921272	1.26874
28	.943806	2.62348	.943768	1.19643
29	1	2.64708	.948257	1.1864
30	1.03682	2.73112	.960453	1.14336
31	1.05165	2.80305	.970367	1.10796
32	1.09247	2.85931	.977804	1.08117
33	1.12566	2.89788	.982748	1.06325
34	1.15649	2.93056	.98684	1.04835
35	1.17988	2.96201	.990697	1.03424
36	1.21813	2.98072	.992956	1.02596
37	1.2437	2.99667	.99486	1.01896
38	1.26215	3.00639	.996009	1.01473
39	1.27509	3.01431	.996941	1.01129
40	1.28654	3.01782	.997354	1.00977
41	1.29335	3.02133	.997765	1.00826
42	1.31056	3.02309	.99797	1.0075
43	1.32575	3.02572	.998277	1.00637
44	1.33769	3.02747	.998481	1.00561
45	1.34451	3.02922	.998684	1.00486
46	1.35145	3.0301	.998786	1.00449
47	1.35855	3.03097	.998888	1.00411
48	1.36172	3.03185	.998989	1.00374
49	1.36255	3.03185	.998989	1.00374
50	1.37574	3.03359	.999192	1.00299
51	1.37745	3.03447	.999293	1.00261
52	1.3779	3.03359	.999192	1.00299
53	1.3811	3.03534	.999394	1.00224
54	1.38955	3.03622	.999496	1.00187
55	1.3911	3.03709	.999597	1.00149
56	1.39631	3.03709	.999597	1.00149
57	1.40202	3.03796	.999698	1.00112
58	1.41995	3.03796	.999698	1.00112
59	1.42766	3.03883	.999798	1.00075
60	1.9316	3.03883	.999798	1.00075
61	2.0148	3.03883	.999798	1.00075
62	2.04088	3.03971	.999899	1.00037
63	2.07644	3.03971	.999899	1.00037
64	2.10726	3.03971	.999899	1.00037
65	2.13809	3.04058	1	1
66	2.1618	3.04145	1.0001	.999629
67	2.20448	3.04058	1	1

3.SUMMARY FOR GROUP NO. 1304

SURFACE CODE: 1
DISTANCE FROM L.E.(CM)= 4
STAGNATION PRESSURE (MM HG ABS)= 600
STATIC PRESSURE (MM HG)= 15.45
NO. OF BAD POINTS: 4

EDGE MACH NO.= 3.04058

EDGE VELOCITY (CM/SEC)= 63835.7
EDGE TEMPERATURE (DEG K)= 109.199
EDGE DENSITY (CGS)= 6.55388E-05
EDGE VISCOSITY (CGS)= 7.60139E-05
EDGE UNIT REYNOLDS NO.)CM-1)= 55038.8

B.L.THICKNESS DELTA (CM)= .07908
MOMENTUM THICKNESS THETA (CM)= 6.56241E-03
DELTA SQUARED (CM2)= 6.25365E-03
THETA SQUARED (CM2)= 4.30652E-05
DELTA/THETA= 12.0505
MOMENTUM REYNOLDS NO.= 361.187
REDELTA*DELTA= 344.193
RETHETA*THETA= 2.37025
REDELTA*DELTA/F(ME)= 109.735
SQYARE ROOT OF REX= 469.207

4.COMPRESSIBLE-TRANSFORMED PROFILE OF 1304

N	Y(CM)	YBAR(CM)	YBAR/THETA	U/UE
5	.0185175	6.97512E-03	1.06289	.215917
6	.02133	.0080471	1.22624	.24252
7	.0237675	.0089843	1.36906	.278195
8	.0263925	.0100054	1.52465	.31166
9	.0286425	.0108922	1.6598	.345966
10	.0308925	.0117917	1.79686	.375218
11	.033705	.0129359	1.97122	.415291
12	.035955	.0138699	2.11353	.446813
13	.0387675	.0150629	2.29534	.483997
14	.0410175	.0160403	2.44427	.515067
15	.043455	.0171261	2.60972	.549114
16	.0462675	.0184159	2.80627	.583917
17	.04833	.0193955	2.95554	.622992
18	.050955	.020693	3.15326	.659946
19	.0533925	.02195	3.34481	.696233
20	.0560175	.0233639	3.56027	.728619
21	.05883	.0249481	3.80168	.760776
22	.0612675	.0263929	4.02184	.79509
23	.06408	.028137	4.2876	.816237
24	.06633	.0296055	4.51138	.850829
25	.06933	.0316833	4.828	.876697
26	.0713925	.0331866	5.05708	.898768
27	.0740175	.0352015	5.36411	.921272
28	.076455	.0371807	5.66572	.943768
29	.07908	.039384	6.00146	.948257
30	.0815175	.0414772	6.32043	.960453
31	.083955	.0436432	6.65048	.970367
32	.0863925	.0458704	6.98988	.977804
33	.0890175	.0483188	7.36297	.982748
34	.091455	.0506276	7.71479	.98684
35	.09408	.0531486	8.09895	.990697
36	.09633	.0553329	8.4318	.992956
37	.0991425	.0580836	8.85097	.99486
38	.101393	.0602964	9.18815	.996009
39	.104393	.0632578	9.63943	.996941
40	.106642	.0654844	9.97872	.997354

B.4 (contd)

41	.10983	.0686434	10.4601	.997765
42	.111705	.0705038	10.7436	.99797
43	.11433	.0731107	11.1408	.998277
44	.11733	.0760928	11.5953	.998481
45	.119768	.0785176	11.9648	.998684
46	.122767	.0815037	12.4198	.998786
47	.12483	.0835573	12.7327	.998888
48	.127455	.0861721	13.1312	.998989
49	.129893	.0886005	13.5012	.998989
50	.132518	.0912167	13.8999	.999192
51	.134393	.0930865	14.1848	.999293
52	.136643	.0953302	14.5267	.999192
53	.139268	.0979483	14.9257	.999394
54	.141518	.100194	15.2678	.999496
55	.14433	.103002	15.6957	.999597
56	.146955	.105623	16.0951	.999597
57	.14883	.107495	16.3805	.999698
58	.15183	.110492	16.8371	.999698
59	.153705	.112365	17.1225	.999798
60	.156705	.115363	17.5794	.999798
61	.15933	.117986	17.9791	.999798
62	.161393	.120047	18.2932	.999899
63	.164205	.122859	18.7216	.999899
64	.166643	.125295	19.0929	.999899
65	.16908	.127732	19.4643	1
66	.170955	.129608	19.75	1.0001
67	.17433	.132983	20.2644	1

DO YOU WISH A FILE MADE FOR GRAPHICS (CR FOR YES,1 FOR NO)? 1
Ok

B.5 The GRAFXXXX Files

These files are outputs of the LAMBL-type programs and contain the same outputs as in the printouts (e.g. see B.4) in a form suitable for plotting on a graphics plotter. For each point of the profile given by the XXXX code, the following properties are provided:

In Order	Quantity
1st	N, i.e. the sequential point number
2nd	y, cm
3rd	y/δ
4th	$\tilde{y}/\theta$
5th	M
6th	u/u_e
7th	T/T_e
8th	ρ/ρ_e

B.6 The TOTALXX Files

These files were prepared for the express purpose of preparing graphics plots of each integral or general profile property vs. the streamwise distance. The XX designates the first two symbols of the profile code (Table II); e.g. TOTAL12 would be called to plot, say, θ vs. x for the smooth wall and P_o = 475 mm. The following properties are listed in these files:

In Order	Property
1st	x(cm)
2nd	δ(cm)
3rd	θ(cm)
4th	Re
5th	Re_δ δ(cm)

6th	$Re_\theta \theta$(cm)
7th	$(Re_x)^{1/2}$
8th	$Re'(cm^{-1})$

APPENDIX C: DATA REDUCTION PROCEDURES

1. Digitization

Referring to Figure C.1, the 10-second data bursts (groups) from the analog tapes were played back at 3 3/4 ips into the Rockland 512 Fast Fourier Transform Computer. In emerging from the latter, the data group was stored in the memory of the IBM 9000 Computer in digital form. Each such group file, called FABCD.BAS, is displayed and explained in Table C-I and is, of course, the spectrum of the AC hot-wire output consisting of 402 numbers grouped into 201 pairs (intensity vs. frequency). The upper frequency was 320 KHZ (10 KHZ in playback time) and the frequencies contained in FABCD.BAS are given as 0, 1, 2.... (to be multiplied later by 1.6 KHZ, which was the real-time window of the spectrum). The A, B, C, D in FABCD.BAS are explained in the Table C-II (this coding is the same as, and an extension of, the coding for the mean flow data shown on Table II).

Once the individual groups were digitized, the next task was to collect the groups belonging to each set and compose a "masterfile" for that set. This was done with the FILEFORM.BAS program of Table C-III. These masterfiles, designated FABZZ.BAS, were used directly as inputs to the data-reduction program STABLE02.BAS (see following section). Note the format of these files from Table C-I and Table C-IV. In the latter, a masterfile structure example (for file F51ZZ.BAS) shows how hot-wire "noise" spectra (groups) were included. In this example there are two noise groups, F51922 and F51932 (the last digit of these two designations is not important to this discussion). It was found that the data obtained for set 51 (smooth wall, free stream, P_o = 350 torr) from x = 1.3" to 3.7" were subject to a different electronic noise (in this case F51922) than were the data obtained from x = 3.8" to 6.6" (this happens because of time-dependence in the lab's electronic noise environment

and is a rather minor point). Thus in this example the net signal for groups 5113 through 5137 is obtained by appropriately subtracting from them group 51922; these groups form one "noise family". This is important since the data reduction program, when commanded to process set F51ZZ, querries the user on the number of such "noise families" (see following section). Table C-V, which summarizes this information for all data sets, is used as an important advisory to the computer operator during data reduction.

2. Description of the STABLE02 PROGRAM

This program, written in BASIC language for the IBM System 9000 Laboratory Computer, is listed in Table C-VI. Relevant information regarding STABLE02 also appears in Table C-VII and Figure C.2. The inputs to this program are the F--ZZ.BAS data files (Table C-IV), which must be in the system storage during the program run.

After the LOAD/RUN command, the system asks the operator seven questions which are answerable by the last seven numbers in each row of Table C-V in that sequence. Note that in the lines 5-711 the program is set to recognize the present data, i.e. modifications are necessary in order to process future data, say, at a P_o not used in this test. Also, on three occasions (lines 546, 556, 566), the program splices together data from two different hot-wires.

The program will next provide the option menu of lines 722-1100. As soon as the operator chooses an option the program jumps to the program line indicated by lines 1110-1220. The function of each option is as follows:

2.1. Option 1: Raw Spectrum

This is a direct display of the data as digitized by the FFT Computer. The results are tabulated on the CRT screen only (volatile).

2.2. Option 2: Noise-Free Spectrum

This is just like Option 1, but the resulting spectral density (the A(f)) is noise-free.

2.3. Option 3: Raw Spectrum Plot

Identical to Option 1, but the computer CRT screen presents a plot of A(f) vs. f (volatile). Control of maximum f and A(f) in this plot allows the operator to magnify portions of the spectrum.

2.4. Option 4: Noise-Free Spectrum Plot

As in Option 2, but a volatile net spectrum plot is obtained as opposed to a tabulation. In addition one can make, on command, a permanent graphics file of the net spectrum. All "graphics" files mentioned herein are suitable for making formal, publication-grade plots by using the Hewlett-Packard 7470A System; they are, of course, suitable for any additional analysis of the data outside of the STABLE02 program.

The data on this separate file prepared in this option are:

1) Filename: SPABCD.BAS

2) Coding: AB: set number
CD: x position in tenths of inch from L.E.

3) Number of variables: 6, as follows:

Variable	Computer Symbol	Explanation	Units
1st	N	Frequency index (1-201)	---
2nd	f	Frequency	KHZ
3rd	F	Non-dim. frequency	---
4th	SA	Raw spectral density (rms)	volt/1.6 KHZ
5th	NA	Noise spectral density (rms)	volt/1.6 KHZ
6th	NET	Net spectral density A(f) (rms)	volt/1.6 KHZ

4) Number of points: 201

2.5. Option 5: RMS Variation Along Plate

The wideband rms hot-wire AC signal is computed in this option vs. position along the plate. The results are given by a volatile CRT screen tabulation or, on command, on hard copy produced by the IBM 9000 printer.

It has been observed that in the free stream the wideband signal is very close to the wideband noise. As is frequently the case, the electronic noise in the laboratory environment underwent small variations from one hour or one day to the next, especially at the high frequencies. Occasionally these small variations made the high-frequency portion of the noise appear bigger than the portion of the signal spectrum itself, producing a negative net signal at the high frequencies. To avoid this, advantage was taken of the fact that the free stream signal in the wind-tunnel was insignificant above about 100 KHZ. Thus, for the "free stream" sets 51.... and 61.... the wideband rms signal and noise were obtained by summing the Fourier components only up to 112 KHZ (line 5512 in the program).

Note that to subtract the noise both for narrowband and wideband options throughout the program, the usual procedure was obtained by assuming that the noise and signal for each Fourier component are uncorrelated (subtraction in the squares). Also, wideband rms signals were obtained by computing the square roots of the sums of the squares of the narrowband Fourier amplitudes.

2.6. Option 6: RMS Variation Along Plate

The only difference between this and Option 5 is the form of the outputs supplied. Option 6 supplies a volatile graph of A(f) vs. x on the CRT screen, and then asks if a permanent graphics datafile should be made. The data for such a file are:

1) Filename: RMSAB.BAS

2) Coding: AB: set number

3) Number of variables: 7, as follows:

Variable	Computer Symbol	Explanation	Units
1st	x	Distance from L.E.	inch
2nd	x	Distance from L.E.	cm
3rd	REX	Re_x	---
4th	SQR(REX)	$R = (Re_x)^{1/2}$	---
5th	RETHNOM	Re_θ nominal (see below)	---
6th	RETHACT	Re_θ actual (see below)	---
7th	RMSI	Net rms	volts

4) Number of Points: These vary according to the following schedule:

SURFACE	P_o(TORR)	BL/FS	CODE	FILENAME	NO. OF POINTS
SMOOTH	350	BL	31	RMS31	63
	475		32	RMS32	55
	600		33	RMS33	44
ROUGH	350		21	RMS21	72
	475		22	RMS22	65
	600		23	RMS23	52
SMOOTH	350	FS	51	RMS51	54
	475		52	RMS52	45
	600		53	RMS53	38
ROUGH	350		61	RMS61	65
	475		62	RMS62	29

The "Re_θ actual" and "Re_θ nominal" are explained in the text.

2.7. Option 7: Amplitude Change With x (Tabulations Only)

In this option the net spectral density A(f) for a given frequency f is found as a function of distance along the plate. The results are given both in volatile form of a CRT screen tabulation and, if desired, also as hard copy. (Note: In this option, as well as in Option 8, the resulting A(x;f) variations denote the directly-measured experimental points; while in Option 9 "theoretical" values of A(f) additionally found by curve-fitting the A(x;f) variations are also given.)

2.8. Option 8: Amplitude Change With x (Graphics)

This is identical to Option 7 except that the results are displayed as a volatile CRT screen plot or, on command, stored into a graphics file with the following characteristics:

1) Filename: AABCDE.BAS

2) Coding: AB: set numbers
CDE: frequency-index number J1 (1-201, where the actual frequency in real time KHZ is given by 1.6(J1-1))

3) Number of points as follows:

Set No.*	No. of Points	Set No.	No. of Points
31	63	51	54
32	55	52	45
33	44	53	38
21	72	61	65
22	65	62	29
23	52		

4) Number of variables: 6, as follows:

NO.	SYMBOL	EXPLANATION	UNITS
1st	x	Distance from L.E.	cm
2nd	REX	Re_x	---
3rd	SQR(REX)	R	---
4th	RETHNOM	Re_θ nominal	---
5th	RETHACT	Re_θ actual	---
6th	NET	A(f) (spectral density)	volts rms/1.6 KHZ

2.9. Option 9: Curve-Fitted Amplitude Change With x

The purpose of this option is to present the A(f) vs. x variation (for chosen f) of Options 7 and 8 in analytic form, by providing least-squares curve-fits to the A(f) vs. x data. Therefore, this option is a "dressing room" in which the degree of the curve-fitting polynomial is chosen and a CRT

*For example, set 31 corresponds to file F31ZZ.BAS.

screen plot is quickly produced both of the actual data points and the fitting polynomial. If the fit, in the judgment of the operator, appears unsuitable then another degree is chosen and the process speedily repeated until the best fit is achieved.

This is a very important option of the STABLE02 program where the data stretch through the laminar and transitional ranges and where preconceptions about the required polynomial fit can result in significant errors in the amplification rates. A more detailed account of how this option was used for the present data appears in Appendix D. This appendix notes that the majority of data were reduced using a 7th-degree polynomial fitting only the points $x <$ '0 cm. The latter range, of x, is also optional during execution of Option 9; some curve-fits were made by taking the entire range of x (these are the so-called EX----- files, see below).

The option querries the operator for the desired frequency to be examined, the maximum x as per above, the maximum value of spectral density (amplitude or spectral density A(f) in each 1.6 KHZ window) and the desired degree of polynomial fit (1-12). When the answers are provided, the CRT screen shows a graph of the data points A(f) vs. x for the chosen frequency, with x ranging from 0 to the limit given, and A(f) from 0 to the amplitude limit given. The computer then also gives, on the same graph, a curve which is the required curve-fit. If the operator wishes a different polynomial degree he so commands until the desired fit is reached.

The program next asks the operator whether graphics data files of the displayed result are desired. If so, the operator is next asked whether files of (a) data points only, (b) amplitude and dimensional amplification, are desired. The former are designated by "PT" and the latter by "CF". The PT files are set up as follows:

1) Filename: PTABCDE.BAS

2) Coding: AB: set number
CDE: frequency index (1-201). Actual frequency is f(KHZ)=1.6 CDE.

3) Number of points: Depends wholly on the desired range of x, as stated during execution (program line 9530). Since the CRT display of this file takes place before a decision to make such a file is taken, the operator can count the data points included in the graph. In analyzing the present test results, the x range was limited to 10 cm for curve-fitting purposes; in $0 < x < 10$ cm the points in PT files were:

Set No.	No. of Points	Set No.	No. of Points
31	36	51	27
32	37	52	31
33	36	53	30
21	36	61	29
22	33	62	29
23	37		

4) Number of variables: 3, as follows:

Variables	Symbol	Explanation	Units
1st	XCF	Distance from L.E.	cm
2nd	RETHNOM	Re_θ nominal	---
3rd	YCF	Spectral density (amplitude A(f))	vrms/1.6 KHZ

Recall that the A----- files of Option 8 produce much the same type file with the total number of x stations recorded for each set.

The files CF produce curve-fits of the data displayed on the CRT screen during this option and stored in the PT files. All data contained in this file are results of the curve fit; for example the 3rd variable in the PT file (see above) is the experimentally determined A(f), whereas CF---- will produce a A(f) which is the theoretical A(f) lying on the polynomial curve. In addition CF produces the dimensional amplification rate dA/dx as well as the usual non-dimensional one:

$$-\alpha_i(R;f) = \frac{1}{2A}\,\frac{\partial A(R;f)}{\partial R}$$

1) Filename: CFABCDEF.BAS

2) Coding: AB: Set number
CDE: frequency index (1-201)
F: polynomial degree

3) Number of points: 100

4) Number of variables: 5, as follows:

Variable	Symbol	Explanation	Units
1st	G(N1)	Distance from L.E.	cm
2nd	R	$R = (Re_x)^{1/2}$	---
3rd	P(N1)	Spectral density (theoretical A(f))	vrms/1.6 KHZ
4th	P1(N1)	Dimensional amplification rate	vrms/cm
5th	$-\alpha_i$	Non-dimensional amplification rate	---

NOTE: In analyzing the present data, this option was occasionally also run using the full available range of x (this was suitable for studying amplification rates of the second mode). In this case, the polynomial degree *was again 7 and the file was prefixed* "EX" *rather than* "CF"; *otherwise* everything was identical to "CF" files. In this case, if one wished to plot both the A(f) points and their curve-fits on the same graph, one produced and used A----- files from Option 8 together with EX----- files (just as one matched PT---- and CF----- files for x < 10 cm).

2.10. Option 10: Poles of the Stability Diagram

The purpose of this option is to provide points in the stability diagram marking the "lower" and "upper" neutral branches as well as the maxima and minima in the amplification rates. This is done exclusively using the curve-fitted curves of $-\alpha_i$ vs. x (or R, Re_θ, etc.). The lower branch is defined as the point on the F, Re_θ plane where $-\alpha_i$ (at a fixed frequency) changes from negative to positive, and the opposite is true for the "upper branch."

The results are presented as a volatile CRT screen tabulation, after

which the operator can obtain hard copy of the tabulation or ask the machine to prepare any of four graphics files as follows:

FILENAME	PURPOSE
LOWERAB.BAS	Locates the lower-branch points in the diagram.
UPPERAB.BAS	Locates the upper-branch points in the diagram.
MAXAMAB.BAS	Locates maxima in the $-\alpha_i$ vs. R curve.
MINAMAB.BAS	Locates minima in the $-\alpha_i$ vs. R curve.

AB: set number

Thus each data set produces four files, as above. Also note that for each of these files, at each frequency there can be more than one point in each file, e.g. there may be two or more upper neutral branches (this was, of course, a key issue in this experiment where the data disclosed the existence of more than one unstable region).

The number of points were as follows:

Set No. (AB)	LOWERAB	UPPERAB	MAXAMAB	MINAMAB
31	184	113	198	271
32	161	67	127	217
33	129	73	129	180
21	224	153	203	266
22	159	110	192	207
23	112	88	200	198
51	303	281	288	317
52	234	236	279	275
53	199	189	261	270
61	375	284	291	381
62	379	290	294	385
VARIABLES:	6	6	7	7

As indicated, the number of variables differ, and were as follows:

Variable	Symbol	Explanation	Units
1st	f(KHZ)	Frequency	KHZ
2nd	F	Non-dimensional frequency	---
3rd	XL(J)	Distance from L.E.	cm
4th	SQR(REX)	R	---
5th	RETHNOM	Re_θ nominal	---
6th	RETHACT	Re_θ actual	---

and for MINAMAB, MAXAMAB only,

7th	PlMAX	$(-\alpha_i)_{maximum}$ for MAXAM	---
7th	PlMIN	$(-\alpha_i)_{minimum}$ for MINAM	---

2.11. Option 11: Amplification-Rate Spectrum

The purpose of this option is to produce amplification spectra, i.e. the variation $-\alpha_i$ vs. F for chosen values of R (or x or Re_θ). Restrictions are: (a) the option is based on 7th degree polynomials, (b) the 7th-degree fit is again done only for $x < 10$ cm, (c) the amplification spectra for R higher than those corresponding to $x = 10$ cm will therefore be possible but unreliable, (d) the spectra are limited below F corresponding to 160 KHZ.

The option produces volatile CRT screen tabulation of $-\alpha_i$ vs. F. On command, graphics files are produced as follows:

1) Filename: ASABCDE.BAS

2) Coding: AB: set number
CDE: R value

3) Number of points: 100

4) Number of variables: 2, as follows:

Variable	Symbol	Explanation	Units
1st	F	Non-dimensional frequency F	---
2nd	RATE (J1)	Non-dimensional amplification rate $-\alpha_i$	---

2.12. Option 12: Total Amplification Spectrum

The purpose of this option is to find the total amplification of the disturbance of a given frequency f between two points x_1 and x_2 on the plate or, rather, R_1 and R_2. The computer does this with the curve-fitted A(R) variations, first by calculating these variations with Option 9 (again curve-fitting with 7th degree polynomials the data in $x < 10$ cm). The initial $R_o = R_1$ is chosen to be 150 (this is near the minimum x measured, near and below which the curve-fits are unreliable). Then, for an operator-chosen R_2 the machine provides $A(R_2)/A(R_1)$. Note that R_1 can be changed in line 12720 of the program.

Graphics files are also made as follows:

1) Filename: TOTABCDE

2) Coding: AB: set number
CDE: R_2 value

3) Number of points: 100 (to 160 KHZ)

4) Number of variables: 2, as follows:

Variable	Symbol	Explanation	Units
1st	F	Non-dimensional frequency	---
2nd	TOT	$A(f;R_2)/A(f;R_1)$	---

2.13. Changes in the Curve-Fitted x-Range

If desired, the curve-fitted x range can be easily changed. For example, to curve-fit from 0 to 15 cm., do the following:

For Option 9: Answer querry (line 9530) with "15"

For Option 10: Change line 10540 to read: LET X1 = 15

For Option 11: Change line 12110 to read: LET X1 = 15

For Option 12: Change line 12630 to read: LET X1 = 15

2.14 Changes in the Curve-Fitting Polynomial Degree

If desired, the curve-fitting polynomial degree (up to 11) can also be changed. For example, to use 6th degree polynomials:

For Option 9: Answer querry (line 9550) with "6"

For Option 10: Change line 10578 to read "LET NCF = 6"

For Option 11: Change line 12150 to read "LET NCF = 6"

For Option 12: Change line 12700 to read "LET NCF = 6"

TABLE C-I

FORMAT OF F-----.BAS AND F--ZZ.BAS FILES

A. FILES F-----.BAS (GROUP DATA)

Numbers in Sequence (Example):

3214	Group Code			
0	First frequency	First pair		
59.86	First A(f)			
1	Second frequency	Second pair	201 pairs	403 numbers
62.59	Second A(f)			
2	Third frequency		(402 numbers)	
....				
200	Last frequency	Last pair		
0.135	Last A(f)			

B. FILES F--ZZ.BAS (SET DATA)

Numbers in Sequence (Example)

3202	Group Code		
0	First frequency		
53.2	First A(f)	First group	
1	Second frequency		
62.12	Second A(f)		
....			
3203	Group code		
0	First frequency	Second group	
55.7	First A(f)		
....			
3216	Group code		
0	First frequency	Last group	Set masterfile F32ZZ.BAS (Number of numbers depends on number of groups and noise groups.).
50.2	First A(f)		
....			
3281	Group code		
0	First frequency	First noise group	
1.32	First A(f)		
1	Second frequency		
0.97	Second A(f)		
....			
3282	Group code		
0	First frequency	Second noise group	
1.02	First A(f)		

TABLE C-II

CODING FOR THE HOT-WIRE ANEMOMETER DATA

In input data files (e.g. FABCD), output graphics files (e.g. GRAFABCD) etc. the sequence ABCD has the following meaning for each data group:

A: For smooth wall (boundary-layer data) A = 3

For smooth wall (free-stream data) = 5

For rough wall (boundary layer data) = 2

For rough wall (free-stream data) = 6

B: P_o = 350 torr, B = 1

475 torr, = 2

600 torr, = 3

CD: Distance from plate L.E. in tenths of an inch

Exceptions to CD: If C = 8 or 9, the group is a noise group:

C = 8 (wire current = 0)

C = 9 (wire current very small)

and:

D = 1, 2, 3..... to simply identify different noise groups.

TABLE C-III. THE FILEFORM PROGRAM

```
Program FILEFORM:
6 DIM Y(55, 405),I(100),J(405)
10 INPUT "TYPE DESIRED SET MASTERFILE NAME (IN QUOTES)";A$
15 IF A$="Q" GOTO 10000
20 OPEN A$ FOR OUTPUT AS FILE #1
30 FOR I=1 TO 100
40 INPUT "TYPE INPUT GROUP FILENAME IN QUOTES ('END' IF DONE)";B$
50 IF B$="END" GOTO 9000
60 OPEN B$ FOR INPUT AS FILE #2
70 FOR J=1 TO 403
80 INPUT #2,Y(I,J)
90 PRINT #1,Y(I,J)
100 NEXT J
105 CLOSE #2
110 NEXT I
9000 CLOSE #1
10000 END
```

TABLE C-IV

DATA-SET FILE FORMAT ACCEPTABLE TO THE STABLE02 PROGRAM

(example shown is set F51ZZ.BAS)

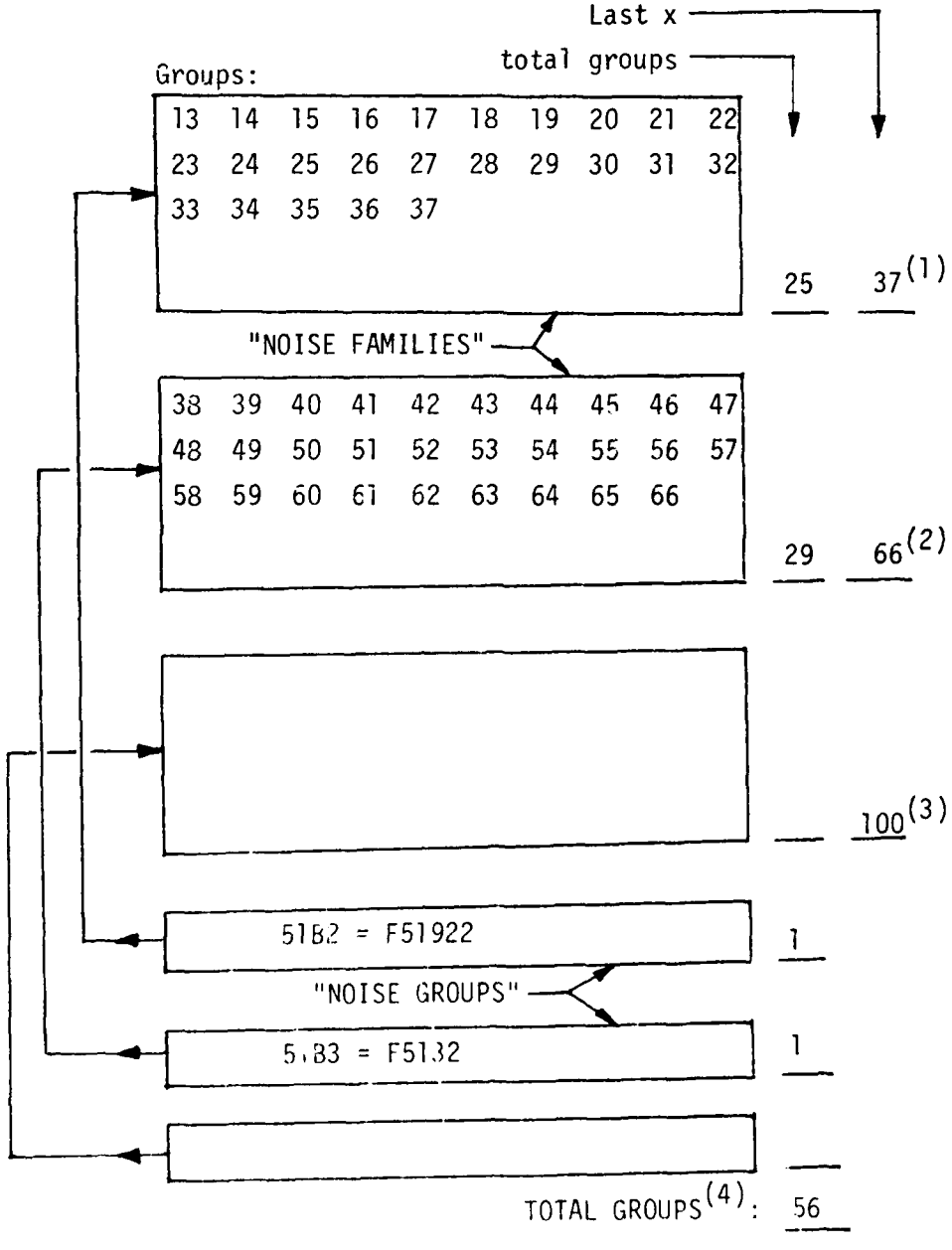

(1): 3rd question of program, (2) 4th question,
(3): 5th question, (4): 1st question

TABLE C-V

SUMMARY OF SET DATA PROCESSED BY THE
DATA-REDUCTION PROGRAM STABLE02

BOUNDARY LAYER DATA

SURFACE	P_o(TORR)	SET NAME	TOTAL GROUPS	NO. OF FREQUENCIES	LAST x(1): 1st FAMILY	2nd FAMILY	3rd FAMILY	NO. OF FAMILIES
SMOOTH	350	F31ZZ(2)	64	201	61	100(3)	100(3)	1
	475	F32ZZ	57	201	29	57	100	2
	600	F33ZZ	45	201	47	100	100	1
ROUGH	350	F21ZZ	75	201	43	72	77	3
	475	F22ZZ	67	201	37	73	100	2
	600	F23ZZ	53	201	56	100	100	1

FREE STREAM DATA

SMOOTH	350	F51ZZ	56	201	37	66	100	2
	475	F52ZZ	47	201	37	53	100	2
	600	F53ZZ	40	201	37	47	100	2
ROUGH	350	F61ZZ	66	201	77	100	100	1
	475	F62ZZ	31	201	17	37	100	2

Notes: 1) Indicates last group in set, in tenths of an inch from L.E.
2) Terminator .BAS needed to process by STABLE02
3) The "100" is a code with no physical meaning

TABLE C-VI. THE STABLE02 PROGRAM.

```
5 REM THIS IS PROGRAM STABLE02
6 REM VERSION OF 4/4/85
10 DIM N(202),S(82,202),A(100)
11 DIM NATOT(100)
12 DIM C(100),P(100)
13 DIM ACF(15),BCF(15),SCF(15),GCF(15),UCF(15)
14 DIM QCF(200),PCF(200),XCF(200),YCF(200),CCF(200)
15 DIM P1(100)
16 DIM P2(100)
17 DIM DX(100)
18 DIM RATE(200)
19 DIM TOT(200)
20 INPUT "TYPE DESIRED INPUT SET FILENAME (IN QUOTES)";A$
30 OPEN A$ FOR INPUT AS FILE #1
40 INPUT "ENTER NUMBER OF GROUPS IN THIS SET: ";I
50 INPUT "ENTER NUMBER OF FREQUENCIES IN EACH GROUP: ";J
52 INPUT "ENTER LAST X OF FIRST NOISE FAMILY (IN TENTHS OF IN.) ";NOISE1
54 INPUT "ENTER LAST X OF SECOND NOISE FAMILY (IN TENTHS OF IN.) ";NOISE2
56 INPUT "ENTER LAST X OF THIRD NOISE FAMILY (IN TENTHS OF IN.) ";NOISE3
58 INPUT "ENTER NO  OF NOISE GROUPS (FAMILIES) IN THIS SET) ",NOISE4
60 FOR I1=1 TO I
65 INPUT #1,A(I1)
70 FOR J1=1 TO J
80 INPUT #1,N(J1),S(I1,J1)
90 NEXT J1
100 NEXT I1
110 IF FIX(A(1)/100)=31 GOTO 510
120 IF FIX(A(1)/100)=32 GOTO 520
130 IF FIX(A(1)/100)=33 GOTO 530
140 IF FIX(A(1)/100)=21 GOTO 540
150 IF FIX(A(1)/100)=22 GOTO 550
160 IF FIX(A(1)/100)=23 GOTO 560
170 IF FIX(A(1)/100)=41 GOTO 570
180 IF FIX(A(1)/100)=42 GOTO 580
190 IF FIX(A(1)/100)=43 GOTO 590
200 IF FIX(A(1)/100)=51 GOTO 600
210 IF FIX(A(1)/100)=52 GOTO 610
220 IF FIX(A(1)/100)=53 GOTO 620
230 IF FIX(A(1)/100)=61 GOTO 630
240 IF FIX(A(1)/100)=62 GOTO 640
250 IF FIX(A(1)/100)=63 GOTO 650
260 IF FIX(A(1)/100)=71 GOTO 660
270 IF FIX(A(1)/100)=72 GOTO 670
280 IF FIX(A(1)/100)=73 GOTO 680
290 IF FIX(A(1)/100)=81 GOTO 690
300 IF FIX(A(1)/100)=82 GOTO 700
310 IF FIX(A(1)/100)=83 GOTO 710
510 LET B$="SOLID PLATE, B.LAYER, P=350"
511 LET RE=29380
512 LET F1=3.31E-9
515 GOTO 720
520 LET B$="SOLID PLATE, B.LAYER, P=475"
521 LET RE=43880
522 LET F1=2.25E-9
525 GOTO 720
530 LET B$="SOLID PLATE, B.LAYER, P=600"
531 LET RE=56120
532 LET F1=1.75E-9
535 GOTO 720
540 LET B$="ROUGH PLATE, B.LAYER, P=350"
541 LET RE=28750
542 LET F1=3.4E-9
543 FOR I1=1 TO I
544 IF A(I1)-100*FIX(A(I1)/100)<40 GOTO 548
545 FOR J1=1 TO J
546 IF A(I1)-100*FIX(A(I1)/100)<80 THEN LET S(I1,J1)=1.438*S(I1,J1)
547 NEXT J1
548 NEXT I1
549 GOTO 720
550 LET B$="ROUGH PLATE, B.LAYER, P=475"
551 LET RE=43080
552 LET F1=2.3E-9
553 FOR I1=1 TO I
554 IF A(I1)-100*FIX(A(I1)/100)<40 GOTO 558
555 FOR J1=1 TO J
556 IF A(I1)-100*FIX(A(I1)/100)<80 THEN LET S(I1,J1)=2.01*S(I1,J1)
557 NEXT J1
558 NEXT I1
559 GOTO 720
560 LET B$="ROUGH PLATE, B.LAYER, P=600"
561 LET RE=55140
562 LET F1=1.79E-9
563 FOR I1=1 TO I
564 IF A(I1)-100*FIX(A(I1)/100)<40 GOTO 568
565 FOR J1=1 TO J
566 IF A(I1)-100*FIX(A(I1)/100)<80 THEN LET S(I1,J1)=1.395*S(I1,J1)
567 NEXT J1
568 NEXT I1
569 GOTO 720
570 LET B$="BLOWING PLATE, B.LAYER, P=350"
571 LET RE=31280
572 LET F1=3.02E-9
575 GOTO 720
580 LET B$="BLOWING PLATE, B.LAYER, P=475"
581 LET RE=44010
582 LET F1=2.22E-9
585 GOTO 720
590 LET B$="BLOWING PLATE, B.LAYER, P=600"
591 LET RE=53540
592 LET F1=1.85E-9
595 GOTO 720
600 LET B$="SOLID PLATE, F.STREAM, P=350"
601 LET RE=29380
602 LET F1=3.31E-9
605 GOTO 720
610 LET B$="SOLID PLATE, F.STREAM, P=475"
611 LET RE=43880
612 LET F1=2.25E-9
615 GOTO 720
620 LET B$="SOLID PLATE, F.STREAM, P=600"
621 LET RE=56120
622 LET F1=1.75E-9
625 GOTO 720
630 LET B$="ROUGH PLATE, F.STREAM, P=350"
631 LET RE=28750
632 LET F1=3.4E-9
635 GOTO 720
640 LET B$="ROUGH PLATE, F.STREAM, P=475"
641 LET RE=43080
642 LET F1=2.3E-9
```

```
645 GOTO 720
650 LET B$="ROUGH PLATE, F.STREAM, P=600"
651 LET RE=55140
652 LET F1=1.79E-9
655 GOTO 720
660 LET B$="BLOWING PLATE, F.STREAM, P=350"
661 LET RE=31280
662 LET F1=3.02E-9
665 GOTO 720
670 LET B$="BLOWING PLATE, F.STREAM, P=475"
671 LET RE=44010
672 LET F1=2.22E-9
675 GOTO 720
680 LET B$="BLOWING PLATE, F.STREAM, P=600"
681 LET RE=53540
682 LET F1=1.85E-9
685 GOTO 720
690 LET B$="EMPTY TUNNEL, P=350"
691 LET RE=29380
695 GOTO 720
700 LET B$="EMPTY TUNNEL, P=475"
701 LET RE=43880
705 GOTO 720
710 LET B$="EMPTY TUNNEL, P=600"
711 LET RE=56120
720 CLS
722 PRINT B$
725 PRINT "----------------------------------------"
730 PRINT
735 PRINT "                              MENU OF OPTIONS"
740 PRINT
750 PRINT "1. RAW SPECTRUM (GROUP) PRINT-OUT"
760 PRINT "2. NOISE-FREE SPECTRUM (GROUP) PRINT-OUT"
770 PRINT "3. RAW SPECTRUM (GROUP) PLOT"
780 PRINT "4. NOISE-FREE SPECTRUM PLOT (W/ HP GRAPHICS OPTION)"
790 PRINT "5. RMS VARIATION WITH X (PRINTOUT)"
800 PRINT "6. NET RMS VARIATION WITH X (PLOT W/ HP GRAPHICS OPTION)"
810 PRINT "7. AMPLITUDE CHANGE WITH X (PRINTOUT W/ HARDCOPY OPTION)"
820 PRINT "8. AMPLITUDE CHANGE WITH X FOR GIVEN N (W/ HP GRAPHICS OPTION)"
830 PRINT "9. CURVE-FIT OF AMPLITUDE CHANGE FOR GIVEN N"
840 PRINT "10. STABILITY DIAGRAM POLES"
850 PRINT "11. AMPLIFICATION RATE SPECTRUM (CRT OR HP GRAPHICS OPTIONS)"
860 PRINT "12. TOTAL AMPLIFICATION SPECTRUM (CRT OR GRAPHICS OPTIONS)"
1095 PRINT
1100 INPUT "ENTER THE NUMBER OF YOUR CHOICE",C
1110 IF C=1 GOTO 1500
1120 IF C=2 GOTO 2500
1130 IF C=3 GOTO 3500
1140 IF C=4 GOTO 4500
1150 IF C=5 GOTO 5500
1160 IF C=6 GOTO 6500
1170 IF C=7 GOTO 7500
1180 IF C=8 GOTO 8500
1190 IF C=9 GOTO 9500
1200 IF C=10 GOTO 10500
1210 IF C=11 GOTO 12000
1220 IF C=12 GOTO 12500
1500 CLS
1510 PRINT B$
1520 PRINT
1530 INPUT "RAW SPECTRUM PRINTOUT:ENTER DESIRED X (IN TENTHS OF IN.): ";X
1540 PRINT
1550 FOR I1=1 TO I
1560 IF A(I1)-100*FIX(A(I1)/100)=X GOTO 1622
1570 NEXT I1
1580 PRINT "NO GROUP AVAILABLE FOR SUCH X IN THIS SET"
1590 INPUT "ENTER 'M' FOR MENU, 'X' FOR ANOTHER X, 'Q' TO QUIT: ";B1$
1600 IF B1$="X" GOTO 1500
1610 IF B1$="M" GOTO 720
1620 IF B1$="Q" GOTO 20000
1622 PRINT "N","FREQUENCY","FREQUENCY","INTENSITY"
1624 PRINT TAB(8),"(KHZ)","2(pi)f/uRe","(VOLTS RMS)"
1626 PRINT
1640 FOR J1=1 TO J
1650 PRINT N(J1),1.6*N(J1),1600*N(J1)*F1,S(I1,J1)
1660 NEXT J1
1670 PRINT "NEXT CHOICE:"
1680 PRINT "                1. PRINT ANOTHER X-POSITION"
1690 PRINT "                2. RETURN TO MENU"
1700 PRINT "                3. QUIT PROGRAM"
1710 PRINT
1720 INPUT "ENTER YOUR CHOICE:";C1
1730 IF C1=1 GOTO 1500
1740 IF C1=2 GOTO 720
1750 IF C1=3 GOTO 20000
2500 CLS
2510 PRINT B$
2520 PRINT
2530 INPUT "NET SPECTRUM PRINTOUT: ENTER DESIRED X (IN TENTHS OF IN.) ";X
2540 PRINT
2550 FOR I1=1 TO I
2560 IF A(I1)-100*FIX(A(I1)/100)=X GOTO 2640
2570 NEXT I1
2580 PRINT "NO GROUP AVAILABLE FOR SUCH X IN THIS SET"
2590 INPUT "ENTER 'X' FOR ANOTHER X, 'M' FOR MENU, 'Q' TO QUIT: ";B1$
2600 IF B1$="X" GOTO 2500
2610 IF B1$="M" GOTO 720
2620 IF B1$="Q" GOTO 20000
2640 PRINT "N","FREQUENCY","N/D FREQ.","RAW INTEN.","NET INTEN."
2643 PRINT TAB(8),"(KHZ)","2(pi)f/uRe'","(VOLTS RMS)","(VOLTS RMS)"
2646 PRINT
2650 IF X<=NOISE1 GOTO 2656
2652 IF X<=NOISE2 GOTO 2670
2654 IF X<=NOISE3 GOTO 2684
2656 FOR J1=1 TO J
2658 LET SA=S(I1,J1)
2660 LET NA=S(I-NOISE4+1,J1)
2662 LET NET=SQR(ABS(SA^2-NA^2))
2664 PRINT N(J1),1.6*N(J1),1600*N(J1)*F1,SA,NET
2666 NEXT J1
2668 GOTO 2700
2670 FOR J1=1 TO J
2672 LET SA=S(I1,J1)
2674 LET NA=S(I-NOISE4+2,J1)
2676 LET NET=SQR(ABS(SA^2-NA^2))
2678 PRINT N(J1),1.6*N(J1),1600*N(J1)*F1,SA,NET
2680 NEXT J1
2682 GOTO 2700
2684 FOR J1=1 TO J
2686 LET SA=S(I1,J1)
```

```
2688 LET NA=S(I-NOISE4+3,J1)
2690 LET NET=SQR(ABS(SA^2-NA^2))
2692 PRINT N(J1),1.6*N(J1),1600*N(J1)*F1,SA,NET
2694 NEXT J1
2700 PRINT
2720 PRINT "NEXT CHOICE. "
2730 PRINT "              1. PRINT ANOTHER X-POSITION"
2740 PRINT "              2. RETURN TO MENU"
2750 PRINT "              3. QUIT PROGRAM"
2760
2770 INPUT "ENTER YOUR CHOICE: ";C1
2780 IF C1=1 GOTO 2500
2790 IF C1=2 GOTO 720
2800 IF C1=3 GOTO 20000
3500 CLS
3510 PRINT B$
3520 PRINT
3530 INPUT "RAW SPECTRUM PLOT. ENTER DESIRED X (IN TENTHS OF IN.): ";X
3540 PRINT
3550 FOR I1=1 TO I
3560 IF A(I1)-100*FIX(A(I1)/100)=X GOTO 3650
3570 NEXT I1
3580 PRINT "NO GROUP AVAILABLE FOR SUCH X IN THIS SET"
3590 INPUT "ENTER 'X' FOR ANOTHER X,'M' FOR MENU OR 'Q' TO QUIT ";B1$
3600 IF B1$="X" GOTO 3500
3610 IF B1$="M" GOTO 720
3620 IF B1$="Q" GOTO 20000
3650 CLS
3660 PRINT B$
3670 PRINT "PLOT OF RAW SPECTRUM AT X=";X/10;"IN. FROM L.E."
3672 PRINT "Choose plot-maximum coordinates, in response to questions which"
3673 PRINT "follow, which are convenient multiples of 5."
3674 INPUT "ENTER MAXIMUM DESIRED FREQUENCY (IN KHZ) ON PLOT ";F2
3676 INPUT "ENTER MAXIMUM DESIRED AMPLITUDE (IN VOLTS RMS) ON PLOT ";A2
3680 CLS
3682 PRINT B$
3684 PRINT "PLOT OF RAW SPECTRUM AT X=";X/10;"IN. FROM THE L.E."
3690 LINE (75,40,575,40)
3700 LINE (75,40,75,390)
3710 LINE (75,390,575,390)
3720 LINE (575,40,575,390)
3730 FOR I2=0 TO 5 STEP 1
3740 TEXT (71+100*I2,31,"+")
3760 TEXT (71+100*I2,381,"+")
3765 TEXT (71+100*I2,20,NUM1$(I2*F2/5))
3770 NEXT I2
3780 TEXT (255,0,"FREQUENCY (KHZ)")
3790 FOR I2=0 TO 5 STEP 1
3800 TEXT (84,36+70*I2,"+",1,1)
3810 TEXT (37,30+70*I2,NUM1$(I2*A2/5))
3820 TEXT (584,36+70*I2,"+",1,1)
3830 NEXT I2
3840 TEXT (30,75,"AMPLIFIER OUTPUT (VRMS/1.6KHZ)",1,1)
3845 FOR J1=1 TO J
3850 IF N(J1)=F2/1.6 GOTO 3860
3852 IF S(I1,J1))=A2 GOTO 3860
3855 LINE (800*N(J1)/F2+75,(S(I1,J1)/A2)*350+40,800*N(J1+1)/F2+75,&
(S(I1,J1+1)/A2)*350+40)
3860 NEXT J1
3900 INPUT "CHOOSE REPLOT SAME (RS),OTHER X (X), MENU (M), OR QUIT (Q) ",A3$
3901 IF A3$="M" GOTO 720
3902 IF A3$="RS" GOTO 3650
3903 IF A3$="X" GOTO 3500
3904 IF A3$="Q" GOTO 20000
4500 CLS
4510 PRINT B$
4520 PRINT
4530 INPUT "NET SPECTRUM PLOT: ENTER DESIRED X (IN TENTHS OF IN.): ";X
4540 PRINT
4550 FOR I1=1 TO I
4560 IF A(I1)-100*FIX(A(I1)/100)=X GOTO 4650
4570 NEXT I1
4580 PRINT "NO GROUP AVAILABLE FOR SUCH X IN THIS SET"
4590 INPUT "ENTER 'X' FOR ANOTHER X, 'M' FOR MENU OR 'Q' TO QUIT ";B1$
4600 IF B1$="X" GOTO 4500
4610 IF B1$="M" GOTO 720
4620 IF B1$="Q" GOTO 20000
4650 CLS
4660 PRINT B$
4670 PRINT "PLOT OF NET SPECTRUM AT X=",X/10;"IN. FROM L.E."
4672 PRINT "Choose plot-maximum coordinates, in response to questions which"
4673 PRINT "follow, which are convenient multiples of 5."
4674 INPUT "ENTER MAXIMUM DESIRED FREQUENCY (IN KHZ) ON PLOT ";F2
4676 INPUT "ENTER MAXIMUM DESIRED AMPLITUDE (IN VOLTS RMS) ON PLOT ";A2
4680 CLS
4682 PRINT B$
4684 PRINT "PLOT OF NET SPECTRUM AT X=",X/10,"IN. FROM THE L.E."
4690 LINE (75,40,575,40)
4700 LINE (75,40,75,390)
4710 LINE (75,390,575,390)
4720 LINE (575,40,575,390)
4730 FOR I2=0 TO 5 STEP 1
4740 TEXT (71+100*I2,31,"+")
4760 TEXT (71+100*I2,381,"+")
4765 TEXT (71+100*I2,20,NUM1$(I2*F2/5))
4770 NEXT I2
4780 TEXT (255,0,"FREQUENCY (KHZ)")
4790 FOR I2=0 TO 5 STEP 1
4800 TEXT (84,36+70*I2,"+",1,1)
4810 TEXT (37,30+70*I2,NUM1$(I2*A2/5))
4820 TEXT (584,36+70*I2,"+",1,1)
4830 NEXT I2
4840 TEXT (30,65,"NET AMPLIFIER OUTPUT (VRMS/1.6KHZ)",1,1)
4850 IF X<=NOISE1 GOTO 4900
4860 IF X<=NOISE2 GOTO 4930
4870 IF X<=NOISE3 GOTO 4960
4900 FOR J1=1 TO J
4910 IF N(J1))=F2/1.6 GOTO 4920
4911 IF S(I1,J1)-S(I-NOISE4+1,J1))=A2 GOTO 4920
4912 LET SA=S(I1,J1)
4913 LET NA=S(I-NOISE4+1,J1)
4914 LET NET=(SQR(ABS(SA^2-NA^2))/A2)*350+40
4915 LET SA1=S(I1,J1+1)
4916 LET NA1=S(I-NOISE4+1,J1+1)
4917 LET NET1=(SQR(ABS(SA1^2-NA1^2))/A2)*350+40
4918 LINE (800*N(J1)/F2+75,NET,800*N(J1+1)/F2+75,NET1)
4920 NEXT J1
4925 GOTO 4983
4930 FOR J1=1 TO J
4940 IF N(J1))=F2/1.6 GOTO 4950
```

```
4942 IF S(I1,J1)-S(I-NOISE4+2,J1))=A2 GOTO 4950
4943 LET SA=S(I1,J1)
4944 LET NA=S(I-NOISE4+2,J1)
4945 LET NET=(SQR(ABS(SA^2-NA^2))/A2)*350+40
4946 LET SA1=S(I1,J1+1)
4947 LET NA1=S(I-NOISE4+2,J1+1)
4948 LET NET1=(SQR(ABS(SA1^2-NA1^2))/A2)*350+40
4949 LINE (800*N(J1)/F2+75,NET,800*N(J1+1)/F2+75,NET1)
4950 NEXT J1
4955 GOTO 4983
4960 FOR J1=1 TO J
4970 IF N(J1))=F2/1.6 GOTO 4980
4972 IF S(I1,J1)-S(I-NOISE4+3,J1))=A2 GOTO 4980
4973 LET SA=S(I1,J1)
4974 LET NA=S(I-NOISE4+3,J1)
4975 LET NET=(SQR(ABS(SA^2-NA^2))/A2)*350+40
4976 LET SA1=S(I1,J1+1)
4977 LET NA1=S(I-NOISE4+3,J1+1)
4978 LET NET1=(SQR(ABS(SA1^2-NA1^2))/A2)*350+40
4979 LINE (800*N(J1)/F2+75,NET,800*N(J1+1)/F2+75,NET1)
4980 NEXT J1
4983 INPUT "DO YOU WISH SEPARATE (HP) GRAPHICS FILE CREATED (Y/N) ";H1$
4984 IF H1$="N" GOTO 5005
4985 INPUT "ENTER NAME OF THIS SEPARATE FILE (IN QUOTES): ";H2$
4987 OPEN H2$ FOR OUTPUT AS FILE #2
4988 FOR J1=1 TO J
4989 LET SA=S(I1,J1)
4990 IF X(=NOISE1 THEN LET NA=S(I-NOISE4+1,J1)
4991 IF X(=NOISE1 GOTO 4996
4992 IF X(=NOISE2 THEN LET NA=S(I-NOISE4+2,J1)
4993 IF X(=NOISE2 GOTO 4996
4994 IF X(=NOISE3 THEN LET NA=S(I-NOISE4+3,J1)
4995 IF X(=NOISE3 GOTO 4996
4996 LET NET=SQR(ABS(SA^2-NA^2))
4997 PRINT #2,N(J1)
4998 PRINT #2,1.6*N(J1)
4999 PRINT #2,1600*N(J1)*F1
5000 PRINT #2,SA
5001 PRINT #2,NA
5002 PRINT #2,NET
5003 NEXT J1
5004 CLOSE #2
5005 INPUT "CHOOSE REPLOT SAME (RS), OTHER X (X),MENU (M), OR QUIT (Q): ";A3$
5010 IF A3$="M" GOTO 720
5020 IF A3$="RS" GOTO 4650
5030 IF A3$="X" GOTO 4500
5040 IF A3$="Q" GOTO 20000
5500 CLS
5501 PRINT B$
5502 PRINT "------------------------------------"
5503 PRINT
5510 PRINT "RMS WIRE VOLTAGE VARIATION ALONG PLATE"
5512 IF FIX(A(1)/1000))=5 THEN LET J=70
5514 REM Line 5512 (and 6512) is specific to the 1983-84 data and
5516 REM restricts the wideband integration of f.s. signals to below
5518 REM 112 khz
5520 PRINT
5530 INPUT "ENTER OUTPUT OPTION: 'CRT' FOR CRT, 'HC' FOR HARDCOPY: ";B1$
5535 IF B1$="HC" THEN INPUT "Put printer ON LINE now and CR: ";JJ$
5540 FOR I1=I-NOISE4+1 TO I
5550 LET NATOT=0
5560 FOR J1=1 TO J
5570 LET NA=S(I1,J1)
5580 LET NATOT=NATOT+NA^2
5590 NEXT J1
5600 LET NATOT(I1)=NATOT
5620 NEXT I1
5630 IF B1$="HC" GOTO 5980
5640 PRINT
5650 PRINT "X","X","REX","RMS(+NOISE)","NET RMS"
5660 PRINT "(INCH)","(CM)"," - ","(VOLTS)","(VOLTS)"
5670 PRINT
5680 FOR I1=1 TO I-NOISE4
5690 LET SATOT=0
5700 LET X=A(I1)-100*FIX(A(I1)/100)
5710 IF X(=NOISE1 GOTO 5740
5720 IF X(=NOISE2 GOTO 5810
5730 IF X(=NOISE3 GOTO 5880
5740 FOR J1=1 TO J
5750 LET SA=S(I1,J1)
5760 LET SATOT=SATOT+SA^2
5770 NEXT J1
5772 IF NOISE4=1 THEN LET MSNOISE=NATOT(I)
5774 IF NOISE4=2 THEN LET MSNOISE=NATOT(I-1)
5776 IF NOISE4=3 THEN LET MSNOISE=NATOT(I-2)
5780 LET RMS1=SQR(SATOT-MSNOISE)
5790 LET RMS2=SQR(SATOT)
5800 GOTO 5940
5810 FOR J1=1 TO J
5820 LET SA=S(I1,J1)
5830 LET SATOT=SATOT+SA^2
5840 NEXT J1
5842 IF NOISE4=2 THEN LET MSNOISE=NATOT(I)
5844 IF NOISE4=3 THEN LET MSNOISE=NATOT(I-1)
5850 LET RMS1=SQR(SATOT-MSNOISE)
5860 LET RMS2=SQR(SATOT)
5870 GOTO 5940
5880 FOR J1=1 TO J
5890 LET SA=S(I1,J1)
5900 LET SATOT=SATOT+SA^2
5910 NEXT J1
5920 LET RMS1=SQR(SATOT-NATOT(I))
5930 LET RMS2=SQR(SATOT)
5940 PRINT X/10,2.54*(X/10),0.254*X*RE,RMS2,RMS1
5950 NEXT I1
5960 INPUT "HARD COPY (Y/N)";B2$
5965 IF B2$="Y" THEN INPUT "Put printer ON LINE now and CR: ";JJ$
5970 IF B2$="N" GOTO 6340
5980 OPEN "0PR" AS FILE #5
5990 PRINT #5,B$
6000 PRINT #5,"----------------------------------------"
6010 PRINT #5
6020 PRINT #5,"RMS WIRE VOLTAGE VARIATION ALONG PLATE"
6030 PRINT #5
6040 PRINT #5,"X","X","REX","RMS(+NOISE)","NET RMS"
6050 PRINT #5,"(INCH)","(CM)"," - ","(VOLTS)","(VOLTS)"
6060 PRINT #5
6070 FOR I1=1 TO I-NOISE4
6080 LET SATOT=0
6090 LET X=A(I1)-100*FIX(A(I1)/100)
```

```
6100 IF X(=NOISE1 GOTO 6130
6110 IF X(=NOISE2 GOTO 6200
6120 IF X(=NOISE3 GOTO 6270
6130 FOR J1=1 TO J
6140 LET SA=S(I1,J1)
6150 LET SATOT=SATOT+SA^2
6160 NEXT J1
6162 IF NOISE4=1 THEN LET MSNOISE=NATOT(I)
6164 IF NOISE4=2 THEN LET MSNOISE=NATOT(I-1)
6166 IF NOISE4=3 THEN LET MSNOISE=NATOT(I-2)
6170 LET RMS1=SQR(SATOT-MSNOISE)
6180 LET RMS2=SQR(SATOT)
6190 GOTO 6330
6200 FOR J1=1 TO J
6210 LET SA=S(I1,J1)
6220 LET SATOT=SATOT+SA^2
6230 NEXT J1
6232 IF NOISE4=2 THEN LET MSNOISE=NATOT(I)
6234 IF NOISE4=3 THEN LET MSNOISE=NATOT(I-1)
6240 LET RMS1=SQR(SATOT-MSNOISE)
6250 LET RMS2=SQR(SATOT)
6260 GOTO 6330
6270 FOR J1=1 TO J
6280 LET SA=S(I1,J1)
6290 LET SATOT=SATOT+SA^2
6300 NEXT J1
6310 LET RMS1=SQR(SATOT-NATOT(I))
6320 LET RMS2=SQR(SATOT)
6330 PRINT #5,X/10,2.54*(X/10),0.254*X*RE,RMS2,RMS1
6340 NEXT I1
6350 CLOSE #5
6360 INPUT "ENTER 'R' TO RERUN,'M' FOR MENU OR 'Q' TO QUIT: ";B3$
6370 IF B3$="R" GOTO 5500
6380 IF B3$="M" GOTO 720
6390 IF B3$="Q" GOTO 20000
6500 CLS
6510 PRINT B$
6512 IF FIX(A(1)/1000))=5 THEN LET J=70
6520 PRINT "---------------------------------"
6530 PRINT
6540 PRINT "PLOT OF RMS WIRE VOLTAGE VARIATION ALONG PLATE"
6550 PRINT "Choose plot-maximum coordinates in response to questions, which"
6560 PRINT "are convenient multiples of 5 "
6570 INPUT "ENTER MAXIMUM DESIRED X ON PLOT (CM): ";X1
6580 INPUT "ENTER MAXIMUM DESIRED RMS VOLTAGE (VOLTS): ",V
6582 CLS
6584 PRINT "NET RMS VARIATION WITH X FOR ";B$
6590 FOR I1=I-NOISE4+1 TO I
6600 LET NATOT=0
6610 FOR J1=1 TO J
6620 LET NA=S(I1,J1)
6630 LET NATOT=NATOT+NA^2
6640 NEXT J1
6650 LET NATOT(I1)=NATOT
6660 NEXT I1
6670 LINE (75,40,575,40)
6680 LINE (75,40,75,390)
6690 LINE (75,390,575,390)
6700 LINE (575,40,575,390)
6710 FOR I2=0 TO 5 STEP 1
6720 TEXT (71+100*I2,31,"+")
6730 TEXT (71+100*I2,381,"+")
6740 TEXT (71+100*I2,20,NUM1$(I2*X1/5))
6750 NEXT I2
6760 TEXT (255,0,"DISTANCE FROM L.E. (CM)")
6770 FOR I2=0 TO 5 STEP 1
6780 TEXT (84,36+70*I2,"+",1,1)
6790 TEXT (37,30+70*I2,NUM1$(I2*V/5))
6800 TEXT (584,36+70*I2,"+",1,1)
6810 NEXT I2
6820 TEXT (30,65,"NET WIDEBAND AMPLIFIER RMS OUTPUT (VOLTS)",1,1)
6830 FOR I1=1 TO I-NOISE4
6840 LET SATOT=0
6850 LET X=A(I1)-100*FIX(A(I1)/100)
6852 IF X(=NOISE1 GOTO 6860
6854 IF X(=NOISE2 GOTO 6920
6856 IF X(=NOISE3 GOTO 6980
6860 FOR J1=1 TO J
6870 LET SA=S(I1,J1)
6880 LET SATOT=SATOT+SA^2
6890 NEXT J1
6892 IF NOISE4=1 THEN LET MSNOISE=NATOT(I)
6894 IF NOISE4=2 THEN LET MSNOISE=NATOT(I-1)
6896 IF NOISE4=3 THEN LET MSNOISE=NATOT(I-2)
6900 LET RMS1=SQR(SATOT-MSNOISE)
6910 GOTO 7030
6920 FOR J1=1 TO J
6930 LET SA=S(I1,J1)
6940 LET SATOT=SATOT+SA^2
6950 NEXT J1
6952 IF NOISE4=2 THEN LET MSNOISE=NATOT(I)
6954 IF NOISE4=3 THEN LET MSNOISE=NATOT(I-1)
6960 LET RMS1=SQR(SATOT-MSNOISE)
6970 GOTO 7030
6980 FOR J1=1 TO J
6990 LET SA=S(I1,J1)
7000 LET SATOT=SATOT+SA^2
7010 NEXT J1
7020 LET RMS1=SQR(SATOT-NATOT(I))
7030 IF 0.254*X)=X1 GOTO 7060
7040 IF RMS1)=V GOTO 7060
7050 TEXT (75+(127*X)/X1,40+(350*RMS1/V),CHR$(111))
7060 NEXT I1
7070 INPUT "DO YOU WISH SEPARATE (HP) GRAPHICS FILE CREATED (Y/N) ";H1$
7080 IF H1$="N" GOTO 7380
7090 INPUT "ENTER NAME (RMS--) OF THIS SEPARATE FILE (IN QUOTES): ";H2$
7100 OPEN H2$ FOR OUTPUT AS FILE #3
7110 FOR I1=1 TO I-NOISE4
7120 LET SATOT=0
7130 LET X=A(I1)-100*FIX(A(I1)/100)
7132 IF X(=NOISE1 GOTO 7140
7134 IF X(=NOISE2 GOTO 7200
7136 IF X(=NOISE3 GOTO 7260
7140 FOR J1=1 TO J
7150 LET SA=S(I1,J1)
7160 LET SATOT=SATOT+SA^2
7170 NEXT J1
7172 IF NOISE4=1 THEN LET MSNOISE=NATOT(I)
7174 IF NOISE4=2 THEN LET MSNOISE=NATOT(I-1)
7176 IF NOISE4=3 THEN LET MSNOISE=NATOT(I-2)
```

```
7180 LET RMS1=SQR(SATOT-MSNOISE)
7190 GOTO 7310
7200 FOR J1=1 TO J
7210 LET SA=S(I1,J1)
7220 LET SATOT=SATOT+SA^2
7230 NEXT J1
7232 IF NOISE4=2 THEN LET MSNOISE=NATOT(I)
7234 IF NOISE4=3 THEN LET MSNOISE=NATOT(I-1)
7240 LET RMS1=SQR(SATOT-MSNOISE)
7250 GOTO 7310
7260 FOR J1=1 TO J
7270 LET SA=S(I1,J1)
7280 LET SATOT=SATOT+SA^2
7290 NEXT J1
7300 LET RMS1=SQR(SATOT-NATOT(I))
7310 PRINT #3,X/10
7312 PRINT #3,0.254*X
7314 LET REX=0.254*X*RE
7316 PRINT #3,REX
7318 PRINT #3,SQR(REX)
7320 PRINT #3,0.664*SQR(REX)
7322 IF FIX(A(1)/1000)=2 THEN LET A1=-0.1354
7324 IF FIX(A(1)/1000)=6 THEN LET A1=-0.1354
7326 IF FIX(A(1)/1000)=3 THEN LET A1=-6.609E-3
7328 IF FIX(A(1)/1000)=5 THEN LET A1=-6.609E-3
7330 IF FIX(A(1)/1000)=4 THEN LET A1=0
7332 IF FIX(A(1)/1000)=7 THEN LET A1=0
7334 IF FIX(A(1)/1000)=8 THEN LET A1=0
7336 IF FIX(A(1)/1000)=2 THEN LET A2=8.741E-4
7338 IF FIX(A(1)/1000)=6 THEN LET A2=8.741E-4
7340 IF FIX(A(1)/1000)=3 THEN LET A2=4.315E-4
7342 IF FIX(A(1)/1000)=5 THEN LET A2=4.315E-4
7344 IF FIX(A(1)/1000)=4 THEN LET A2=0
7346 IF FIX(A(1)/1000)=7 THEN LET A2=0
7348 IF FIX(A(1)/1000)=8 THEN LET A2=0
7349 IF C=10 GOTO 11370
7350 PRINT #3,0.664*SQR(REX)+A1*(REX/1000)+A2*((REX/1000)^2)
7356 PRINT #3,RMS1
7360 NEXT I1
7370 CLOSE #3
7380 INPUT "CHOOSE TO RE-DO ('R'),MENU ('M') OR QUIT ('Q'): ";A3$
7390 IF A3$="R" GOTO 6500
7400 IF A3$="M" GOTO 720
7410 IF A3$="Q" GOTO 20000
7500 CLS
7510 PRINT "AMPLITUDE CHANGE WITH X FOR ",B$
7520 PRINT
7530 INPUT "ENTER CHOICE OF FREQUENCY INDEX N=J1 (0-200): ";J1
7540 INPUT "ENTER CHOICE OF CRT PRINTOUT ('CRT') OR HARDCOPY ('HC') ";B7$
7545 IF B7$="HC" THEN INPUT "Now put printer on line and CR";J00
7550 IF B7$="HC" GOTO 8000
7555 CLS
7560 PRINT "AMPLITUDE CHANGE WITH X FOR ";B$
7570 PRINT "FREQUENCY INDEX N(J1)=";N(J1);" (f=";1.6*N(J1);" KHZ"
7580 PRINT "N/D FREQUENCY F=2(pi)f/uRe'=";1600*N(J1)*F1
7590 PRINT
7600 PRINT "X","REX","RETHNOM","RETHACT","NET INTEN."
7610 PRINT "(CM)"," - "," -    "," -    ","VOLTS/1.6KHZ"
7620 PRINT
7630 FOR I1=1 TO I-NOISE4
7640 LET X=A(I1)-100*FIX(A(I1)/100)
7650 IF X(=NOISE1 GOTO 7680
7660 IF X(=NOISE2 GOTO 7720
7670 IF X(=NOISE3 GOTO 7760
7680 LET SA=S(I1,J1)
7690 LET NA=S(I-NOISE4+1,J1)
7700 LET NET=SQR(ABS(SA^2-NA^2))
7710 GOTO 7790
7720 LET SA=S(I1,J1)
7730 LET NA=S(I1-NOISE4+2,J1)
7740 LET NET=SQR(ABS(SA^2-NA^2))
7750 GOTO 7790
7760 LET SA=S(I1,J1)
7770 LET NA=S(I1-NOISE4+3,J1)
7780 LET NET=SQR(ABS(SA^2-NA^2))
7790 IF FIX(A(1)/1000)=2 THEN LET A1=-0.1354
7800 IF FIX(A(1)/1000)=6 THEN LET A1=-0.1354
7810 IF FIX(A(1)/1000)=3 THEN LET A1=-6.609E-3
7820 IF FIX(A(1)/1000)=5 THEN LET A1=-6.609E-3
7830 IF FIX(A(1)/1000)=4 THEN LET A1=0
7840 IF FIX(A(1)/1000)=7 THEN LET A1=0
7850 IF FIX(A(1)/1000)=8 THEN LET A1=0
7860 IF FIX(A(1)/1000)=2 THEN LET A2=8.741E-4
7870 IF FIX(A(1)/1000)=6 THEN LET A2=8.741E-4
7880 IF FIX(A(1)/1000)=3 THEN LET A2=4.315E-4
7890 IF FIX(A(1)/1000)=5 THEN LET A2=4.315E-4
7900 IF FIX(A(1)/1000)=4 THEN LET A2=0
7910 IF FIX(A(1)/1000)=7 THEN LET A2=0
7920 IF FIX(A(1)/1000)=8 THEN LET A2=0
7925 IF C=10 GOTO 11510
7930 LET REX=0.254*X*RE
7940 LET RETHACT=0.664*SQR(REX)+A1*(REX/1000)+A2*((REX/1000)^2)
7950 PRINT 0.254*X,REX,0.664*SQR(REX),RETHACT,NET
7960 NEXT I1
7970 PRINT
7980 INPUT "DO YOU WISH HARD COPY (Y/N): ";C7$
7985 IF C7$="Y" THEN INPUT "Now put printer ON LINE and CR";J00
7990 IF C7$="N" GOTO 8420
8000 OPEN "0PR" AS FILE #7
8010 PRINT #7,"AMPLITUDE CHANGE WITH X FOR ";B$
8020 PRINT #7,"FREQUENCY INDEX N(J1)=";N(J1);"(f=";1.6*N(J1);" KHZ)"
8030 PRINT #7,"N/D FREQUENCY F=2(pi)f/uRe'=";1600*N(J1)*F1
8040 PRINT #7
8050 PRINT #7,"X","REX","RETHNOM","RETHACT","NET INTEN."
8060 PRINT #7,"(CM)"," - "," -    "," -    ","(VOLTS/1.6KHZ)"
8070 PRINT #7
8080 FOR I1=1 TO I-NOISE4
8090 LET X=A(I1)-100*FIX(A(I1)/100)
8100 IF X(=NOISE1 GOTO 8130
8110 IF X(=NOISE2 GOTO 8170
8120 IF X(=NOISE3 GOTO 8210
8130 LET SA=S(I1,J1)
8140 LET NA=S(I-NOISE4+1,J1)
8150 LET NET=SQR(ABS(SA^2-NA^2))
8160 GOTO 8240
8170 LET SA=S(I1,J1)
8180 LET NA=S(I-NOISE4+2,J1)
8190 LET NET=SQR(ABS(SA^2-NA^2))
8200 GOTO 8240
8210 LET SA=S(I1,J1)
```

```
8220 LET NA=S(I-NOISE4+3,J1)
8230 LET NET=SQR(ABS(SA^2-NA^2))
8240 IF FIX(A(1)/1000)=2 THEN LET A1=-0.1354
8250 IF FIX(A(1)/1000)=6 THEN LET A1=-0.1354
8260 IF FIX(A(1)/1000)=3 THEN LET A1=-6.609E-3
8270 IF FIX(A(1)/1000)=5 THEN LET A1=-6.609E-3
8280 IF FIX(A(1)/1000)=4 THEN LET A1=0
8290 IF FIX(A(1)/1000)=7 THEN LET A1=0
8300 IF FIX(A(1)/1000)=8 THEN LET A1=0
8310 IF FIX(A(1)/1000)=2 THEN LET A2=8.741E-4
8320 IF FIX(A(1)/1000)=6 THEN LET A2=8.741E-4
8330 IF FIX(A(1)/1000)=3 THEN LET A2=4.315E-4
8340 IF FIX(A(1)/1000)=5 THEN LET A2=4.315E-4
8350 IF FIX(A(1)/1000)=4 THEN LET A2=0
8360 IF FIX(A(1)/1000)=7 THEN LET A2=0
8370 IF FIX(A(1)/1000)=8 THEN LET A2=0
8375 IF C=10 GOTO 10970
8380 LET REX=0.254*X*RE
8390 LET RETHACT=0.664*SQR(REX)+A1*(REX/1000)+A2*((REX/1000)^2)
8400 PRINT #7,0.254*X,REX,0.664*SQR(REX),RETHACT,NET
8410 NEXT I1
8415 CLOSE #7
8420 INPUT "ENTER OTHER N ('NN'),MENU ('M'), OR QUIT ('Q') ";D7$
8425 IF D7$="NN" GOTO 7500
8430 IF D7$="M" GOTO 720
8435 IF D7$="Q" GOTO 20000
8500 CLS
8505 PRINT "AMPLITUDE CHANGE WITH X FOR ";B$
8510 PRINT
8515 INPUT "ENTER CHOICE OF FREQUENCY INDEX J1 (1-201): ";J1
8520 INPUT "CRT PLOT ('CRT') OR HP GRAPHICS FILE ('HP')? ";B8$
8525 IF B8$="HP" GOTO 8760
8530 PRINT "Choose plot-maximum coordinates in response to questions, which"
8535 PRINT "are convenient multiples of 5"
8540 INPUT "ENTER MAXIMUM DESIRED X ON PLOT (CM): ";X1
8545 INPUT "ENTER MAXIMUM DESIRED RMS SIGNAL (VOLTS): ";V
8550 CLS
8555 PRINT "AMPLITUDE CHANGE WITH X FOR ";B$
8560 PRINT "J1=",J1," N(J1)=";N(J1)," f=";1.6*N(J1);" KHZ  F=",1600*N(J1)*F1
8565 LINE (75,40,575,40)
8570 LINE (75,40,75,390)
8575 LINE (75,390,575,390)
8580 LINE (575,40,575,390)
8585 FOR I2=0 TO 5 STEP 1
8590 TEXT (71+100*I2,31,"+")
8595 TEXT (71+100*I2,381,"+")
8600 TEXT (71+100*I2,20,NUM1$(I2*X1/5))
8605 NEXT I2
8610 TEXT (255,0,"DISTANCE FROM L.E. (CM)")
8615 FOR I2=0 TO 5 STEP 1
8620 TEXT (84,36+70*I2,"+",1,1)
8625 TEXT (37,30+70*I2,NUM1$(I2*V/5))
8630 TEXT (584,36+70*I2,"+",1,1)
8635 NEXT I2
8640 TEXT (30,65,"NET SIGNAL PER 1.6 KHZ (VRMS)",1,1)
8645 FOR I1=1 TO I-NOISE4
8650 LET X=A(I1)-100*FIX(A(I1)/100)
8652 IF 0.254*X>X1 GOTO 8745
8655 IF X<=NOISE1 GOTO 8675
8660 IF X<=NOISE2 GOTO 8695
8665 IF X<=NOISE3 GOTO 8715
8675 LET SA=S(I1,J1)
8680 LET NA=S(I-NOISE4+1,J1)
8685 LET NET=SQR(ABS(SA^2-NA^2))
8690 GOTO 8735
8695 LET SA=S(I1,J1)
8700 LET NA=S(I-NOISE4+2,J1)
8705 LET NET=SQR(ABS(SA^2-NA^2))
8710 GOTO 8735
8715 LET SA=S(I1,J1)
8720 LET NA=S(I-NOISE4+3,J1)
8725 LET NET=SQR(ABS(SA^2-NA^2))
8735 IF NET>V GOTO 8745
8740 TEXT (75+(127*X)/X1,40+(350*NET/V),CHR$(111))
8745 NEXT I1
8748 IF C=9 GOTO 9570
8750 INPUT "DO YOU WISH SEPARATE HP GRAPHICS FILE CREATED (Y/N): ";H8$
8755 IF H8$="N" GOTO 9020
8760 INPUT "ENTER NAME (A------) OF THIS SEPARATE HP FILE (IN QUOTES): ";A8$
8765 OPEN A8$ FOR OUTPUT AS FILE #8
8770 FOR I1=1 TO I-NOISE4
8775 LET X=A(I1)-100*FIX(A(I1)/100)
8780 IF X<=NOISE1 GOTO 8800
8785 IF X<=NOISE2 GOTO 8820
8790 IF X<=NOISE3 GOTO 8840
8800 LET SA=S(I1,J1)
8805 LET NA=S(I-NOISE4+1,J1)
8810 LET NET=SQR(ABS(SA^2-NA^2))
8815 GOTO 8860
8820 LET SA=S(I1,J1)
8825 LET NA=S(I-NOISE4+2,J1)
8830 LET NET=SQR(ABS(SA^2-NA^2))
8835 GOTO 8860
8840 LET SA=S(I1,J1)
8845 LET NA=S(I-NOISE4+3,J1)
8850 LET NET=SQR(ABS(SA^2-NA^2))
8860 IF FIX(A(1)/1000)=2 THEN LET A1=-0.1354
8865 IF FIX(A(1)/1000)=6 THEN LET A1=-0.1354
8870 IF FIX(A(1)/1000)=3 THEN LET A1=-6.609E-3
8875 IF FIX(A(1)/1000)=5 THEN LET A1=-6.609E-3
8880 IF FIX(A(1)/1000)=4 THEN LET A1=0
8885 IF FIX(A(1)/1000)=7 THEN LET A1=0
8890 IF FIX(A(1)/1000)=8 THEN LET A1=0
8895 IF FIX(A(1)/1000)=2 THEN LET A2=8.741E-4
8900 IF FIX(A(1)/1000)=6 THEN LET A2=8.741E-4
8905 IF FIX(A(1)/1000)=3 THEN LET A2=4.315E-4
8910 IF FIX(A(1)/1000)=5 THEN LET A2=4.315E-4
8915 IF FIX(A(1)/1000)=4 THEN LET A2=0
8920 IF FIX(A(1)/1000)=7 THEN LET A2=0
8925 IF FIX(A(1)/1000)=8 THEN LET A2=0
8927 IF C=10 GOTO 11100
8930 LET REX=0.254*X*RE
8935 LET RETHACT=0.664*SQR(REX)+A1*(REX/1000)+A2*((REX/1000)^2)
8940 PRINT #8,0.254*X
8950 PRINT #8,REX
8960 PRINT #8,SQR(REX)
8970 PRINT #8,0.664*SQR(REX)
8980 PRINT #8,RETHACT
8990 PRINT #8,NET
9000 NEXT I1
```

```
9010 CLOSE #8
9020 INPUT "'R' TO RE-RUN,'N' FOR OTHER N, 'M' FOR MENU, 'Q' TO QUIT:";C8$
9030 IF C8$="R" GOTO 8520
9040 IF C8$="N" GOTO 8515
9050 IF C8$="M" GOTO 720
9060 IF C8$="Q" GOTO 20000
9500 CLS
9510 PRINT "CURVE-FIT OF AMPLITUDE FOR ";B$
9520 INPUT "ENTER CHOICE OF FREQUENCY INDEX J1 (1-201): ";J1
9530 INPUT "MAXIMUM DESIRED X ON PLOT (CM): ";X1
9540 INPUT "MAXIMUM DESIRED RMS SIGNAL DENSITY (VRMS): ";V
9550 INPUT "ENTER DESIRED POLYNOMIAL DEGREE (11 IS MAX): ";NCF
9555 LET MCF=0
9560 GOTO 8550
9570 FOR I1=1 TO I-NOISE4
9572 LET ICF=I1
9580 LET X=A(I1)-100*FIX(A(I1)/100)
9590 IF 0.254*X)X1 GOTO 9782
9600 LET G=0.254*X
9610 IF X(=NOISE1 GOTO 9640
9620 IF X(=NOISE2 GOTO 9680
9630 IF X(=NOISE3 GOTO 9720
9640 LET SA=S(I1,J1)
9650 LET NA=S(I-NOISE4+1,J1)
9660 LET P=SQR(ABS(SA^2-NA^2))
9670 GOTO 9750
9680 LET SA=S(I1,J1)
9690 LET NA=S(I-NOISE4+2,J1)
9700 LET P=SQR(ABS(SA^2-NA^2))
9710 GOTO 9750
9720 LET SA=S(I1,J1)
9730 LET NA=S(I-NOISE4+3,J1)
9740 LET P=SQR(ABS(SA^2-NA^2))
9750 IF P)V GOTO 9782
9760 LET YCF(ICF)=P
9770 LET XCF(ICF)=G
9780 LET MCF=MCF+1
9782 NEXT I1
9791 LET ZCF=0
9792 LET OCF=1
9793 LET KCF=12
9794 LET NCF=NCF+1
9795 IF MCF(NCF GOTO 9500
9796 LET T7CF=ZCF
9797 LET T8CF=ZCF
9798 LET W7CF=ZCF
9799 FOR ICF=1 TO MCF
9800 LET W7CF=W7CF+XCF(ICF)
9801 LET T7CF=T7CF+YCF(ICF)
9802 LET T8CF=T8CF+YCF(ICF)^2
9803 NEXT ICF
9804 LET T9CF=(MCF*T8CF-T7CF^2)/(MCF^2-MCF)
9805 FOR ICF=1 TO MCF
9806 LET PCF(ICF)=ZCF
9807 LET QCF(ICF)=OCF
9808 NEXT ICF
9809 FOR ICF=1 TO 11
9810 LET ACF(ICF)=ZCF
9811 LET BCF(ICF)=ZCF
9812 LET SCF(ICF)=ZCF
9813 NEXT ICF
9814 LET E1CF=ZCF
9815 LET F1CF=ZCF
9816 LET W1CF=MCF
9817 LET N4CF=KCF
9818 LET ICF=1
9819 LET K1CF=2
9820 IF NCF=0 THEN 9822
9821 LET K1CF=N4CF
9822 LET WCF=ZCF
9823 FOR LCF=1 TO MCF
9824 LET WCF=WCF+YCF(LCF)*QCF(LCF)
9825 NEXT LCF
9826 LET SCF(ICF)=WCF/W1CF
9827 IF ICF-N4CF)=0 THEN 9847
9828 IF ICF-MCF)=0 THEN 9847
9829 LET E1CF=ZCF
9830 FOR LCF=1 TO MCF
9831 LET E1CF=E1CF+XCF(LCF)*QCF(LCF)*QCF(LCF)
9832 NEXT LCF
9833 LET E1CF=E1CF/W1CF
9834 LET ACF(ICF+1)=E1CF
9835 LET WCF=ZCF
9836 FOR LCF=1 TO MCF
9837 LET VCF=(XCF(LCF)-E1CF)*QCF(LCF)-F1CF*PCF(LCF)
9838 LET PCF(LCF)=QCF(LCF)
9839 LET QCF(LCF)=VCF
9840 LET WCF=WCF+VCF*VCF
9841 NEXT LCF
9842 LET F1CF=WCF/W1CF
9843 LET BCF(ICF+2)=F1CF
9844 LET W1CF=WCF
9845 LET ICF=ICF+1
9846 GOTO 9822
9847 FOR LCF=0 TO 12
9848 LET GCF(LCF)=ZCF
9849 NEXT LCF
9850 LET GCF(1)=OCF
9851 FOR JCF=1 TO NCF
9852 LET S1CF=ZCF
9853 FOR LCF=1 TO NCF
9854 IF LCF=1 THEN 9856
9855 LET GCF(LCF)=GCF(LCF)-ACF(LCF)*GCF(LCF-1)-BCF(LCF)*GCF(LCF-2)
9856 LET S1CF=S1CF+SCF(LCF)*GCF(LCF)
9857 NEXT LCF
9858 LET UCF(JCF)=S1CF
9859 LET LCF=NCF
9860 FOR I2CF=2 TO NCF
9861 LET GCF(LCF)=GCF(LCF-1)
9862 LET LCF=LCF-1
9863 NEXT I2CF
9864 LET GCF(1)=ZCF
9865 NEXT JCF
9866 LET TCF=ZCF
9867 FOR LCF=1 TO MCF
9868 LET CCF(LCF)=ZCF
9869 LET JCF=NCF
9870 FOR I2CF=1 TO NCF
9871 LET CCF(LCF)=CCF(LCF)*XCF(LCF)+UCF(JCF)
9872 LET JCF=JCF-1
```

```
9873 NEXT ICF
9874 LET T3CF=YCF(LCF)-CCF(LCF)
9875 LET TCF=TCF+T3CF^2
9876 NEXT LCF
9877 IF MCF<>NCF THEN 9880
9878 LET T3CF=0
9879 GOTO 9881
9880 LET T3CF=TCF/(MCF-NCF)
9881 LET Q7CF=1-TCF/(T9CF*(MCF-1))
9882 IF C=11 GOTO 11200
9883 IF C=12 GOTO 11720
9910 FOR N1=0 TO 100
9913 LET G(N1)=N1*E1/100
9914 LET P=0
9916 FOR L=1 TO NCF
9918 LET P=P+UCF(L)*(G(N1)^(L-1))
9920 NEXT L
9921 LET P(N1)=P
9923 NEXT N1
9923 IF C=10 GOTO 10610
9924 FOR N1=1 TO 99
9926 LINE(75+(G(N1)*500)/E1,40+(350*P(N1)/V),75+(G(N1+1)*500/E1),.6
40+(350*P(N1+1)/V))
9930 NEXT N1
9940 PRINT "CURVE IS FOR FITTING POLYNOMIAL OF DEGREE";NCF-1
9951 INPUT "'R' RERUN, 'F' FILES,'D' NEW DEGREE,'M' MENU,'Q' TO QUIT: ";B1$
9953 IF B1$="R" GOTO 9500
9954 IF B1$="D" GOTO 9550
9955 CLS
9957 IF B1$="M" GOTO 720
9959 IF B1$="Q" GOTO 20000
9960 PRINT "You can now prepare files on the data and curve fits. The X"
9965 PRINT "and Y range, and N, will be the same as just shown previously."
9970 PRINT "In these ranges you can load HP-ready files with the data "
9975 PRINT "points (PT------) or files called 'CF------' of fitted curves"
9980 PRINT "of the amplitudes (to the polynomial degree last chosen) and"
9985 PRINT "the amplification rates."
9990 PRINT
9991 REM In the HP file prepared below, the variables are as follows:
9992 REM 1) x in cm 2)R (the sq. root of Rex) 3) the rms spectral density
9993 REM in vrms per 1.6 khs, 4) the derivative de/dx of the latter and
9994 REM 5) the non-dimensional amplification rate (the minus alpha sub i)
10000 PRINT "1  DATA POINTS ONLY"
10010 PRINT "2  AMPLITUDE AND AMPLIFICATION (DIMENSIONAL)"
10015 PRINT
10020 INPUT "ENTER YOUR CHOICE: ";C9
10030 IF C9=1 THEN INPUT "DATA-POINT FILENAME (PT------) IN QUOTES: ";C9$
10040 IF C9=2 THEN INPUT "AMPL/AMPLIFICATION FILENAME (CF------) QUOTES.";C9$
10050 IF C9=2 GOTO 10120
10060 OPEN C9$ FOR OUTPUT AS FILE #1
10070 FOR ICF=1 TO MCF
10080 PRINT #1,XCF(ICF)
10081 PRINT #1,0.664*SQR(RE*XCF(ICF))
10085 PRINT #1,YCF(ICF)
10090 NEXT ICF
10100 CLOSE #1
10110 IF C9=1 GOTO 10215
10120 OPEN C9$ FOR OUTPUT AS FILE #1
10130 FOR N1=1 TO 100
10140 LET P1=0
10150 FOR L=1 TO NCF
10160 LET P1=P1+UCF(L)*(L-1)*(G(N1)^(L-2))
10170 NEXT L
10180 LET P1(N1)=P1
10190 PRINT #1,G(N1)
10191 PRINT #1,SQR(RE*G(N1))
10193 PRINT #1,P(N1)
10196 PRINT #1,P1(N1)
10197 PRINT #1,(P1(N1)/P(N1))*SQR(G(N1)/RE)
10200 NEXT N1
10210 CLOSE #1
10215 PRINT
10220 PRINT "DONE WITH LOADING FILE";C9$
10230 PRINT
10240 PRINT "1. RETURN TO CRT GRAPHICS, START OF OPTION 9"
10250 PRINT "2. DITTO, BUT START BY FITTING NEW DEGREE"
10260 PRINT "3. GO TO MENU"
10270 PRINT "4. QUIT"
10280 PRINT
10290 INPUT "YOUR CHOICE: ";C10
10300 IF C10=1 GOTO 9500
10310 IF C10=2 GOTO 9550
10320 IF C10=3 GOTO 720
10330 IF C10=4 GOTO 20000
10500 CLS
10501 INPUT "CHOOSE BETWEEN HARDCOPY (H) AND SCREEN PRINTOUT (S): ";Q$
10502 INPUT "ENTER '1' TO MAKE GRAPHICS FILES, OTHERWISE CR: ";CC
10503 IF CC=1 THEN INPUT "FILENAME FOR LOWER BRANCH ('LOWER--' IN QUOTES):";GR2$
10504 IF CC=1 THEN INPUT "FILENAME FOR UPPER BRANCH ('UPPER--' IN QUOTES):";GR3$
10505 IF CC=1 THEN INPUT "FILENAME FOR MAX.AMPLIF. ('MAXAM--' IN QUOTES):";GR4$
10506 IF CC=1 THEN INPUT "FILENAME FOR MIN.AMPLIF. ('MINAM--' IN QUOTES):";GR5$
10507 IF Q$="H" THEN OPEN "0FR" AS FILE #1
10508 IF Q$="H" THEN INPUT "Turn printer on and CR";JJJ$
10509 IF Q$="H" THEN PRINT #1,"LIST OF POLES & ZEROES OF STABILITY DIAGRAM"
10510 PRINT "LIST OF POLES & ZERO CROSSINGS OF STABILITY DIAGRAM"
10511 IF Q$="H" THEN PRINT #1,"FOR ";B$
10512 PRINT B$
10513 IF CC=1 THEN OPEN GR2$ FOR OUTPUT AS FILE #2
10514 IF CC=1 THEN OPEN GR3$ FOR OUTPUT AS FILE #3
10515 IF CC=1 THEN OPEN GR4$ FOR OUTPUT AS FILE #4
10516 IF CC=1 THEN OPEN GR5$ FOR OUTPUT AS FILE #5
10519 IF Q$="H" THEN PRINT #1,"Based on 7th-deg polyfits of x(10 cm points"
10520 PRINT "Based on 7th-degree polyfits of the x(10 cm ponts only"
10529 IF Q$="H" THEN PRINT #1,"and limited to f(160 khs"
10530 PRINT "and limited to f(160 khs"
10532 LET NN2=0
10534 LET NN3=0
10536 LET NN4=0
10538 LET NN5=0
10540 LET E1=10
10550 LET V=1
10570 FOR J1=1 TO 100
10575 LET MCF=8
10578 LET NCF=7
10579 IF Q$="H" THEN PRINT #1
10580 PRINT
10588 IF Q$="H" THEN PRINT #1,"----------------------------------------"
10589 IF Q$="H" THEN PRINT #1,"J1=";J1;" N(J1)=";N(J1),," f=";1.6*N(J1),.6
"KHZ F=";1600*N(J1)*E1
10590 PRINT "J1=";J1;" N(J1)=",N(J1),," f=";1.6*N(J1),," KHZ F=",1600*N(J1)*E1
```

```
10600 GOTO 9570
10610 FOR N1=1 TO 100
10620 LET P1=0
10630 FOR L=1 TO NCF
10640 LET P1=P1+UCF(L)*(L-1)*(G(N1)^(L-2))
10650 NEXT L
10655 LET DX(N1)=P1
10660 LET P1(N1)=(P1/P(N1))*SQR(G(N1)/RE)
10670 NEXT N1
10680 FOR N1=1 TO 100
10690 LET P2=0
10700 FOR L=1 TO NCF
10710 LET P2=P2+UCF(L)*(L-1)*(L-2)*(G(N1)^(L-3))
10720 NEXT L
10730 LET P2(N1)=(P2*SQR(G(N1))/P(N1)+DX(N1)/(2*P(N1)*SQR(G(N1)))&
-((DX(N1)/P(N1))^2)*SQR(G(N1))/SQR(RE))
10740 NEXT N1
10750 FOR N1=1 TO 99
10760 IF P1(N1)*P1(N1+1)<0 GOTO 10810
10770 NEXT N1
10780 IF KK+LL<0.5 GOTO 11130
10790 IF KK>0.5 GOTO 10880
10800 IF LL>0.5 GOTO 11010
10810 IF P1(N1)>0 GOTO 10850
10820 LET KK=KK+1
10830 LET XL(KK)=(G(N1)+G(N1+1))/2
10840 GOTO 10770
10850 LET LL=LL+1
10860 LET XU(LL)=(G(N1)+G(N1+1))/2
10870 GOTO 10770
10879 IF Q$="H" THEN PRINT #1
10880 PRINT
10889 IF Q$="H" THEN PRINT #1,"LOWER BRANCH POINTS:"
10890 PRINT "LOWER BRANCH POINTS:"
10899 IF Q$="H" THEN PRINT #1
10900 PRINT
10909 IF Q$="H" THEN PRINT #1,"X(CM)","R","RETH(NOM)","RETH(ACT)"
10910 PRINT "X(CM)","R","RETH(NOM)","RETH(ACT)"
10919 IF Q$="H" THEN PRINT #1
10920 PRINT
10930 FOR J=1 TO KK
10940 LET REX=RE*XL(J)
10950 LET RETHNOM=0.664*SQR(REX)
10960 GOTO 8240
10970 LET RETHACT=RETHNOM+A1*(REX/1000)+A2*((REX/1000)^2)
10979 IF Q$="H" THEN PRINT #1,XL(J),SQR(REX),RETHNOM,RETHACT
10980 PRINT XL(J),SQR(REX),RETHNOM,RETHACT
10981 IF CC=1 THEN PRINT #2,1.6*N(J1)
10982 IF CC=1 THEN PRINT #2,1600*N(J1)*F1
10983 IF CC=1 THEN PRINT #2,XL(J)
10984 IF CC=1 THEN PRINT #2,SQR(REX)
10985 IF CC=1 THEN PRINT #2,RETHNOM
10986 IF CC=1 THEN PRINT #2,RETHACT
10987 LET NN2=NN2+1
10990 NEXT J
11000 IF LL<0.5 GOTO 11130
11009 IF Q$="H" THEN PRINT #1
11010 PRINT
11019 IF Q$="H" THEN PRINT #1,"UPPER BRANCH POINTS:"
11020 PRINT "UPPER BRANCH POINTS"
11029 IF Q$="H" THEN PRINT #1
11030 PRINT
11039 IF Q$="H" THEN PRINT #1,"X(CM)","R","RETH(NOM)","RETH(ACT)"
11040 PRINT "X(CM)","R","RETH(NOM)","RETH(ACT)"
11049 IF Q$="H" THEN PRINT #1
11050 PRINT
11060 FOR J=1 TO LL
11070 LET REX=RE*XU(J)
11080 LET RETHNOM=0.664*SQR(REX)
11090 GOTO 8840
11100 LET RETHACT=RETHNOM+A1*(REX/1000)+A2*((REX/1000)^2)
11109 IF Q$="H" THEN PRINT #1,XU(J),SQR(REX),RETHNOM,RETHACT
11110 PRINT XU(J),SQR(REX),RETHNOM,RETHACT
11111 IF CC=1 THEN PRINT #3,1.6*N(J1)
11112 IF CC=1 THEN PRINT #3,1600*N(J1)*F1
11113 IF CC=1 THEN PRINT #3,XU(J)
11114 IF CC=1 THEN PRINT #3,SQR(REX)
11115 IF CC=1 THEN PRINT #3,RETHNOM
11116 IF CC=1 THEN PRINT #3,RETHACT
11118 LET NN3=NN3+1
11120 NEXT J
11130 FOR N1=1 TO 99
11140 IF P2(N1)*P2(N1+1)<0 GOTO 11190
11150 NEXT N1
11160 IF KK1+LL1<0.5 GOTO 11540
11170 IF KK1>0.5 GOTO 11279
11180 IF LL1>0.5 GOTO 11409
11190 IF P2(N1)<0 GOTO 11240
11200 LET KK1=KK1+1
11210 LET XMAX(XK1)=(G(N1)+G(N1+1))/2
11220 LET P1MAX(KK1)=(P1(N1)+P1(N1+1))/2
11230 GOTO 11150
11240 LET LL1=LL1+1
11250 LET XMIN(LL1)=(G(N1)+G(N1+1))/2
11260 LET P1MIN(LL1)=(P1(N1)+P1(N1+1))/2
11270 GOTO 11150
11279 IF Q$="H" THEN PRINT #1
11280 PRINT
11289 IF Q$="H" THEN PRINT #1,"AMPLIFICATION MAXIMA LOCATIONS."
11290 PRINT "AMPLIFICATION MAXIMA LOCATIONS:"
11299 IF Q$="H" THEN PRINT #1
11300 PRINT
11309 IF Q$="H" THEN PRINT #1,"X(CM)","R","RETH(NOM)","RETH(ACT)","AMP RATE"
11310 PRINT "X(CM)","R","RETH(NOM)","RETH(ACT)","AMP RATE"
11319 IF Q$="H" THEN PRINT #1
11320 PRINT
11330 FOR J=1 TO KK1
11340 LET REX=RE*XMAX(J)
11350 LET RETHNOM=0.664*SQR(REX)
11360 GOTO 7322
11370 LET RETHACT=RETHNOM+A1*(REX/1000)+A2*((REX/1000)^2)
11379 IF Q$="H" THEN PRINT #1,XMAX(J),SQR(REX),RETHNOM,RETHACT,P1MAX(J)
11380 PRINT XMAX(J),SQR(REX),RETHNOM,RETHACT,P1MAX(J)
11381 IF CC=1 THEN PRINT #4,1.6*N(J1)
11382 IF CC=1 THEN PRINT #4,1600*N(J1)*F1
11383 IF CC=1 THEN PRINT #4,XMAX(J)
11384 IF CC=1 THEN PRINT #4,SQR(REX)
11385 IF CC=1 THEN PRINT #4,RETHNOM
11386 IF CC=1 THEN PRINT #4,RETHACT
11387 IF CC=1 THEN PRINT #4,P1MAX(J)
```

```
11380 LET NN4=NN4+1
11390 NEXT J
11400 IF LL1(0.3 GOTO 11540
11409 IF Q$="M" THEN PRINT #1
11410 PRINT
11419 IF Q$="M" THEN PRINT #1,"AMPLIFICATION MINIMA LOCATIONS:"
11420 PRINT "AMPLIFICATION MINIMA LOCATIONS:"
11429 IF Q$="M" THEN PRINT #1
11430 PRINT
11439 IF Q$="M" THEN PRINT #1,"X(CM)","R","RETH(NOM)","RETH(ACT)","AMP.RATE"
11440 PRINT "X(CM)","R","RETH(NOM)","RETH(ACT)","AMP.RATE"
11449 IF Q$="M" THEN PRINT #1
11450 PRINT
11460 FOR J=1 TO LL1
11470 LET REX=RE*XMIN(J)
11480 LET RETHNOM=0.664*SQR(REX)
11500 GOTO 7790
11510 LET RETHACT=RETHNOM+A1*(REX/1000)+A2*((REX/1000)^2)
11519 IF Q$="M" THEN PRINT #1,XMIN(J),SQR(REX),RETHNOM,RETHACT,PIMIN(J)
11520 PRINT XMIN(J),SQR(REX),RETHNOM,RETHACT,PIMIN(J)
11521 IF CC=1 THEN PRINT #3,1.6*N(J1)
11522 IF CC=1 THEN PRINT #3,1600*N(J1)*F1
11523 IF CC=1 THEN PRINT #3,XMIN(J)
11524 IF CC=1 THEN PRINT #3,SQR(REX)
11525 IF CC=1 THEN PRINT #3,RETHNOM
11526 IF CC=1 THEN PRINT #3,RETHACT
11527 IF CC=1 THEN PRINT #3,PIMIN(J)
11528 LET NN5=NN5+1
11530 NEXT J
11532 LET KK=0
11534 LET LL=0
11536 LET KK1=0
11538 LET LL1=0
11540 NEXT J1
11541 PRINT #1
11542 PRINT #1,"NO. OF POINTS IN FILE ";GR2$;"=";NN2
11543 PRINT #1,"NO. OF POINTS IN FILE ";GR3$;"=";NN3
11544 PRINT #1,"NO. OF POINTS IN FILE ";GR4$;"=";NN4
11545 PRINT #1,"NO. OF POINTS IN FILE ";GR5$;"=";NN5
11546 CLOSE #1
11547 CLOSE #2
11548 CLOSE #3
11549 CLOSE #4
11550 CLOSE #5
11551 PRINT
11552 PRINT "NO. OF POINTS IN FILE ";GR2$;"=";NN2
11553 PRINT "NO. OF POINTS IN FILE ";GR3$;"=";NN3
11554 PRINT "NO. OF POINTS IN FILE ";GR4$;"=";NN4
11555 PRINT "NO. OF POINTS IN FILE ";GR5$;"=";NN5
11560 INPUT "CHOOSE RERUN (RR), MENU (M),OR QUIT (Q): ";A10$
11570 IF A10$="RR" GOTO 10500
11580 IF A10$="M" GOTO 720
11590 IF A10$="Q" GOTO 20000
12000 CLS
12010 PRINT "AMPLIFICATION SPECTRA FOR ";B$
12010 PRINT "All spectra are for 7-deg polyfits of points x(10 cm and are"
12025 PRINT "limited to f(160 khs."
12030 INPUT "ENTER DESIRED R(=SQR(REX))  ";R
12040 INPUT "CHOOSE BETWEEN HP GRAPHICS FILES (H) AND SCREEN PRINTOUT(S) ";Q$
12050 IF Q$="H" THEN INPUT "ENTER DESIRED FILENAME (AS-----) IN QUOTES: ";AS$
12060 IF Q$="H" THEN OPEN AS$ FOR OUTPUT AS FILE #1
12070 IF Q$="S" THEN CLS
12080 IF Q$="S" THEN PRINT B$
12090 IF Q$="S" THEN PRINT "AMPLIFICATION SPECTRUM FOR R(=SQR(REX))=";R
12100 IF Q$="S" THEN PRINT "Based on 7th-deg polyfits in x(10 cm, of a ve"
12105 IF Q$="S" THEN PRINT "R @ constant f"
12110 LET X1=10
12120 LET V=1
12122 PRINT
12124 IF Q$="S" THEN PRINT "J1","N(J1)","f(KHZ)","F","AMP.RATE (N/D)"
12126 PRINT
12130 FOR J1=1 TO 100
12140 LET MCF=0
12150 LET NCF=7
12190 GOTO 9570
12200 LET X2=(R^2)/RE
12210 LET P=0
12220 LET P1=0
12230 FOR L=1 TO NCF
12240 LET P=P+UCF(L)*(X2^(L-1))
12250 LET P1=P1+UCF(L)*(L-1)*(X2^(L-2))
12260 NEXT L
12270 LET RATE(J1)=(F1/P)*SQR(X2/RE)
12280 IF Q$="S" THEN PRINT J1,N(J1),1.6*N(J1),1600*N(J1)*F1,RATE(J1)
12290 IF Q$="M" THEN PRINT #1,1600*N(J1)*F1
12300 IF Q$="M" THEN PRINT #1,RATE(J1)
12310 NEXT J1
12320 IF Q$="M" THEN PRINT "FILE ";AS$;" HAS BEEN LOADED"
12322 PRINT CHR$(7)
12330 CLOSE #1
12340 PRINT
12350 PRINT
12360 INPUT "REPEAT (R), MENU (M) OR QUIT (Q): ";C11$
12370 IF C11$="R" GOTO 12000
12380 IF C11$="M" GOTO 720
12390 IF C11$="Q" GOTO 20000
12500 CLS
12510 PRINT "TOTAL AMPLIFICATION SPECTRA FOR ";B$
12520 PRINT "All spectra are for 7-deg. polyfits of points x(10 cm and"
12530 PRINT "are limited to f(160 khs. In this option, for each frequency,"
12540 PRINT "we get the ratio of the amplitude (spectral density) at some"
12545 PRINT "Reynolds no. r to the same amplitude at R=150 "
12550 INPUT "ENTER DESIRED R(=SQR(REX)).  ",R
12560 INPUT "CHOOSE BETWEEN HP GRAPHICS FILES (H) AND SCREEN PRINTOUT (S) ";Q$
12570 IF Q$="H" THEN INPUT "ENTER DESIRED FILENAME (TOT-----) IN QUOTES  ";TOT$
12580 IF Q$="H" THEN OPEN TOT$ FOR OUTPUT AS FILE #1
12590 IF Q$="S" THEN CLS
12600 IF Q$="S" THEN PRINT B$
12610 IF Q$="S" THEN PRINT "TOTAL AMPLIFICATION FOR R(=SQR(REX))=";R
12615 IF Q$="S" THEN PRINT "referred to the amplitude at R=150"
12616 IF Q$="S" THEN PRINT "By 7-deg polyfits of x(10 cm points only"
12630 LET X1=10
12640 LET V=1
12650 PRINT
12660 IF Q$="S" THEN PRINT "J1","N(J1)","f(KHZ)","F","TOT  AMPL."
12670 PRINT
12680 FOR J1=1 TO 100
12690 LET MCF=0
12700 LET NCF=7
12710 GOTO 9570
```

```
12720 LET X2=22500/RE
12730 LET X3=(R^2)/RE
12740 LET P=0
12750 LET PREF=0
12760 FOR L=1 TO NCF
12770 LET PREF=PREF+UCF(L)*(X2^(L-1))
12780 LET P=P+UCF(L)*(X3^(L-1))
12790 NEXT L
12800 LET TOT(J1)=P/PREF
12810 IF Q$="S" THEN PRINT J1,N(J1),1.6*N(J1),1600*N(J1)*F1,TOT(J1)
12820 IF Q$="H" THEN PRINT #1,1600*N(J1)*F1
12830 IF Q$="H" THEN PRINT #1,TOT(J1)
12840 NEXT J1
12850 IF Q$="H" THEN PRINT "FILE ";TOT$;" HAS BEEN LOADED"
12860 CLOSE #1
12870 PRINT
12880 PRINT
12890 INPUT "REPEAT (R),MENU (M), OR QUIT (Q): ";C12$
12900 IF C12$="R" GOTO 12500
12910 IF C12$="M" GOTO 720
12920 IF C12$="Q" GOTO 20000
20000 END
```

AD-A166 188 BOUNDARY LAYER STABILITY MEASUREMENTS OVER A FLAT PLATE AT MACH 3(U) MONTANA STATE UNIV BOZEMAN SUPERSONIC WIND TUNNEL LAB A DEMETRIADES NOV 85 SWT-TR-85-1 3/3

UNCLASSIFIED AFOSR-TR-86-0056 AFOSR-80-0267 F/G 20/4 NL

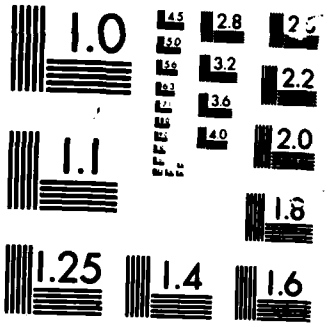

MICROCOPY RESOLUTION TEST CHART

TABLE C-VII

OUTPUTS PROVIDED BY STABLE02.BAS

OPTION	PURPOSE	CRT* TABLE	CRT* PLOT	HARDCOPY	NAME(S) OF CREATED FILE(S)
1	Raw spectrum, each group	x			
2	Net spectrum, each group	x			
3	Raw spectrum, each group		x		
4	Net spectrum, each group		x		SP-----.BAS
5	RMS variation with x, entire set	x		x	
6	RMS variation with x, entire set		x		RMS--.BAS
7	Amplitude variation with x, single frequency	x		x	
8	Amplitude variation with x, single frequency		x		A------.BAS
9	Curve-fits of single-frequency amplitude variation with x			x	PT------.BAS CF-------.BAS (EX-------.BAS)
10	Stability Diagram Poles			x	LOWER--.BAS UPPER--.BAS MAXAM--.BAS MINAM--.BAS
11	Amplification rate spectrum at some fixed x (or Re_x)	x			AS------.BAS
12	Total amplification between R_o= 150 and given R	x			TOT------.BAS

*Volatile outputs

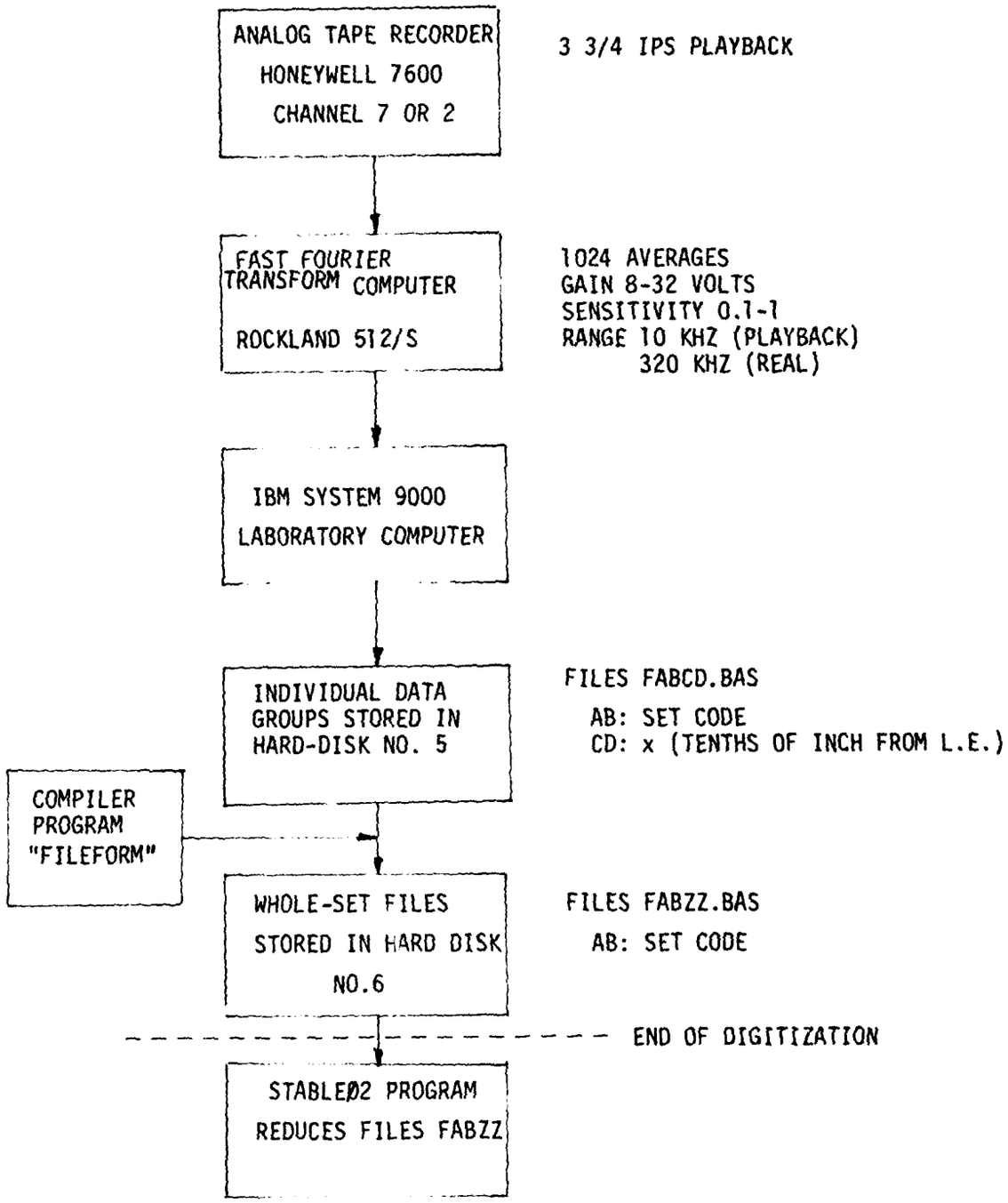

C.1 Data reduction operations for stability measurements.

OVERVIEW OF STABLEØ2 PROGRAM

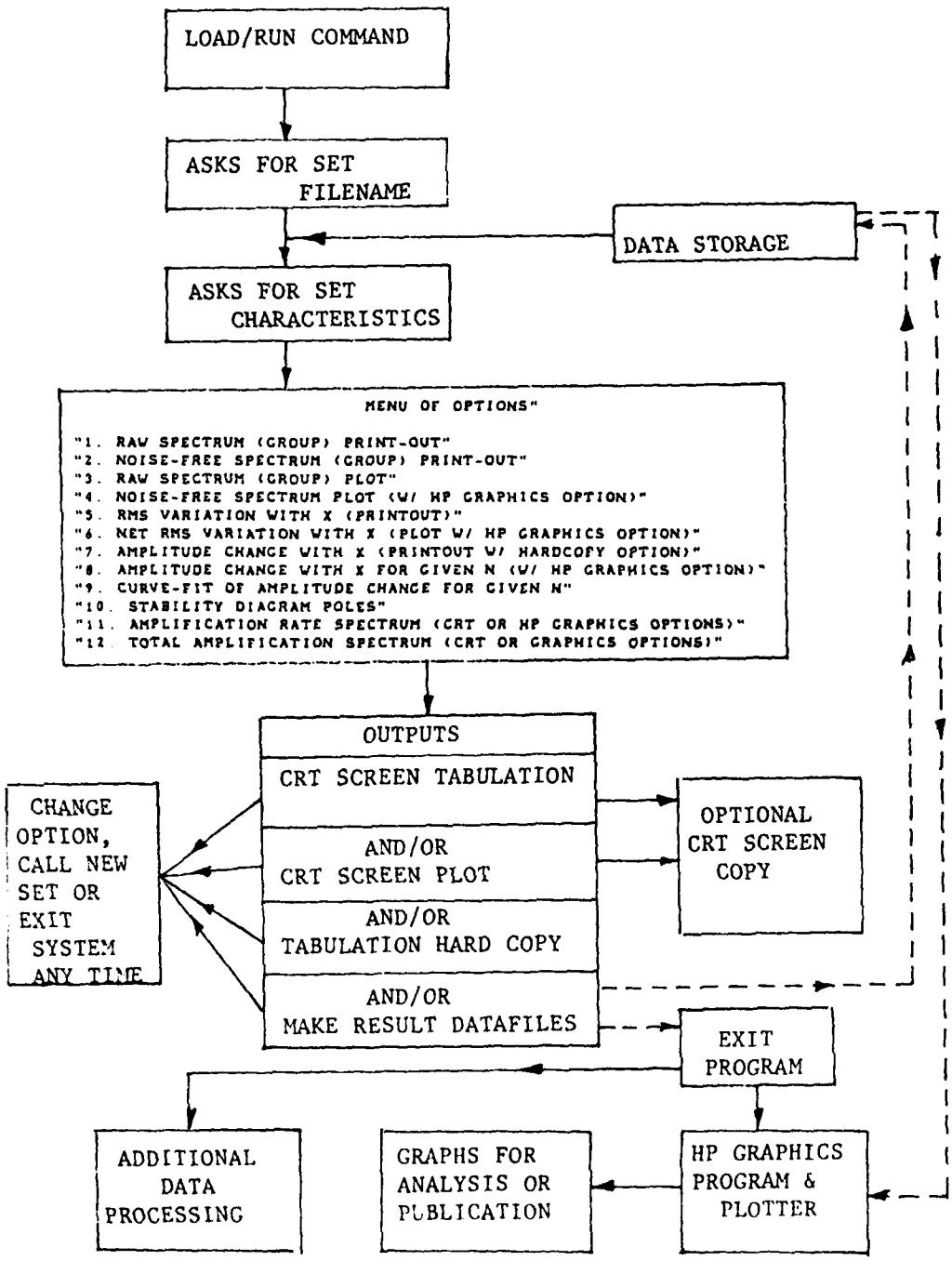

C.2 Overview of the STABLE02 Program.

APPENDIX D

CURVE-FITS OF THE AMPLITUDES AND AMPLIFICATION RATES

Nomenclature, Definitions and Objectives

The important variables in the discussion of stability are the net spectral density $e^2(f,R)$ and the amplification rate $-\alpha_i(f,R)$. The $e^2(f,R)$ is measured as mean-square volts (VMS) within a narrow frequency window which in our case was 1.6 KHZ. In the present experiment too, the data were collected and are presented as the square root of $e^2(f,R)$, which is called A(f) or simply A. The spectra of the amplifier output at a given R are then, in this test, given by A(f) vs. f. The variation A(R) at some fixed frequency f will be called the "amplitude change" and can also be alternately shown as A vs. x or vs. Re_θ, or versus any other such variable connected with variations along x.

In order to illustrate the role of the flow as an amplifier, most stability discussions and comparisons with theory deal with the amplification rate

$$-\alpha_i = \frac{1}{2A}\frac{\partial A}{\partial R}$$

Thus $-\alpha_i$ depends on taking derivatives of curves formed by data points, which introduces inaccuracies deserving a brief discussion of past work. The data of Demetriades (References 6, 7 and 8) and Stetson (Reference 9) were obtained by first measuring the spectra A(f) at a series of R values, crossplotting these vs. R at fixed f, and finally passing some sort of continuous curve A(R) through the points in the A-R plane from which dA/dR was computed. Demetriades (References 6 and 7) and Stetson et al. (References 9, 10 and 11) chose 4th-degree polynomials to curve-fit their points with the least-squares method. Laufer and Vrebalovich (Reference 5) and Kendall (Reference 12) do

not specify the curve-fitting method. In their case, however, it should be noted that amplitude data A(R) vs. R were available in the form of a continuous line, i.e. an "infinite" number of points in the A-R plane (this was done by plotting directly a single Fourier component output vs. distance on an x-y plotter). Such a large number of points should improve the accuracy of measuring slopes, although "scatter" can exist on a continuous line also.

In the present work the A(R) data were least-squares curve-fitted as in References 8 and 9 but with considerable reservations which apply in retrospect to these references as well. If a set of data points is not too badly scattered and defines, to the naked eye, a fairly simple curve, then it is true that just about any higher-degree polynomial will fit the set well. Even then, however, the slope of any fitted curve will depend on (a) the polynomial degree and (b) the number of points included. This dependence can become intolerable if there is data scatter and/or the data imply a "complex" curve (e.g. several inflection points). No justification has been given in References 8 and 9 as to why the polynomial degree was chosen at 4, and therefore, it is not easy to determine the accuracy of their results (Figure 6 of Reference 8, Figures 16 of Reference 9).

Even if the curve-fits for the calculations in References 8 and 9 were to be justified by the evidently "good behavior" of the points to be fitted, curve-fitting of the present data looked much more difficult at the beginning. For example, in Figure D.1, we see that there are as many as three extrema defined by the A(R) (in this case the A(x)) curves, even in the limited range $0 < x < 10$ cm. Furthermore, in most cases the large signal increases at high x tended to so dominate the A(R) picture that any curve fitting it would fit poorly the small but significant changes seen at small x. It therefore appeared unreasonable to make a single curve-fit of the entire x range or to

favor some polynomial degree in advance. It was instead decided to study in some detail the regions into which x should be divided for individual curve-fits and the degree fitting the data best. To avoid biasing, however, it was decided to use the same polynomial degree for all curve-fits once this proper degree was determined. The judgment of the latter was made by plotting the polynomial slopes.

The Effect of the Polynomial Degree

The search for the proper degree, shown by examples on Figures D.1-D.3, was done by first looking at the data in $0 < x < 10$ cm, i.e. mostly in the "first mode" region. In this region the figures show the data fitted by six polynomials of degree 2-8. In each example of Figures D.1-D.3 there are two plots, the first plotting A (i.e. spectral density) vs. x, and the second the amplification rate (actually dA/dx) vs. x. Each polynomial was found solely by using the points in $0 < x < 10$ cm, even though one example in Figure D.3 presents a detail of the curves confined into $0 < x < 4$ cm. Note that the examples are so chosen as to include different types of amplitude changes ranging from near-monotonic amplification (e.g. f = 40 KHZ, smooth wall, p_o = 475 mm) to near-monotonic damping (e.g. f = 76.8 KHZ, 350 mm).

Judging especially from the amplification rate plots, it is seen that the polynomial degree has to be rather high (6-8) before the curves begin to settle toward a shape nearly independent of it. After studying such curves it was decided to curve-fit with 7th degree polynomials.

The Effect of the X-Range

Once the suitable polynomial degree was "narrowed down", a test of the appropriate x-range was made with plots such as those on Figures D.4 and D.5. The procedure here was as follows. First, the polynomial degree is chosen

(only degrees 7 and 8 are used since those were the most promising; see above). Then the points in the x range 0-5 cm are fitted with such a polynomial. The procedure is then repeated for the ranges 0-10 and 0-20 cm. The results are again plotted in the A-x and dA/dx-x planes.

Figure D.4 shows a case where in the range $1 < x < 4$ cm (a critical range of the first-mode region) the amplification rates are not sensitive to the polynomial degree choice (7 or 8), whether the points in the range $5 < x < 10$ cm are included or not. When the points in $10 < x < 20$ cm are included in the curve-fit, then the curve-fit seems improper. On Figure D.5 another case is shown where the insensitivity to the polynomial degree remains but where a consideration only of the points in the range $0 < x < 5$ cm produces an inappropriate curve-fit.

On the basis of this test, it was decided that the curve-fits needed would consist of 7th degree polynomials fitting the range $0 < x < 10$ cm. This was the method employed for the majority of the figures in the text and for the bulk of the analysis and discussion. Seventh-degree polynomials fitting the range $0 < x < 20$ cm were also used for a small segment of the text where it was desired to study and discuss the second-mode region.

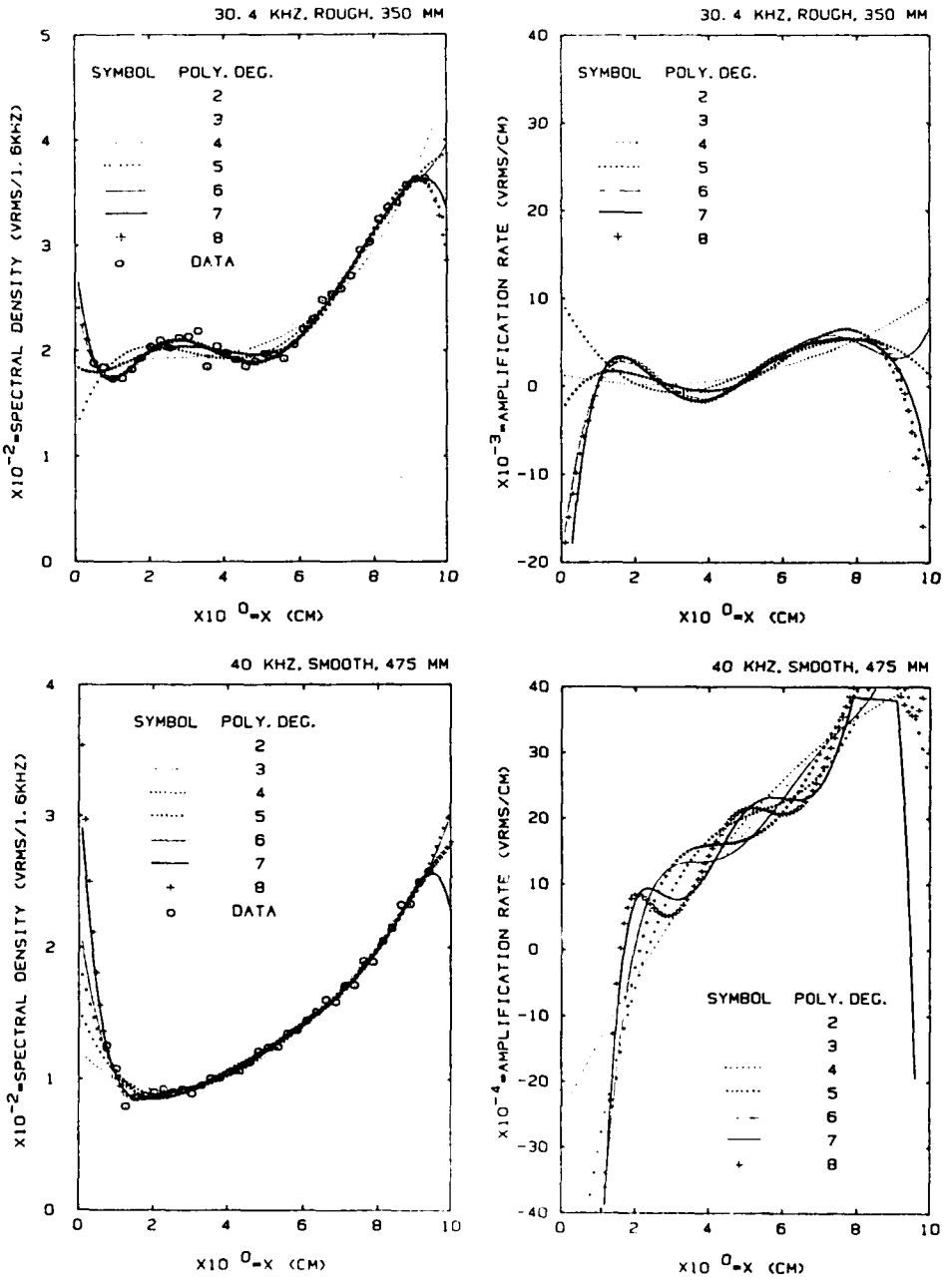

D.1 Curve-fit examples at 30.4 and 40 KHz.

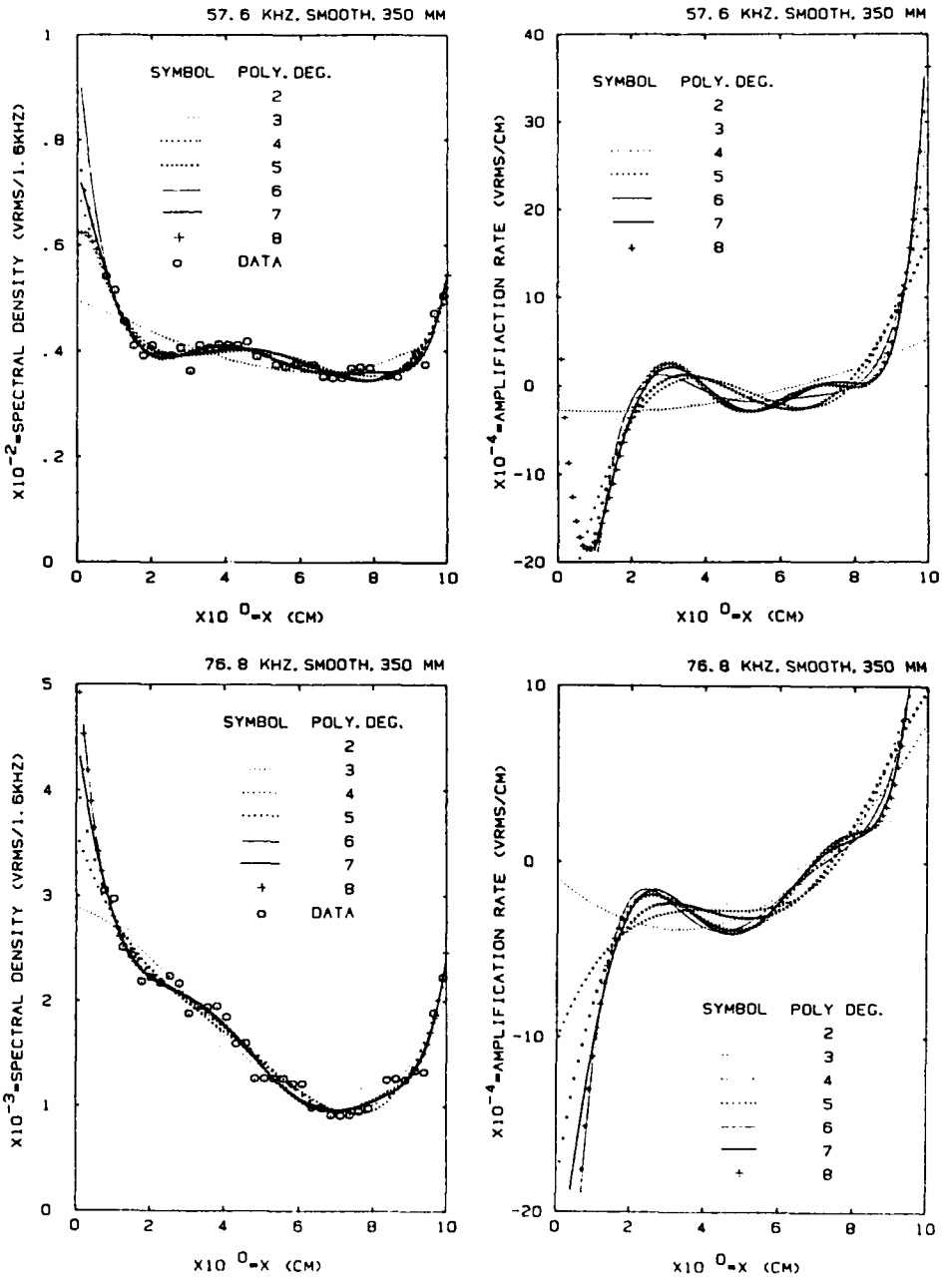

D.2 Curve-fit examples at 57.6 and 76.8 KHz.

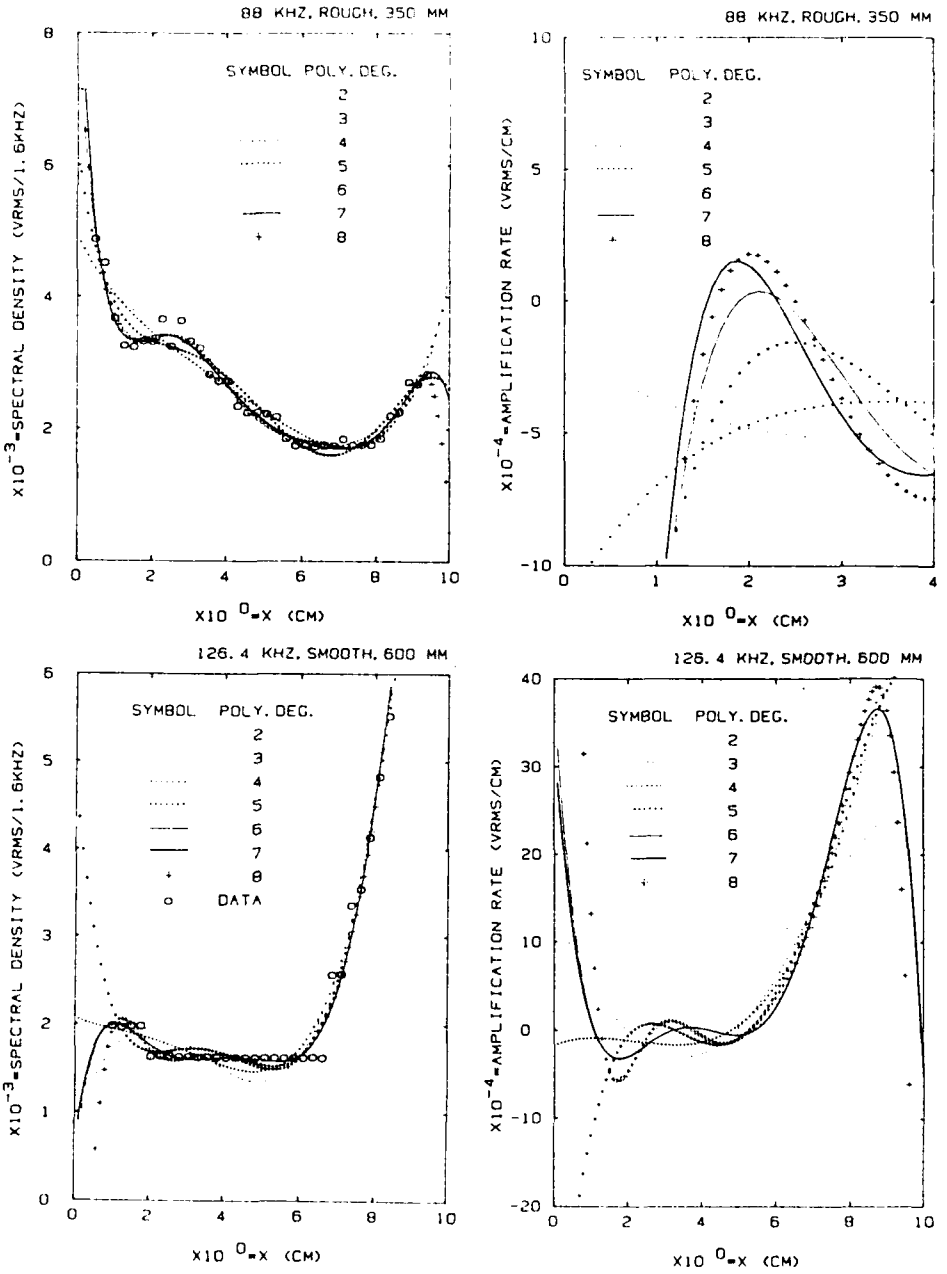

D.3 Curve-fit examples at 88 and 126.4 KHz.

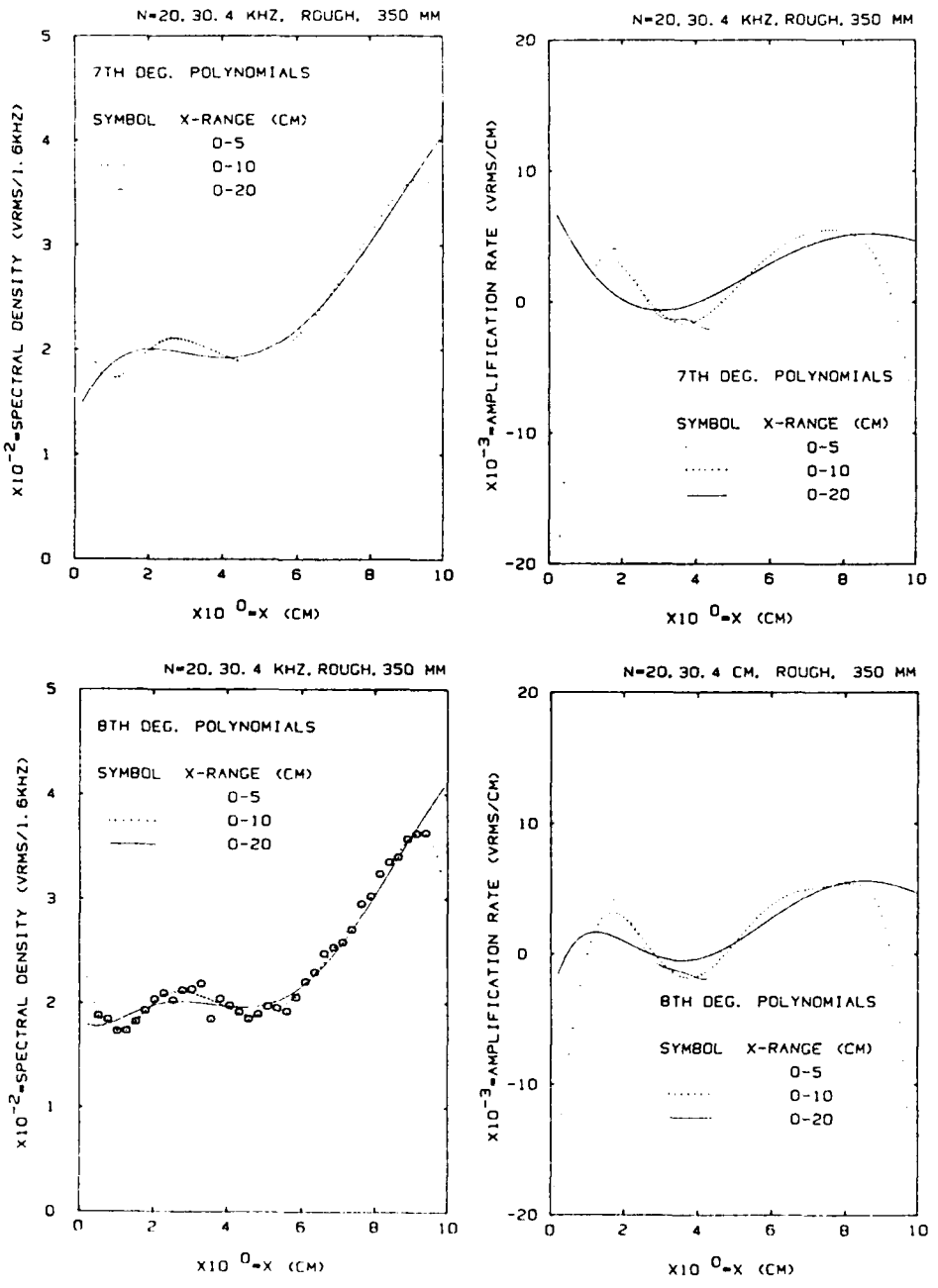

D.4 Influence of included x range on curve-fits.

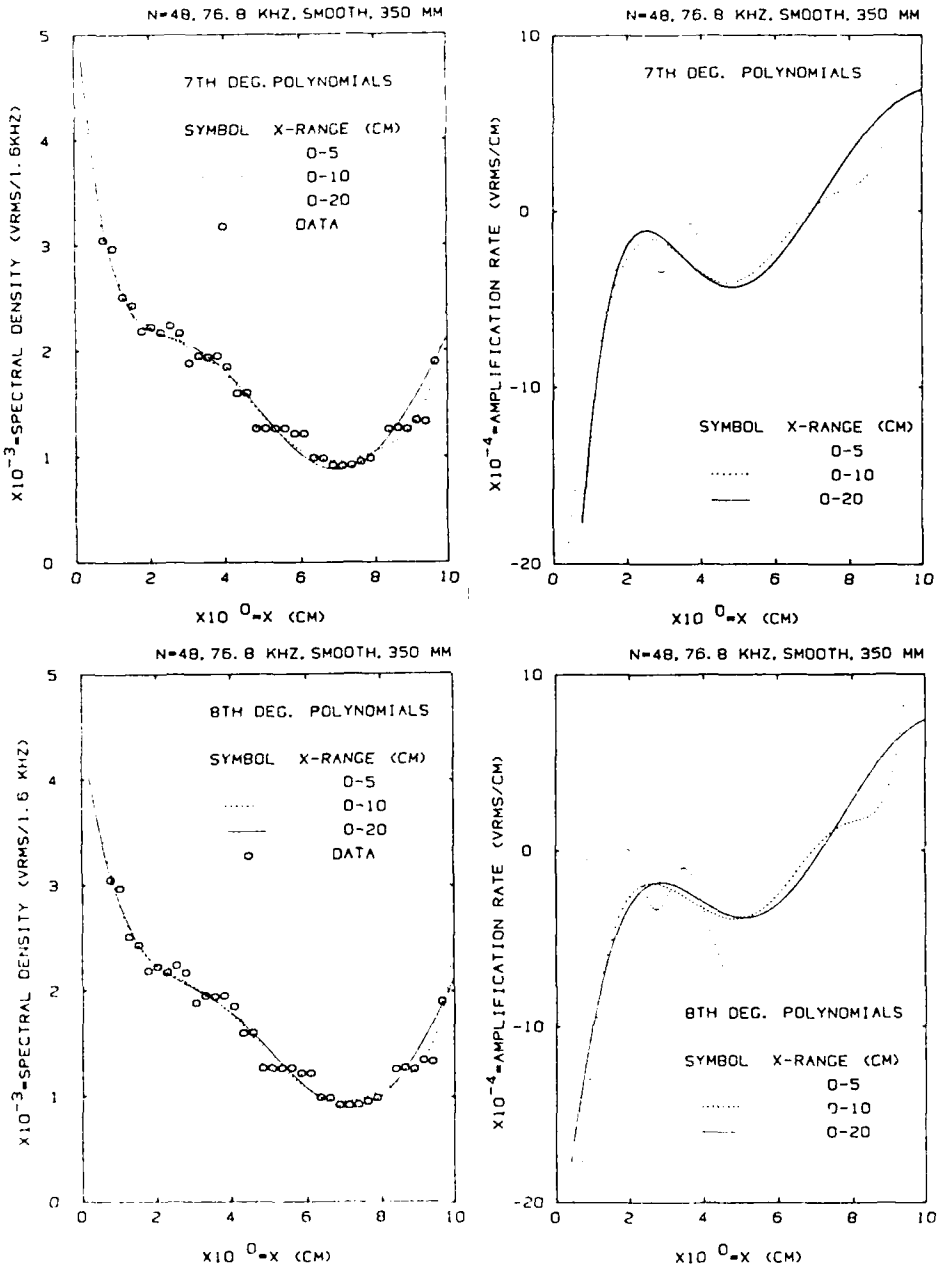

D.5 Influence of included x range on curve-fits.

END

FILMED

5-86

DTIC